Synthesis and Characterisation of MOP-phosphonite Complexes and their Applications in Asymmetric Catalysis

PhD Thesis Submitted by

James T. Fleming

Supervisor: Dr Lee J. Higham

School of Chemistry

Faculty of Science, Agriculture and Engineering

Newcastle University

Newcastle upon Tyne

United Kingdom

Abstract

In this thesis we report our synthesis of user-friendly, chiral phosphonite ligands, based upon Hayashi's MOP backbone, and their application in asymmetric catalytic transformations. Chapter 1 gives an introduction to organophosphorus ligands in catalysis and the use of air-stable primary phosphines as precursors in the synthesis of functionalised phosphorus compounds.

Chapter 2 details our synthesis and characterisation of the enantiopure MOP-phosphonite ligands (*S*)-**28a** and (*R*)-**28b** containing two phenoxy substituents, (*S*)-**29a** and (*R*)-**29b** with a biphenoxy moiety and (*S*)-**30a** and (*R*)-**30b** with a 3,3'-dimethylbiphenoxy group. These ligands are proven to be very successful in high-yielding, regio- and enantioselective palladium-catalysed hydrosilylation reactions of substituted styrenes, affording important chiral secondary alcohols, with (*S*)-**30a** achieving *ee*s of up to 95%. In-depth NMR studies reveal the hemilabile nature of the bonding of (*R*)-**30a** in a palladium 2-methylallyl complex, where the phosphonite ligand acts as a chelating P,C-π-donor.

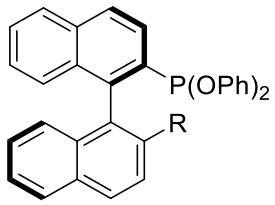

(*S*)-**28a**: R = H
(*R*)-**28b**: R = OMe

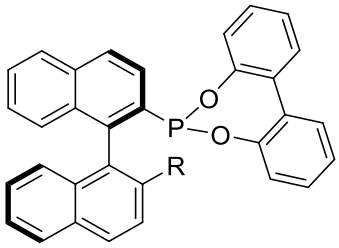

(*S*)-**29a**: R = H
(*R*)-**29b**: R = OMe

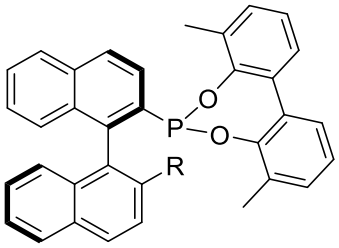

(*S*)-**30a**: R = H
(*R*)-**30b**: R = OMe

In Chapter 3 we compare our series of novel ligands via experimental and computational methods in an effort to quantify their differing structural and electronic profiles. Four [Rh(L^P)(η^2:η^2-cod)Cl] and two [Rh(L^P)$_2$]BF_4 complexes were synthesised and characterised by NMR spectroscopy, HRMS and, in all but one case, by X-ray crystallography. Rh(I) complexes were used as catalysts in industrially relevant asymmetric hydrogenation and hydroformylation reactions. Pd(II) complexes were successfully employed in asymmetric Suzuki-Miyaura cross-coupling reactions yielding binaphthyl products and two of the [Pd(L^P)$_2$$Cl_2$] catalysts were isolated and characterised by X-ray crystallography.

The final chapter details the preparation of copper, silver and gold complexes of our MOP-phosphonites. Six [Au(L^P)Cl] complexes were prepared as was the complex [Au((*S*)-**30a**)$_2$]SbF_6. Six [Ag(L^P)OTf] complexes were synthesised, as were six [Cu(L^P)(MeCN)$_2$]PF_6 complexes. Extensive NMR and X-ray crystallographic analyses undertaken on these compounds reveals that any M–π interactions appear weak, if present at all.

Acknowledgements

I would like to thank my supervisor Dr Lee Higham for his support and guidance during my PhD. I have had the opportunity to learn many different skills throughout my time in his research group, with interesting and varied projects, and have been given a great deal of freedom to pursue my own ideas and interests. Specifically thank you for sending me to numerous conferences and summer schools, I greatly appreciate every opportunity and I enjoyed them all. My second supervisor Dr Michael Hall has also always given helpful advice, alongside a few pints of beer, and I very much appreciate the conversations we have had over the years.

My time in the lab was made enjoyable and memorable by many people. Notably, Dr Manuel Abelairas-Edesa, Dr Arne Ficks and Dr Connor Sibbald who taught me most of what I know and have become great friends – hopefully our annual holiday will continue for many years! I have also had unforgettable times with Jennifer Wallis and Antonio Sanchez-Cid, thank you for keeping me cheerful as I wrote multiple papers and a thesis during the cold winter months. To complete the LJH research group I must thank Dr Laura Davies, Dr Ana Cioran, Graeme Bowling and Charlotte Hepples. Dr Thomas Winstanley deserves a special mention as an honorary LJH alumnus. I have also made many friends over the years with MChem, Erasmus and summer students who have passed through the lab – in particular Giorgia Fagnani and Bebhinn Tully-Penon.

I must thank the school of chemistry for funding my PhD and all members of the department who have made this work possible through their hard work and helpful support. With specific regards to my research: NMR – Dr Corinne Wills and Prof. William McFarlane; X-ray – Dr Paul Waddell, Dr Ross Harrington, Dr Michael Probert and Prof. William Clegg; Computing – Dr Jerry Hagon.

A special thank you to my parents, family and Hannah who have always been so enthusiastic and supportive about my academic adventures. I have always placed far more pressure upon myself to succeed than anyone else has, so thank you for keeping me calm and grounded.

List of Publications

I. N. Fey, S. Papadouli, P. G. Pringle, A. Ficks, J. T. Fleming, L. J. Higham, J. F. Wallis, D. Carmichael, N. Mézailles and C. Müller, Setting P-Donor Ligands into Context: An Application of the Ligand Knowledge Base (LKB) Approach, *Phosphorus Sulfur Silicon Relat. Elem.*, 2014, **190**, 706.

II. J. T. Fleming and L. J. Higham, Primary phosphine chemistry, *Coord. Chem. Rev.*, 2015, **297–298**, 127.

III. J. T. Fleming, A. Ficks, P. G. Waddell, R. W. Harrington and L. J. Higham, The design of second generation MOP-phosphonites: efficient chiral hydrosilylation of functionalised styrenes, *Dalton Trans.*, 2016, **45**, 1886.

IV. J. T. Fleming, C. Wills, P. G. Waddell, R. W. Harrington and L. J. Higham, A comparison of MOP-phosphonite ligands and their applications in Rh(I)- and Pd(II)-catalysed asymmetric transformations, *Dalton Trans.*, 2016, **45**, 15660.

Abbreviations

General

aq.	Aqueous solution
L	Arbitrary ligand
R	Arbitrary organic substituent
L^P	Arbitrary phosphorus ligand
Ar	Aryl
AHF	Asymmetric hydroformylation
AH	Asymmetric hydrogenation
AHS	Asymmetric hydrosilylation
AM1	Austin model one
B3LYP	Becke, three-parameter, Lee-Yang-Parr
Bn	Benzyl
Bu	Butyl
Cy	Cyclohexyl
DFT	Density functional theory
de	Diastereomeric excess
ee	Enantiomeric excess
Et	Ethyl
GC	Gas chromatography
ΔG	Gibbs free energy
η	Hapticity
HOMO	Highest occupied molecular orbital
HPLC	High-performance liquid chromatography
θ	Ligand cone angle
LKB	Ligand knowledge base
LUMO	Lowest unoccupied molecular orbital
MP	Melting point
Me	Methyl
Ph	Phenyl
Pr	Propyl
R_f	Retention factor
SOMO	Singly occupied molecular orbital

$[\alpha]_D^{20}$	Specific Rotation (20 °C, D = Wavelength of the sodium D line (589 nm))
*S*4'	Symmetric deformation coordinate
BAr^F	Tetrakis[3,5-bis(trifluoromethyl)phenyl]borate
TLC	Thin-layer chromatography
TM	Transition metal
TS	Transition state
Tf / Triflate	Trifluoromethanesulfonyl
Trip	2,4,6-Triisopropylphenyl
Mes	2,4,6-Trimethylphenyl
TMS	Trimethylsilyl
Mes*	2,4,6-Tri-*tert*-butylphenyl
2D	Two-dimensional
UV	Ultraviolet
UV-Vis	Ultraviolet-visible

Chemicals

acac	Acetylacetone
SEGPHOS	4,4'-Bi-1,3-benzodioxole-5,5'-diylbis(diphenylphosphine)
H-MOP	([1,1'-Binaphthalen]-2-yl)diphenylphosphine
BINOL	1,1'-Bi-2-naphthol
BINAP	2,2'-Bis(diphenylphosphino)-1,1'-binaphthalene
DPPP	1,3-Bis(diphenylphosphino)propane
COD	1,5-Cyclooctadiene
DCE	Dichloroethane
DCM	Dichloromethane
DIPEA	*N,N*-Diisopropylethylamine
MeO-BIPHEP	6,6'-Dimethoxy-2,2'-bis(diphenylphosphino)-1,1'-biphenyl
BIPHEMP	6,6'-Dimethyl-2,2'-bis(diphenylphosphino)-1,1'-biphenyl
DMI	Dimethyl itaconate
DMSO	Dimethyl sulfoxide
HO-MOP	(2'-Hydroxy-[1,1'-binaphthalen]-2-yl)diphenylphosphine
DIOP	2,3-*o*-Isopropylidene-2,3-dihydroxy-1,4-bis(diphenylphosphino)butane
MeO-MOP	(2'-Methoxy-[1,1'-binaphthalen]-2-yl)diphenylphosphine
PMB	*p*-Methoxybenzyl

MAA	Methyl 2-acetamidoacrylate
MAC	Methyl (Z)-2-acetamidocinnamate
KenPhos	(2'-Dimethylamino-[1,1'-binaphthalen]-2-yl)dicyclohexylphosphine
CAMP	Methylcycohexyl-*o*-anisylphosphine
PAMP	Methylphenyl-*o*-anisylphosphine
Ph-MOP	(2'-Phenyl-[1,1'-binaphthalen]-2-yl)diphenylphosphine
TADDOL	α,α,α',α'-Tetraaryl-1,3-dioxolane-4,5-dimethanol
THF	Tetrahydrofuran
tht	Tetrahydrothiophene
TMEDA	*N*,*N*,*N*',*N*'-Tetramethylethylenediamine

Infrared (IR) Spectroscopy

FT	Fourier transform
ν	Frequency
m	Medium
s	Strong
w	Weak

Mass Spectrometry

ASAP	Atmospheric-pressure solids analysis probe
HRMS	High-resolution mass spectrometry
LRMS	Low-resolution mass spectrometry
MALDI	Matrix-assisted laser desorption ionisation
NSI	Nanospray ionisation

Nuclear Magnetic Resonance (NMR) Spectroscopy

br	Broad
δ	Chemical shift
COSY	Correlation spectroscopy
J	Coupling constant
d	Doublet
EXSY	Exchange spectroscopy
HSQC	Heteronuclear single quantum correlation
HMBC	Heteronuclear multiple-bond correlation
m	Multiplet

NOE	Nuclear Overhauser effect
NOESY	Nuclear Overhauser effect spectroscopy
I	Quantum spin number
q	Quartet
ROE	Rotating frame Overhauser effect
ROESY	Rotating frame Overhauser effect spectroscopy
s	Singlet
t	Triplet
VT	Variable temperature

Units

Å	Ångström
cm	Centimetre
°	Degree
^{o}C	Degrees Celsius
eV	Electron volt
eq.	Equivalent
g	Grams
Hz	Hertz
h	Hour
K	Kelvin
MHz	MegaHertz
µmol	Micromoles
mg	Milligram
mL	Millilitre
mm	Millimetre
mmol	Millimoles
ms	Millisecond
min	Minute
M	Molar concentration
ppm	Parts per million

Table of Contents

1. Background and Introduction

1.1 Organophosphorus Ligands in Catalysis

A catalyst is a substance that increases the rate of a reaction but is both a reactant and product of the reaction.[1] Homogeneous catalysis is when only one phase is involved, usually the reactants and catalyst are contained in a single liquid phase or are in a gaseous state. Many soluble organometallic compounds have been used as homogeneous catalysts, both in academia and industry.[2] This differs from heterogeneous catalysis where the phase of the catalyst and reactants are not the same: typical examples use a solid catalyst with liquid or gaseous reactants.

Trivalent phosphorus compounds are commonly used in coordination chemistry as ligands in the formation of organometallic compounds. In 1965, Wilkinson (Nobel Prize for Chemistry 1973) discovered that the complex $[Rh(PPh_3)_3Cl]$ (Wilkinson's catalyst) catalysed the hydrogenation of unhindered alkenes (Scheme 1.1) with comparable rates to those found in the more developed field of heterogeneous catalysis.[3] Soon after, Vaska showed that complexes of the type *trans*-$[M(PPh_3)_2(CO)X]$ (M = Ir, Rh and X = halogen) were able to catalyse the hydrogenation of alkenes.[4] Wilkinson developed rhodium phosphine chemistry further with a report on catalysed alkene hydroformylation reactions.[5] This work was expanded by Pruett (Union Carbide Corporation) only a few months later, who showed that the rate and selectivity of hydroformylation reactions could be tuned by using triaryl-phosphite ligands.[6] Since these early breakthroughs, organophosphorus ligands have frequently been bound to transition metals in low oxidation states to form stable complexes which exhibit reactivity in homogeneous catalysis.[2] Popular metals from rows 2 and 3 of the transition series include ruthenium, rhodium, palladium and iridium.

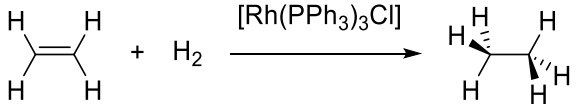

Scheme 1.1 The homogeneous hydrogenation of ethene, catalysed by Wilkinson's catalyst.

1.1.1 Electronic and steric parameters

Organophosphorus ligands (P-ligands) typically behave as Lewis bases and bind to transition metals through the phosphorus lone pair (σ-donor). In addition to this, they can accept electron density from filled metal orbitals into empty P–R antibonding σ*-orbitals (π-acceptor) (Fig. 1.1). The LUMO of the phosphorus ligand contains P–R antibonding orbitals, not empty phosphorus 3d-orbitals as was originally thought, as they are too high in energy.[7] Crystallographic studies by Orpen and co-workers have proven the application of this theory in transition metal complexes.[8] By varying the electronic

and steric properties of the substituents on the phosphorus atom, changes in the behaviour of the free ligands and their transition metal compounds have been observed.[9] The relative ease with which electronic and steric modification can be made to phosphorus compounds, in comparison to other common ligand classes such as alcohols and amines, makes them an attractive area of research for organometallic chemists.

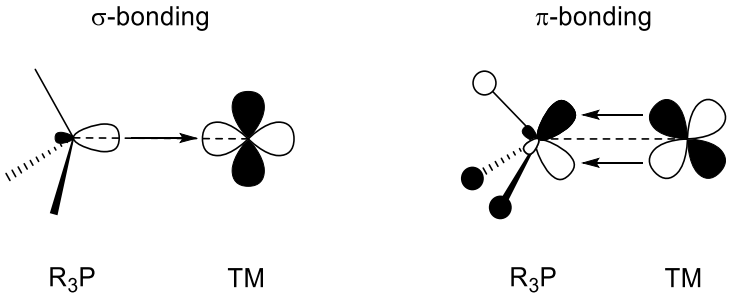

Fig. 1.1 A schematic diagram showing σ-bonding (left) and π-bonding (right) in transition metal P-ligand complexes.

A useful attribute of phosphorus compounds is the ability to study them by NMR spectroscopy. The ^{31}P nucleus is found in 100% abundance, has a high magnetogyric ratio (this property is directly proportional to the NMR signal strength) and has a nuclear spin quantum number of ½. These physical characteristics mean that ^{31}P NMR spectra often yield sharp lines with well resolved scalar coupling, allowing relatively easy interpretation of spectra. Therefore, this technique provides a fast and facile route to characterisation of ligands and their complexes, due to a noticeable coordination shift between the free ligand and complex. It can also be used to monitor reaction conversions and to observe synthetic intermediates.

In P-ligands, as the electronegativity of the substituents increases, the σ-donor character of the phosphorus atom decreases. On the other hand this may result in enhanced π back-donation in complexes of the type R_3P–TM (Fig. 1.1), especially from late transition metals in low oxidation states, with regards to partially filled d-orbitals. The amount of back-bonding has important consequences for stabilising the oxidation state of the metal. This can be seen in the length of P–TM and P–R bonds obtained from crystal structures, as oxidation of the metal results in lengthening of the P–TM bonds and shortening of the P–R bonds due to decreased π-back-bonding.[8a,b] For example, an elegant study by McKinney and co-workers illustrated this principle in the complexes $[CpCo(PEt_3)_2]$ (18 electron, +1 oxidation state) and $[CpCo(PEt_3)_2]BF_4$ (17 electron, +2 oxidation state), where the oxidation is largely metal based (Fig. 1.2).[10] The Co–P bond lengths increase on oxidation of the metal, from 2.218(1) Å to 2.230(1) Å (averages), whereas there is a decrease in the length of the P–C bonds in the two homoleptic phosphine ligands, from 1.846(3) Å to 1.829(3) Å (averages).[8a]

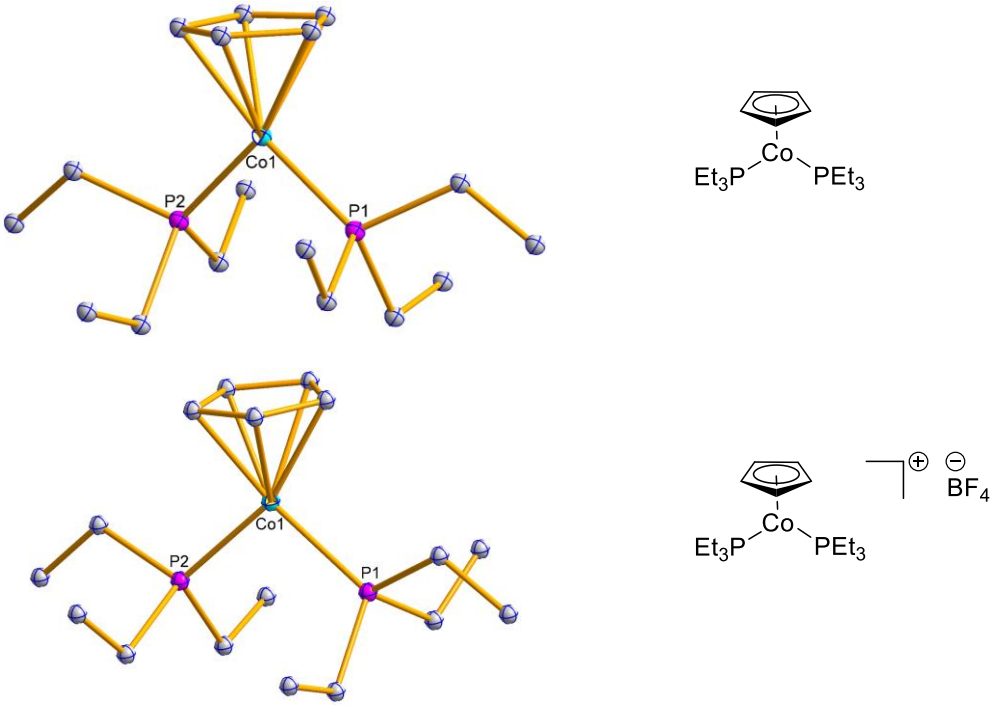

Fig. 1.2 View of the molecular structure of $[CpCo(PEt_3)_2]$ (top) and the cation of $[CpCo(PEt_3)_2]BF_4$ (bottom). Hydrogen atoms bound to carbon atoms have been omitted for clarity. (CCDC: 1125281 and 1125282 respectively). Crystal structure data was obtained from the Cambridge Structural Database (CSD).[11]

The Tolman steric and electronic parameters are a historically important means of evaluating the properties of a phosphorus(III) donor ligand.[9] Electronic effects result from transmission along chemical bonds. A popular method for assessing this is the Tolman electronic parameter (ν), the wavenumber of the A_1 carbonyl stretching mode in the IR spectra of $[(PR_3)Ni(CO)_3]$ complexes, recorded as a solution in DCM.[9] Reaction of $[Ni(CO)_4]$ with one equivalent of ligand at room temperature results in rapid formation of the complex and the sharp A_1 band is readily measurable, making this a convenient technique for synthetic chemists. The value of ν correlates well with the net donor properties of the ligand, for example, the electron rich ligand tri-*tert*-butylphosphine gives a value of 2056.1 cm^{-1} whereas the electron poor ligand phosphorus trifluoride has a value of 2110.8 cm^{-1}. The electron poor ligand competes more effectively with CO for π-backbonding, resulting in a stronger CO bond. Transition metal complexes of CO continue to play an important role in ranking the net donor properties of P-ligands.[12]

Tolman also noted that steric effects play an important role and that features of ligand binding in Ni(0) complexes could not solely be explained in terms of their electronic character. To quantify this, the magnitude of the steric bulk can be measured in terms of its ligand cone angle (θ) (Table 1.1).[9] For symmetrical ligands, the cone angle is calculated by modelling the van der Waals radii of the atoms and measuring angles to the outermost atoms of the model, where the apex angle of the cylindrical cone is 2.28 Å from the phosphorus atom (*n.b.* the calculation differs for unsymmetrical ligands).

Increasing the steric bulk of the substituents of the phosphorus results in a larger value for θ (Table 1.1). Following on from the work of Tolman, variations to the method of calculating cone angles and estimating the steric requirement of ligands have been proposed, which may better account for the properties of real ligands and their complexes, particularly where the substituent groups of the phosphorus atom differ greatly.[13]

Table 1.1 Calculated ligand cone angles (θ) for a selection of symmetrical phosphorus ligands.[9]

Ligand	θ	Ligand	θ
PH_3	87	$P(CF_3)_3$	137
PF_3	104	PPh_3	145
PMe_3	118	PCy_3	170
PCl_3	124	$P(C_6F_5)_3$	184
PBr_3	131	$P(Mes)_3$	212

Large cone angles can favour lower coordination numbers, which is important in transition metal catalysis providing the substrate is of the appropriate size to bind to the vacant metal coordination site. A significant realisation is that electronic and steric effects are not mutually exclusive, they are in fact intimately related, and hence are difficult to isolate completely. For example, changes in the angles between substituents can affect the s-character of the phosphorus lone pair; similarly, bond lengths and angles can be tuned by varying the electronegativity of the substituents.[9]

An alternative means of evaluating the steric bulk of phosphorus ligands is the symmetric deformation coordinate (*S*4'), introduced by Orpen and co-workers using data obtained from crystal structures,[8c] which seeks to evaluate P-ligands based on a geometric calculation using phosphine angles from species with the general formula Z–PR_3 (Z = transition-, main group- or non-metal) (Fig. 1.3). *S*4' is a measure of the flattening or pyramidality around the phosphorus atom, and the value is calculated by subtracting the sum of the R–P–R angles (β) from the sum of the Z–P–R angles (α). Small values for *S*4 can suggest substituents with increasing steric bulk.

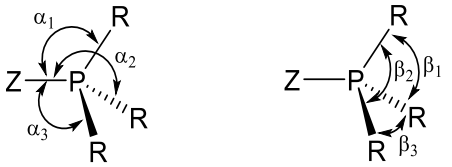

Fig. 1.3 Angles used in the calculation of Orpen's symmetric deformation coordinate (*S*4').

1.1.2 Ligand knowledge base

The Ligand Knowledge Base (LKB), developed by Fey and co-workers,[14] is a DFT-computational method designed to aid the discovery of novel ligands and to predict ligand effects before experimentation. Monodentate P-donor (LKB-P)[15] and C-donor (LKB-C)[16] ligands and chelating P,P- and P,N-donor (LKB-PP)[17] ligands have been described to create a database containing more than 1000 ligands.

Computational ligand parameters/descriptors have been developed using the optimised structures of the ligand in a number of different coordination environments: the free ligand (L), the protonated ligand ($[LH]^+$), the borane adduct ($[LBH_3]^+$), three transition metal complexes ([LAuCl], $[LPdCl_3]$ and $[LPt(PH_3)_3]$) and the interaction between the ligand and a ring of 8 helium atoms ($L{\cdot}He_8$). Parameters such as calculated versions of the Tolman parameters, adduct binding energies and electronic frontier molecular orbital energies are extracted, 28 in total.

The LKB uses Principal Component Analysis (PCA) to reduce the dimensionality of datasets where descriptors are correlated, giving fewer variables. This technique is designed to capture as much of the variation in the dataset in as few dimensions as possible, hence the data can be expressed into 3D scattering plots. Clustering of ligands with similar properties can help establish patterns and a chemical context (*i.e.* ligands which are close in space are more likely to have similar properties than those further away). The LKB is a highly useful tool with potential industrial applications, the results from calculations can be analysed and used to reduce the scale of an experimental catalyst screening.

The LKB-P has recently been updated to include a selection of unusual MOP ligands which Higham *et al*. have reported, including phosphiranes and phosphonites (*vide infra*) (Chart 1.1). The LKB-P has been used, alongside experimental results, to direct the catalytic application of novel ligands presented in this thesis in asymmetric catalytic transformations.[18]

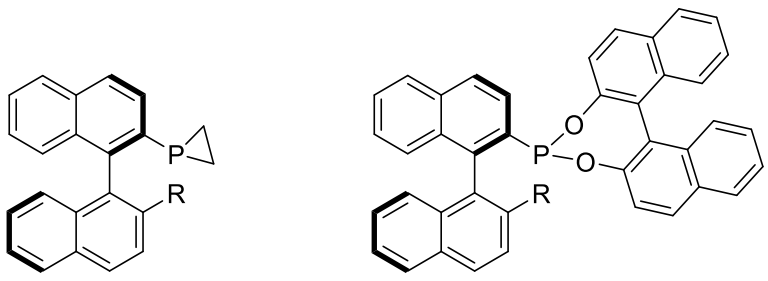

R = H or OMe
Phosphiranes

R = H or OMe
Phosphonites

Chart 1.1 A selection of MOP ligands synthesised by the Higham research group which are in the LKB-P.

1.2 Organophosphorus Ligands in Asymmetric Catalysis

1.2.1 Asymmetric catalysis

Organophosphorus molecules are a popular choice of ligand in homogeneous catalysis because, by altering the choice of P-substituent, the electronic and steric properties of the ligand – and any derived organometallic complex – can be finely tuned.[19] By choosing a chiral substituent, or alternatively making the P atom itself a chiral centre (P-chiral), it is possible to synthesise complexes which can catalyse reactions asymmetrically. Chirality is a feature found in many pharmaceuticals and agrochemicals – hence catalysts that can selectively synthesise one enantiomer over another are in high demand.

The synthesis of chiral, enantiopure compounds can begin with commercially available starting materials. If these compounds are sourced from nature, then it is commonly referred to as a chiral-pool source. Otherwise, optical purity can be achieved by chiral resolution techniques or by asymmetric synthesis using chiral auxiliaries or catalysts. The development of enantioselective catalytic reactions has been driven by the industrial need for enantiopure compounds, without time consuming and inherently expensive chiral resolution techniques, based on crystallisations or chromatography.[20] Advances in the field of homogeneous asymmetric catalysis were recognised in 2001 with the awarding of the Nobel Prize for Chemistry to Knowles, Noyori and Sharpless for their work on asymmetric hydrogenation and oxidation reactions.[21]

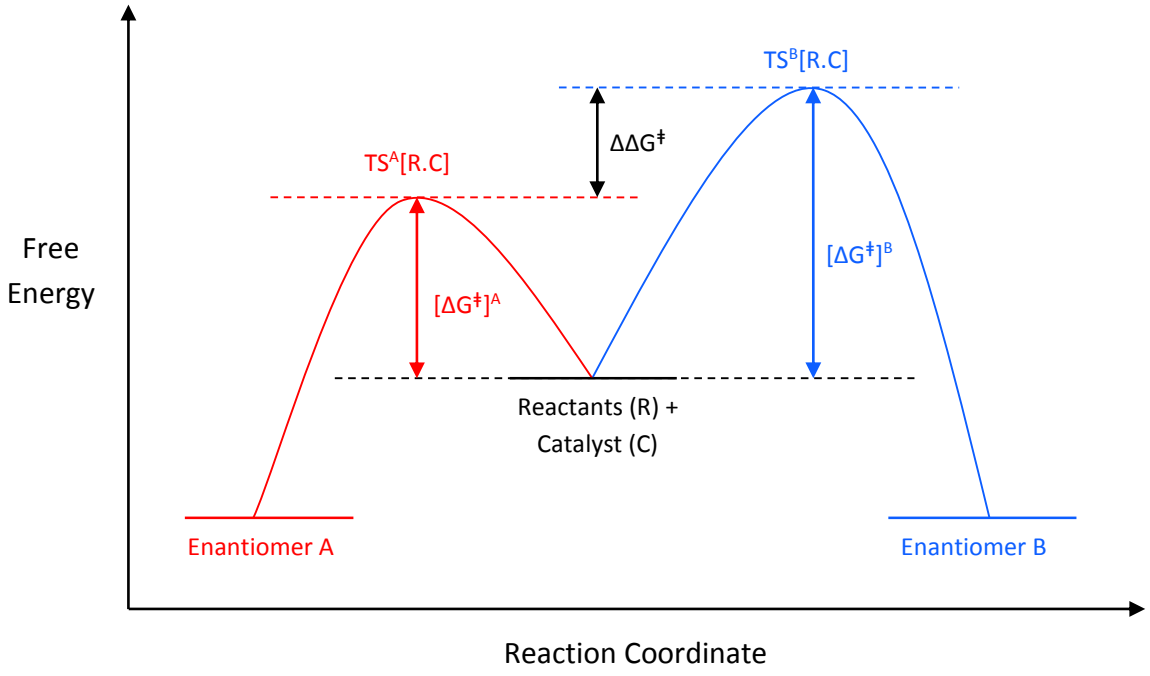

Fig. 1.4 An energy level diagram illustrating the origin of selectivity in asymmetric catalysis.

An asymmetric catalyst lowers the transition state (TS) energy for the formation of one enantiomer, more than it lowers the TS energy for the formation of the other enantiomer, making the lower energy route kinetically favourable (Fig. 1.4). The catalyst must itself be a non-racemic chiral species; this results in the TS complexes becoming a pair of diastereomers as opposed to enantiomers. Diastereomers have different physical and chemical properties and this is the cause of the difference in energy of the two transition states.

1.2.2 P-chiral, monodentate phosphorus ligands

A chiral compound has the property of being non-superimposable on its mirror image, its enantiomer. The most commonly encountered form of asymmetry found in organic molecules is a centre of chirality, a tetrahedral atom with four non-identical substituents. This type of chirality is seen in trivalent phosphorus compounds when three different groups are bound to the phosphorus atom (P-chirality) – the P lone pair is the fourth non-identical group. In P-chiral ligands, the pyramidal inversion barrier of the molecule must be sufficiently high to prevent racemisation: typically the energy barrier is 35-40 kcal/mol,[22] which is usually adequate to prevent inversion at room temperatures.

Early work using organophosphorus complexes as asymmetric catalysts was based on Wilkinson's catalyst, replacing triphenylphosphine with chiral phosphorus ligands where the phosphorus atom is the centre of chirality. Horner first noted the possibility of stereospecific hydrogenation reactions with optically active tertiary phosphines and later carried out reactions to prove this theory.[23] However, Knowles (Nobel Prize for Chemistry 2001) and Sabacky at the Monsanto Company were the first to report the use of P-chiral phosphines in asymmetric catalysis: the asymmetric hydrogenation of α-phenylacrylic acid, using an optically enriched isopropyl(methyl)(phenyl)phosphine rhodium(III) complex, yielded the product in a 15% *ee*.[24] Knowles pioneered further research in this field with the synthesis of the PAMP and CAMP ligands (Chart 1.2), which proved increasingly successful in asymmetric hydrogenation reactions, with enantiomeric excesses of up to 90% reported using (*R*)-CAMP.[25] However, P-chiral alkyl phosphine ligands have their drawbacks, their synthesis and purification can be laborious and as commonly encountered with alkyl phosphines, a rigorous air-free procedure may be necessary to prevent phosphorus oxidation.[26]

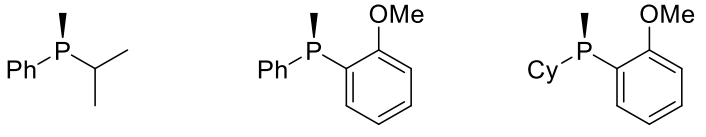

(*S*)-PMePh(*i*Pr) (*R*)-PAMP (*R*)-CAMP

Chart 1.2 A selection of ligands used by Knowles in homogeneous asymmetric hydrogenation reactions.

1.2.3 Chiral, bidentate phosphorus ligands

Later work more often concentrated on using bidentate P-ligands. Bidentate binding reduces the number of conformations available to the chiral ligand, and it is often the case that the more defined the steric environment of the complex, the more selective it is in asymmetric catalysis. The first major successes of bidentate phosphine ligands in asymmetric hydrogenation reactions were achieved by Kagan and Dang with (*R*,*R*)-DIOP, which is prepared from the naturally occurring form of tartaric acid (Chart 1.3).[27] In their study it was shown that (*R*,*R*)-DIOP was able to efficiently catalyse the hydrogenation of α-acetamidocinnamic acid (a precursor of the amino acid phenylalanine) with a yield of 95% and a 72% *ee*,[27a] and subsequent work revealed that a range of α-acetamidoacrylic acid precursors of amino acids were reduced with high enantioselectivities by the Rh/(*R*,*R*)-DIOP catalyst.[27b] Kagan was somewhat controversially not given a share of the 2001 Nobel Prize for Chemistry awarded for catalytic asymmetric synthesis.[28] Development in this field led to the synthesis of (*R*,*R*)-DiPAMP by Knowles, where the methyl group in (*R*)-PAMP was replaced by an ethyl bridge to form a chelating bisphosphine, C_2 symmetric ligand.[29] The Monsanto Company quickly adapted their commercial process to synthesise L-DOPA, a drug used for treating Parkinson's disease, to include a rhodium complex of (*R*,*R*)-DiPAMP, which could hydrogenate a key prochiral precursor with an *ee* of 95%.[30]

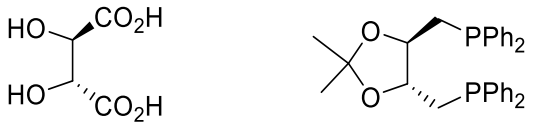

(*R*,*R*)-tartaric acid (*R*,*R*)-DIOP

Chart 1.3 (*R*,*R*)-Tartaric acid and (*R*,*R*)-DIOP.

1.2.4 Atropisomeric phosphorus ligands

Atropisomerism results from the non-planar arrangement of four groups in pairs about an axis of chirality.[31] It is observed for *ortho*-substituted biphenyls (Fig. 1.5, where $a \neq b$ and $c \neq d$), where the energy barrier for free rotation is large enough to prevent rotation, except at high temperatures.[32] The stereochemistry of the molecule is assigned by the Cahn-Ingold-Prelog priority rules.[33]

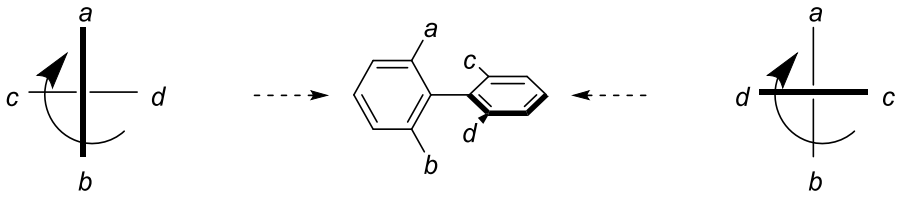

Fig. 1.5 The view along an *ortho*-substituted biphenyl along its axis of chirality (broken arrow) and assigning its configuration by the Cahn-Ingold-Prelog priority rules.

Priority is designated for each substituent with respect to its atomic number, and the molecule is viewed along its axis of chirality with the highest priority group given the position of *a*. The absolute configuration of (*R*)- for clockwise and (*S*)- for anti-clockwise can thus be assigned by analysing the direction of transition from the second highest priority substituent on the proximal ring to the highest priority substituent on the distal ring (Fig. 1.5: b to c (left hand view) and d to a (right hand view)). This is the source of chirality found in binaphthyl and will be used to assign the absolute stereochemistry.

At room temperature, the minimum free energy barrier to rotation (*i.e.* racemisation) is approximately 23 kcal/mol for biphenyl derivatives.[34] The rotational barrier for 1,1'-binaphthyl is also approximately 23 kcal/mol and hence it will racemise under standard conditions (Fig. 1.6),[35] the values for 2/2'-substituted binaphthyls are higher and hence they may exist as single enantiomers.[31]

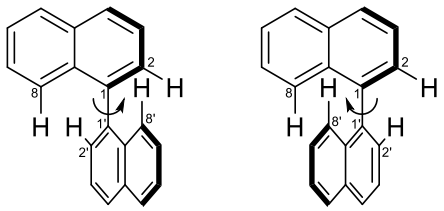

Fig. 1.6 Anti-transition (H2–C1–C1'–H8' = 0°) (left) and syn-transition (H2–C1–C1'–H8' = 180°) (right) in the racemisation pathway of 1,1'-binaphthyl.

A milestone in chiral bidentate ligand synthesis was the discovery of the C_2-symmetric ligand BINAP in 1980 by Noyori (Nobel Prize for Chemistry 2001) (Chart 1.4).[36] BINAP is one of the most widely used and useful ligands found in the field of homogeneous asymmetric catalysis, and has become one of the few chiral ligands produced on an industrial scale.[37] There have also been many BINAP-analogues reported in the literature, for example the BIPHEMP and MeO-BIPHEP series developed by the pharmaceutical company Roche (Chart 1.4),[38] and the SEGPHOS ligand class developed by the research team at Takasago International Corporation (Chart 1.4).[39] Consequently, axially chiral bidentate ligands have become an important ligand class in homogeneous asymmetric catalysis.[40]

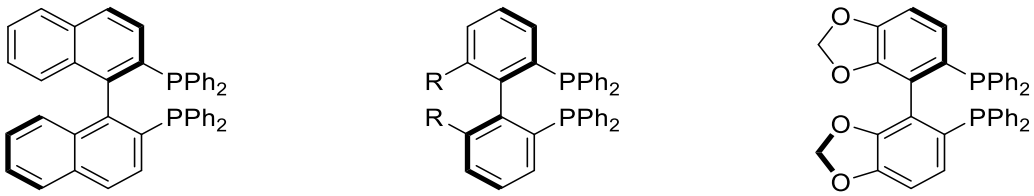

(*R*)-BINAP (*R*)-BIPHEMP: R = Me (*R*)-MeO-BIPHEP: R = OMe (*R*)-SEGPHOS

Chart 1.4 A selection of axially chiral, biaryl-diphosphine ligands.

One of the major advances in BINAP catalysis was the discovery that transition metal-bound BINAP can hydrogenate many substrates with a high *ee* and turnover. BINAP-based ruthenium(II) and rhodium(I) complexes have shown high chiral selectivity in a variety of catalytic reactions.[41] Early examples included the demonstration that BINAP is an effective ligand for the asymmetric hydrogenation of prochiral alkenes under mild conditions: Ru(II) complexes achieved up to 95% *ee*[42] and Rh(I) complexes could achieve complete enantioselectivity with α-acetamidoacrylic acid substrates (Scheme 1.2).[36,43]

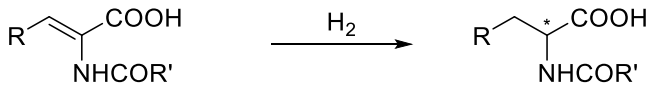

a. R = H, R' = Me
b. R = Ph, R' = Me
c. R = Ph, R' = Ph

Scheme 1.2 The asymmetric hydrogenation of α-acetamidoacrylic acids.

Although bidentate P-ligands have dominated the research, there have been noteworthy examples of asymmetric catalysis using monodentate phosphines.[44] Hayashi has featured prominently in this field. His early work featured chiral ferrocenylphosphines,[45] and later he synthesised the MOP ligand class (Chart 1.5). MOP ligands have been proven to be effective in the asymmetric hydrosilylation of alkenes,[46] as well as other catalytic transformations.[47]

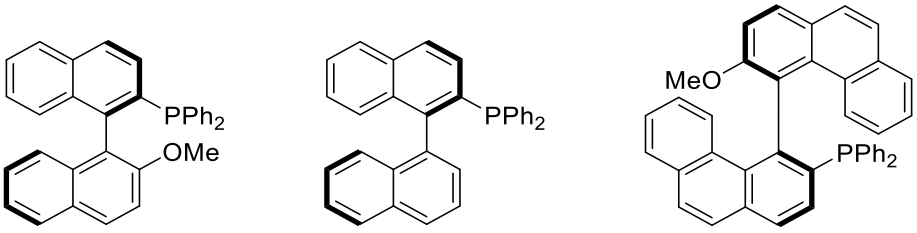

(*R*)-MeO-MOP (*S*)-H-MOP (*R*)-MOP-phen

Chart 1.5 Examples of ligands from the MOP-family.

1.3 Primary Phosphines

Primary phosphines[48] are highly versatile precursors in the synthesis of functionalised phosphorus compounds due to the high reactivity of the P–H bonds, and allow access to a range of molecules that are otherwise inaccessible or difficult to reach by other methods. Scheme 1.3 provides a representation of reaction types which can be used to modify the phosphorus atom.[49] Primary phosphines have been used as starting materials in the fields of asymmetric catalysis,[49c] carbohydrate research,[50] macrocyclic synthesis,[51] medicinal chemistry[52] and polymer science.[53] Despite these diverse applications, there are still only a limited number of reports on this functionality, in part due to certain

preconceived ideas about their supposed high sensitivity to oxidation and noxious character, which lends them a reputation as being difficult to handle.

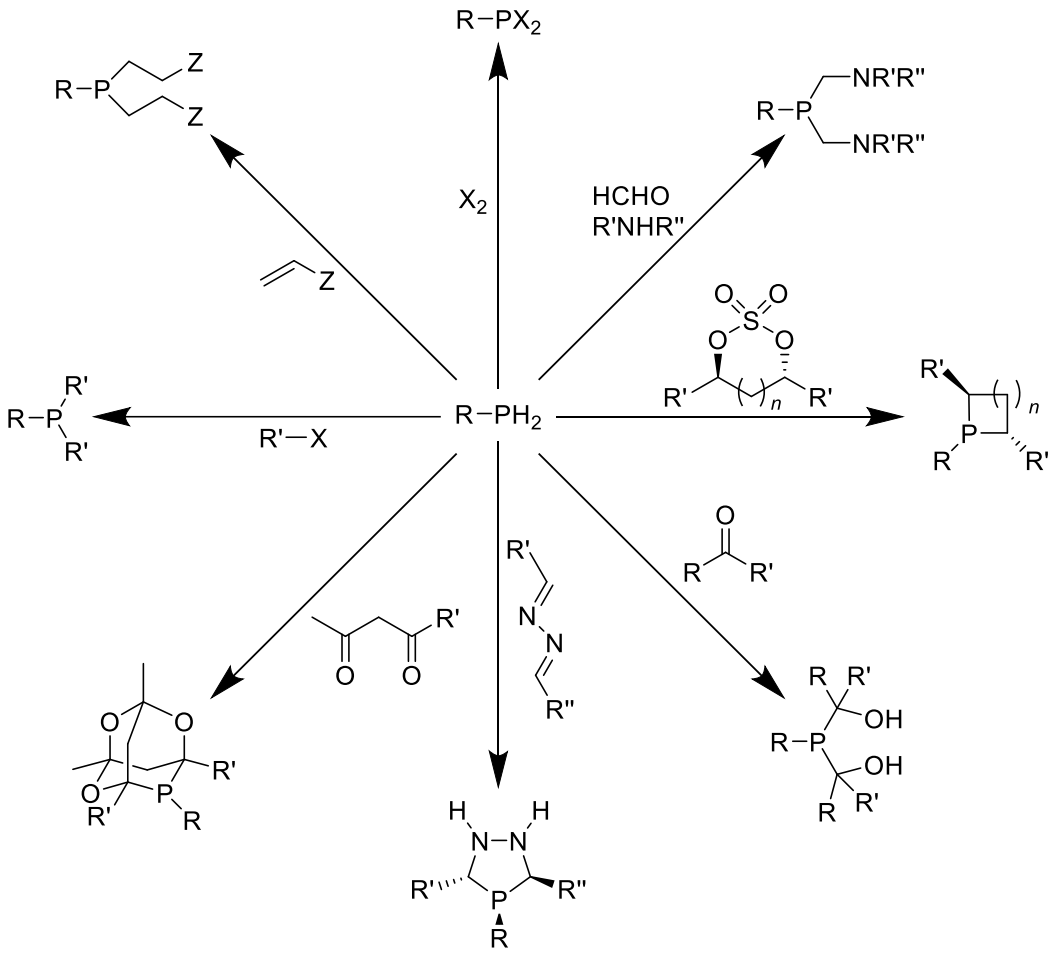

Scheme 1.3 Reactions to functionalise the P–H bonds in a primary phosphine (n = number, R/R'/R'' = organic substituent, X = halogen and Z = R_2N, R_2P).

The reputation of primary phosphines as air-sensitive compounds, many of which are highly pyrophoric, is well deserved, especially those which are of a low molecular weight and lack steric encumbrance.[54] Decomposition occurs through an exothermic oxidation reaction which can be very rapid, even at room temperature (Scheme 1.4).[55] This factor, in addition to other common characteristics of volatility, toxicity and unpleasant odour, appear to be the reasons why primary phosphines are not employed more routinely in the synthesis of organophosphorus compounds.[56]

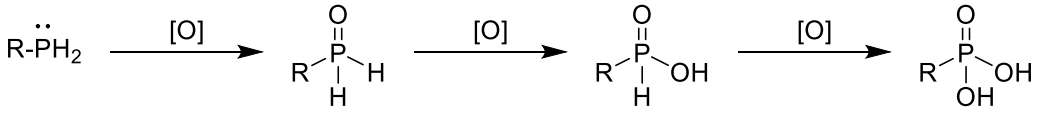

Scheme 1.4 A simplified reaction showing the stepwise oxidation of primary phosphines.

In 2005 Brynda published a review covering those primary pnictanes which are found to be 'user-friendly' and they focus on the strategy of using bulky substituents in close proximity to the phosphino group to afford steric protection to air-oxidation – the review details the first examples of this approach dating back to the late 1960s. Some recently discovered examples of surprisingly air-stable primary phosphines containing heteroatoms or a ferrocenyl backbone were also introduced.[48a] Since the publication of Brynda's fascinating review, the number of 'user-friendly' primary phosphines has steadily increased. While the air-stability of certain primary phosphines can be attributed to the well-known phenomenon of steric encumbrance, there have been a growing number of examples where the authors were unable to rationalise this unexpected stability. In order to account for their resistance to air oxidation, Higham *et al*. have developed a theoretical model of phosphine oxidation, and these DFT calculations have also proven to be a useful tool to rationalise the air-stability/sensitivity of other primary phosphines with previously unexplained air-stability. The model has also proven successful in predicting how novel primary phosphines behave towards air-oxidation.[54,57]

1.4 Air-stable Primary Phosphines

It is prudent at the outset to explain how we interpret 'air-stability', in this instance we mean the resistance of a primary phosphine to undergo oxidation by aerobic (or occasionally elemental) oxygen, in the absence of other oxidising agents. It is also worth noting that it is not always straightforward to compare literature examples of air-stability, as different authors judge this somewhat subjectively, in the absence of an accepted definition. Here, we regard air-stable primary phosphines as those that display inertness to oxidation over several weeks. As will be shown, certain primary phosphines are not air-stable but oxidise slowly, and this still confers a number of advantages in terms of their ease-of-handling over their more reactive counterparts. It is also important to clarify that an environment containing certain transition metals, or one which allows for the production of peroxides, such as aged ether solvents or prolonged exposure to sunlight, can result in an air-stable phosphine undergoing oxidation – these conditions must, therefore, be avoided. It is useful for the purposes of classification to separate out the air-stable primary phosphines into those that are stabilised by steric encumbrance, and those compounds whose behaviour cannot be explained in this way.

1.4.1 Steric protection

There are a small number of 'user-friendly' primary phosphines reported in the literature, whose enhanced stability results from kinetic stabilisation by bulky substituents, which inhibits the reaction with dioxygen (Chart 1.6).[48a] For example, phenylphosphine **1** is a pyrophoric, highly air-sensitive liquid which rapidly oxidises; however, mesitylphosphine **2** is only mildly sensitive to air-oxidation and was the first primary phosphine characterised by X-ray crystallography.[58] With a further increase in the

steric bulk of the substituents on the phosphorus, as in supermesitylphosphine **3**, described as air-stable and odourless,[59] and again in 2,6-$Trip_2H_3C_6PH_2$ **4** which possesses remarkable thermal stability,[60] it becomes possible to isolate primary phosphines that have long-term stability and which can be handled freely in air. These tactics allow such compounds to be used in the synthesis and characterisation of what would otherwise be highly reactive molecules. Of course, this confined space around the phosphorus atom renders further functionalisation more difficult.

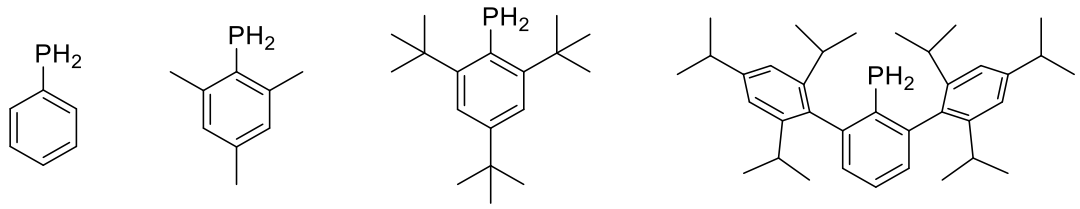

1 **2** **3** **4**

Chart 1.6 Primary phosphines: increasing steric encumbrance results in a greater resistance to air-oxidation.

1.4.2 Unexplained stability

There are sporadic reports in the literature of primary phosphines that are resistant to air-oxidation but where steric hindrance does not appear to be the protecting factor – examples of compounds of this nature include **5**, **6**, **8a** and **8b** (Chart 1.7). Analysis of the solid-state structure of the primary diphosphine **5** (Fig. 1.7),[61] revealed intermolecular hydrogen-bonding interactions between the amide and carbonyl groups, but no direct hydrogen-bonds to the primary phosphine-bound hydrogen atoms. Thus, hydrogen-bonding does not appear to be responsible for the surprising resistance to air-oxidation of a molecule which bears two phosphino groups. The authors postulated that negative hyperconjugation arising from the electronegative heteroatoms to the phosphorus centres may be the causative factor in this regard;[61] similarly, the thioether-functionalised diprimary phosphine **6** also demonstrated an unexpected degree of air-stability.[52] From unpublished AM1 calculations, Katti *et al*. suggested that the heteroatom atomic orbitals in **5**, **6** and related molecules could contribute to the frontier molecular orbitals, providing some support to the negative hyperconjugation theory.[49b]

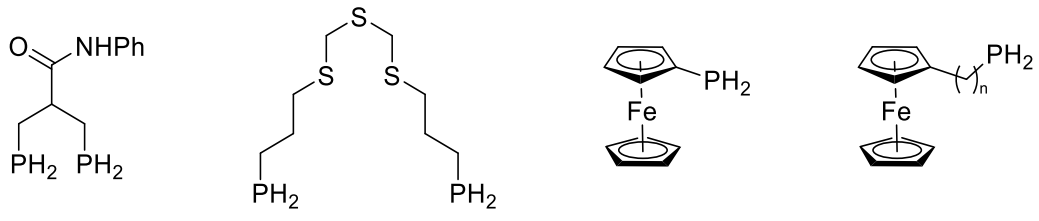

5 **6** **7** **8a**, n = 1 **8b**, n = 2

Chart 1.7 Primary phosphines **5**, **6**, **8a** and **8b** resist air-oxidation but possess little steric encumbrance – the ferrocenyl derivative **7** is air-sensitive.

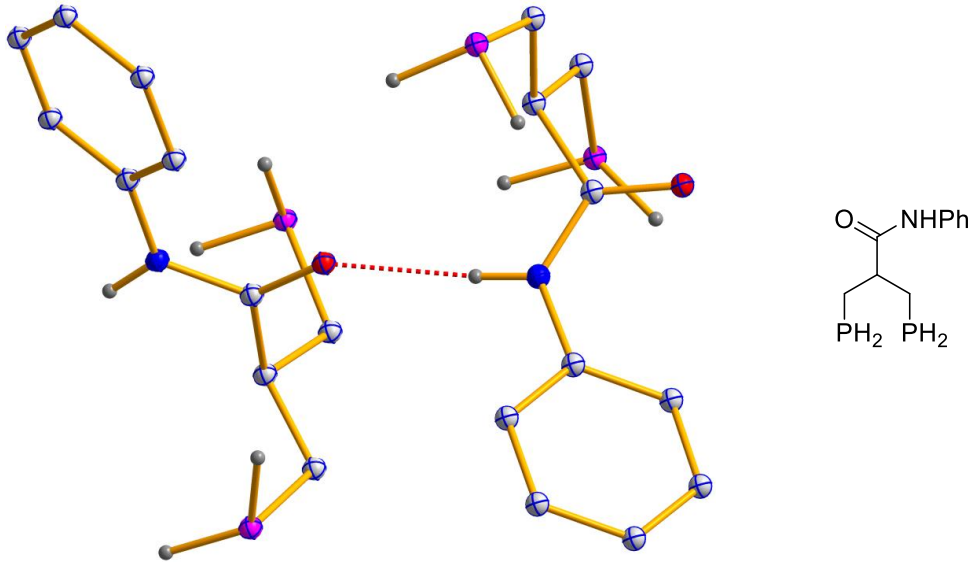

Fig. 1.7 View of the molecular structure of **5** with intermolecular hydrogen bonding between the amide and carbonyl groups indicated (red broken line). Hydrogen atoms bound to carbon atoms have been omitted for clarity. (CCDC: 138440). Crystal structure data was obtained from the Cambridge Structural Database (CSD).[11]

A second example of note is the exceptional long-term stability of the methylene-bridged ferrocenyl-phosphine **8a** which was synthesised by Henderson and co-workers.[62] This primary phosphine has only a very slight odour and is completely air-stable.[63] Furthermore, the ethylene-bridged ferrocenyl-phosphine **8b** was found to show a similar resistance to aerobic oxidation. Neither steric encumbrance nor the presence of the iron centre were thought to be responsible for this behaviour, which was instead attributed to the alkane spacer group separating the phosphorus from the cyclopentadienyl ring.[64] The corresponding derivative without such a spacer **7** is sensitive to oxidation in air;[65] however, the underlying reason for this observation has yet to be determined.[64]

1.4.3 Electronic protection

More recently, Higham *et al*. have synthesised air-stable primary phosphines which possess neither steric encumbrance nor heteroatoms other than the phosphorus (**12a** for instance, Chart 1.8).

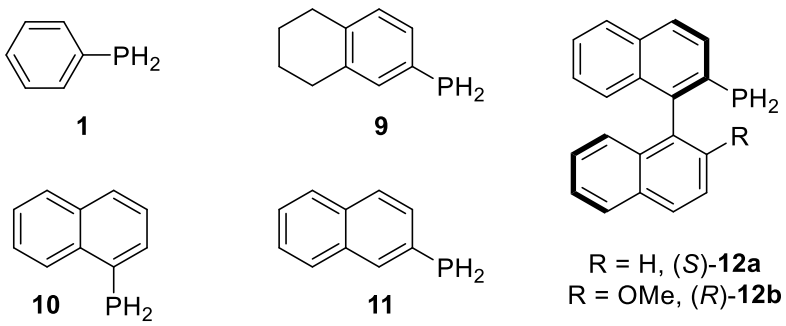

Chart 1.8 Phenyl-, naphthyl- and binaphthyl-derived primary phosphines. The three classes exhibit differing degrees of air-stability – the more π-conjugation present in the molecule, the greater the resistance to air-oxidation.

It has been found that those phosphines which contain a relatively high degree of π-conjugation in their backbone demonstrate resistance to air-oxidation – as the extent of π-conjugation decreases, the air-stability falls too (Chart 1.8).[54] Phenylphosphine **1** is a highly air-sensitive liquid – a neat sample completely oxidised within one week, whilst a chloroform solution showed only 42% of **1** remained after the same length of time. The monoarene oil **9** is also air-sensitive but oxidises less readily – 59% remained in solution after the same time frame. In comparison, 2-naphthylphosphine **11** is a relatively air-stable white solid and its regioisomer, 1-naphthylphosphine **10**, shares a similar degree of solution air-stability (72% and 74% remaining after seven days, respectively). It should be noted, however, that neat samples of the oil **10** *do* oxidise more rapidly in air than the solid **11**. Increasing the degree of π-conjugation still further, it is observed that the crystalline compounds (*S*)-**12a** and (*R*)-**12b**, based on a binaphthyl backbone, possess long-term air-stability. No oxidation was observed in solution after seven days, and solid samples were found to be stable to air indefinitely.[54] The solid-state structure of (*R*)-**12b**, obtained by X-ray crystallography (Fig. 1.8), reveals that the phosphino group is not interacting with the methoxy substituent, thereby ruling this out as a source of stabilisation in the solid state.[66]

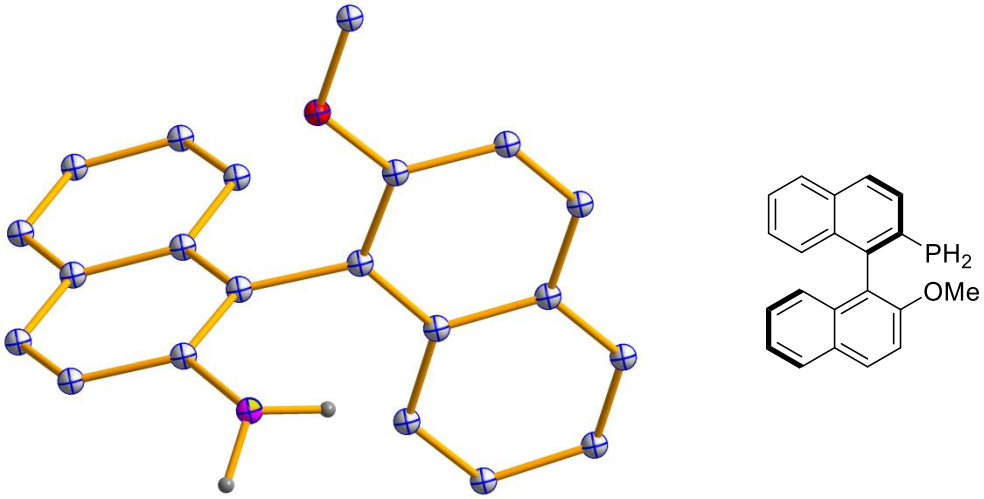

Fig. 1.8 View of the molecular structure of (*R*)-**12b**. Hydrogen atoms bound to carbon atoms have been omitted for clarity. (CCDC: 281451). Crystal structure data was obtained from the Cambridge Structural Database (CSD).[11]

The sensitivity of phosphines to molecular oxygen has been explained by the thermodynamically favourable formation of phosphine oxides and acids (Scheme 1.4), the driving-force being the strength of the phosphorus-oxygen bond.[55] However, the mechanism for the aerobic oxidation of primary phosphines has yet to be established. Even for tertiary phosphines there are relatively few reports concerned with their oxidation by air or oxygen.[67] Those studies that have tackled the matter generally point to the implication of a phosphorus radical cation in the oxidative process. Recent reports by Yasui and Majima provided spectroscopic evidence, through laser flash photolysis experiments, that the formation of the triarylphosphine radical cation $[R_3P]^{+\bullet}$, led to the generation of the peroxy radical

cation $[R_3POO]^{+\bullet}$ in the presence of molecular oxygen. This transient intermediate subsequently undergoes a radical reaction with a second equivalent of phosphine, to form the dimeric radical cation $[R_3POOPR_3]^{+\bullet}$ (Scheme 1.5), which eventually breaks down into the corresponding phosphine oxide.[67i,j,l,m] A related reaction pathway was noted when the radical cation was generated by radiolysis rather than photolysis.[67g,h] Two recent reports have revealed the first examples of single crystal X-ray structures of triarylphosphine radical cations.[68] It has been suggested that sterically bulky or rigid substituents can result in higher stability in the $[R_3P]^{+\bullet}$ radical cations.[67i,j,n,68a]

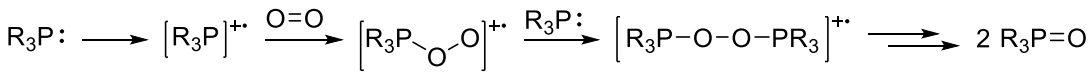

Scheme 1.5 Postulated steps in the photolytic oxidation of a tertiary phosphine; a radical cation forms and reacts with dioxygen to give a peroxy radical which leads to two molecules of phosphine oxide via its reaction with a second tertiary phosphine.

Higham *et al*. have recently developed a quantum mechanical model based upon density functional theory (DFT), in an attempt to provide an explanation for both the air-stability observed for the series of π-conjugated primary phosphines and the unexplained stability of those introduced in Chart 1.7.[54]

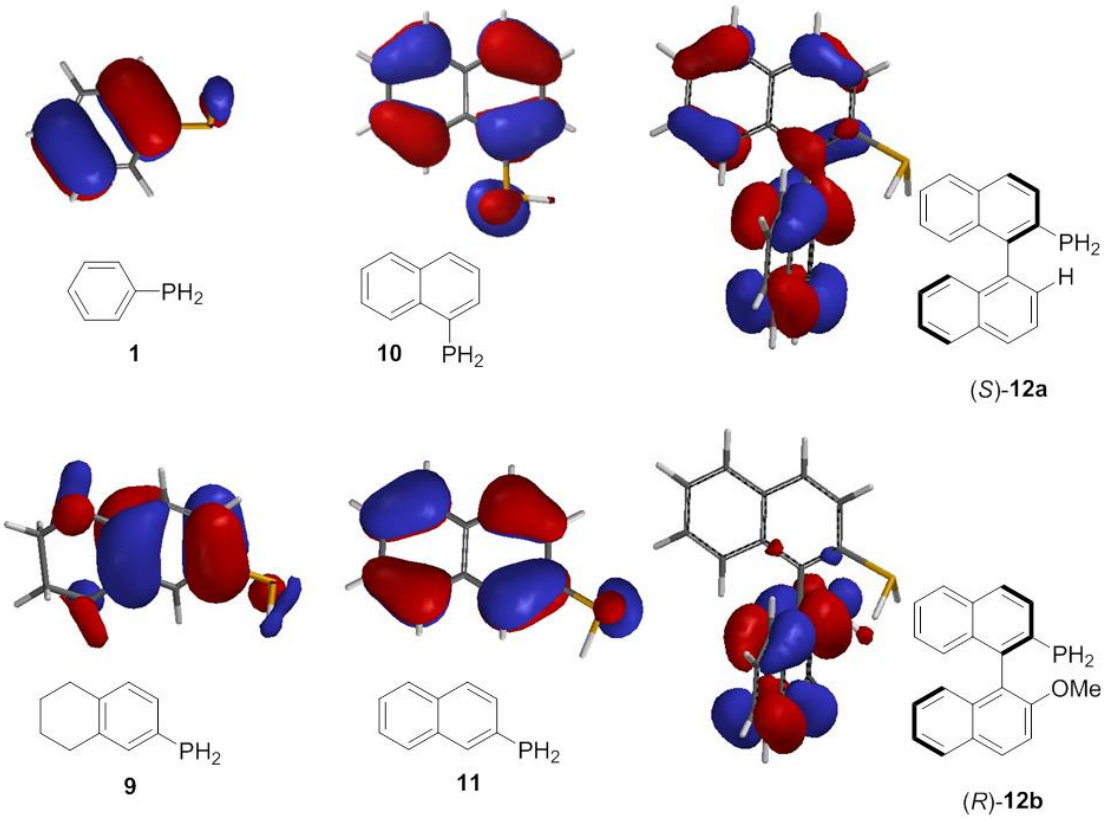

Chart 1.9 HOMO distributions for the primary phosphines **1**, **9**, **10**, **11**, (*S*)-**12a** and (*R*)-**12b**.

The model uses the B3LYP/6-31G* level of theory to ascertain the electronic properties of a primary phosphine, and it considers specifically the nature of the HOMO of the neutral phosphine (Chart 1.9),

and that of the SOMO of their radical cation counterparts. The model was used to try and explain how varying the degree of conjugation in the molecule has a significant impact on the orbital distributions and energies, and the consequences of this for the degree of air-stability of the phosphino group with regard to a radical cation mechanism.[54]

Results from the DFT calculations show a qualitative trend in the HOMO distribution for the aryl primary phosphines studied (Chart 1.9). Those with extended π-conjugation have a low (or no) phosphorus contribution to the HOMO, and those with less conjugation show more significant phosphorus character in this orbital. Experimentally, the phosphines found to be air-sensitive are those that have phosphorus participation in the HOMO (**1**, **9**, **10** and **11**), and those which resist reaction with molecular oxygen have a HOMO delocalised away from the phosphorus (**12a** and **12b**). Despite this resistance to oxidation, increasing the degree of conjugation in the molecule generally raises the energy of the orbital as expected (Table 1.2), although note that the HOMO of the air-stable binaphthyl **12a** (−5.82 eV) is comparable to that of the air-sensitive naphthylphosphine **10** (−5.80 eV).

Table 1.2 HOMO and SOMO energy values (in eV) for **1**, **5**, **6**, **7**, **8b**, **9**, **10**, **11**, **12a** and **12b**.

	1	**5**	**6**	**7**	**8b**	**9**	**10**	**11**	**12a**	**12b**
HOMO	−6.87	−5.90	−5.99	−5.34	−5.17	−6.41	−5.80	−5.88	−5.82	−5.50
SOMO	−11.73	−9.94	−9.51	−10.67	−9.58	−10.96	−10.63	−10.64	−9.29	−9.02

The corresponding radical cations were then modelled and it was found that the phosphorus atom is incorporated into the SOMO surface in each case. It also noted that there appeared to be a threshold value for resistance to air-oxidation; those primary phosphines with a SOMO energy above −10 eV are found to be experimentally air-stable and those below this value are air-sensitive (Table 1.2 and Fig. 1.9). To explain these observations it was proposed that a radical cation with a lower energy SOMO, has a higher reactivity towards oxidation than one originating from a SOMO of higher energy. This would also be consistent with the aforementioned mechanistic insights of other researchers.

The model is not limited to aryl primary phosphines – those phosphines from Chart 1.7 with unexplained resistance to air-oxidation, **5**, **6** and **8b**, were also found to have a radical cation SOMO energy above the proposed threshold (Fig. 1.9). Conversely, the air-sensitive ferrocenyl-phosphine **7** has a value below the threshold, implying that the presence of the alkylidene spacer groups in **8a** and **8b** provide the requisite 'electronic insulation' for the phosphino functionality to become air-stable.

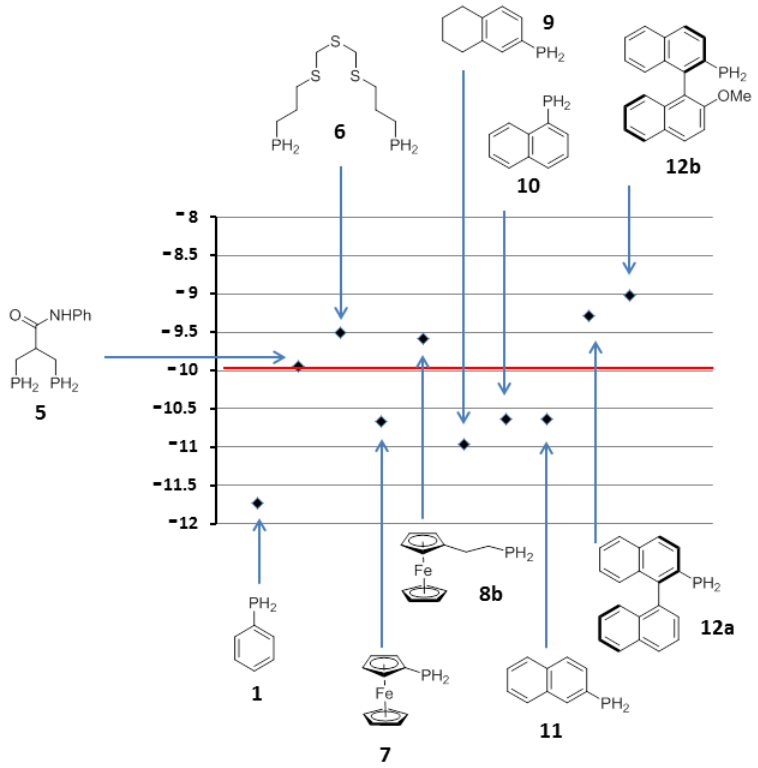

Fig. 1.9 Plot showing the SOMO energies of the primary phosphines and the 'threshold air-stability' line at −10 eV. Phosphines above the red line are found to be experimentally air-stable, whereas those below it oxidise in air.

From the molecules modelled, it was deduced that small primary phosphines lacking (i) steric hindrance, or (ii) appropriate conjugation and/or sufficient heteroatom presence to raise the energy of the SOMO, are likely to oxidise rapidly. This conclusion matches further experimental findings; the primary phosphines **13**-**15** are all stabilised beyond the −10 eV limit (Chart 1.10), and are highly oxygen sensitive. Hence, it is predicted that a wide variety of primary phosphines are likely to be air-stable, if they incorporate a backbone containing the appropriate aforementioned features.[54]

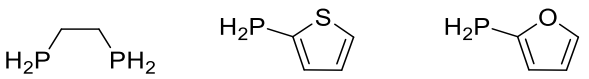

13 −11.83 **14** −11.71 **15** −11.94

Chart 1.10 Three highly air-sensitive primary phosphines (**13**-**15**) and their SOMO energies (in eV).

Protasiewicz and co-workers have synthesised a series of primary phosphines for use as synthons to benzoxaphospholes with interesting luminescent properties (Chart 1.11).[69] 3-Phosphino-2-naphthol (**16**) was prepared as an air-stable, white solid, in a high yielding synthesis. It was found that *d*-chloroform solutions of **16** could be stored for over a month without signs of oxidation, and that this air-stability could be extended into several months in the solid state.[69a] This finding is in contrast to experimental results for 2-naphthylphosphine (**11**) which shows mild air-sensitivity.[54] This is in accord

with the hypothesis that incorporating π-conjugation, or as in this case an additional heteroatom, will increase a primary phosphine's resistance to air-oxidation. However, DFT calculations on the SOMO energy level of the radical cation of **16** gave an energy value of −10.72 eV, below the assigned threshold for air-stability. Inspection of the SOMO energy distribution shows that there is no significant phosphorus contribution to the orbital, unlike the previous phosphines studied, and hence this is a potential explanation for the lack of reactivity with molecular oxygen. An alternative explanation could be that the hydroxy substituent plays an inhibitory role in the oxidation process.[69a]

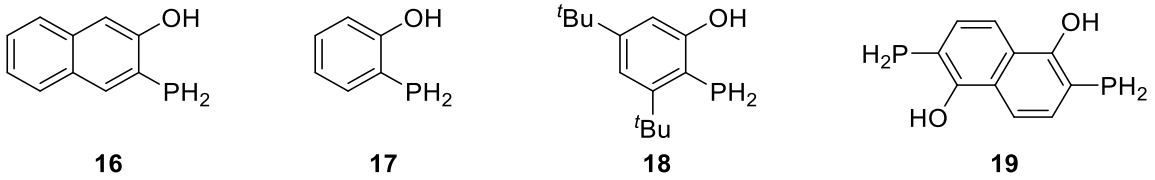

16 **17** **18** **19**

Chart 1.11 Primary phosphines (**16**-**19**) prepared by Protasiewicz and co-workers.

More curious still is 2-phosphinophenol (**17**); this and the related 3,5-di-*tert*-butyl-2-phosphinophenol (**18**) were synthesised and their air-stability investigated.[69b] DFT calculations on compounds **17** and **18** showed little phosphorus character in the HOMO of the neutral molecule, a possible indication of air-stability. The SOMO energy levels of the radical cations on the other hand, −11.3 eV and −10.5 eV respectively, do not predict that the molecules will be stable to air oxidation. Furthermore, the SOMO orbital distribution appears to have a phosphorus contribution. Surprisingly, **17** was found to be completely stable in a *d*-chloroform solution left open to air over a period of 6 days. However, **18** showed complete decomposition in an equivalent experiment. A key observation was that the major product in the decomposition of **18** was not the corresponding phosphine oxide, but 3,5-di-*tert*-butyl-2-phenol and PH_3. It was proven experimentally that the decomposition of **18** was highly dependent on an acid-catalysed mechanism; repeating the aforementioned stability study with the addition of acid rapidly increased the rate of decomposition.[69b] It is noteworthy that repeating the experiment with acid- and moisture-free *d*-chloroform in an environment of dry air resulted in little or no decomposition of **18**, implying that the compound is stable with respect to oxidation to the phosphine oxide. Corresponding experiments with **17** revealed no sensitivity to acids, and interestingly, the methoxy analogue of **18** was observed to retain its phosphorus centre and form a phosphine oxide.[70] The precise reasoning for the decomposition of **18** is still unclear, as is the apparent stability of **17** and **18** towards oxidation. In collaboration with the Protasiewicz research group, Higham *et al*. are investigating further the intriguing properties of **17**. Finally, the diprimary phosphine **19** was described as an air-stable, white solid with similar characteristics to **16**; however, DFT calculations have not yet been completed for this molecule.[69c]

The research group of Goicoechea have recently synthesised the primary phosphine containing phosphinecarboxamide **20** (Scheme 1.6), an analogue of urea, from the 2-phosphaethynolate ion.[71] The novel compound was characterised by multinuclear NMR, IR spectroscopy and X-ray crystallography. The ^{31}P NMR spectrum was assigned as a triplet of doublets due to the inequivalence of the amide protons (δ = −134.4 ppm, $^{1}J_{PH}$ = 209 Hz and $^{3}J_{PH}$ = 12 Hz) and the ^{31}P{^{1}H} NMR spectrum as a singlet (δ = −134.4 ppm). Crystallographic characterisation was made possible by synthesising compound **20**·0.5(18-crown-6). From the NMR and crystallographic data it was deduced that π-delocalisation between the carbonyl and phosphine group was insignificant, whereas there was a strong interaction between the carbonyl and amide groups – Scheme 4 depicts the possible resonance forms of **20**. This small molecule demonstrates a reasonable level of air-stability; it was reported that a pyridine-d_5 solution that had been exposed to air had a half-life of 9 days.[71] DFT calculations on **20** revealed that the phosphorus lone pair has a significant HOMO contribution (44.38%). It was suggested by the authors that a large HOMO-LUMO energy gap (6.62 eV) and mixing of π-orbitals could explain the surprising stability of **20**, although in accordance with the model, the presence of an unsaturated bond and two additional heteroatoms would be expected to raise the SOMO energy level and resistance to oxidation.

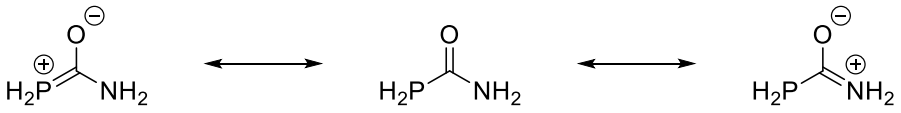

20

Scheme 1.6 Phosphinecarboxamide **20** and its possible resonance forms.

1.4.4 Metallocenes

The excellent air-stability of compounds **8a** and **8b**,[62-64] and how the model can be used to rationalise their behaviour has been previously mentioned. Henderson and co-workers, in collaboration with Hey-Hawkins, have recently expanded on this earlier work and increased the number of known alkylidene-tethered ferrocenyl primary phosphines (**21a-c**), as well as presenting the first example of a ruthenocenyl primary phosphine (**21d**) (Chart 1.12).[72]

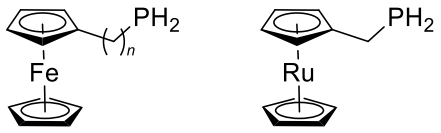

21a, n = 4
21b, n = 6
21c, n = 11

21d

Chart 1.12 Ferrocenyl and ruthenocenyl alkyl-tethered primary phosphines.

The ferrocenyl primary phosphines **21a**-**c** (Chart 1.12), with longer alkylidene spacer groups than **8a** and **8b**, were prepared and characterised by various spectroscopic means, although **21b** and **21c** could not be isolated pure. The ^{31}P NMR chemical shift (~δ = −136 ppm) and the $^{1}J_{HP}$ (~194 Hz) and $^{3}J_{HH}$ (~7 Hz) coupling constants were found to be comparable in all of the compounds.[72] Crystal structures of the primary phosphines were not obtained; however, the borane adduct of **21b**·BH_3 was synthesised and the molecular structure elucidated. The primary phosphines were found to be considerably stabilised toward air-oxidation, with **21a** lasting several weeks. In addition to the ferrocenyl compounds reported, the ruthenocene derived primary phosphine **21d** (Chart 1.12), an analogue of **8a**, was synthesised in an investigation which would show if the stabilising effects observed are transferrable to other metallocene systems.[72] Compound **21d** was isolated as a pale-yellow oil, characterised by various spectroscopic means and was noted to have a distinctive odour. The ^{31}P NMR spectrum showed a distinctive triplet at δ = −132.5 ppm with a $^{1}J_{HP}$ coupling constant of 193 Hz. The resistance to air-oxidation of the compound was found to be lower than that of the related ferrocenyl compounds; a *d*-chloroform solution in a capped NMR tube showed that approximately half of **21d** had oxidised after one month.

Hey-Hawkins and co-workers have reported the first two chiral, primary aminoalkyl(phosphanyl)ferrocene complexes **22** and **23**,[73] and in subsequent publications presented the molecules **24**, **25a** and **25b** (Chart 1.13).[74] Compound **22** is a high boiling point liquid that was obtained as a racemate. The related ferrocenyl phosphine (*S*,*R*)-**23** was prepared as a *S*,*R*/*S*,*S* diastereomeric mixture in 92% *de* and similarly, (*R*,*S*)-**23** can be prepared with (*R*,*R*)-**23** as the minor isomer.[73] The racemic crystalline solid **24** has also been synthesised and characterised by X-ray crystallography – it is air-stable in the solid state and shows an inertness to solution oxidation over a period greater than two weeks.[74a] Two further crystalline primary phosphines (**25a** and **25b**) were reported to be air-stable in solution over a minimum period of 5 days.[74b] The ^{31}P NMR spectral signals corresponding to the phosphanyl groups in **25a** and **25b** appear as characteristic triplets (~δ = −150 ppm and ~$^{1}J_{PH}$ = 200 Hz). The 1,1'-bis(diphenylphosphino)ferrocene derivative **25b** was also structurally characterised by X-ray crystallography. Marinetti and co-workers have reported the synthesis and X-ray crystal structure of [2-(phosphinomethyl)ferrocenyl]diphenylphosphine, an air-stable primary phosphine precursor for synthesising ferrocenyl-based diphosphines.[75]

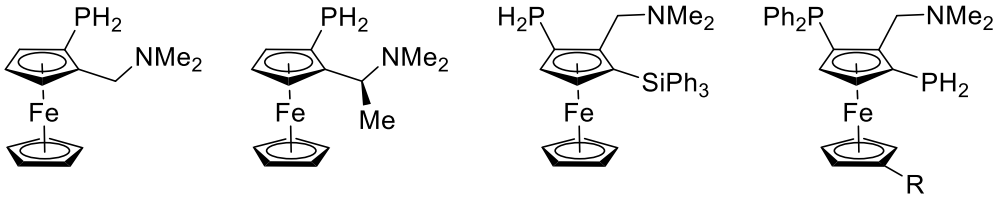

(*R*)-**22** (*S*,*R*)-**23** (*R*)-**24** R = H, (*R*)-**25a**
R = PPh_2, (*R*)-**25b**

Chart 1.13 Primary aminoalkyl(phosphanyl)ferrocene complexes developed by the Hey-Hawkins research group.

1.5 Reactivity of Primary Phosphines

The coordination chemistry of tertiary and secondary phosphines is extensive and well reported in the literature, whereas the equivalent research involving primary phosphines is far less developed.[48a] As well as often being difficult to handle, primary phosphines have different steric and electronic properties. The P–H bonds are relatively weak and hybridisation effects mean the lone-pair orbital has a higher s-character and is, therefore, a weaker donor to a transition metal.[76] Consequently, P–H bonds often cleave in the presence of transition metals to form phosphido or phosphinidine ligands, unless the co-ligands are carefully considered.[77] We have detailed their emerging coordination chemistry in a published review.[48b]

Manners and co-workers reported the catalytic dehydrocoupling reaction of primary- and secondary-phosphine–borane adducts to prepare poly(phosphinoborane) compounds.[53,78] In a rhodium(I)-catalysed reaction, dehydrocoupling of $PhPH_2{\cdot}BH_3$ resulted in the formation of the high molecular weight polymer, poly(phenylphosphinoborane), an air- and moisture-stable solid (Scheme 1.7).[53]

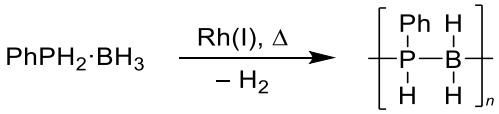

Scheme 1.7 Rhodium-catalysed synthesis of the polymer poly(phenylphosphinoborane).

A new class of functional polymer networks has been synthesised from air-stable primary phosphines, using phosphine-ene chemistry, analogous to the thiol-ene reaction.[79] A major benefit of these systems, compared to the sulfur-based derivatives, is the ability to use ^{31}P solid-state NMR spectroscopy to investigate the chemical structures of the networks. Further functionalisation of the phosphorus moieties incorporated into the networks was proven to be possible, and the polymers show potential as oxygen-scavenging materials. Incorporating **8b** resulted in the formation of a redox-active polymer network.

Alkyl and aryl primary phosphines have been shown to react with aldehydes in the presence of trifluoroacetic acid to form secondary phosphine oxides.[80] A broad range of aldehydes were reacted, including formaldehyde, and it was shown that using 1,5-dialdehydes provides a convenient route to bis(phosphine oxides).

The synthesis of polydentate 1,5-diaza-3,7-diphosphacyclooctane ligands incorporating nitrogen atoms was reported via the condensation of primary phosphines with formaldehyde and primary amines.[81]

Secondary and tertiary functionalised vinylphosphines were synthesised from the stereoselective hydrophosphination of dichloroacetylene by primary phosphines and their complexes.[82] The use of a sterically hindered primary phosphine in the hydrophosphination of 1-hexene has also been reported, the reaction proceeding via an intermediate nickel phosphanido hydride complex.[83]

Fermin and Stephan reported the catalytic dehydrocyclooligomerisation of primary phosphines using a zirconium(IV) hydride complex.[84] Waterman has since used a triamidoamine zirconium catalyst to selectively dehydrocouple primary and secondary phosphines, via an intermediate phosphido complex [(N_3N)ZrPHR], with high selectivity for the diphosphine product (Scheme 1.8).[85]

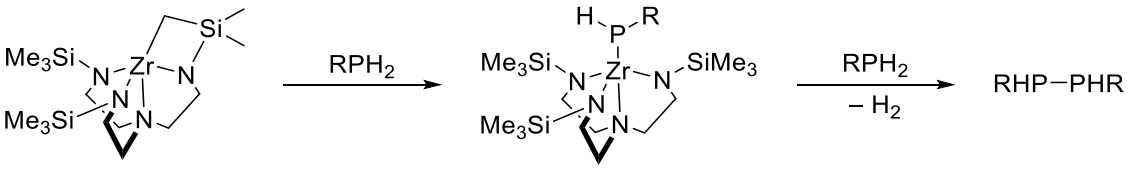

Scheme 1.8 Selective dehydrocoupling of a primary phosphine, catalysed by a triamidoamine zirconium complex (R = Ph, Mes, *p*-Tol, 2-EtC_6H_4, Cy, *t*-Bu).

This work was followed up with a report on the intermolecular hydrophosphination of primary phosphines with a variety of alkenes and dienes using the triamidoamine zirconium catalyst. It was shown that adjustment of the reaction conditions can change the selectivity between the formation of secondary or tertiary phosphine products, and the reactions are unusually successful with unactivated alkenes.[86] Finally, a collaboration between the groups of Waterman and Higham has yielded chiral, air-stable secondary and tertiary phosphines from the catalytic hydrophosphination of alkenes using (*R*)-MeO-MOPH_2 ((*R*)-**12b**).[87] The reaction proceeds selectively to afford anti-Markovnikov secondary phosphines as a mixture of diastereomers. A single-crystal of the phosphido reaction intermediate was also prepared, the compound crystallised with two diastereomeric, independent molecules in the unit cell (Fig. 1.10).

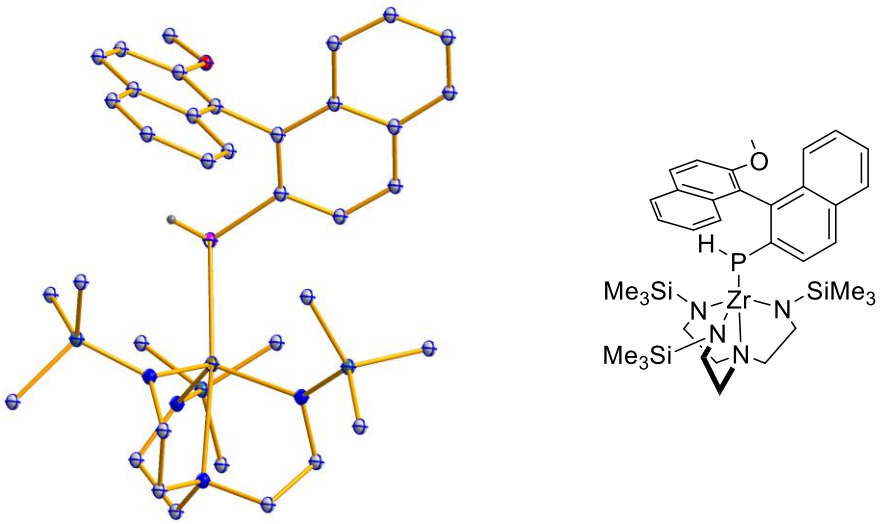

Fig. 1.10 View of the molecular structure of one of the diastereomers of [(N_3N)Zr((*R*)-MeO-MOPH)]. Hydrogen atoms bound to carbon atoms have been omitted for clarity. (CCDC: 1421827). Crystal structure data was obtained from the Cambridge Structural Database (CSD).[11]

Lammertsma and Slootweg have reported a method to synthesise phosphaamidines through the reaction of primary phosphines with readily available nitrilium triflates, and treatment of the phosphaamidines with *n*-butyllithium allowed for the synthesis of the corresponding phosphaamidinates (Scheme 1.9).[88] Simply changing the substituents on either substrate may allow access to a diverse range of P,N ligands with potential applications in catalysis.

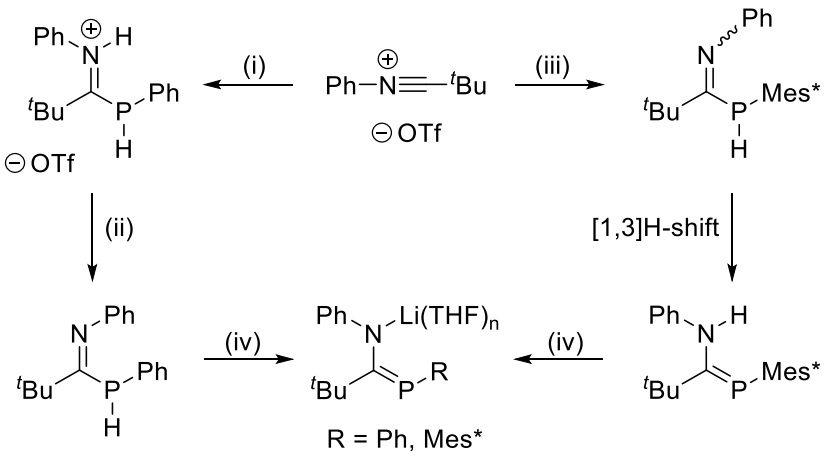

Scheme 1.9 Synthesis of phosphaamidinates from the reaction of nitrilium triflates with primary phosphines via phosphaamidines: (i) $PhPH_2$, (ii) NEt_3, (iii) 1. Mes^*PH_2 2. NEt_3, (iv) *n*-BuLi, THF.

1.6 Chiral Primary Phosphines and their Applications

The first enantiomerically pure primary phenylphosphine derivatives were reported by Brauer and co-workers in 2003 (Chart 1.14),[89] the chirality in the primary phosphinoamines originating from a carbon stereocentre on the *ortho*-$CMeNMe_2$ substituent. Novel P,N chelating ligands were prepared from these precursors and used in rhodium-catalysed asymmetric hydrogenation reactions.[89]

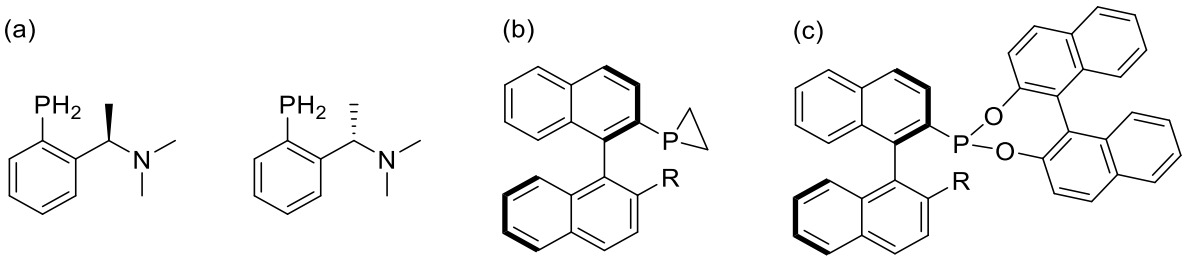

R = H, (*S*)-**26a**
R = OMe, (*R*)-**26b**

R = H, (*S*,R_b)-**27a**, (*S*,S_b)-**27a**
R = OMe, (*R*,R_b)-**27b**, (*R*,S_b)-**27b**

Chart 1.14 Chiral phosphorus compounds: (a) primary phosphinoamines, (b) phosphiranes and (c) phosphonites.

Higham *et al*. previously reported the synthesis of the remarkably air-stable primary phosphines (*S*)-**12a** and (*R*)-**12b**,[66] which are atropisomeric by nature of their binaphthyl backbone; these phosphines can be readily synthesised on a multigram scale.[90] These chiral precursors have been exploited to prepare new, enantiopure MOP ligands with interesting functionality,[49c] including phosphiranes,[91] alkylphosphines,[92] aminophosphines[92] and phosphonites.[92-93] The previously inaccessible phosphiranes (*S*)-**26a** and (*R*)-**26b** have demonstrated unusual chemical properties (Chart 1.14). Phenylphosphirane readily undergoes decomposition above 0 °C, whereas (*S*)-**26a** and (*R*)-**26b** are thermally stable when heated overnight in refluxing toluene and can be stored in air indefinitely. In the non-optimised asymmetric hydrosilylation of styrene, (*S*)-**26a** achieved an enantioselectivity of 80% with full conversion.[91] The synthesis and characterisation of the diastereomeric, optically pure MOP-phosphonite ligands **27a** and **27b** (Chart 1.14) was also described, as was their application in the same catalytic reaction, achieving enantioselectivities of 79% with (*R*,S_b)-**27b** and 80% with (*S*,S_b)-**27a** (*b* is the absolute configuration of the BINOL moiety).[93a] Higham *et al*. recently detailed the synthesis of previously inaccessible or difficult to access functionalities from (*S*)-**12a** and (*R*)-**12b**, covering a range of tuneable structural and electronic donor properties.[92] This complements work by Fey and co-workers who have developed an extensive ligand knowledge base for monodentate P-donors (LKB-P), which may be useful for identifying applications for ligands and for reaction optimisation (*vide supra*).

Pringle and co-workers reported the synthesis of diastereomeric diphosphine ligands with mixed dimethylphospholane and 6-phospa-2,4,8-trioxa-adamantane donors, prepared from a primary phosphine (Scheme 1.10). The ligands were successful in rhodium-catalysed asymmetric hydrogenation reactions, and exhibited substrate-matching with the diastereomeric catalysts.[94]

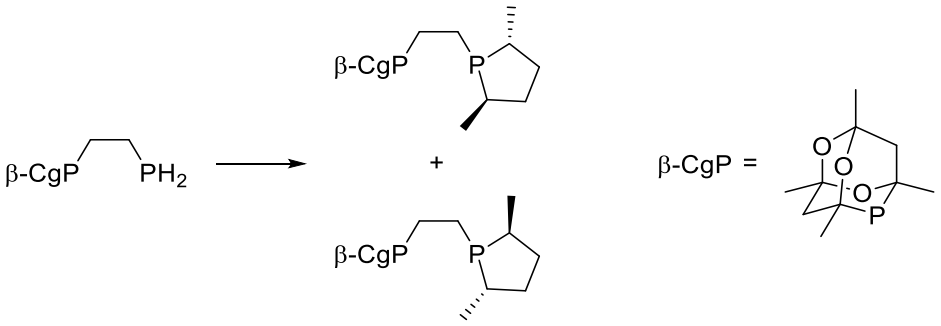

Scheme 1.10 Pringle's synthesis of the chiral mixed cage-phospholane diphosphine.

A series of P-stereogenic 1-phosphaacenaphthenes have been synthesised by Glueck and co-workers, using a platinum catalyst for the enantioselective tandem alkylation/arylation of primary phosphines.[95] In a one-pot synthesis the benzyl chloride was reacted with mono- and diprimary phosphines to yield new phosphacycles, including C_2-symmetric P-stereogenic diphosphines (Scheme 1.11).

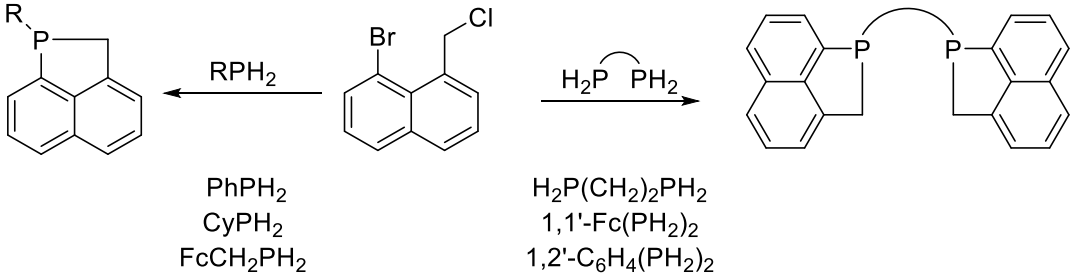

Scheme 1.11 Glueck's synthesis of P-stereogenic 1-phosphaacenaphthenes from mono- and diprimary phosphines.

Novel, hydrophilic aryl MeO-BIPHEP (Chart 1.4) analogues have been synthesised from the parent bis-primary phosphine (MeO-BIPHEPH_2, Scheme 1.12) via palladium-catalysed P–C coupling reactions.[96] The resulting atropisomeric ligands were successfully applied in the C–C bond forming, asymmetric rhodium-catalysed 1,4-addition of boronic acids to enones in water, with high isolated yields (up to 99%) and enantioselectivities (up to 96%) obtained (Scheme 1.12).[96]

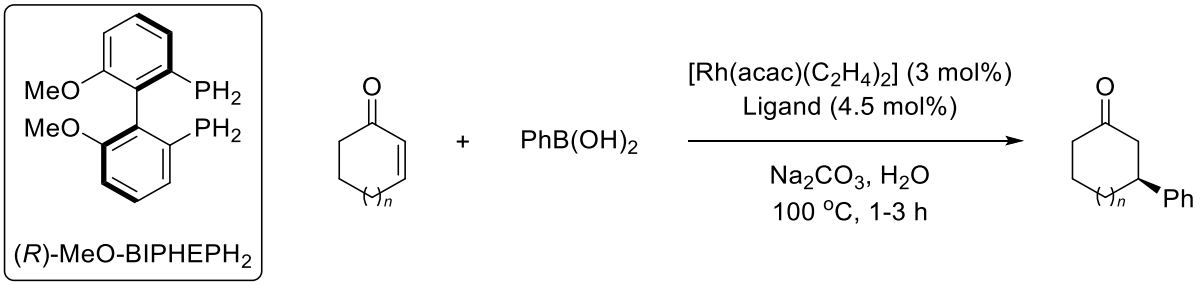

Scheme 1.12 Rhodium-catalysed addition of phenylboronic acid to 5- and 7-membered ring enones, employing water soluble MeO-BIPHEP-type ligands, synthesised from MeO-BIPHEPH_2 (left).

1.7 Phosphonites

Phosphines are characterised by having three P–C bonds, and by altering the C-substituents, changes can be made to the σ-donor properties of the ligand. The electronic properties are more dramatically adjusted by introducing P–O or P–N bonds and primary phosphines provide a convenient way to construct molecules with this functionality, via conversion to their dichlorophosphine analogues. Phosphonites (arylphosphonous esters) are P-ligands with one P–C bond and two P–O bonds (Fig. 1.11), which results in enhanced π-acceptor abilities and decreased basicity of the phosphorus lone pair when compared to phosphines.

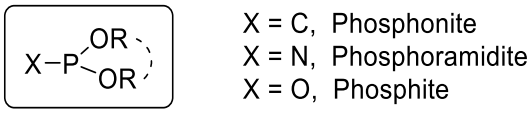

Fig. 1.11 Nomenclature for phosphorous(III) ligands containing two P–O bonds.

Phosphonites are valuable phosphorus ligands used in homogeneous catalysis, with characteristic properties of being a poor σ-donor but strong π-acceptor.[97] The energy of the σ* orbitals is lowered compared to arylphosphines due to the electronegative substituents, allowing the ligand to better stabilise transition metals in low oxidation states. A typical method to prepare phosphonites is by direct alcoholysis of a dichlorophosphine in the presence of an organic base,[98] or via a diaminophosphine (Scheme 1.13).[99] An alternative method is the reaction of phosphorus trichloride with a diol followed by treatment of the resulting phosphorochloridite intermediate with a carbon nucleophile in the presence of an organic base. Oestreich and co-workers suggest that this method is particularly suitable for the synthesis of sterically congested ligands.[100]

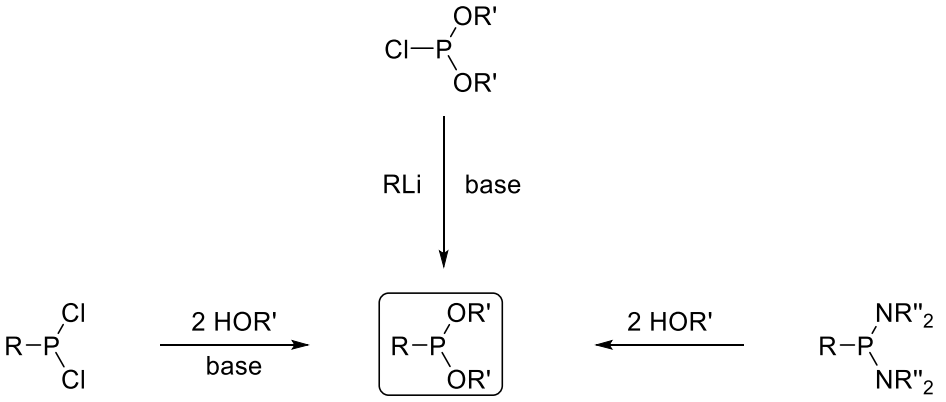

Scheme 1.13 Typical procedure for the synthesis of phosphonites from dichlorophosphines, diaminophosphines and chlorophosphites.

There are a range of examples where transition metal complexes of chiral mono- and bidentate phosphonite ligands have proven to be efficient catalysts in enantioselective homogeneous catalytic

reactions: the copper-catalysed conjugate addition of diethylzinc to cyclic and acyclic enones,[101] the nickel-catalysed hydrocyanation of alkenes,[102] the palladium-catalysed hydrovinylation of styrene,[103] the Suzuki-Miyaura cross-coupling of aryl chlorides,[104] the rhodium-catalysed conjugate addition of arylboronic acids,[105] the hydroformylation of alkenes,[106] the hydrogenation of alkenes[107] and the hydrosilylation of aromatic ketones.[108]

Common examples of chiral phosphonite ligands use the BINOL[109] and TADDOL[100] architectures (Chart 1.15). BINOL contains an atropisomeric 1,1'-binaphthyl backbone which is synthesised by the oxidative coupling of 2-naphthol, and is a commercially available in its enantiopure form.[110] The auxiliary TADDOL was developed by Seebach and is derived from (*R*,*R*)-tartaric acid (Chart 1.3), which is sourced from the chiral pool.[111]

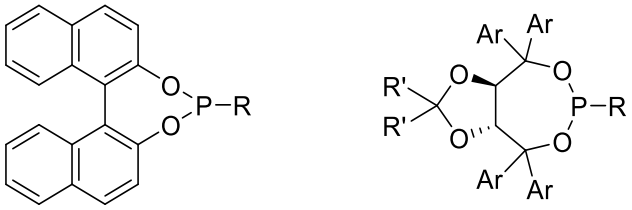

Chart 1.15 Chiral phosphonites based on BINOL (left) and TADDOL (right).

Higham *et al*. have recently reported a convenient synthetic route to enantiopure MOP-phosphonite ligands containing a BINOL moiety, via their dichlorophosphine analogues, starting with the air-stable, chiral primary phosphine precursors (*S*)-H-MOPH$_2$ ((*S*)-**12a**) and (*R*)-MeO-MOPH$_2$ ((*R*)-**12b**) (Scheme 1.14). Reaction of the primary phosphines (*S*)-**12a** and (*R*)-**12b** with phosphorus pentachloride to make the corresponding dichlorophosphines, followed by the addition of enantiopure BINOL in the presence of triethylamine gave the desired products (*S*,*R*$_b$)-**27a**, (*S*,*S*$_b$)-**27a**, (*R*,*R*$_b$)-**27b** and (*R*,*S*$_b$)-**27b** (Chart 1.14) – in a high yielding, one-pot synthesis.[93a] Similarly, dimethoxy MOP-phosphonites were made by adding two equivalents of methanol under the same conditions; however, the ligand is very susceptible to hydrolysis, lowering the isolated yield.[92] These ligands proved to be particularly useful in the palladium-catalysed asymmetric hydrosilylation of styrene.[92-93]

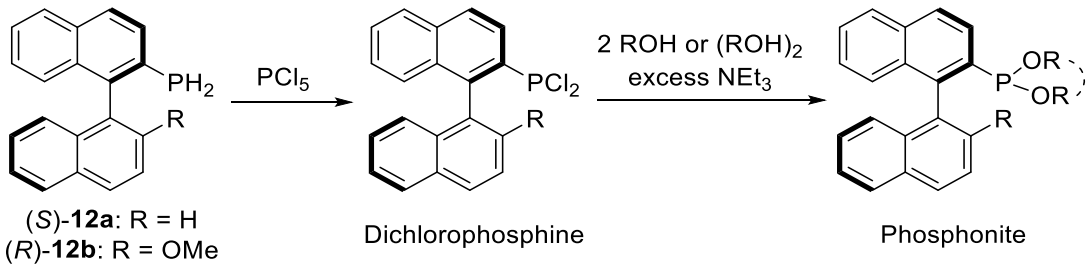

Scheme 1.14 Synthetic procedure for MOP-phosphonite ligands.

1.8 Objectives

Chiral monophosphorus ligands have found applications in a variety of organometallic catalysis. However, they are often neglected in favour of the more established diphosphorus ligand class.[44] Therefore, we were keen to explore the potential of monophosphorus ligands, with unusual functionality on the phosphorus,[92] to fill voids left by their diphosphorus ligand counterparts in the field of asymmetric catalysis.

The aim of this project was to synthesise user-friendly, chiral phosphonite ligands, based upon Hayashi's MOP backbone, and to apply the enantiopure ligands in asymmetric catalytic transformations. Promising results have been reported in the palladium-catalysed asymmetric hydrosilylation of styrene with first generation MOP-phosphonites based on the BINOL architecture (**27a** and **27b**, Chart 1.14), and detailed the hemilabile nature of the bonding of the ligands in transition metal complexes.[93] It was unknown if the reduction from two stereocentres in those ligands – at the binaphthyl backbone and the BINOL auxiliary – to just one with an achiral auxiliary, would have any detrimental effects on the stability, reactivity and asymmetric induction of the phosphonites. Therefore, we sought to remove this second axis of chirality by replacing the BINOL moiety with non-chelating phenoxy groups and also with an achiral 2,2'-biphenoxy moiety. Removing the need to have the second axis of chirality within the ligand is beneficial as it would greatly reduce the synthetic costs of making the phosphonite and also enable more flexibility in the tuning of the ligand architecture by making a more diverse set of aryl diols available to the synthetic methodology.[†]

We sought to detail the individual steric and electronic parameters of the phosphonite molecules via computational, spectroscopic and crystallographic techniques to help establish a chemical context and allow the directed application of the ligands in catalysis. Higham *et al*. reported on the coordination chemistry of **27a** and **27b** with a selection of group 9 and 10 transition metals.[93] Replicating the coordination chemistry and catalytic reactions reported for these ligands is important if one is to comprehend the effect of removing the second axis of chirality. We, therefore, sought to optimise the group of ligands to improve upon the fledgling, but promising, results achieved for the palladium-catalysed asymmetric hydrosilylation of styrene, and also to apply the novel organometallic compounds as catalysts in untested asymmetric syntheses. We also had yet to explore the chemistry of the group 11 metals with the MOP ligand class; therefore, another aim of the project was to examine the coordination chemistry of the chiral MOP-phosphonites in copper, silver and gold complexes.

[†](*R*)- and (*S*)-BINOL retail at £33.70 and £34.60 (respectively) for 1 g, whereas phenol and 2,2'-biphenol retail at £11.70 and £21.10 (respectively) for 100 g: www.sigmaaldrich.com, 99% purity or greater. (12/01/2016)

2. The design of second generation MOP-phosphonites: efficient chiral hydrosilylation of functionalised styrenes

Abstract: A series of enantiopure MOP-phosphonite ligands, with tailored steric profiles, have been synthesised and are proven to be very successful in high-yielding, regio- and enantioselective catalytic hydrosilylation reactions of substituted styrenes, affording important chiral secondary alcohols.

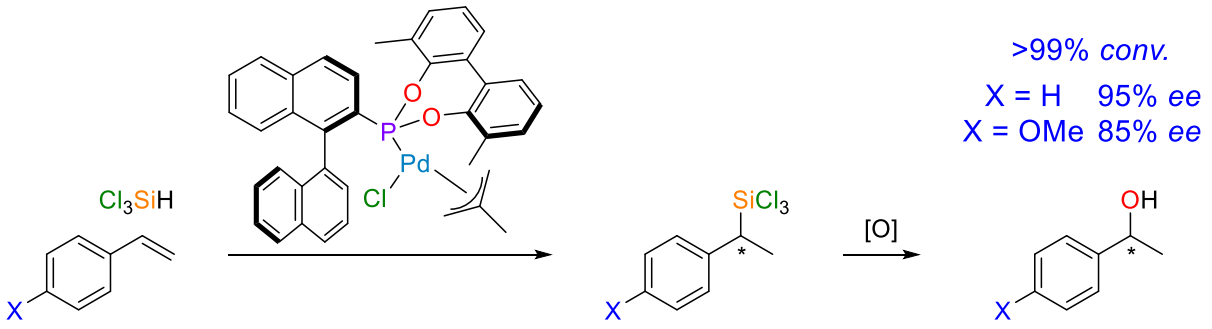

2.1 Introduction

Chiral phosphorus ligands have achieved considerable acclaim in a variety of transition metal-catalysed transformations.[19] Atropisomeric monophosphines with a binaphthyl backbone (Chart 2.1)[44,47,49c] have proven to be particularly successful in the palladium-catalysed asymmetric hydrosilylation (AHS) of alkenes to produce organosilanes (Scheme 2.1).[112]

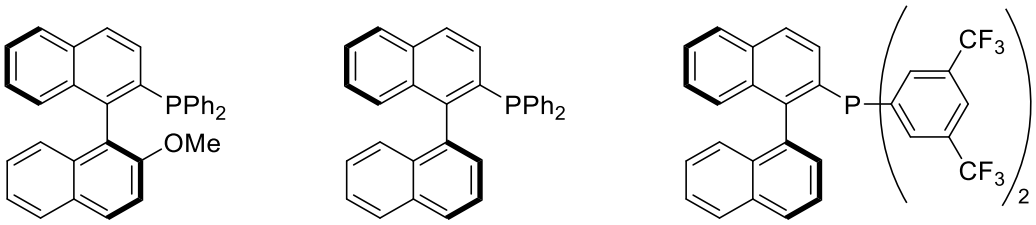

(*S*)-MeO-MOP (*R*)-H-MOP (*R*)-H-MOP(*m*,*m*-2CF$_3$)

Chart 2.1 Examples of ligands from the MOP-family which have proven to be highly enantioselective in palladium-catalysed asymmetric hydrosilylation reactions.

Hydrosilylation is the addition of hydrosilanes to unsaturated substrates, in the case of alkenes this is the addition of a Si–H bond across a C–C double bond (Scheme 2.2).[112] For example, (*S*)-MeO-MOP was able to catalyse the AHS of alkyl-substituted terminal alkenes regioselectivity, to give 2-(trichlorosilyl)alkanes with enantiomeric excesses of up to 97% (Chart 2.1).[113] (*R*)-H-MOP and its electron deficient derivative (*R*)-H-MOP(*m*,*m*-2CF$_3$) have been employed in the completely regioselective AHS of styrenes with enantiomeric excesses of up to 98% reported (Chart 2.1).[114]

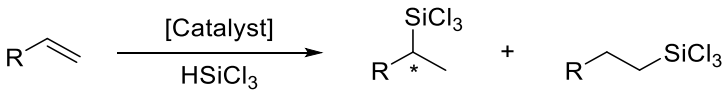

Scheme 2.1 Palladium-catalysed asymmetric hydrosilylation of terminal alkenes.

Two proposed catalytic cycles for transition metal-catalysed hydrosilylation reactions are depicted in Scheme 2.2. Both cycles begin with a reversible oxidative addition of the hydrosilane to the metal to give a metal alkene silyl hydride complex. The Chalk-Harrod mechanism (Scheme 2.2, right hand side),[115] follows with a hydrometallation step, the reversible migratory insertion of the alkene into the M–H bond. The alkyl-silyl complex formed then undergoes irreversible Si–C reductive elimination to form the organosilane product. An alternative mechanism proposes a reversible silylmetallation step to give a β-silylalkyl-hydrido complex (Scheme 2.2, left hand side),[116] via alkene insertion into the M–Si bond, followed by an irreversible, C–H reductive elimination to release the product.

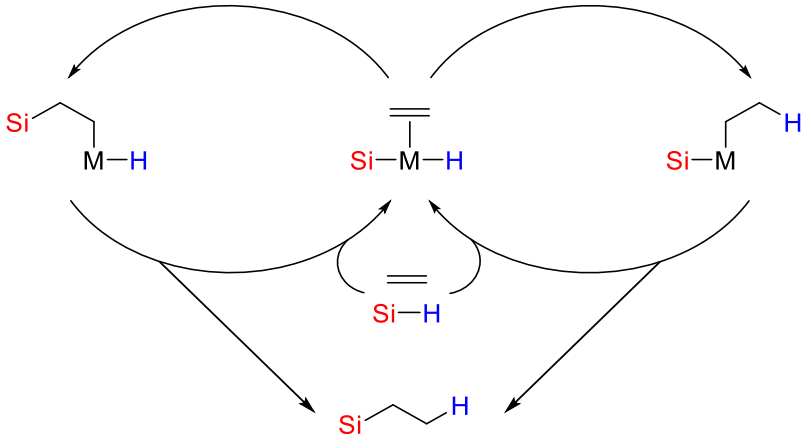

Scheme 2.2 Proposed catalytic cycles for the transition metal-catalysed hydrosilylation of alkenes.

In AHS reactions, the transformation is generally catalysed by a transition metal complex incorporating a chiral ligand. In many AHS reactions the catalyst must not only be enantioselective, but also regioselective (Scheme 2.1). The palladium-catalysed AHS reaction of styrene derivatives, using a monophosphine ligand, with trichlorosilane has been the focus of mechanistic studies by Hayashi;[114a,117] the catalytic cycle was shown to proceed via the classical Chalk-Harrod mechanism, with hydropalladation onto the vinyl group (Scheme 2.3). The hydropalladation step is reversible, with β–hydride elimination reverting the intermediate (**C**) back to the palladium alkene silyl hydride complex (**B**). The reaction generally is regioselective for the branched 1-aryl-1-silylethane product over the linear 2-aryl-1-silylethane isomer, which is often explained by the formation of stable π-benzylpalladium intermediates (Scheme 2.3).[114a] Pedersen and Johannsen have suggested that the mechanism shown in Scheme 2.3 differs depending on the P:Pd ratio used to prepare the catalyst, and that there are two competing catalytic cycles (see Results and Discussion and Scheme 2.9).[118] They

concluded that the conversion time is also highly dependent on the ratio, and that the reaction rate changed significantly when comparing different ligands, implying that the steric and electronic properties of the ligand play an important role.[118]

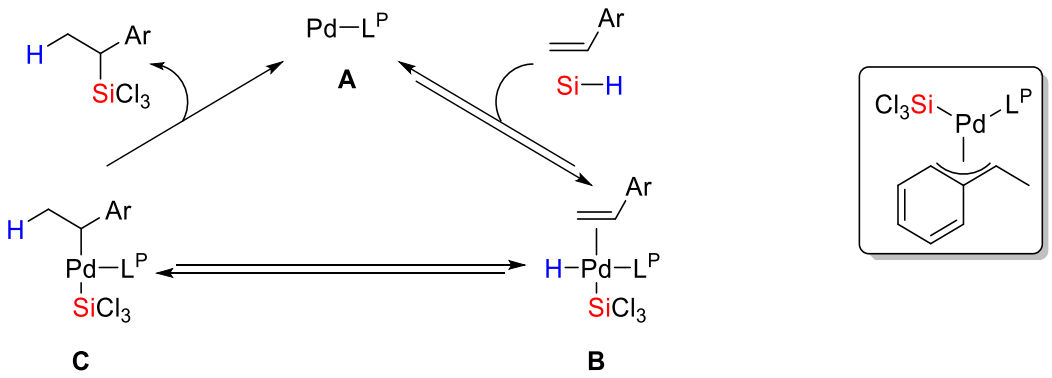

Scheme 2.3 Proposed reaction mechanism for the palladium-catalysed AHS of styrenes with a monophosphine ligand and a representation of a stabilised (η^3-benzyl)(silyl)palladium intermediate.

The high enantioselectivities observed in palladium-catalysed AHS of styrenes with H-MOP ligands has been investigated mechanistically by Hayashi and co-workers by comparing (*R*)-H-MOP and (*R*)-H-MOP(*m*,*m*-2CF$_3$) (Chart 2.1), chosen due to the very high enantioselectivities obtained (up to 98%) with the trifluoromethane substituted ligand (Scheme 2.4).[114a] The study concluded that β–hydride elimination from the alkyl palladium intermediates **C** is fast compared to reductive elimination in the complexes of (*R*)-H-MOP(*m*,*m*-2CF$_3$), and also that the β–hydride elimination is much more rapid for (*R*)-H-MOP(*m*,*m*-2CF$_3$) complexes when compared to the (*R*)-H-MOP analogues. A highly selective reductive elimination from the diastereomeric intermediate (*S*)-**C** over (*R*)-**C**, in addition to reversible β–hydride elimination and hydropalladation processes putting (*S*)-**C** and (*R*)-**C** in a fast equilibrium, accounts for the high optical purity obtained in the chiral product when employing (*R*)-H-MOP(*m*,*m*-2CF$_3$) as the ligand (up to a 98% enantiomeric excess of the (*S*)-organosilane).

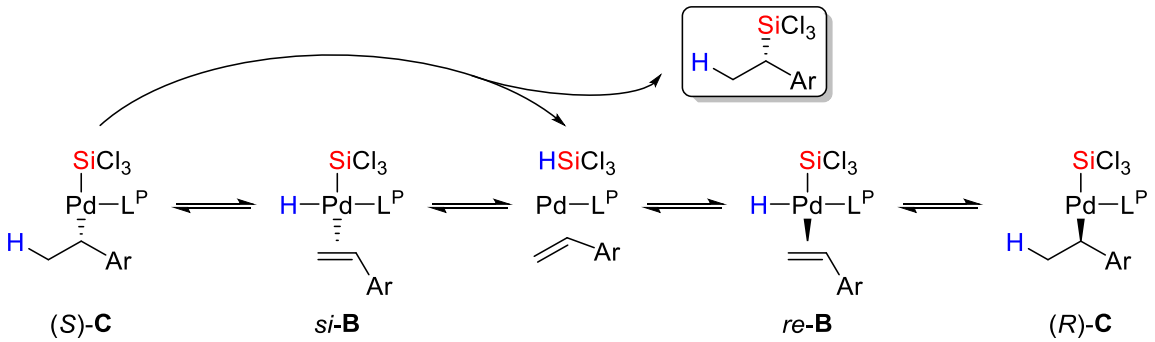

Scheme 2.4 Proposed reaction mechanism to explain the high enantioselectivity for (*S*)-organosilane products observed in the palladium-catalysed AHS of styrenes with the ligand (*R*)-H-MOP(*m*,*m*-2CF$_3$).

The chiral alkyl silanes produced in AHS reactions with alkenes are useful and versatile intermediates in organic synthesis,[119] especially as precursors in the synthesis of enantioenriched alcohols. Using Fleming–Tamao oxidation procedures, the Si–C bond is cleaved to form a C–O bond with complete retention of configuration and in high yields.[120]

Higham *et al*. recently reported a new class of MOP-phosphonite ligands (**27a** and **27b**, Chapter 1), based on a MOP/XuPhos-type hybrid (Chart 2.2).[93a] Chiral phosphonites are ligands with good π-acceptor properties and are effective in a range of asymmetric hydrocyanations,[102c] hydroformylations[106c] and hydrogenations.[107b,c] Ligands **27a** and **27b** possess a phosphorus donor bound directly to a binaphthyl backbone – the **a** series has a hydrogen in the 2' position of the lower naphthyl ring whilst a methoxy group occupies the site in the **b** series (Chart 2.2). This difference has profound implications for the catalytic performance of the parent (*S*)-H-MOP and (*R*)-MeO-MOP ligands. Importantly, the authors sought to examine the effect of incorporating a second chiral moiety, which was achieved by appending either (*R*)- or (*S*)-BINOL to isolate the diastereomeric pairs (*S*,R_b)-**27a**/(*S*,S_b)-**27a** and (*R*,R_b)-**27b**/(*R*,S_b)-**27b**. By investigating the coordination chemistry and catalytic performance of the four ligand pairs, it was demonstrated that subtle differences in the position of the palladium atom relative to the lower naphthyl ring in these complexes appears to have important consequences for chiral induction in the catalytic hydrosilylation of styrene.[93a] The authors did not determine whether the large chiral BINOL group was necessary for effective asymmetric catalysis with MOP-phosphonites.

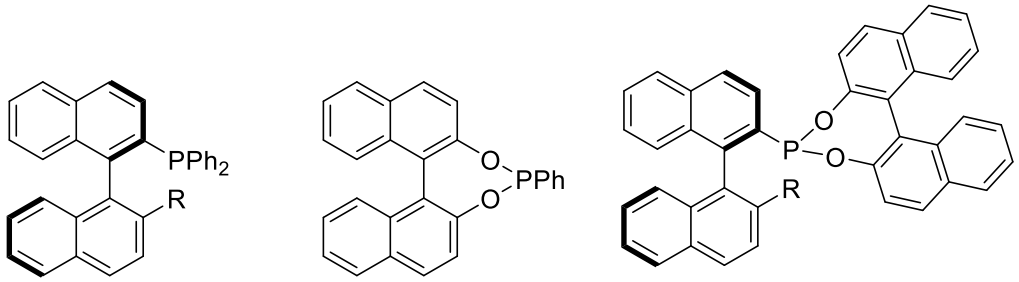

(*S*)-H-MOP: R = H
(*R*)-MeO-MOP: R = OMe

XuPhos

R = H, (*S*,R_b)-**27a**, (*S*,S_b)-**27a**
R = OMe, (*R*,R_b)-**27b**, (*R*,S_b)-**27b**

Chart 2.2 A selection of binaphthyl-containing monophosphorus-donor ligands.

In this study, the effect of replacing the BINOL moiety of **27a** and **27b** with achiral ancillary aryloxides was investigated, in order to establish if the enantioselectivities remain high by virtue of the phosphorus-bonded binaphthyl backbone, and thus eliminate the requirement for a second chiral centre. To the best of our knowledge this has not been demonstrated for MOP-phosphonites, which are likely to catalyse alternative substrates to their phosphine analogues, owing to their differing

electronic properties. Herein we present the synthesis of the phenoxy derivatives (*S*)-**28a** and (*R*)-**28b**, which allowed us to probe the effect of removing the chelating element of the added aryloxide. We then describe how the sensitivity of these ligands to hydrolysis, demanded the design of next generation 2,2'-biphenoxy-based MOP-phosphonites (*S*)-**29a** and (*R*)-**29b**. These were further improved upon to yield the user-friendly, chiral phosphonites (*S*)-**30a** and (*R*)-**30b**, which perform better than the corresponding phosphines in the hydrosilylation of functionalised styrenes (Chart 2.3).

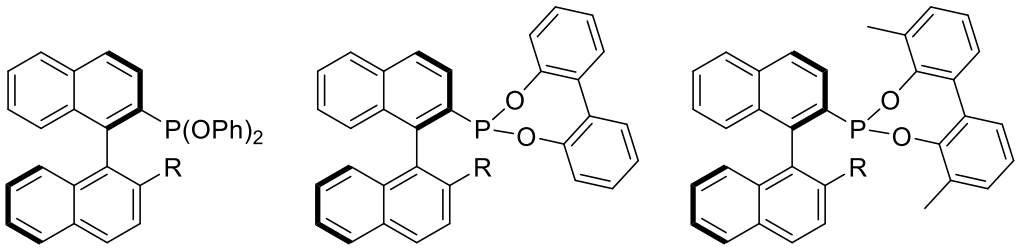

(*S*)-**28a**: R = H
(*R*)-**28b**: R = OMe

(*S*)-**29a**: R = H
(*R*)-**29b**: R = OMe

(*S*)-**30a**: R = H
(*R*)-**30b**: R = OMe

Chart 2.3 Phosphonite ligands (*S*)-**28a**, (*R*)-**28b**, (*S*)-**29a**, (*R*)-**29b**, (*S*)-**30a** and (*R*)-**30b** prepared in this study.

2.2 Results and Discussion

The six new MOP-phosphonite ligands depicted in Chart 2.3 were synthesised following a procedure developed by Higham *et al*., starting with the air-stable, chiral primary phosphine precursors (*S*)-**12a** and (*R*)-**12b**.[66,90] It was previously demonstrated that this synthesis can be carried out on a multigram scale, and with high yields at each stage, starting from enantiopure BINOL (Scheme 2.5).[90] It is more convenient to store the stable primary phosphine than the target phosphonite ligands due to the susceptibility of phosphonites to undergo hydrolysis during storage.

In a two-step, one-pot reaction, the primary phosphine was treated with phosphorus pentachloride, quantitatively yielding their dichlorophosphine analogues (Scheme 2.6).[93a] Our initial targets (*S*)-**28a** and (*R*)-**28b** were synthesised by employing two equivalents of phenol (Chart 2.3). However, both syntheses proved to be unreliable as a result of product sensitivity to hydrolysis, with (*S*)-**28a** particularly low-yielding ((*S*)-**28a** = 74% compared to (*R*)-**28b** = 97%). Therefore, we sought to replace the two phenol groups with the achiral, chelating 2,2'-biphenol, in order to ascertain whether we could inhibit this decomposition. This approach led to the successful preparation of the enantiopure compounds (*S*)-**29a** and (*R*)-**29b** (Chart 2.3). The isolated yields are lower than for (*S*)-**28a** and (*R*)-**28b** ((*S*)-**29a** = 70% and (*R*)-**29b** = 68%), beneficially though, the ligands can be stored under nitrogen for a period of weeks with only minimal decomposition. However, during our initial investigations into the coordination chemistry of these ligands, we noticed slow decomposition in solution and their performance in catalytic hydrosilylation required improvement (*vide infra*).

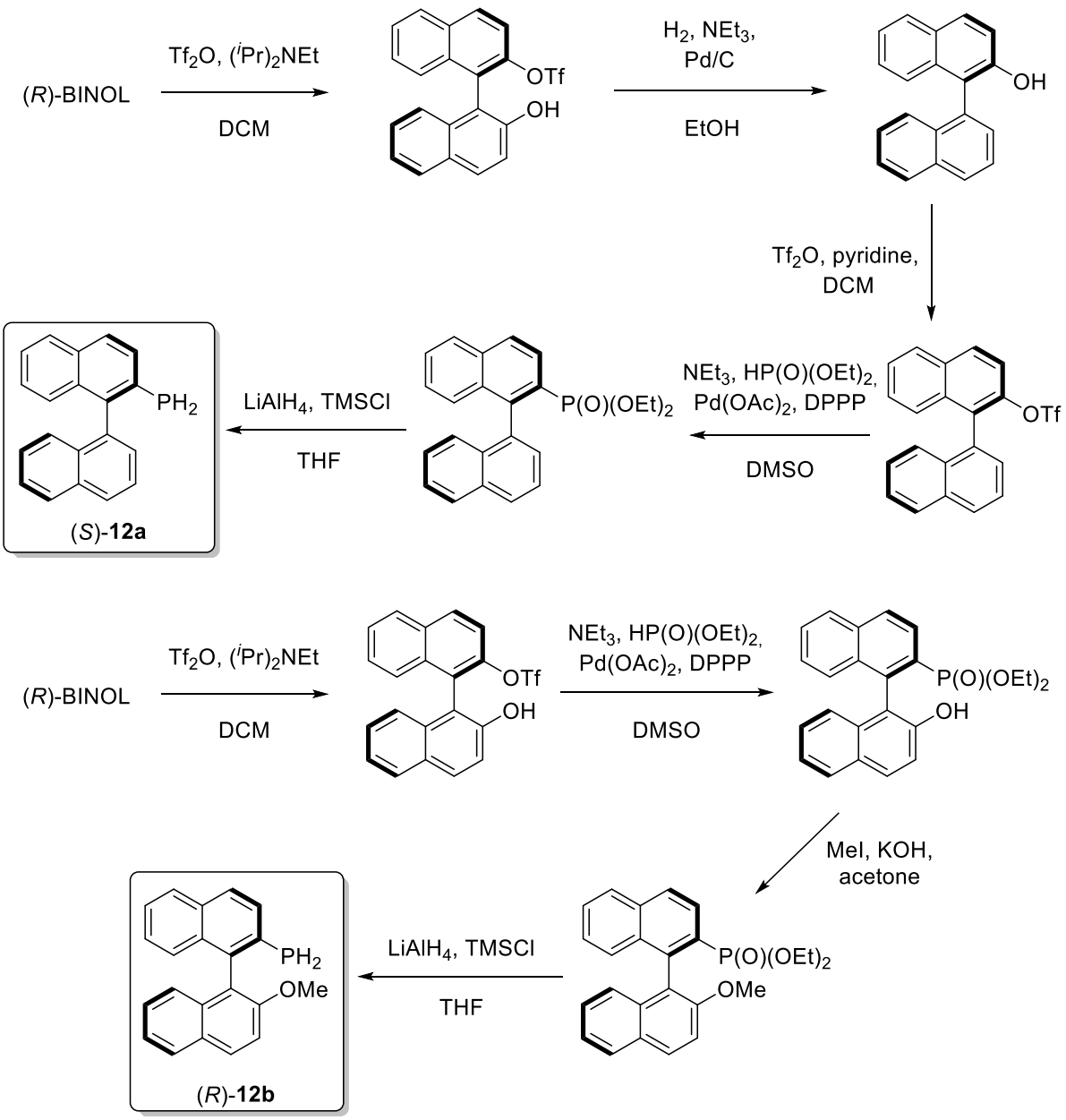

Scheme 2.5 Procedure followed to synthesise (*S*)-**12a** and (*R*)-**12b**.

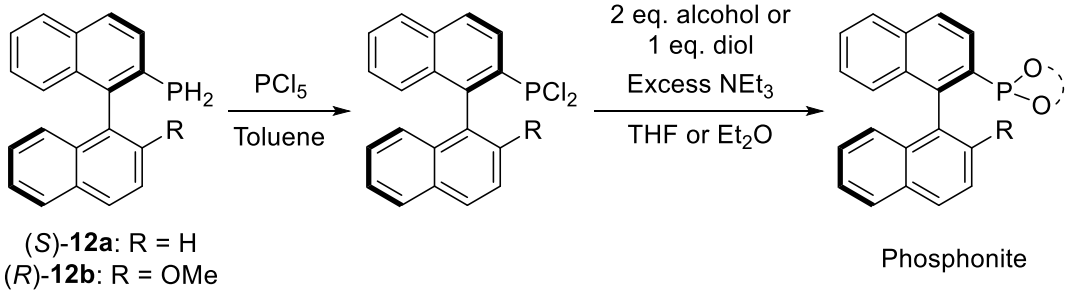

Scheme 2.6 The synthesis of phosphonite ligands (*S*)-**28a**, (*R*)-**28b**, (*S*)-**29a**, (*R*)-**29b**, (*S*)-**30a** and (*R*)-**30b** from primary phosphines (*S*)-**12a** and (*R*)-**12b**.

Thus, in order to push the design concept still further and optimise both ligand stability and catalytic capability, we synthesised the bulky *ortho*-methyl substituted precursor 2,2'-dihydroxy-3,3'-dimethyl-1,1'-biphenyl from 2,2'-dihydroxy-1,1'-biphenyl (Scheme 2.7), and used it to prepare the ligands (*S*)-**30a** and (*R*)-**30b** which possess a more imposing steric profile (Chart 2.3). Both phosphonites were isolated in high yield ((*S*)-**30a** = 91% and (*R*)-**30b** = 88%), and are purified by passing through a plug of alumina in air. They can be stored under nitrogen without decomposition over several months, and their coordination complexes also exhibit better stability. All the phosphonites were fully characterised by multinuclear NMR spectroscopy and HRMS. Their $^{31}P\{^{1}H\}$ spectra show characteristic singlet peaks: δ (ppm) = (*S*)-**28a** (154.8), (*R*)-**28b** (155.6), (*S*)-**29a** (177.7), (*R*)-**29b** (180.0), (*S*)-**30a** (172.4) and (*R*)-**30b** (174.2). The resonances for the phenoxy-derived phosphonites have a notable upfield shift compared to the biphenoxy analogues.

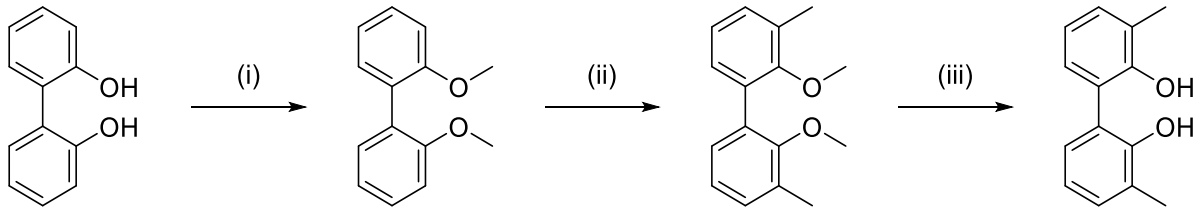

Scheme 2.7 Procedure followed to synthesise 2,2'-dihydroxy-3,3'-dimethyl-1,1'-biphenyl. Reagents: (i) MeI, KOH and acetone. (ii) ^{n}BuLi, TMEDA, MeI and Et_2O. (iii) BBr_3 and DCM.

Single crystals of (*R*)-**28b** and (*R*)-**29b** suitable for X-ray crystallographic analysis were obtained (Fig. 2.1, and Fig. 2.2); there are two crystallographically independent molecules in the asymmetric unit of (*R*)-**28b**. The phosphorus atoms have a trigonal pyramidal structure, the P–C bonds (1.812(7)-1.830(2) Å) are considerably longer than the P–O bonds (1.6461(17)-1.6675(17) Å).

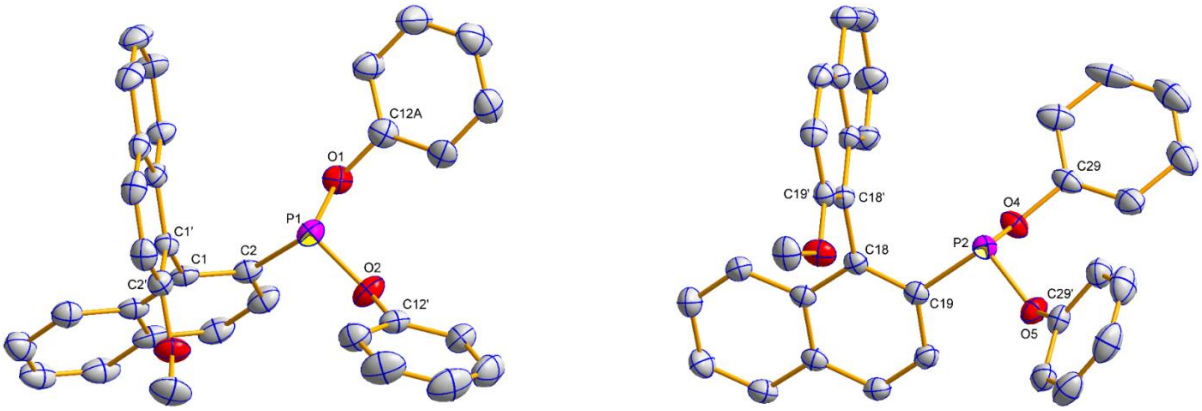

Fig. 2.1 Molecular structure of (*R*)-**28b** (the asymmetric unit comprises two molecules in different conformations). Hydrogen atoms have been omitted for clarity. Selected average bond distances (Å) and angles (°): (left) P1–C2 1.818(3), P1–O1 1.6489(18), P1–O2 1.6675(17), O1–C12A 1.400(10), O2–C12' 1.390(3), C1–C1' 1.495(3); O1–P1–O2 98.80(9), O1–P1–C2 96.62(10), O2–P1–C2 97.37(10), C2–C1–C1'–C2' –102.2(3); (right) P2–C19 1.830(2), P2–O4 1.6461(17), P2–O5 1.6619(18), O4–C29 1.402(3), O5–C29' 1.391(3); O4–P2–O5 99.13(9), O4–P2–C19 93.63(9), O5–P2–C19 97.85(10), C19–C18–C18'–C19' –86.5(3).

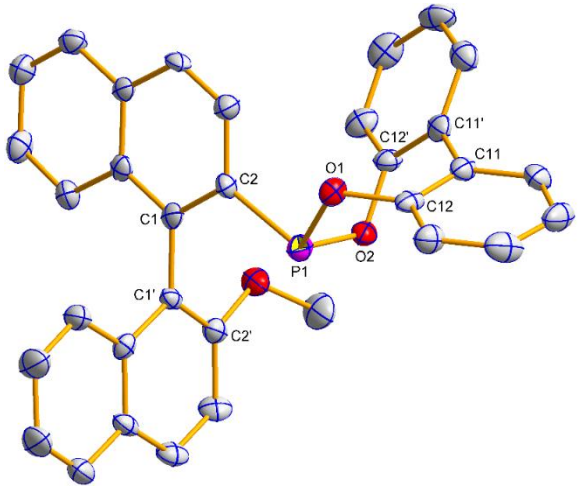

Fig. 2.2 Molecular structure of (*R*)-**29b**. Hydrogen atoms have been omitted for clarity. Selected average bond distances (Å) and angles (°): P1–C2 1.812(7), P1–O1 1.658(4), P1–O2 1.657(4), O1–C12 1.411(7), O2–C12' 1.396(7), C11–C11' 1.482(9); O1–P1–O2 99.5(2), O1–P1–C2 96.6(2), O2–P1–C2 100.3(3), C2–C1–C1'–C2' –86.5(7), C12–C11–C11'–C12' –48.6(8).

Density Functional Theory calculations at the B3LYP/6-31G* level of theory, performed on the optimised structures of the MOP-phosphonite ligands and the parent compounds (*S*)-H-MOP and (*R*)-MeO-MOP, revealed that the phosphonites have lower HOMO and LUMO energies than their aryl counterparts (Section 2.6, Fig. 2.8, Fig. 2.9, Fig. 2.10 and Fig. 2.11). They also have a lower phosphorus contribution to the HOMO, implying that the phosphonites are weaker P-ligand σ-donors. To study the coordination chemistry of our ligands with Pd(II), we reacted them with $[Pd(\eta^3\text{-}C_4H_7)Cl]_2$ in a 1:1, P:Pd ratio, to quantitatively synthesise complexes with the molecular formula $[Pd(L^P)(\eta^3\text{-}C_4H_7)Cl]$. Single crystals of $[Pd((S)\text{-}\mathbf{29a})(\eta^3\text{-}C_4H_7)Cl]$ ((*S*)-**31a**) and $[Pd((S)\text{-}\mathbf{30a})(\eta^3\text{-}C_4H_7)Cl]$ ((*S*)-**32a**) suitable for X-ray analysis were grown (Fig. 2.3 and Fig. 2.4). The asymmetric unit of (*S*)-**32a** comprises two molecules in different conformations and there is twofold disorder of the 2-methylallyl ligand and the palladium atom in one of these independents. The phosphonites show monodentate coordination through the phosphorus donor atom, and there is a *pseudo*-square-planar geometry around the palladium centre. The allyl carbons *trans* to phosphorus exhibit a longer Pd–C bond length (2.119(8)-2.206(4) Å) than the allyl carbons *cis* to the phosphorus (2.091(9)-2.096(4) Å), which is consistent with the stronger *trans* influence of the phosphonite compared to the chloride ligand. In the solid state, the lower naphthyl fragment of the binaphthyl backbone in (*S*)-**31a** is face-to-face with the palladium centre (Fig. 2.3). Neither of the two independent structures of (*S*)-**32a** display this feature, with the lower naphthyl group being orientated away from the palladium centre and facing the biphenyl moiety (Fig. 2.4). In the two independent structures of (*S*)-**32a**, the torsion angle of the dimethyl substituted biphenyl moiety is of opposite sign (Fig. 2.5), and also when comparing the biphenyl moiety in the structures of (*R*)-**29b** and (*S*)-**31a**, implying no restriction to rotation about the C11–C11' bond.

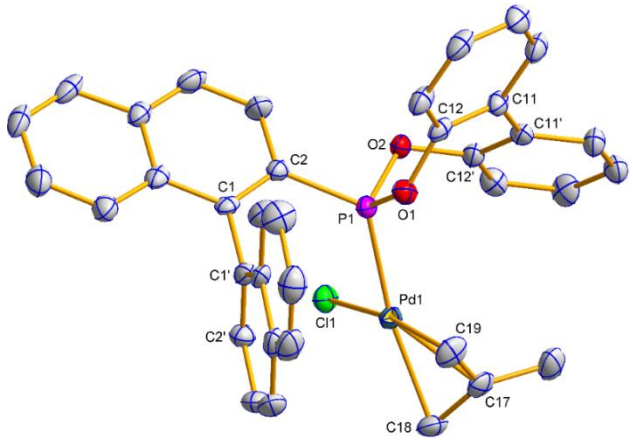

Fig. 2.3 Molecular structure of (*S*)-**31a**. Hydrogen atoms have been omitted for clarity. Selected average bond distances (Å) and angles (°): Pd1–P1 2.2478(10), Pd1–Cl1 2.3583(9), Pd1–C17 2.162(4), Pd1–C18 2.195(4), Pd1–C19 2.096(4), P1–C2 1.815(4), P1–O1 1.619(3), P1–O2 1.610(3), C11–C11' 1.477(5); P1–Pd1–Cl1 91.55(4), P1–Pd1–C18 165.51(11), P1–Pd1–C19 98.27(13), C18–Pd1–C19 67.46(16), C18–C17–C19 114.6(4), C2–C1–C1'–C2' –80.8(5), C12–C11–C11'–C12' 42.3(6).

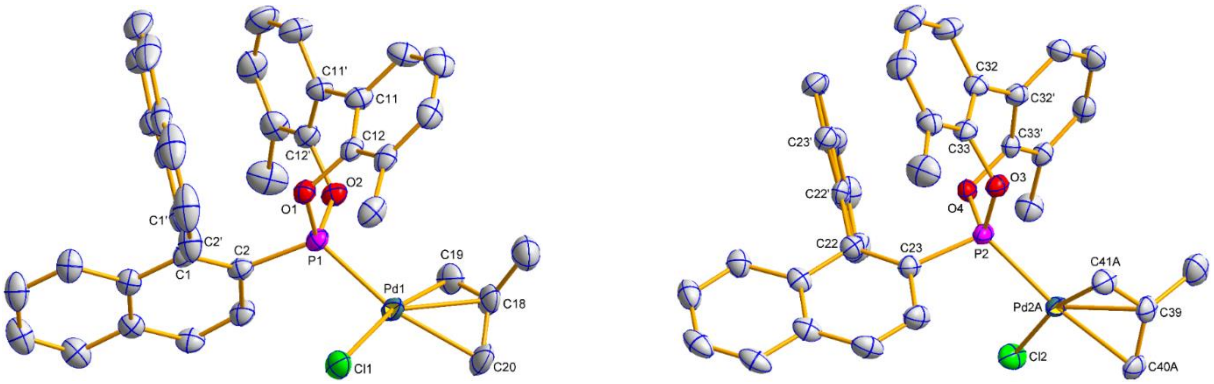

Fig. 2.4 Molecular structure of (*S*)-**32a** (the asymmetric unit comprises two molecules in different conformations). Hydrogen atoms have been omitted for clarity. Selected average bond distances (Å) and angles (°): (left) Pd1–P1 2.2368(11), Pd1–Cl1 2.3739(11), Pd1–C18 2.152(4), Pd1–C19 2.095(4), Pd1–C20 2.206(4), P1–C2 1.804(4), P1–O1 1.610(3), P1–O2 1.622(3), C11–C11' 1.485(6); P1–Pd1–Cl1 94.59(4), P1–Pd1–C19 96.50(15), P1–Pd1–C20 162.95(15), C19–Pd1–C20 66.8(2), C19–C18–C20 117.4(5), C2–C1–C1'–C2' –81.9(6), C12–C11–C11'–C12' –46.0(7); (right) Pd2A–P2 2.250(3), Pd2A–Cl2 2.363(3), Pd2A–C39 2.166(5), Pd2A–C40A 2.119(8), Pd2A–C41A 2.091(9), P2–C23 1.814(4), P2–O3 1.625(3), P2–O4 1.606(3), C32–C32' 1.475(6); P2–Pd2A–Cl2 93.59(11), P2–Pd2A–C40A 165.9(3), P2–Pd2A–C41A 98.50(3), C40A–Pd2A–C41A 67.5(3), C40A–C39–C41A 118.5(6), C23–C22–C22'–C23' –96.7(5), C33–C32–C32'–C33' 48.6(6).

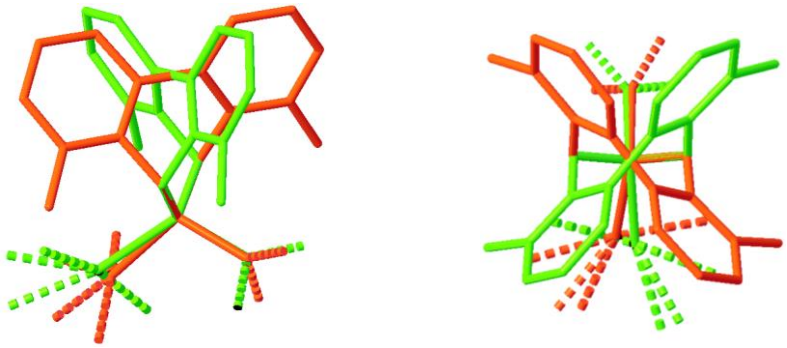

Fig. 2.5 Two views of an overlay image of the biphenyl moiety in the two independent molecules of (*S*)-**32a**.

The $^{31}P\{^1H\}$ NMR peaks of (*S*)-**31a** and (*S*)-**32a** experience slight shifts compared to the free ligands, and show the presence of two independent resonances due to the two isomers formed: δ (ppm) = (*S*)-**31a** (172.0 and 173.6) and (*S*)-**32a** (172.9 and 177.6). The isomers are a result of the rotation of the allyl moiety, via a selective *syn*/*anti* exchange of the allyl protons *cis* to the phosphorus, by an η^3-η^1-η^3 mechanism (Scheme 2.8), due to the stronger *trans* effect of the phosphonite donor ligand.[93a,121]

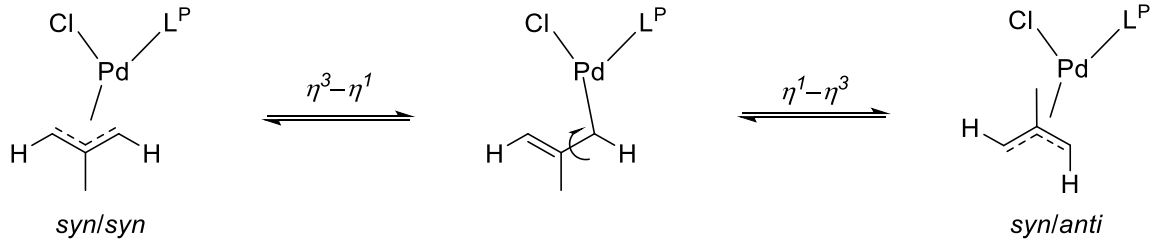

Scheme 2.8 *Syn*/*anti* exchange mechanism in 2-methylallyl palladium chloride complexes.

The rapid exchange process resulted in broadened peaks in the NMR spectra at room temperature. Cooling of CD_2Cl_2 solutions of the complexes to −20 °C sharpened the resonances and allowed for full characterisation of the 2-methylallyl ligands in both isomers. Reaction of (*S*)-**32a** with $NaBAr^F$ resulted in loss of NaCl and the formation of $[Pd((S)\text{-}\mathbf{30a})(\eta^3\text{-}C_4H_7)]BAr^F$ ((*S*)-**33a**), where the phosphonite ligand acts as a chelating P,C-π-donor. The upfield $^{13}C\{^1H\}$ NMR coordination chemical shifts for both C1' and C2' suggest an η^2-binding mode (Fig. 2.6), which is in agreement with the results of a NMR study reported by Pregosin and co-workers.[121]

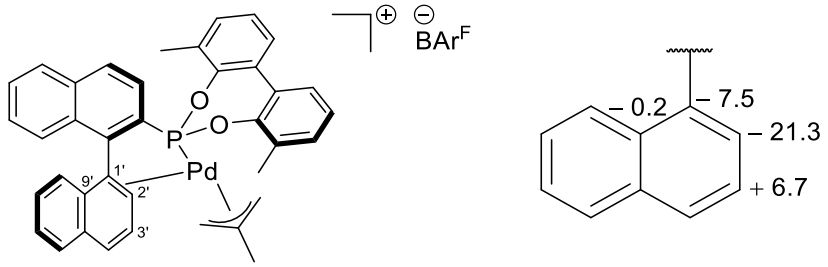

Fig. 2.6 Proposed structure of (*S*)-**33a** (left) and a fragment showing the $^{13}C\{^1H\}$ NMR coordination chemical shift (ppm) between the major isomers of (*S*)-**32a** and (*S*)-**33a** (right).

As discussed, MOP-phosphine ligands are known to give high enantioselectivity in the palladium-catalysed AHS of C–C double bonds in 1-alkenes, styrenes, and 1,3-dienes to give chiral secondary alcohols.[114b] To gain an insight into how the different stereoelectronic profiles of our phosphonites impacts upon their catalytic activity in the same transformation, we prepared catalysts by reacting each phosphonite with $[Pd(\eta^3\text{-}C_3H_5)Cl]_2$ (Table 2.1). We chose to test the phosphonites in the AHS of styrene and against the well-known phosphines H-MOP and MeO-MOP (the latter is a commercial compound), employing P:Pd ratios of 1:1 and 2:1 at room temperature.

Table 2.1 The asymmetric synthesis of 1-phenylethanol via the palladium-catalysed asymmetric hydrosilylation of styrene and subsequent stereoseospecific oxidation of the hydrosilylation product.[a]

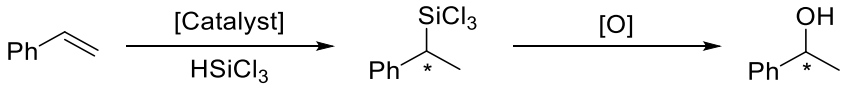

	Ligand	P:Pd	Temperature	Time[b]	Conversion[c]	*ee*[d]
1	(*S*)-**H-MOP**	1:1	rt	1 min	>99%	74 (*R*)
2	(*S*)-**H-MOP**	1:1	0 °C	4 h	>99%	93 (*R*)
3	(*S*)-**H-MOP**	2:1	rt	1 h	>99%	75 (*R*)
4	(*S*)-**H-MOP**	2:1	0 °C	12 h	>99%	94 (*R*)
5	(*R*)-**MeO-MOP**	1:1	rt	10 min	>99%	22 (*R*)
6	(*R*)-**MeO-MOP**	2:1	rt	1 h	>99%	20 (*R*)
7	(*S*)-**28a**	1:1	rt	24 h	>99%	63 (*R*)
8	(*S*)-**28a**	2:1	rt	24 h	>99%	73 (*R*)
9	(*R*)-**28b**	1:1	rt	24 h	>99%	7 (*S*)
10	(*R*)-**28b**	2:1	rt	24 h	>99%	1 (*S*)
11	(*S*)-**29a**	1:1	rt	6 min	>99%	73 (*R*)
12	(*S*)-**29a**	2:1	rt	1 h	>99%	79 (*R*)
13	(*R*)-**29b**	1:1	rt	10 min	>99%	23 (*R*)
14	(*R*)-**29b**	2:1	rt	1 h	>99%	27 (*R*)
15	(*S*)-**30a**	1:1	rt	2 min	>99%	79 (*R*)
16	(*S*)-**30a**	1:1	0 °C	5 h	>99%	92 (*R*)
17	(*S*)-**30a**	2:1	rt	2 h	>99%	80 (*R*)
18	(*S*)-**30a**	2:1	0 °C	72 h	>99%	95 (*R*)
19	(*R*)-**30b**	1:1	rt	1 h	>99%	45 (*R*)
20	(*R*)-**30b**	2:1	rt	70 min	>99%	51 (*R*)
21	(S,R_b)-**27a**	1:1	0 °C	168 h	88%[e]	4 (*S*)
22	(S,R_b)-**27a**	2:1	0 °C	168 h	>99%	60 (*R*)
23	(S,S_b)-**27a**	1:1	0 °C	72 h	>99%	59 (*R*)
24	(S,S_b)-**27a**	2:1	0 °C	168 h	22%[e]	77 (*R*)

[a] The catalyst was generated *in situ* from the ligand (0.25 or 0.50 mol%) and $[Pd(\eta^3\text{-}C_3H_5)Cl]_2$ (0.125 mol%), and reacted with styrene (10 mmol) and trichlorosilane (12 mmol). Fleming–Tamao procedures were used for the oxidation reaction: K_2CO_3, KF and H_2O_2 in MeOH/THF. [b] Time taken for reaction to reach completion. [c] Determined by ^{1}H NMR spectroscopy. [d] % *ee* determined by chiral GC; absolute configuration assigned by comparison of the sign of optical rotation to literature data. [e] Reaction stopped.

The reaction was performed without solvent and was monitored by ^{1}H NMR spectroscopy – full conversion and regioselectivity for the branched isomer were obtained in all cases. The 1-phenyl(trichlorosilyl)ethane product was stereospecifically oxidised to 1-phenylethanol using Fleming–Tamao procedures to obtain the *ee*. We noted a general increase in enantioselectivity and reaction rate in the order (*S*)-**30a**/(*R*)-**30b**>(*S*)-**29a**/(*R*)-**29b**>(*S*)-**28a**/(*R*)-**28b**, with the introduction of the biphenyl moiety, and subsequently the methyl groups, markedly improving the ligand performance. At a reduced temperature of 0 °C, phosphonite (*S*)-**30a** gave excellent enantioselectivity for (*R*)-1-phenylethanol (95%, Table 2.1, entry 18), which is slightly higher than that for the phosphine (*S*)-H-MOP (94%, Table 2.1, entry 4), although the latter reaction reached conversion more quickly. We also tested the H-MOP BINOL-appended phosphonite ligands (*S*,R_b)-**27a** and (*S*,S_b)-**27a** at 0 °C (Table 2.1, entries 21-24) and these ligands proved to be far less selective than (*S*)-**30a**.[93a] Interestingly, although the methoxy-substituted ligands (*R*)-MeO-MOP and (*R*)-**30b** performed poorly compared to their H-substituted counterparts – an established trend for this ligand family[122] – the phosphonite ligand gave much higher *ee*s than the corresponding phosphine (51% versus 20%, Table 2.1, entries 20 and 6), demonstrating further the potential these derivatives have to improve existing toolkits.

It is notable that at room temperature, the hydrosilylation occurs as a highly exothermic, quite violent reaction upon addition of trichlorosilane to the yellow homogeneous solution of catalyst and styrene, which is accompanied by a spontaneous colour change to black; similar observations with arylmonophosphinoferrocenes have also been made.[118] When a 2:1, P:Pd ratio was used there was often a significant delay in the time taken to observe this phenomenon (from 1-8 h, Table 2.1). Pedersen and Johannsen attributed the 'ultrafast' reaction to two competing catalytic cycles following the Chalk-Harrod mechanism (Scheme 2.9). The slower cycle I dominates with a twofold excess of ligand due to the superior donating abilities of phosphorus ligands over alkenes, whereas the faster cycle II is preferred with an equimolar quantity of P-ligand and palladium(0). The exothermic reactions accompanied by colour changes were not observed when the external temperature of the flask was kept at 0 °C. Consequently, the catalysis performed at 0 °C using both (*S*)-H-MOP and the sterically bulky (*S*)-**30a** resulted in longer reaction times; however, this was offset by an increased *ee* of the product – phosphonite (*S*)-**30a** gave the best *ee* with a value of 95%.

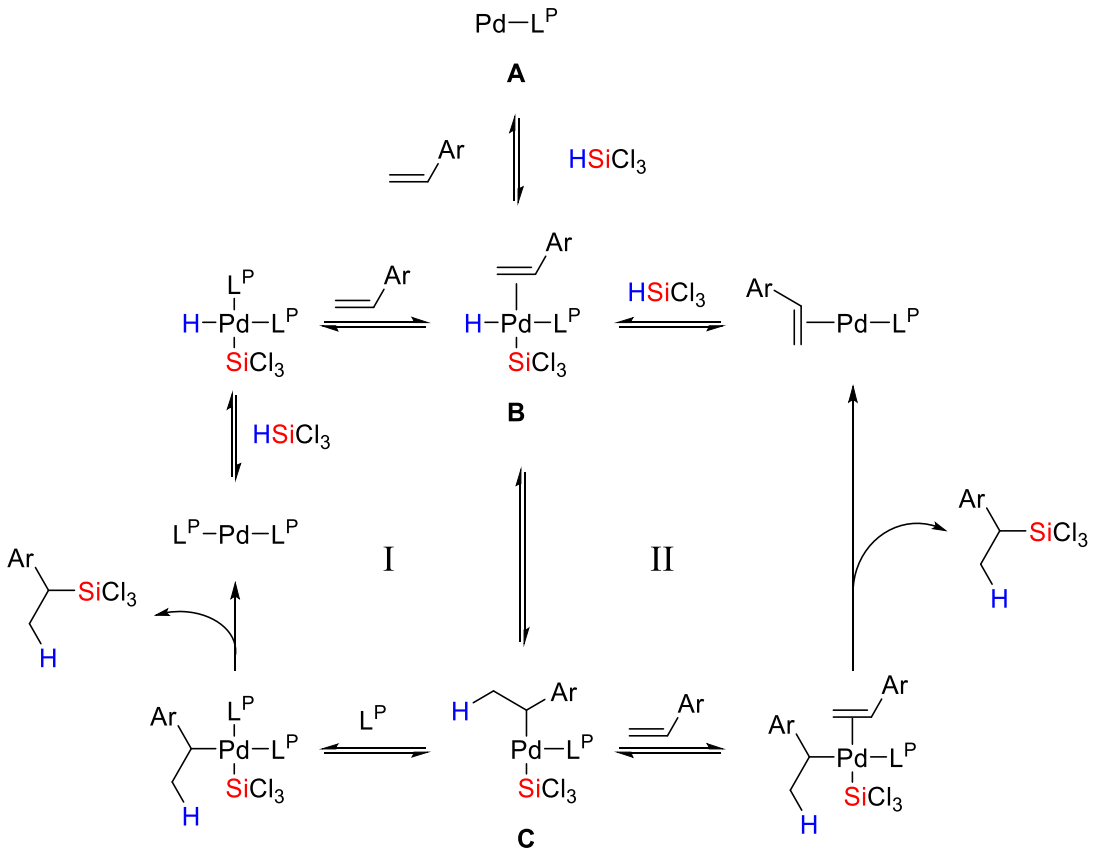

Scheme 2.9 Proposed catalytic cycles for the palladium-catalysed AHS of styrenes with a monophosphine ligand.

The final objective in this study was to extend our styrene screening regimen to substrates that MOP-phosphine palladium-complexes struggle to catalyse, or confer only low or moderate enantioselectivity in the product, with the aim that the unique stereoelectronic properties of the phosphonites would allow for improvements to be made. Thus, we extended our screening with (*S*)-**30a** to include the *para*-substituted styrenes listed in Table 2.2. Introducing an electron withdrawing chloride group resulted in much longer reaction times; however, full conversion and a high *ee*, better than (*S*)-H-MOP, were again obtained (Table 2.2, entries 1 and 3; note entry 2 for improving the *ee* generated by the latter). The chloro-substituted chiral secondary alcohol product was used to synthesise the antihistamine Clemastine enantioselectively by Clayden and co-workers.[123] More significantly, when an electron donating 4-methoxy substituent was incorporated onto the styrene precursor, (*S*)-**30a** was found to be a remarkably superior ligand, generating a much higher *ee* than (*S*)-H-MOP, albeit more slowly (85% versus 58%, Table 2.2, entries 8 and 6). It is of note that the product alcohol from this reaction was used to prepare antagonists of lysophosphatidic receptors, which may have implications in the treatment of lung fibrosis, liver disease and cancer.[124] A preliminary result with 4-dimethylamino styrene at room temperature suggested only a moderate enantioselectivity when employing (*S*)-**30a** (Table 2.2, entry 9). Due to the high cost of the substituted styrene, optimised reaction conditions were not sought for this reaction.[125]

Table 2.2 The synthesis of chiral secondary alcohols via the palladium-catalysed asymmetric hydrosilylation and subsequent stereoseospecific oxidation of styrene derivatives.[a]

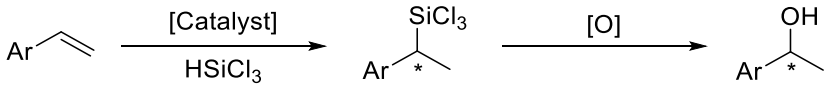

	Ligand	Ar	Temperature	Time[d]	Conversion[e]	*ee*[g]
1	(*S*)-**H-MOP**	4-ClC_6H_4[b]	rt	1 h	>99%	78 (*R*)[h]
2	(*S*)-**H-MOP**	4-ClC_6H_4[b]	0 °C	24 h	>99%	94 (*R*)[h]
3	(*S*)-**30a**	4-ClC_6H_4[b]	rt	18 h	>99%	86 (*R*)[h]
4	(*S*)-**30a**	4-ClC_6H_4[b]	0 °C	336 h	<5%[f]	–
5	(*S*)-**H-MOP**	4-$MeOC_6H_4$[b]	rt	10 min	>99%	35 (*R*)[h]
6	(*S*)-**H-MOP**	4-$MeOC_6H_4$[b]	0 °C	12 h	>99%	58 (*R*)[h]
7	(*S*)-**30a**	4-$MeOC_6H_4$[b]	rt	70 min	>99%	78 (*R*)[h]
8	(*S*)-**30a**	4-$MeOC_6H_4$[b]	0 °C	240 h	>99%	85 (*R*)[h]
9	(*S*)-**30a**	4-$Me_2NC_6H_4$[c]	rt	2.5 min	>99%	45 (*R*)[i]

[a] The catalyst was generated *in situ* from the ligand (0.50 mol%) and $[Pd(\eta^3\text{-}C_3H_5)Cl]_2$ (0.125 mol%). Fleming–Tamao procedures were used for the oxidation reaction: K_2CO_3, KF and H_2O_2 in MeOH/THF. [b] Styrene (10 mmol) and trichlorosilane (12 mmol). [c] Styrene (3.4 mmol) and trichlorosilane (4.1 mmol). [d] Time taken for reaction to reach completion. [e] Determined by ^{1}H NMR spectroscopy. [f] Reaction stopped. [g] Absolute configuration assigned by comparison of the sign of optical rotation to literature data. [h] % *ee* determined by chiral GC (Supelco β-dex). [i] % *ee* determined by chiral HPLC (Lux Cellulose) with hexane/2-propanol (98:2).

2.3 Summary

We have synthesised a series of novel MOP-phosphonite ligands from air-stable, chiral primary phosphine precursors, and have demonstrated the ease with which both the sterics and the hydrolytic stability of the ligands can be tuned, by modifying the aryl groups of the aryloxy moiety. In comparison to the previously reported **27a** and **27b**,[4] a major finding here is that a second chiral element is not necessary for the chiral induction, crucially both the *ee* and reaction rates can be increased without it. In the palladium-catalysed asymmetric hydrosilylation of functionalised styrenes, our new ligands proved to be high yielding, and both regio- and enantioselective: phosphonite (*S*)-**30a** achieved *ee*s of up to 95%. With the substrate 4-methoxystyrene, (*S*)-**30a** was significantly more enantioselective than Hayashi's benchmark phosphine (*S*)-H-MOP, demonstrating how MOP-phosphonite ligands have the potential to fill voids left by their phosphine counterparts in the field of asymmetric catalysis. Our future work will seek to extend the substrate scope to styrenes bearing other important functional groups. Having already proven that *para*-substituted styrenes are excellent AHS substrates for (*S*)-**30a**, we aim to apply the ligand to *ortho*- and *meta*-substituted styrenes, the regioisomers were shown to

react with large differences in reaction rates with arylphosphines.[114a] However, the stereoelectronic properties of the phosphonite may allow improvements to me made with these challenging groups.

2.4 Experimental Procedures

All air- and/or water-sensitive reactions were performed under a nitrogen atmosphere using standard Schlenk line techniques in oven dried glassware. Solvents were freshly distilled prior to use; toluene was dried over sodium, tetrahydrofuran and diethyl ether were dried over sodium/benzophenone, dichloromethane was dried over calcium hydride and *d*-chloroform was dried over phosphorus pentoxide, distilled and stored over molecular sieves. (*S*)-H-MOP,[126] (*R*)-MeO-MOP,[127] (*S*,R_b)-[1,1'-binaphthalene]-2,2'-diyl [1,1'-binaphthalen]-2-yl phosphonite ((*S*,R_b)-**27a**)[93a] and (*S*,S_b)-[1,1'-binaphthalene]-2,2'-diyl [1,1'-binaphthalen]-2-yl phosphonite ((*S*,S_b)-**27a**)[93a] were prepared according to literature procedures. All other chemicals were used as received without further purification. Flash chromatography was performed on silica gel (Fluorochem, 60A, 40-63 μm) or neutral aluminum oxide (Acros Organics, 60A, 50-200 μm). Thin-layer chromatography was performed on Merck silica gel coated aluminium sheets with fluorescent indicator (UV_{254}) or Machery-Nagel aluminum oxide coated polyester sheets with fluorescent indicator (UV_{254}), UV light was used for indicating. Melting points were determined in open glass capillary tubes on a Stuart SMP3 melting point apparatus. Optical rotation values were determined on an Optical Activity Polaar 2001 device. Infrared spectra were measured on a Varian 800 FT-IR Scimitar Series spectrometer. ^{1}H, ^{11}B, $^{13}C\{^{1}H\}$, ^{19}F and $^{31}P\{^{1}H\}$ NMR spectra were recorded on a Bruker 500 (^{1}H 500.15 MHz), JEOL 400 (^{1}H 399.78 MHz) or Bruker 300 (^{1}H 300.13 MHz) spectrometer at room temperature (21-25°C) if not otherwise stated, using the indicated solvent as internal reference. 2D NMR experiments (^{1}H-^{1}H COSY, ^{1}H-^{1}H NOESY, HSQC and HMBC) were used for the assignment of proton and carbon resonances, the numbering schemes are given in Fig. 2.7. High-resolution mass spectrometry was carried out by the EPSRC National Mass Spectrometry Facility, Swansea. Analytical gas chromatography was performed on a Shimadzu GC2014 instrument with a flame ionisation detector, using a Supelco β-dex™ 225 capillary column (L = 30 m, I.D. = 0.25 mm, d_f = 0.25 μm) and helium (purge flow 3 ml/min) as the carrier gas. High-performance liquid chromatography was performed on a Shimadzu Prominence UFLC instrument with a UV-Vis absorbance detector, using a Lux® 5μ Cellulose-1 column (250 × 4.6 mm).

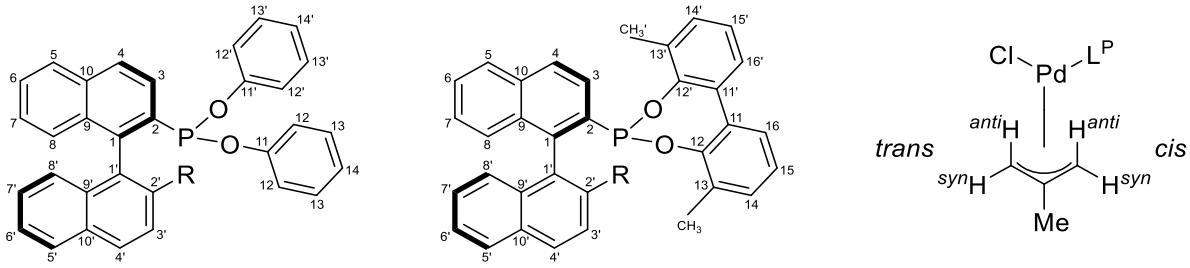

Fig. 2.7 Numbering schemes used to assign proton and carbon resonances in the NMR spectra: phenoxy-derived ligands (left), 2,2'-biphenoxy-derived ligands (middle) and 2-methylallyl ligands (right).

2.4.1 (*R*)-2'-Hydroxy-[1,1'-binaphthalen]-2-yl trifluoromethanesulfonate

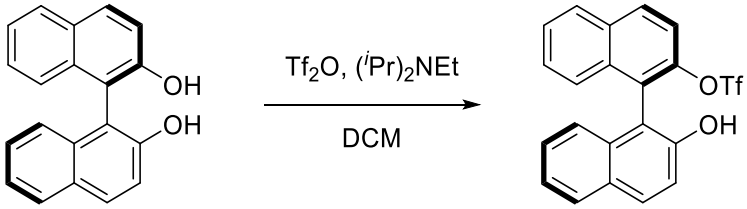

(*R*)-BINOL (8.00 g, 27.9 mmol, 1.0 eq.) was dissolved in DCM (500 mL). The solution was cooled to 0 °C and DIPEA (4.9 mL, 3.6 g, 28 mmol, 1.0 eq.) was added, the reaction mixture was stirred for 5 min, after which triflic anhydride (4.7 mL, 7.9 g, 28 mmol, 1.0 eq.) was added dropwise over 15 min. The reaction mixture was allowed to warm to room temperature and stirred for 18 h. TLC analysis showed complete consumption of the starting material. After concentration to approximately half volume, the organic phase was washed with water (100 mL), 1.0 M aq. HCl (100 mL) and brine (100 mL), dried over $MgSO_4$ and the volatiles were removed *in vacuo*. The title compound was obtained as a pale yellow oil (11.50 g, 27.5 mmol, 99%) which was reacted without further purification. R_f = 0.30 (silica gel; toluene). The ^{1}H and ^{19}F NMR spectroscopic data matched that of data reported in the literature.[90]

^{1}H NMR (400 MHz, $CDCl_3$): δ (ppm) = 8.12 (d, $^3J_{HH}$ = 8.2 Hz, 1H), 8.02 (d, $^3J_{HH}$ = 8.2 Hz, 1H), 7.97 (d, $^3J_{HH}$ = 8.2 Hz, 1H), 7.88 (d, $^3J_{HH}$ = 8.2 Hz, 1H), 7.60 (m, 2H), 7.44 (m, 2H), 7.37-7.24 (m, 3H), 7.01 (d, $^3J_{HH}$ = 8.2 Hz, 1H), 4.90 (br s, 1H). **^{19}F NMR** (376 MHz, $CDCl_3$): δ (ppm) = −74.3 (s).

2.4.2 (*S*)-[1,1'-Binaphthalen]-2-ol

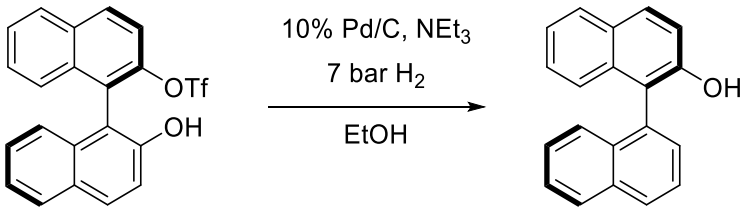

(*R*)-2'-Hydroxy-[1,1'-binaphthalen]-2-yl trifluoromethanesulfonate (5.76 g, 13.8 mmol, 1.0 eq.) was dissolved in ethanol (50 mL) in a miniclave vessel. Triethylamine (5.8 mL, 4.2 g, 42 mmol, 3.0 eq.) and palladium on carbon (10% wt. loading, 147 mg, 0.138 mmol Pd, 0.01 eq. Pd) were added, and the vessel

was pressurised to 7 bar with hydrogen gas. The suspension was stirred for 48 h, after which TLC analysis showed complete consumption of the starting material. The reaction mixture was filtered and the volatiles were removed *in vacuo*. The resulting yellow oil was dissolved in DCM (40 mL) and washed with water (2 x 20 mL), 1.0 M aq. HCl (2 x 20 mL), 0.1 M aq. $NaHCO_3$ (2 x 20 mL) and brine (2 x 20 mL), dried over $MgSO_4$ and the volatiles were removed *in vacuo*. The title compound was obtained as a white solid (3.08 g, 11.4 mmol, 83%) which was reacted without further purification. R_f = 0.50 (silica gel; toluene). The ^{1}H NMR spectroscopic data matched that of data reported in the literature.[90]

^{1}H NMR (400 MHz, $CDCl_3$): δ (ppm) = 8.03 (d, $^3J_{HH}$ = 8.2 Hz, 1H), 7.98 (d, $^3J_{HH}$ = 8.2 Hz, 1H), 7.91 (d, $^3J_{HH}$ = 8.7 Hz, 1H), 7.86 (d, $^3J_{HH}$ = 7.8 Hz, 1H), 7.65 (*apparent*-t (dd), $^3J_{HH}$ = 8.2 Hz, 1H), 7.53 (m, 2H), 7.41-7.21 (m, 5H), 7.01 (d, $^3J_{HH}$ = 8.2 Hz, 1H), 4.91 (br s, 1H).

2.4.3 (*S*)-[1,1'-Binaphthalen]-2-yl trifluoromethanesulfonate

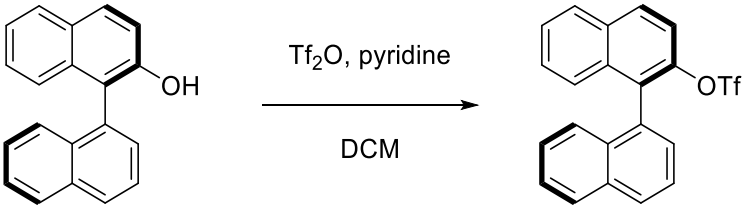

(*S*)-[1,1'-Binaphthalen]-2-ol (7.05 g, 26.1 mmol, 1.0 eq.) was dissolved in DCM (95 mL) and pyridine (3.1 mL, 3.0 g, 38 mmol, 1.5 eq.) was added. The solution was cooled to 0 °C and triflic anhydride (6.6 mL, 11 g, 39 mmol, 1.5 eq.) was added dropwise over 10 min. The reaction mixture was allowed to warm to room temperature and stirred for 18 h. TLC analysis showed complete consumption of the starting material. The organic phase was washed with water (2 x 30 mL), 1.0 M aq. HCl (2 x 30 mL), 0.1 M aq. $NaHCO_3$ (2 x 30 mL) and brine (2 x 20 mL), dried over $MgSO_4$ and the volatiles were removed *in vacuo*. The title compound was obtained as a pale orange solid (9.38 g, 23.3 mmol, 89%) which was reacted without further purification. R_f = 0.90 (silica gel; toluene). The ^{1}H and ^{19}F NMR spectroscopic data matched that of data reported in the literature.[90]

^{1}H NMR (400 MHz, $CDCl_3$): δ (ppm) = 8.06-7.95 (m, 4H), 7.64 (m, 1H), 7.58-7.47 (m, 4H), 7.42-7.29 (m, 3H), 7.21 (d, $^3J_{HH}$ = 7.8 Hz, 1H). **^{19}F NMR** (376 MHz, $CDCl_3$): δ (ppm) = −74.4 (s).

2.4.4 (*S*)-Diethyl [1,1'-binaphthalen]-2-yl phosphonate

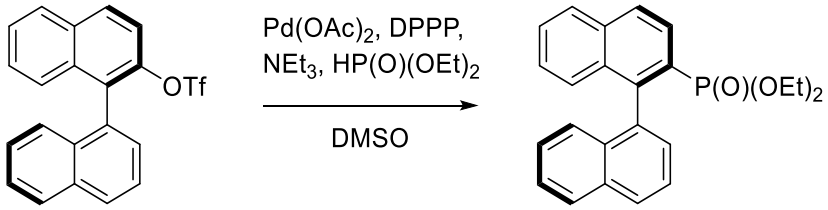

(*S*)-[1,1'-Binaphthalen]-2-yl trifluoromethanesulfonate (9.38 g, 23.3 mmol, 1.0 eq.) was dissolved in DMSO (80 mL) and water (0.2 mL). Palladium acetate (263 mg, 1.17 mmol, 0.05 eq.) and DPPP (722 mg, 1.75 mmol, 0.075 eq.) were added, and the solution purged with nitrogen for 15 min. Triethylamine (4.9 mL, 3.6 g, 36 mmol, 1.5 eq.) and diethyl phosphite (3.6 mL, 3.9 g, 28 mmol, 1.2 eq.) were added, and the reaction mixture heated to 90 °C and stirred for 18 h. The reaction mixture was diluted with water (50 mL) and extracted with DCM (3 x 50 mL). The combined organic extracts were washed with brine (3 x 50 mL), dried over $MgSO_4$ and the solvent removed *in vacuo*. Silica gel flash chromatography (ethyl acetate/hexane, 2:1) yielded the pure title compound as a white solid (6.47 g, 16.6 mmol, 71%). R_f = 0.30 (silica gel; ethyl acetate/hexane, 2:1). The ^{1}H and $^{31}P\{^{1}H\}$ NMR spectroscopic data matched that of data reported in the literature.[90]

^{1}H NMR (400 MHz, $CDCl_3$): δ (ppm) = 8.20 (dd, $^{3}J_{HP}$ = 12.4 Hz, $^{3}J_{HH}$ = 8.7 Hz, 1H), 8.01 (dd, $^{3}J_{HH}$ = 8.7 Hz, $^{4}J_{HP}$ = 3.7 Hz, 1H), 7.97-7.90 (m, 3H), 7.59 (d, $^{3}J_{HH}$ = 7.8 Hz, 1H), 7.54-7.47 (m, 2H), 7.42 (*apparent*-t (dd), $^{3}J_{HH}$ = 7.8 Hz, 1H), 7.27-7.15 (m, 3H), 7.07 (d, $^{3}J_{HH}$ = 8.2 Hz, 1H), 3.81-3.50 (m, 4H), 0.96 (t, $^{3}J_{HH}$ = 6.9 Hz, 3H), 0.69 (t, $^{3}J_{HH}$ = 6.9 Hz, 3H).**^{31}P{^{1}H} NMR** (162 MHz, $CDCl_3$): δ (ppm) = 18.6 (s).

2.4.5 (*R*)-Diethyl (2'-hydroxy-[1,1'-binaphthalen]-2-yl) phosphonate

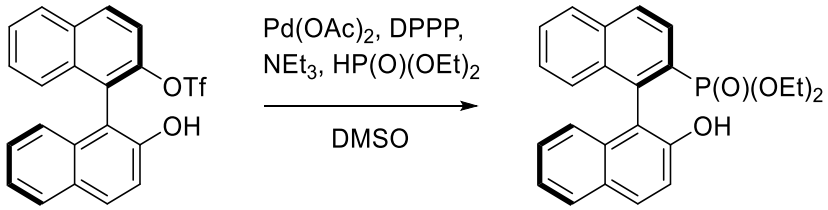

(*R*)-2'-Hydroxy-[1,1'-binaphthalen]-2-yl trifluoromethanesulfonate (11.20 g, 26.8 mmol, 1.0 eq.) was dissolved in DMSO (90 mL) and water (0.2 mL). Palladium acetate (300 mg, 1.34 mmol, 0.05 eq.) and DPPP (829 mg, 2.01 mmol, 0.075 eq.) were added, and the solution purged with nitrogen for 15 min. Triethylamine (5.6 mL, 4.1 g, 41 mmol, 1.5 eq.) and diethyl phosphite (4.2 mL, 4.5 g, 33 mmol, 1.2 eq.) were added, and the reaction mixture heated to 90 °C and stirred for 18 h. The reaction mixture was diluted with water (50 mL) and extracted with DCM (3 x 50 mL). The combined organic extracts were washed with brine (3 x 50 mL), dried over $MgSO_4$ and the volatiles were removed *in vacuo*. The title compound was obtained as a pale orange solid (7.62 g, 18.7 mmol, 70%) which was reacted without

further purification. R_f = 0.35 (silica gel; DCM/methanol, 50:1). The ^{1}H and ^{31}P{^{1}H} NMR spectroscopic data matched that of data reported in the literature.[90]

^{1}H NMR (400 MHz, $CDCl_3$): δ (ppm) = 8.08 (dd, $^3J_{HP}$ = 11.8 Hz, $^3J_{HH}$ = 8.5 Hz, 1H), 8.01 (dd, $^3J_{HH}$ = 8.5 Hz, $^4J_{HH}$ = 4.3 Hz, 1H), 7.92 (d, $^3J_{HH}$ = 8.2 Hz, 1H), 7.87 (d, $^3J_{HH}$ = 8.9 Hz, 1H), 7.83 (d, $^3J_{HH}$ = 8.9 Hz, 1H), 7.53 (m, 1H), 7.35 (dd, $^3J_{HH}$ = 8.7 Hz, $^4J_{HH}$ = 1.2 Hz, 1H), 7.29-7.23 (m, 2H), 7.19 (d, $^3J_{HH}$ = 8.5 Hz, 1H), 7.14 (m, 1H), 6.77 (d, $^3J_{HH}$ = 8.5 Hz, 1H), 6.52 (br s, 1H) 3.99-3.85 (m, 2H), 3.58 (m, 1H), 3.22 (m, 1H), 1.05 (t, $^3J_{HH}$ = 6.9 Hz, 3H), 0.69 (t, $^3J_{HH}$ = 6.9 Hz, 3H). **^{31}P{^{1}H} NMR** (162 MHz, $CDCl_3$): δ (ppm) = 18.6 (s).

2.4.6 (*R*)-Diethyl (2'-methoxy-[1,1'-binaphthalen]-2-yl) phosphonate

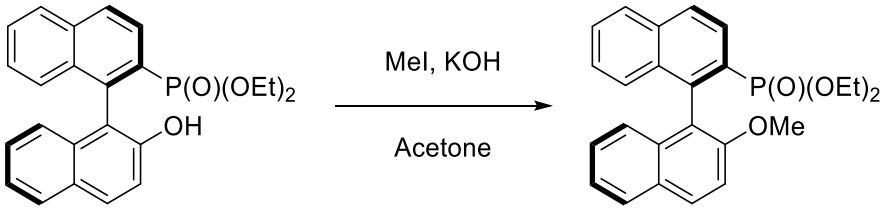

(*R*)-Diethyl (2'-hydroxy-[1,1'-binaphthalen]-2-yl) phosphonate (7.62 g, 18.7 mmol, 1.0 eq.) was dissolved in acetone (300 mL). Potassium hydroxide (4.20 g, 74.8 mmol, 4.0 eq.) and methyl iodide (4.8 mL, 11 g, 77 mmol, 4.0 eq.) were added, and the reaction mixture was stirred for 18 h. TLC analysis showed complete consumption of the starting material. The volatiles were removed *in vacuo* and the residue dissolved in DCM (100 mL). The organic phase was washed with water (50 mL), 1.0 M aq. HCl (50 mL), 0.1 M aq. $NaHCO_3$ (50 mL) and brine (50 mL), dried over $MgSO_4$ and the solvent removed *in vacuo*. Silica gel flash chromatography (ethyl acetate/hexane, 3:1) yielded the pure title compound as a white solid (5.89 g, 14.0 mmol, 75%). R_f = 0.25 (silica gel; ethyl acetate/hexane, 3:1). The ^{1}H and ^{31}P{^{1}H} NMR spectroscopic data matched that of data reported in the literature.[90]

^{1}H NMR (400 MHz, $CDCl_3$): δ (ppm) = 8.20 (dd, $^3J_{HP}$ = 11.9 Hz, $^3J_{HH}$ = 8.2 Hz, 1H), 8.00 (m, 2H), 7.93 (d, $^3J_{HH}$ = 8.2 Hz, 1H), 7.83 (d, $^3J_{HH}$ = 8.2 Hz, 1H), 7.52 (m, 1H), 7.41 (d, $^3J_{HH}$ = 9.2 Hz, 1H), 7.25 (m, 3H), 7.15 (m, 1H), 6.86 (d, $^3J_{HH}$ = 8.7 Hz, 1H), 3.80-3.48 (m, 4H), 3.76 (s, 3H), 0.96 (t, $^3J_{HH}$ = 7.3 Hz, 3H), 0.76 (t, $^3J_{HH}$ = 7.3 Hz, 3H). **^{31}P{^{1}H} NMR** (162 MHz, $CDCl_3$): δ (ppm) = 18.6 (s).

2.4.7 (*S)*-[1,1'-Binaphthalen]-2-yl phosphine (*S*)-**12a**

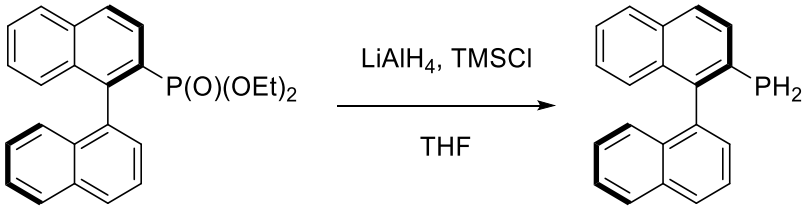

A suspension of lithium aluminium hydride (1.89 g, 49.8 mmol, 3.0 eq.) in THF (50 mL) was cooled to −78 °C and TMSCl (6.3 mL, 5.4 g, 50 mmol, 3.0 eq.) was added dropwise. The reaction mixture was allowed to warm to room temperature over 30 min, cooled to −78 °C and a solution of (*S*)-diethyl [1,1'-binaphthalen]-2-yl phosphonate (6.47 g, 16.6 mmol, 1.0 eq.) in THF (50 mL) was added dropwise. The reaction mixture was allowed to warm to room temperature and stirred for 18 h. The reaction was quenched by the dropwise addition of water (15 mL) and extracted with diethyl ether (2 x 40 mL). The combined organic extracts were washed with water (20 mL), dried over $MgSO_4$ and the solvent removed *in vacuo*. Silica gel flash chromatography (DCM/hexane, 1:1) yielded the pure title compound as a white solid (3.98 g, 13.9 mmol, 84%). R_f = 0.70 (silica gel; DCM/hexane, 1:1). The ^1H and $^{31}P\{^1H\}$ NMR spectroscopic data matched that of data reported in the literature.[66]

^{1}H NMR (400 MHz, $CDCl_3$): δ (ppm) = 7.98 (m, 2H), 7.90 (d, $^3J_{HH}$ = 8.2 Hz, 1H), 7.86 (d, $^3J_{HH}$ = 8.2 Hz, 1H), 7.72 (dd, $^3J_{HH}$ = 8.7 Hz, $^3J_{HH}$ = 5.5 Hz, 1H), 7.72 (dd, $^3J_{HH}$ = 8.2 Hz, $^3J_{HH}$ = 6.9 Hz, 1H), 7.51-7.40 (m, 3H), 7.32-7.15 (m, 4H), 3.67 (AB quartet, $^1J_{PHa}$ = 204.7 Hz, $^1J_{PHb}$ = 206.5 Hz, $^2J_{HH}$ = 11.9 Hz, 2H). **$^{31}P\{^1H\}$ NMR** (162 MHz, $CDCl_3$): δ (ppm) = −124.8 (s).

2.4.8 (*R*)-(2'-Methoxy-[1,1'-binaphthalen]-2-yl) phosphine (*R*)-**12b**

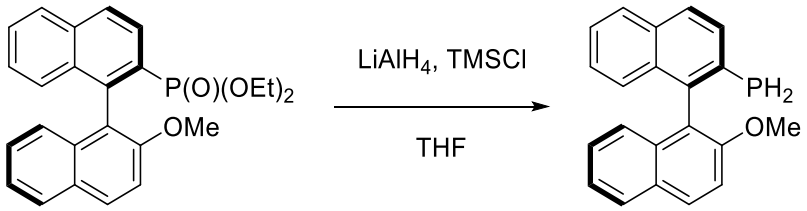

A suspension of lithium aluminium hydride (1.41 g, 37.2 mmol, 3.0 eq.) in THF (40 mL) was cooled to −78 °C and TMSCl (4.7 mL, 4.0 g, 37 mmol, 3.0 eq.) was added dropwise. The reaction mixture was allowed to warm to room temperature over 30 min, cooled to −78 °C and a solution of (*R*)-diethyl (2'-methoxy-[1,1'-binaphthalen]-2-yl) phosphonate (5.21 g, 12.4 mmol, 1.0 eq.) in THF (40 mL) was added dropwise. The reaction mixture was allowed to warm to room temperature and left to stir for 18 h. The reaction was quenched by the dropwise addition of water (15 mL) and extracted with diethyl ether (2 x 40 mL). The combined organic extracts were washed with water (20 mL), dried over $MgSO_4$ and the solvent removed *in vacuo*. Silica gel flash chromatography (DCM/hexane, 1:1)

yielded the pure title compound as a white solid (3.03 g, 9.58 mmol, 77%). R_f = 0.40 (silica gel; DCM/hexane, 1:1). The ^{1}H and ^{31}P{^{1}H} NMR spectroscopic data matched that of data reported in the literature.[66]

^{1}H NMR (400 MHz, $CDCl_3$): δ (ppm) = 8.03 (d, $^3J_{HH}$ = 9.2 Hz, 1H), 7.89 (m, 2H), 7.86 (d, $^3J_{HH}$ = 8.7 Hz, 1H), 7.75 (dd, $^3J_{HH}$ = 8.3 Hz, $^3J_{HH}$ = 5.5 Hz, 1H), 7.44 (m, 2H), 7.34 (*apparent*-t (dd), $^3J_{HH}$ = 6.9 Hz, 1H), 7.24 (m, 2H), 7.16 (d, $^3J_{HH}$ = 8.3 Hz, 1H), 6.97 (d, $^3J_{HH}$ = 8.3 Hz, 1H), 3.80 (s, 3H), 3.64 (AB quartet, $^1J_{PHa}$ = 203.9 Hz, $^1J_{PHb}$ = 204.8 Hz, $^2J_{HH}$ = 12.4 Hz, 2H). **^{31}P{^{1}H} NMR** (162 MHz, $CDCl_3$): δ (ppm) = −125.7 (s).

2.4.9 (*S*)-Diphenyl [1,1'-binaphthalen]-2-yl phosphonite (*S*)-**28a**

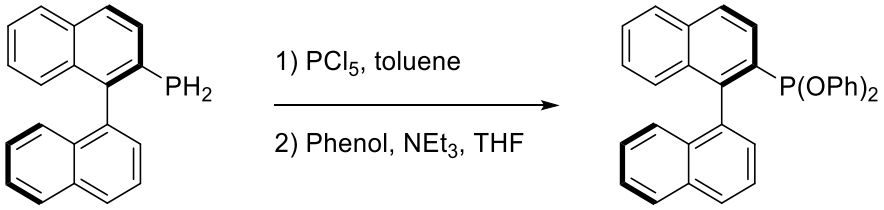

(*S*)-[1,1'-Binaphthalen]-2-yl) phosphine ((*S*)-**12a**, 286 mg, 1.00 mmol, 1.0 eq.) was dissolved in toluene (10 mL) and phosphorus pentachloride (458 mg, 2.20 mmol, 2.2 eq.) was added. The reaction mixture was stirred for 45 min, after which the volatiles were removed *in vacuo*. The residue was dissolved in THF (8 mL) and triethylamine (0.61 mL, 450 mg, 4.4 mmol, 4.4 eq.) was added. The reaction mixture was then left to stir for 10 min, before phenol (188 mg, 2.00 mmol, 2.0 eq.) was added and stirring continued overnight. The volatiles were removed *in vacuo* and the crude compound was filtered through a plug of alumina (diethyl ether) to yield the pure title compound as a white sticky solid (350 mg, 0.74 mmol, 74%). R_f = 0.95 (alumina; diethyl ether).

$[\alpha]_D^{20}$ = +56° ($CHCl_3$, *c* = 0.1). **IR** (neat): ν = 3055.1 (w), 1589.8 (m), 1483.3 (m), 1217.2 (m), 1193.4 (s), 1162.4 (m), 1120.2 (w), 1070.8 (w), 1023.4 (w), 852.9 (s), 758.7 (s), 716.5 (m), 687.3 (s), 632.4 (m) cm^{-1}. **^{1}H NMR** (400 MHz, $CDCl_3$): δ (ppm) = 8.30 (dd, $^3J_{HH}$ = 8.6 Hz, $^3J_{HP}$ = 2.8 Hz, 1H, *H*3), 8.08 (d, $^3J_{HH}$ = 8.6 Hz, 1H, *H*4), 7.98-7.94 (m, 2H, *H*4'/*H*5'), 7.91 (d, $^3J_{HH}$ = 8.3 Hz, 1H, *H*5), 7.56-7.51 (m, 3H, *H*2'/*H*3'/*H*6'), 7.56 (ddd, $^3J_{HH}$ = 8.2 Hz, $^3J_{HH}$ = 8.2 Hz, $^4J_{HH}$ = 1.9 Hz, 1H, *H*6), 7.32-7.21 (m, 4H, *H*7/*H*7'/*H*8/*H*8'), 7.19-7.13 (m, 2H, *H*13'), 7.04-6.96 (m, 3H, *H*13/*H*14'), 6.90-6.83 (m, 3H, *H*12'/*H*14), 6.53-6.49 (m, 2H, *H*12). **^{13}C{^{1}H} NMR** (101 MHz, $CDCl_3$): δ (ppm) = 155.3 (*overlapping*-d, *C*11/*C*11'), 143.2 (d, $^2J_{CP}$ = 36.5 Hz, *C*1), 137.7 (d, $^1J_{CP}$ = 14.0 Hz, *C*2), 135.4 (d, $^3J_{CP}$ = 9.2 Hz, *C*1'), 134.6 (*C*10'), 133.6 (*C*10), 133.5 (*C*9'), 132.9 (d, $^3J_{CP}$ = 5.8 Hz, *C*9), 129.6 (d, $^4J_{CP}$ = 3.9 Hz, *C*2'), 129.5 (*C*13'), 129.3 (*C*13), 128.8 (*C*4), 128.3, 128.2, 128.2, 127.4 (*C*6'), 127.1 (d, $^4J_{CP}$ = 2.8 Hz, *C*8), 126.8 (*C*6), 126.6, 126.5, 126.1, 125.1 (*C*3'), 125.0 (d, $^2J_{CP}$ = 3.3 Hz, *C*3), 123.3 (*C*14'), 123.1 (*C*14), 119.9 (d, $^3J_{CP}$ = 8.6 Hz, *C*12'), 119.6 (d, $^3J_{CP}$ = 8.9 Hz, *C*12).

^{31}P{^{1}H} NMR (162 MHz, $CDCl_3$): δ (ppm) = 154.8 (s). **HRMS** (ASAP$^+$, solid): Found: m/z = 471.1499. Calculated for $[M + H]^+$: m/z = 471.1508.

2.4.10 (*R*)-Diphenyl (2'-methoxy-[1,1'-binaphthalen]-2-yl) phosphonite (*R*)-**28b**

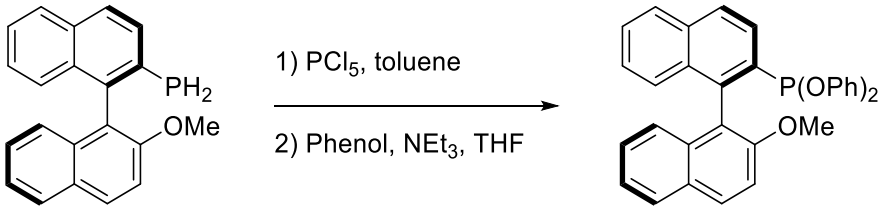

(*R*)-(2'-Methoxy-[1,1'-binaphthalen]-2-yl) phosphine ((*R*)-**12b**, 316 mg, 1.00 mmol, 1.0 eq.) was dissolved in toluene (10 mL) and phosphorus pentachloride (458 mg, 2.20 mmol, 2.2 eq.) was added. The reaction mixture was stirred for 45 min, after which the volatiles were removed *in vacuo*. The residue was dissolved in THF (8 mL) and triethylamine (0.61 mL, 450 mg, 4.4 mmol, 4.4 eq.) was added. The reaction mixture was then left to stir for 10 min, before phenol (188 mg, 2.00 mmol, 1.0 eq.) was added and stirring continued overnight. The volatiles were removed *in vacuo* and the crude compound was filtered through a plug of alumina (toluene) to yield the pure title compound as a white solid (488 mg, 0.97 mmol, 97%). R_f = 0.95 (alumina; toluene).

MP: 142-144 °C. $[\boldsymbol{\alpha}]_{\boldsymbol{D}}^{\boldsymbol{20}}$ = +24° ($CHCl_3$, *c* = 0.1). **IR** (neat): ν = 3233.1 (w), 3054.6 (w), 2935.7 (w), 2840.8 (w), 1592.2 (m), 1486.3 (m), 1334.5 (w), 1191.8 (s), 1162.9 (m), 1079.3 (m), 1052.5 (m), 1022.0 (m), 967.6 (m), 922.2 (s), 868.4 (m), 809.7 (s), 747.2 (s), 689.4 (s), 633.3 (m) cm^{-1}. **^{1}H NMR** (400 MHz, $CDCl_3$): δ (ppm) = 8.32 (dd, $^3J_{HH}$ = 8.5 Hz, $^3J_{HP}$ = 2.8 Hz, 1H, *H*3), 8.11 (d, $^3J_{HH}$ = 8.5 Hz, 1H, *H*4), 8.03 (d, $^3J_{HH}$ = 9.1 Hz, 1H, *H*4'), 8.00 (d, $^3J_{HH}$ = 8.3 Hz, 1H, *H*5), 7.89 (d, $^3J_{HH}$ = 8.2 Hz, 1H, *H*5'), 7.56 (*apparent*-t (dd), $^3J_{HH}$ = 7.3 Hz, 1H, *H*6), 7.41 (d, $^3J_{HH}$ = 9.1 Hz, 1H, *H*3'), 7.37-7.30 (m, 3H, *H*6'/*H*7/*H*8), 7.25-7.17 (m, 3H, *H*7'/*H*13'), 7.11 (d, $^3J_{HH}$ = 8.5 Hz, 1H, *H*8'), 7.06-7.00 (m, 3H, *H*13/*H*14), 6.94-6.88 (m, 3H, *H*12'/*H*14'), 6.52 (d, $^3J_{HH}$ = 8.3 Hz, 2H, *H*12), 3.72 (s, 3H, OCH_3). **^{13}C{^{1}H} NMR** (101 MHz, $CDCl_3$): δ (ppm) = 155.5 (*overlapping*-d, *C*11/*C*11'), 155.3 (d, $^4J_{CP}$ = 2.4 Hz, *C*2'), 139.9 (d, $^2J_{CP}$ = 38.3 Hz, *C*1), 138.0 (d, $^1J_{CP}$ = 13.4 Hz, *C*2), 135.1 (*C*10), 134.8 (d, $^4J_{CP}$ = 2.1 Hz, *C*9'), 132.9 (d, $^3J_{CP}$ = 6.4 Hz, *C*9), 130.7 (*C*4'), 129.5 (*C*13'), 129.3 (*C*13), 128.9 (*C*10'), 128.4 (*C*5), 128.3 (d, $^3J_{CP}$ = 1.0 Hz, *C*4), 128.0 (*C*5'), 127.5 (*C*6), 127.1 (*C*7'), 126.6 (*C*7), 126.5 (d, $^4J_{CP}$ = 2.8 Hz, *C*8), 125.6 (*C*8'), 125.3 (d, $^2J_{CP}$ = 3.2 Hz, *C*3), 123.8 (*C*6'), 123.2 (*C*14'), 123.2 (*C*14), 120.9 (d, $^3J_{CP}$ = 7.1 Hz, *C*1'), 120.0 (d, $^3J_{CP}$ = 9.1 Hz, *C*12'), 119.8 (d, $^3J_{CP}$ = 8.8 Hz, *C*12), 113.1 (*C*3'), 56.3 (O*C*H_3). **^{31}P{^{1}H} NMR** (162 MHz, $CDCl_3$): δ (ppm) = 155.6 (s). **HRMS** (ASAP$^+$, solid): Found: m/z = 501.1602. Calculated for $[M + H]^+$: m/z = 501.1614.

2.4.11 (*S*)-[1,1'-Biphenyl]-2,2'-diyl [1,1'-binaphthalen]-2-yl phosphonite (*S*)-**29a**

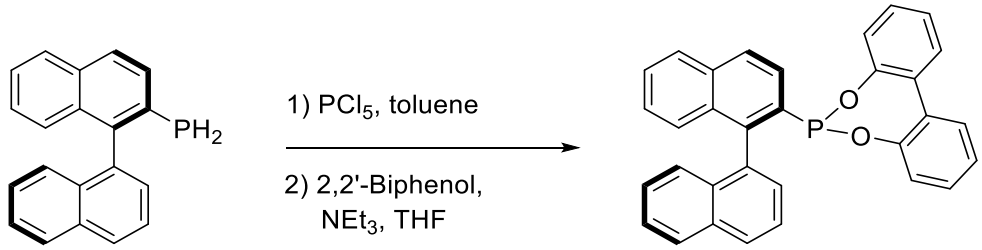

(*S*)-[1,1'-Binaphthalen]-2-yl) phosphine ((*S*)-**12a**, 429 mg, 1.50 mmol, 1.0 eq.) was dissolved in toluene (12 mL) and phosphorus pentachloride (687 mg, 3.30 mmol, 2.2 eq.) was added. The reaction mixture was stirred for 45 min, after which the volatiles were removed *in vacuo*. The residue was dissolved in THF (12 mL) and triethylamine (0.92 mL, 670 mg, 6.6 mmol, 4.4 eq.) was added. The reaction mixture was then left to stir for 10 min before 2,2'-biphenol (279 mg, 1.50 mmol, 1.0 eq.) was added and stirring continued overnight. The volatiles were removed *in vacuo* and the crude compound was filtered through a plug of silica gel (toluene) to yield the pure title compound as a white solid (492 mg, 1.05 mmol, 70%). R_f = 0.90 (silica gel; toluene).

MP: 137-139 °C. $[\boldsymbol{\alpha}]_{\boldsymbol{D}}^{\boldsymbol{20}}$ = +116° ($CHCl_3$, *c* = 0.1). **IR** (neat): ν = 3048.0 (w), 1497.0 (m), 1473.1 (w), 1432.8 (m), 1244.5 (m), 1205.7 (m), 1180.0 (m), 1095.0 (w), 1022.0 (w), 946.1 (w), 893.2 (s), 851.6 (s), 821.3 (m), 800.7 (m), 761.8 (s), 700.2 (m), 630.5 (w), 603.2 (w) cm^{-1}. **^{1}H NMR** (400 MHz, $CDCl_3$): *δ* (ppm) = 8.04 (d, $^3J_{HH}$ = 8.1 Hz, 1H, *H*4'), 7.98 (d, $^3J_{HH}$ = 8.2 Hz, 1H, *H*5'), 7.90 (d, $^3J_{HH}$ = 8.2 Hz, 1H, *H*5), 7.77-7.70 (m, 2H, *H*2'/*H*4), 7.69-7.64 (m, 1H, *H*3'), 7.57-7.49 (m, 3H, *H*3/*H*6/*H*6'), 7.48-7.43 (m, 2H, H16/H16'), 7.40-7.31 (m, 4H, H7/H7'/H8/H8'), 7.28-7.16 (m, 4H, H14/H14'/H15/H15'), 6.98-6.94 (m, 1H, *H*13'), 6.83 (d, $^3J_{HH}$ = 7.8 Hz, 1H, *H*13). **^{13}C{^{1}H} NMR** (101 MHz, $CDCl_3$): *δ* (ppm) = 151.5 (d, $^2J_{CP}$ = 4.4 Hz, *C*12), 151.3 (d, $^2J_{CP}$ = 6.7 Hz, *C*12'), 145.0 (d, $^2J_{CP}$ = 37.1 Hz, *C*1), 136.8 (d, $^1J_{CP}$ = 39.1 Hz, *C*2), 135.0 (d, $^3J_{CP}$ = 9.8 Hz, *C*1'), 134.9 (*C*10), 133.7 (d, $^4J_{CP}$ = 2.6 Hz, *C*9'), 133.4 (*C*10'), 133.1 (d, $^3J_{CP}$ = 4.6 Hz, *C*9), 132.3 (d, $^3J_{CP}$ = 4.0 Hz, *C*11'), 131.9 (d, $^3J_{CP}$ = 3.2 Hz, *C*11), 130.3 (d, $^4J_{CP}$ = 5.4 Hz, *C*2'), 130.0 (*C*16 or *C*16'), 129.9 (*C*16 or *C*16'), 129.3 (*C*14 or *C*14'), 129.1 (*C*14 or *C*14'), 129.0 (*C*4'), 128.4 (*C*5'), 128.2 (*C*5), 127.7 (*C*6 or *C*6'), 127.3 (d, $^4J_{CP}$ = 2.7 Hz, *C*8), 127.1 (*C*4), 126.9 (*C*8'), 126.6 (*C*7 or *C*7'), 126.5 (*C*7 or *C*7'), 126.2 (*C*6 or *C*6'), 125.1 (*C*3'), 125.0 (*C*15 or *C*15'), 124.9 (*C*15 or *C*15'), 124.4 (d, $^2J_{CP}$ = 2.6 Hz, *C*3), 122.2 (*overlapping*-d, *C*13/*C*13'). **^{31}P{^{1}H} NMR** (162 MHz, $CDCl_3$): *δ* (ppm) = 177.7 (s). **HRMS** ($ASAP^+$, solid): Found: *m*/*z* = 469.1344. Calculated for $[M + H]^+$: *m*/*z* = 469.1352.

2.4.12 (*R*)-[1,1'-Biphenyl]-2,2'-diyl (2'-methoxy-[1,1'-binaphthalen]-2-yl) phosphonite (*R*)-**29b**

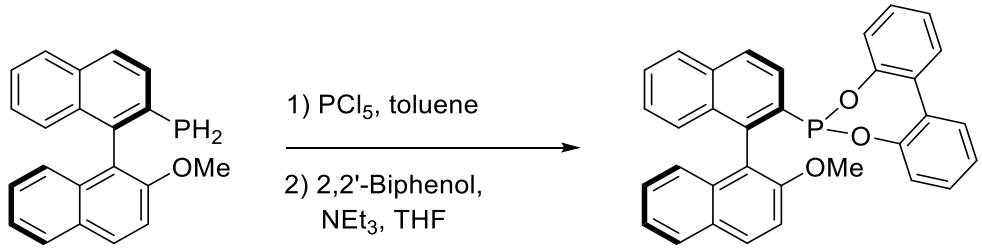

(*R*)-(2'-Methoxy-[1,1'-binaphthalen]-2-yl) phosphine ((*R*)-**12b**, 474 mg, 1.50 mmol, 1.0 eq.) was dissolved in toluene (12 mL) and phosphorus pentachloride (687 mg, 3.30 mmol, 2.2 eq.) was added. The reaction mixture was stirred for 45 min, after which the volatiles were removed *in vacuo*. The residue was dissolved in THF (12 mL) and triethylamine (0.92 mL, 670 mg, 6.6 mmol, 4.4 eq.) was added. The reaction mixture was then left to stir for 10 min before 2,2'-biphenol (279 mg, 1.50 mmol, 1.0 eq.) was added and stirring continued overnight. The volatiles were removed *in vacuo* and the crude compound was filtered through a plug of silica gel (toluene) to yield the pure title compound as a white solid (510 mg, 1.02 mmol, 68%). R_f = 0.80 (silica gel; toluene).

MP: 225-227 °C. $[\boldsymbol{\alpha}]_{\boldsymbol{D}}^{\mathbf{20}}$ = +162° ($CHCl_3$, *c* = 0.1). **IR** (neat): ν = 3062.8 (w), 2969.0 (w), 1619.9 (w), 1592.5 (w), 1496.0 (m), 1471.6 (w), 1435.6 (m), 1269.1 (m), 1248.4 (s), 1197.6 (s), 1181.9 (m), 1124.4 (w), 1077.5 (m), 1049.8 (w), 1020.3 (w), 867.9 (m), 839.6 (m), 811.5 (m), 769.3 (s), 745.0 (s), 693.4 (m), 631.9 (m) cm^{-1}. **^{1}H NMR** (400 MHz, $CDCl_3$): *δ* (ppm) = 8.05 (d, $^3J_{HH}$ = 9.1 Hz, 1H, *H*4'), 7.94 (*apparent*-t (dd), $^3J_{HH}$ = 8.3 Hz, 2H, *H*5/*H*5'), 7.71 (d, $^3J_{HH}$ = 8.6 Hz, 1H, *H*4), 7.55-7.22 (m, 5H, *H*3/*H*3'/*H*6/*H*16/*H*16'), 7.38-7.26 (m, 4H, *H*6'/*H*7/*H*7'/*H*8), 7.25-7.20 (m, 3H, *H*14 or *H*14'/*H*15/*H*15'), 7.17 (*apparent*-t (dd), $^3J_{HH}$ = 7.8 Hz, 1H, *H*14 or *H*14'), 7.08 (d, $^3J_{HH}$ = 8.5 Hz, 1H, *H*8'), 6.95-6.92 (m, 1H, *H*13'), 6.82 (d, $^3J_{HH}$ = 8.0 Hz, 1H, *H*13), 3.89 (s, 3H, O*C*H_3). **^{13}C{^{1}H} NMR** (101 MHz, $CDCl_3$): *δ* (ppm) = 155.9 (d, $^4J_{CP}$ = 3.3 Hz, *C*2'), 151.5 (*overlapping*-d, *C*12/*C*12'), 141.6 (d, $^2J_{CP}$ = 38.0 Hz, *C*1), 136.7 (d, $^1J_{CP}$ = 37.3 Hz, *C*2), 135.3 (*C*10), 135.0 (d, $^4J_{CP}$ = 2.4 Hz, *C*9'), 132.9 (d, $^3J_{CP}$ = 5.0 Hz, *C*9), 132.4 (d, $^3J_{CP}$ = 4.0 Hz, *C*11'), 132.1 (d, $^3J_{CP}$ = 2.9 Hz, *C*11), 130.8 (*C*4'), 129.9 (*C*16 or *C*16'), 129.7 (*C*16 or *C*16'), 129.2 (*C*14 or *C*14'), 129.0 (*C*14 or *C*14'), 128.7 (*C*10'), 128.3 (*C*5 or *C*5'), 128.1 (*C*5 or *C*5'), 127.6 (*C*6), 127.0 (*C*4), 126.9 (*C*7 or *C*7'), 126.6 (d, $^4J_{CP}$ = 2.3 Hz, *C*8), 126.4 (*C*7 or *C*7'), 125.7 (*C*8'), 125.0 (*C*15'), 124.8 (*C*15), 124.6 (d, $^2J_{CP}$ = 1.9 Hz, *C*3), 123.8 (*C*6'), 122.6 (*C*13), 122.3 (*C*13'), 119.3 (d, $^3J_{CP}$ = 10.1 Hz, *C*1'), 112.9 (*C*3'), 56.3 (O*C*H_3). **^{31}P{^{1}H} NMR** (162 MHz, $CDCl_3$): *δ* (ppm) = 180.0 (s). **HRMS** (ASAP$^+$, solid): Found: *m*/*z* = 499.1449. Calculated for $[M + H]^+$: *m*/*z* = 499.1458.

2.4.13 (*S*)-3,3'-Dimethyl-[1,1'-biphenyl]-2,2'-diyl [1,1'-binaphthalen]-2-yl phosphonite (*S*)-**30a**

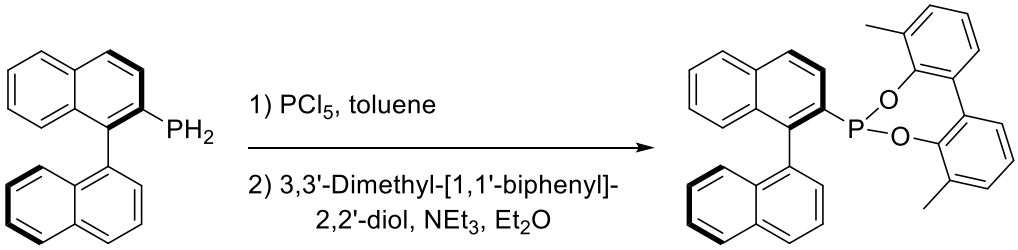

(*S*)-[1,1'-Binaphthalen]-2-yl) phosphine ((*S*)-**12a**, 429 mg, 1.50 mmol, 1.0 eq.) was dissolved in toluene (10 mL) and phosphorus pentachloride (687 mg, 3.30 mmol, 2.2 eq.) was added. The reaction mixture was stirred for 45 min, after which the volatiles were removed *in vacuo*. The residue was dissolved in diethyl ether (14 mL) and triethylamine (0.92 mL, 668 mg, 6.60 mmol, 4.4 eq.) was added. The reaction mixture was then left to stir for 10 min before 3,3'-dimethyl-[1,1'-biphenyl]-2,2'-diol (321 mg, 1.50 mmol, 1.0 eq.) was added and stirring continued overnight. The volatiles were removed *in vacuo* and the crude compound was filtered through a plug of alumina (diethyl ether) to yield the pure title compound as a white solid (678 mg, 1.37 mmol, 91%). R_f = 0.95 (alumina; diethyl ether).

MP: 202-203 °C. $[\boldsymbol{\alpha}]_{\boldsymbol{D}}^{\boldsymbol{20}}$ = +58° ($CHCl_3$, *c* = 0.1). **IR** (neat): ν = 3054.7 (w), 1455.4 (s), 1417.0 (m), 1364.0 (w), 1318.2 (w), 1250.4 (w), 1195.6 (m), 1165.0 (m), 1120.5 (w), 1082.0 (m), 1025.4 (w), 922.0 (w), 878.1 (s), 798.4 (m), 769.2 (s), 736.0 (s), 696.0 (s), 630.7 (m) cm^{-1}. **^{1}H NMR** (400 MHz, $CDCl_3$): *δ* (ppm) = 8.02 (dd, $^3J_{HH}$ = 7.8 Hz, $^4J_{HH}$ = 1.5 Hz, 1H, *H*4'), 7.97 (d, $^3J_{HH}$ = 8.3 Hz, 1H, *H*5'), 7.90 (d, $^3J_{HH}$ = 8.2 Hz, 1H, *H*5), 7.74 (d, $^3J_{HH}$ = 8.5 Hz, 1H, *H*4), 7.69-7.62 (m, 2H, *H*2'/*H*3'), 7.56-7.47 (m, 3H, *H*3/*H*6/*H*6'), 7.39-7.23 (m, 6H, *H*7/*H*7'/*H*8/*H*8'/*H*16/*H*16'), 7.16-7.07 (m, 4H, *H*14/*H*14'/*H*15/*H*15'), 2.00 (s, 3H, CH_3), 1.84 (s, 3H, CH_3'). **^{13}C{^{1}H} NMR** (101 MHz, $CDCl_3$): *δ* (ppm) = 149.6 (*overlapping*-d, *C*12/*C*12'), 144.6 (d, $^2J_{CP}$ = 38.2 Hz, *C*1), 138.3 (d, $^1J_{CP}$ = 39.0 Hz, *C*2), 135.5 (d, $^3J_{CP}$ = 10.4 Hz, *C*1'), 135.0 (*C*10), 134.0 (d, $^4J_{CP}$ = 3.7 Hz, *C*9'), 133.4 (*C*10'), 133.0 (d, $^3J_{CP}$ = 4.9 Hz, *C*9), 132.4 (d, $^3J_{CP}$ = 4.6 Hz, *C*11 or *C*11'), 131.9 (d, $^3J_{CP}$ = 2.7 Hz, *C*11 or *C*11'), 130.9, 130.7, 130.6 (*C*14'), 130.4 (*C*14), 129.7 (d, $^4J_{CP}$ = 5.5 Hz, *C*2'), 128.8 (*C*4'), 128.5 (*C*5'), 128.2 (*C*5), 128.0, 127.8, 127.7, 127.4, 127.4 (*C*4), 126.7, 126.6, 126.5, 126.1, 125.0 (*C*3'), 124.6 (*C*15 or *C*15'), 124.4 (*C*15 or *C*15'), 123.9 (*C*3), 16.7 (*C*H_3'), 16.4 (*C*H_3). **^{31}P{^{1}H} NMR** (162 MHz, $CDCl_3$): *δ* (ppm) = 172.4 (s). **HRMS** (ASAP$^+$, solid): Found: *m*/*z* = 497.1657. Calculated for $[M + H]^+$: *m*/*z* = 497.1665.

2.4.14 (*R*)-3,3'-Dimethyl-[1,1'-biphenyl]-2,2'-diyl (2'-methoxy-[1,1'-binaphthalen]-2-yl) phosphonite (*R*)-**30b**

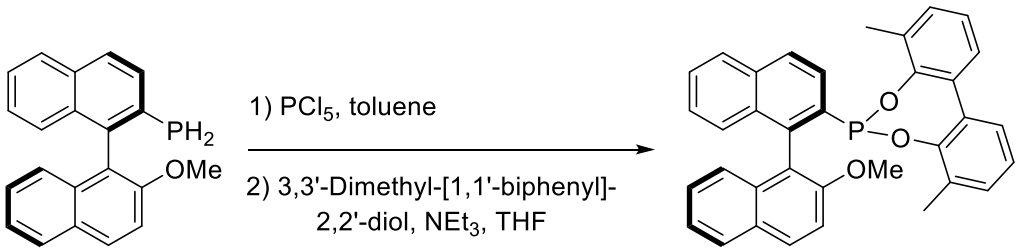

(*R*)-(2'-Methoxy-[1,1'-binaphthalen]-2-yl) phosphine ((*R*)-**12b**, 474 mg, 1.50 mmol, 1.0 eq.) was dissolved in toluene (10 mL) and phosphorus pentachloride (687 mg, 3.30 mmol, 2.2 eq.) was added. The reaction mixture was stirred for 45 min, after which the volatiles were removed *in vacuo*. The residue was dissolved in THF (14 mL) and triethylamine (0.92 mL, 668 mg, 6.60 mmol, 4.4 eq.) was added. The reaction mixture was then left to stir for 10 min, before 3,3'-dimethyl-[1,1'-biphenyl]-2,2'-diol (321 mg, 1.50 mmol, 1.0 eq.) was added and stirring continued overnight. The volatiles were removed *in vacuo* and the crude compound was filtered through a plug of alumina (diethyl ether) to yield the pure title compound as a white solid (695 mg, 1.32 mmol, 88%). R_f = 0.90 (alumina; diethyl ether).

MP: 203-205 °C. $[\alpha]_D^{20}$ = +48° ($CHCl_3$, *c* = 0.1). **IR** (neat): ν = 3054.3 (w), 2924.8 (w), 1602.1 (w), 1593.6 (w), 1510.1 (w), 1458.7 (m), 1414.9 (m), 1333.9 (w), 1250.2 (m), 1203.6 (m), 1077.0 (m), 1021.5 (m), 918.0 (w), 885.0 (m), 869.0 (m), 809.8 (m), 769.6 (m), 746.5 (m), 696.6 (m), 632.1 (m) cm^{-1}. **^{1}H NMR** (400 MHz, $CDCl_3$): *δ* (ppm) = 8.05 (d, $^3J_{HH}$ = 9.1 Hz, 1H, *H*4'), 7.94 (d, $^3J_{HH}$ = 8.2 Hz, 2H, *H*5/*H*5'), 7.74 (d, $^3J_{HH}$ = 8.5 Hz, 1H, *H*4), 7.53 (*apparent*-t (dd), $^3J_{HH}$ = 7.4 Hz, 1H, *H*6), 7.49-7.44 (m, 2H, *H*3/*H*3'), 7.38-7.24 (m, 6H, *H*6'/*H*7/*H*7'/*H*8/*H*16/*H*16'), 7.17-7.15 (m, 2H, *H*14/H14'), 7.13-7.10 (m, 3H, *H*8'/*H*15/*H*15'), 3.86 (s, 3H, OCH_3), 1.99 (s, 3H, CH_3'), 1.87 (s, 3H, CH_3). **^{13}C{^{1}H} NMR** (101 MHz, $CDCl_3$): *δ* (ppm) = 155.4 (d, $^4J_{CP}$ = 3.3 Hz, *C*2'), 149.8 (*overlapping*-d, *C*12/*C*12'), 141.4 (d, $^2J_{CP}$ = 40.6 Hz, *C*1), 138.4 (d, $^1J_{CP}$ = 37.8 Hz, *C*2), 135.4 (*C*10), 135.0 (d, $^4J_{CP}$ = 3.2 Hz, *C*9'), 132.8 (d, $^3J_{CP}$ = 5.9 Hz, *C*9), 132.3 (d, $^3J_{CP}$ = 3.8 Hz, *C*11 or *C*11'), 132.1 (d, $^3J_{CP}$ = 3.4 Hz, *C*11 or *C*11'), 131.0 (*C*16 or *C*16'), 130.7 (*C*16 or *C*16'), 130.6 (*C*4'), 130.5 (*C*14'), 130.5 (*C*14), 128.8 (*C*10'), 128.3 (*C*5), 128.2 (*C*5'), 127.9 (*C*13 or *C*13'), 127.8 (*C*13 or *C*13'), 127.6 (*C*6), 127.3 (*C*4), 127.0 (d, $^4J_{CP}$ = 2.4 Hz, *C*8), 126.9 (*C*7'), 126.5 (*C*7), 125.5 (*C*8'), 124.5 (*C*15 or *C*15'), 124.4 (*C*15 or *C*15'), 124.2 (d, $^2J_{CP}$ = 1.2 Hz, *C*3), 123.7 (*C*6'), 119.9 (d, $^3J_{CP}$ = 10.6 Hz, *C*1'), 112.8 (*C*3'), 56.3 (OCH_3), 16.4 (CH_3'), 16.2 (CH_3). **^{31}P{^{1}H} NMR** (162 MHz, $CDCl_3$): *δ* (ppm) = 174.2 (s). **HRMS** (NSI^+, DCM/MeOH): Found: *m*/*z* = 527.1761. Calculated for $[M + H]^+$: *m*/*z* = 527.1771.

2.4.15 2,2'-Dihydroxy-3,3'-dimethyl-1,1'-biphenyl

2,2'-Dimethoxy-1,1'-biphenyl

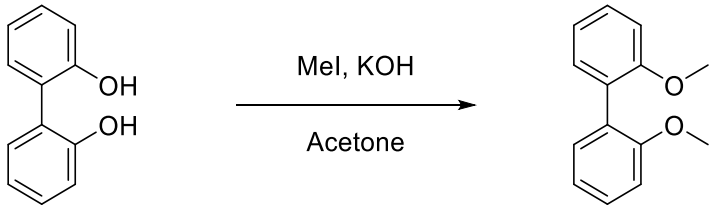

2,2'-Dihydroxy-1,1'-biphenyl (5.00 g, 26.9 mmol, 1.0 eq.) was dissolved in acetone (100 mL). Potassium hydroxide (6.04 g, 108 mmol, 4.0 eq.) was added to the solution and the reaction mixture was stirred for 15 min, after which methyl iodide (6.70 mL, 15.3 g, 108 mmol, 4.0 eq.) was added. The reaction mixture was stirred for 16 h, the volatiles were removed *in vacuo* and the residue dissolved in diethyl ether (100 mL). The organic phase was washed with water (100 mL), 1.0 M aq. HCl (50 mL) and 0.2 M aq. $NaHCO_3$ (50 mL), dried over $MgSO_4$ and the volatiles were removed *in vacuo*. Silica gel flash chromatography (petrol/ethyl acetate, 9:1) yielded the pure title compound as a white solid (4.63 g, 21.6 mmol, 80%). R_f = 0.50 (silica gel; petrol/ethyl acetate, 9:1). The physical and spectroscopic properties matched those reported in the literature.[128]

MP: 156-158 °C (Lit.[128] 155-156 °C). **^{1}H NMR** (400 MHz, $CDCl_3$): δ = 7.33 (ddd, $^3J_{HH}$ = 7.8 Hz, $^3J_{HH}$ = 7.8 Hz, $^4J_{HH}$ = 1.8 Hz, 2H), 7.25 (dd, $^3J_{HH}$ = 7.4 Hz, $^4J_{HH}$ = 1.8 Hz, 2H), 7.03-6.96 (m, 4H), 3.77 (s, 6H) ppm. **^{13}C{^{1}H} NMR** (101 MHz, $CDCl_3$): δ = 157.1, 131.6, 128.7, 127.9, 120.4, 111.2, 55.8 ppm.

2,2'-Dimethoxy-3,3'-dimethyl-1,1'-biphenyl

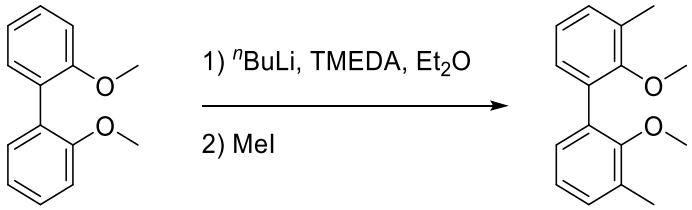

2,2'-Dimethoxy-1,1'-biphenyl (2.00 g, 9.33 mmol, 1.0 eq.) was dissolved in diethyl ether (120 mL). TMEDA (6.8 mL, 5.3 g, 45 mmol, 4.8 eq.) was added and the reaction mixture was cooled to 0 °C. *n*-Butyllithium (2.2 M solution in hexanes, 19 mL, 2.7 g, 42 mmol, 4.5 eq.) was added and the reaction mixture was left to stir at 0 °C for 1 h, after which it was heated to 40 °C and refluxed for 18 h. After cooling to 0 °C, methyl iodide (3.0 mL, 6.8 g, 48 mmol, 5.1 eq.) was added and the reaction mixture was left to stir for 1.5 h, before the reaction was quenched with 1.0 M aq. HCl (20 mL). The organic layer was separated, washed with 2.0 M aq. $NaHCO_3$ (2 x 50 mL) and brine (2 x 50 mL), dried over $MgSO_4$ and the volatiles were removed *in vacuo*. The title compound was obtained as a yellow oil

(2.12 g, 8.75 mmol, 94%) and reacted without purification. The ^{1}H NMR spectroscopic data matched that of data reported in the literature.[129]

^{1}H NMR (400 MHz, $CDCl_3$): δ = 7.20-7.14 (m, 4H), 7.25 (*apparent*-t (dd), $^{3}J_{HH}$ = 7.5 Hz, 2H), 3.40 (s, 6H), 2.34 (s, 6H) ppm.

2,2'-Dihydroxy-3,3'-dimethyl-1,1'-biphenyl

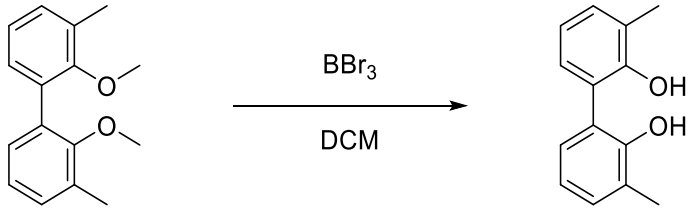

Boron tribromide (1.0 M solution in DCM, 12 mL, 3.0 g, 12 mmol, 4.0 eq.) was diluted with DCM (10 mL) and cooled to 0 °C. 2,2'-Dimethoxy-3,3'-dimethyl-1,1'-biphenyl (730 mg, 3.01 mmol, 1.0 eq.) was dissolved in DCM (20 mL) and added to the solution. The reaction mixture was allowed to warm to room temperature and stirred for 18 h. The reaction mixture was cooled to 0 °C and quenched with water (20 mL). The organic phase was separated and the aqueous phase extracted with DCM (20 mL). The combined organic extracts were washed with brine (3 x 20 mL), dried over $MgSO_4$ and the volatiles were removed *in vacuo*. Silica gel flash chromatography (petrol/ethyl acetate, 20:1) yielded the pure title compound as a dark pink solid (540 mg, 2.52 mmol, 84%). R_f = 0.20 (silica gel; petrol/ethyl acetate, 20:1).

MP: 90-92 °C (Lit.[130] 85-86 °C). **IR** (neat): ν = 3029.6 (s), 1587.5 (w), 1451.4 (m), 1324.0 (m), 1240.1 (m), 1198.9 (s), 1165.9 (m), 1124.9 (m), 1088.9 (m), 839.6 (m), 759.5 (s) cm^{-1}. **^{1}H NMR** (400 MHz, $CDCl_3$): δ = 7.19 (d, $^{3}J_{HH}$ = 7.5 Hz, 2H, *H*4), 7.06 (d, $^{3}J_{HH}$ = 7.5 Hz, 2H, *H*6), 6.93 (dd, $^{3}J_{HH}$ = 7.5 Hz, $^{3}J_{HH}$ = 7.5 Hz, 2H, *H*5), 5.17 (br s, 2H, O*H*), 2.31 (s, 6H, CH_3) ppm. **^{13}C{^{1}H} NMR** (101 MHz, $CDCl_3$): δ = 151.6 (*C*2), 131.6 (*C*4), 128.4 (*C*6), 125.6 (*C*3), 122.1 (*C*1), 121.0 (*C*5), 16.3 (*C*H_3) ppm. **HRMS** (ASAP^{+}, solid): Found: *m*/*z* = 215.1067. Calculated for $[M + H]^{+}$: *m*/*z* = 215.1067.

2.4.16 [Pd((*S*)-**29a**)(η^3-C_4H_7)Cl] (*S*)-**31a**

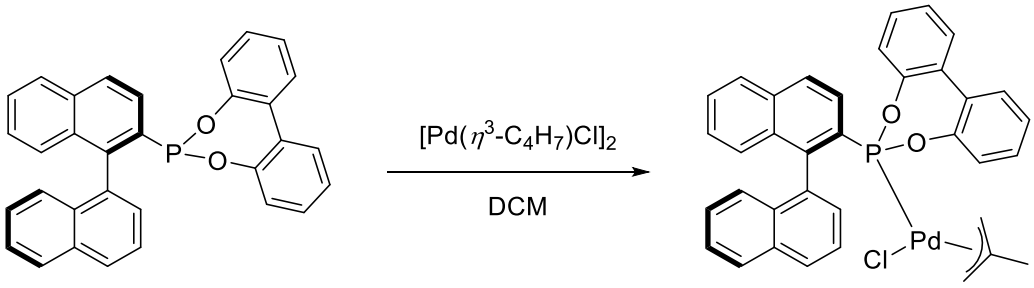

(*S*)-**29a** (18.7 mg, 39.9 µmol, 1.0 eq.) and chloro(2-methylallyl)palladium(II) dimer (7.9 mg, 20 µmol, 0.5 eq.) were dissolved in DCM (0.5 mL) and stirred for 10 min; the title complex formed quantitatively as two isomers (isomer A 58%; isomer B 42%). Single crystals were grown by slow diffusion of diethyl ether into a DCM solution.

MP: 142-144 °C (decomp.). **IR** (neat): ν = 3059.6 (w), 1497.7 (m), 1475.9 (m), 1433.1 (m), 1367.6 (w), 1247.4 (m), 1202.6 (m), 1120.4 (w), 1095.7 (m), 1044.3 (w), 946.6 (w), 905.8 (s), 884.8 (m), 834.6 (w), 783.6 (s), 771.5 (s), 713.3 (m), 688.9 (m), 636.6 (m), 605.6 (m) cm^{-1}. **^{1}H NMR** (500 MHz, CD_2Cl_2, −20 °C): *δ* (ppm) = 8.16 (dd, $^3J_{HH}$ = 7.0 Hz, $^3J_{HH}$ = 0.9 Hz, 1H, *H*4'^{A}), 8.04-7.96 (m, 6H), 7.95-7.89 (m, 3H, *H*3^B/*H*4^A/*H*4^B), 7.83 (dd, $^3J_{HH}$ = 7.0 Hz, $^3J_{HH}$ = 0.9 Hz, 1H, *H*4'^{B}), 7.76 (dd, $^3J_{HH}$ = 8.7 Hz, $^3J_{HP}$ = 5.1 Hz, 1H, *H*3^A), 7.75-7.70 (m, 2H, *H*3'^{A}/*H*3'^{B}), 7.65-7.61 (m, 2H), 7.60-7.46 (m, 10H), 7.44-7.30 (m, 10H), 7.29-7.24 (m, 2H), 7.22 (d, $^3J_{HH}$ = 8.6 Hz, 1H, *H*^{A}), 7.18 (d, $^3J_{HH}$ = 8.6 Hz, 1H, *H*^{B}), 6.97 (d, $^3J_{HH}$ = 8.1 Hz, 1H, *H*13^B), 6.78 (d, $^3J_{HH}$ = 8.1 Hz, 1H, *H*13^A), 4.20 (dd, $^3J_{HP}$ = 10.1 Hz, $^4J_{HH}$ = 2.9 Hz, 1H, allyl-*H*t$_{syn}^A$), 3.77 (dd, $^3J_{HP}$ = 9.8 Hz, $^4J_{HH}$ = 2.9 Hz, 1H, allyl-*H*t$_{syn}^B$), 2.67-2.62 (m, 2H, allyl-*H*c$_{syn}^B$/allyl-*H*t$_{anti}^A$), 2.44 (br s, 1H, allyl-*H*c$_{syn}^A$), 1.58 (d, $^3J_{HP}$ = 14.1 Hz, 1H, allyl-*H*t$_{anti}^B$), 1.17 (s, 3H, allyl-C*H*$_3^A$), 1.16 (s, 3H, allyl-C*H*$_3^B$), 0.82 (br s, 1H, allyl-*H*c$_{anti}^B$), 0.61 (br s, 1H, allyl-*H*c$_{anti}^A$). **^{13}C{^{1}H} NMR** (126 MHz, CD_2Cl_2, −20 °C): *δ* (ppm) = 150.1 (m, *C*12^A/ *C*12^B/*C*12'^{A}/*C*12'^{B}), 144.7 (*overlapping*-d, *C*1^A/ *C*1^B), 135.3 , 135.1, 134.4 (d, $^3J_{CP}$ = 10.1 Hz, *C*1'^{A}), 134.2 (d, $^3J_{CP}$ = 9.4 Hz, *C*1'^{B}), 133.9 (*C*9'^{A}), 133.6, 133.5, 133.5, 133.4, 133.3, 133.2, 133.1, 132.8 (*C*9'^{B}), 131.2 (*C*4'^{A}), 131.1 (*C*4'^{B}), 130.8, 130.8, 130.7, 130.5, 130.4, 130.3, 129.9, 129.4, 129.2, 129.1, 128.9, 128.6, 128.4, 128.3, 128.2, 127.9, 127.7, 127.5, 127.2, 127.1, 127.0, 126.9, 126.9, 126.8, 126.5, 126.3, 126.2, 126.1, 125.9, 125.8, 125.6, 125.4, 124.7, 124.3, 123.2, 123.0, 121.6 (*C*13^A), 120.9 (*C*13^B), 77.4 (d, $^2J_{CP}$ = 46.3 Hz, allyl-*C*t^A), 76.5 (d, $^2J_{CP}$ = 44.8 Hz, allyl-*C*t^B), 57.4 (allyl-*C*c^A), 56.3 (allyl-*C*c^B), 22.8 (allyl-*C*H$_3^A$/allyl-*C*H$_3^B$). **^{31}P{^{1}H} NMR** (202 MHz, CD_2Cl_2, −20 °C): *δ* (ppm) = 173.6 (s, *P*^{B}), 172.0 (s, *P*^{A}). **HRMS** (ASAP$^+$, solid): Found: *m*/*z* = 625.0888. Calculated for [M − Cl]$^+$: *m*/*z* = 625.0878.

2.4.17 [Pd((*S*)-**30a**)(η^3-C_4H_7)Cl] (*S*)-**32a**

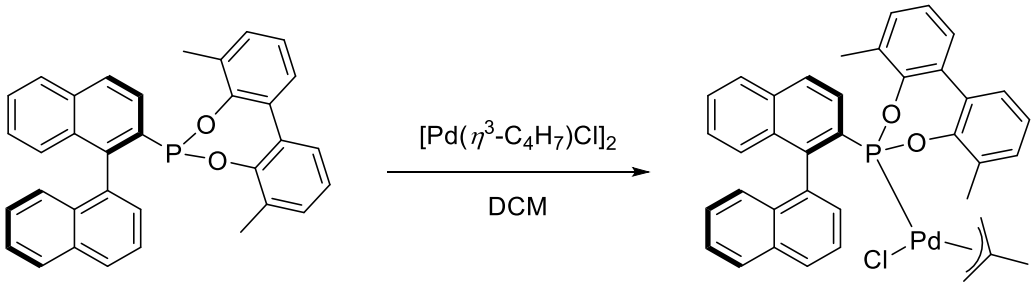

(*S*)-**30a** (19.9 mg, 40.0 µmol, 1.0 eq.) and chloro(2-methylallyl)palladium(II) dimer (7.9 mg, 20 µmol, 0.5 eq.) were dissolved in DCM (0.5 mL) and stirred for 10 min; the title complex formed quantitatively as two isomers (isomer A 58%; isomer B 42%). Single crystals were grown by hexane layering of a DCM solution.

MP: 147-149 °C (decomp.). **IR** (neat): ν = 3048.8 (w), 1558.2 (w), 1454.9 (m), 1418.3 (m), 1187.0 (m), 1126.3 (w), 1087.3 (m), 1025.8 (w), 947.3 (w), 888.3 (s), 802.3 (m), 770.3 (s), 710.2 (m), 635.1 (s), 610.1 (m) cm^{-1}. **^{1}H NMR** (500 MHz, CD_2Cl_2, −20 °C): δ (ppm) = 8.33 (dd, $^3J_{HP}$ = 14.0 Hz, $^3J_{HH}$ = 8.7 Hz, 1H, *H*3^B), 8.17 (d, $^3J_{HH}$ = 8.7 Hz, 1H, *H*4^B), 8.04-7.95 (m, 4H, *H*3^A), 7.91-7.87 (m, 2H, *H*4'^{A}/*H*5'^{A}), 7.79 (d, $^3J_{HH}$ = 8.3 Hz, 1H, *H*^{B}), 7.70 (d, $^3J_{HH}$ = 8.2 Hz, 1H, *H*^{B}), 7.63-7.58 (m, 2H), 7.52 (d, $^3J_{HH}$ = 6.9 Hz, 1H, *H*2'^{A}), 7.48-7.38 (m, 3H), 7.35-7.09 (m, 20H, *H*8^A/*H*8^B/*H*14'A/*H*14'^{B}/*H*15^A/*H*15^B/*H*15'^{A}/*H*15'^{B}/*H*16^A/*H*16^B/*H*16'^{A}/*H*16'^{B}), 7.05-7.01 (m, 2H, *H*14^A/*H*14^B), 4.34 (dd, $^3J_{HP}$ = 9.9 Hz, $^4J_{HH}$ = 2.8 Hz, 1H, allyl-*H*t$_{syn}^B$), 4.06 (dd, $^3J_{HP}$ = 10.2 Hz, $^4J_{HH}$ = 2.8 Hz, 1H, allyl-*H*t$_{syn}^A$), 3.25 (br s, 1H, allyl-*H*c$_{syn}^A$), 3.16 (d, $^3J_{HP}$ = 13.8 Hz, 1H, allyl-*H*t$_{anti}^B$), 3.00 (br s, 1H, allyl-*H*c$_{syn}^B$), 2.57 (d, $^3J_{HP}$ = 14.3 Hz, 1H, allyl-*H*t$_{anti}^A$), 2.27 (br s, 1H, allyl-*H*c$_{anti}^A$), 2.24 (s, 3H, C*H*$_3$'^{A}), 2.13 (br s, 1H, allyl-*H*c$_{anti}^B$), 1.81 (s, 3H, C*H*$_3$'^{B}), 1.63 (s, 6H, C*H*$_3^A$/C*H*$_3^B$), 1.52 (s, 3H, allyl-C*H*$_3^B$), 1.47 (s, 3H, allyl-C*H*$_3^A$). **^{13}C{^{1}H} NMR** (126 MHz, CD_2Cl_2, −20 °C): δ (ppm) = 148.8 (d, $^2J_{CP}$ = 13.4 Hz, *C*12'^{B}), 148.4 (d, $^2J_{CP}$ = 12.8 Hz, *C*12^A), 148.0 (d, $^2J_{CP}$ = 7.4 Hz, *C*12'^{A}), 147.3 (d, $^2J_{CP}$ = 7.6 Hz, *C*12^B), 143.3 (d, $^2J_{CP}$ = 18.2 Hz, *C*1^A), 142.6 (d, $^2J_{CP}$ = 6.7 Hz, *C*1^B), 135.5 (d, $^3J_{CP}$ = 2.5 Hz, *C*1'^{B}), 135.2 (d, $^3J_{CP}$ = 7.1 Hz, *C*1'^{A}), 134.9, 134.8, 134.7 (d, $^2J_{CP}$ = 8.8 Hz, allyl-*C*^{B}), 134.0 (d, $^2J_{CP}$ = 9.0 Hz, allyl-*C*^{A}), 133.9 (*C*9'^{A}), 133.5, 133.2, 133.1, 133.0, 132.5, 131.5, 131.5, 131.3, 131.2 (d, J_{CP} = 2.8 Hz), 131.0 (d, J_{CP} = 2.2 Hz), 130.9, 130.8, 130.7 (d, J_{CP} = 2.2 Hz), 130.7, 130.5 (d, J_{CP} = 2.8 Hz), 130.4 (d, J_{CP} = 2.8 Hz), 130.2 (d, J_{CP} = 2.2 Hz), 130.2 (d, J_{CP} = 1.9 Hz), 128.8 (*C*2'^{A}), 128.6, 128.4, 128.3 (*C*4'^{A}), 128.3, 128.3, 128.1, 128.0, 127.9, 127.8, 127.6, 127.6, 127.5, 127.0, 126.9, 126.8, 126.8, 126.0, 125.9, 125.8, 125.8, 125.6, 125.5, 125.4, 125.4, 125.1, 124.3 (*C*3'^{A}/*C*3'^{B}), 78.3 (d, $^2J_{CP}$ = 44.7 Hz, allyl-*C*t^B), 77.8 (d, $^2J_{CP}$ = 45.7 Hz, allyl-*C*t^A), 59.3 (d, $^2J_{CP}$ = 5.1 Hz, allyl-*C*c^A), 57.4 (d, $^2J_{CP}$ = 3.5 Hz, allyl-*C*c^B), 22.9 (allyl-*C*H$_3^A$), 22.8 (allyl-*C*H$_3^B$), 17.6 (*C*H$_3$'^{A}), 17.2 (*C*H$_3^A$), 16.8 (*C*H$_3$'^{B}), 16.5 (*C*H$_3^B$). **^{31}P{^{1}H} NMR** (202 MHz, CD_2Cl_2, −20 °C): δ (ppm) = 177.6 (s, *P*^{B}), 172.9 (s, *P*^{A}). **HRMS** (NSI$^+$, DCM/MeOH + NH_4OAc): Found: *m*/*z* = 653.1190. Calculated for [M − Cl]$^+$: *m*/*z* = 653.1191.

2.4.18 [Pd((*S*)-**30a**)(η^3-C_4H_7)]BAr^F (*S*)-**33a**

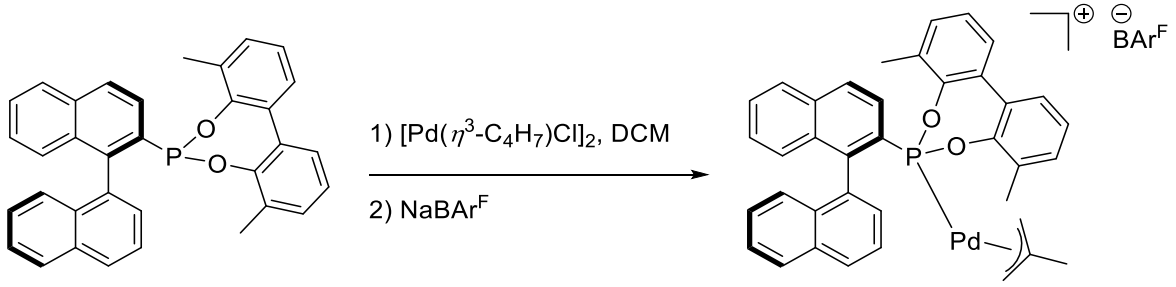

(*S*)-**30a** (19.9 mg, 40.0 µmol, 1.0 eq.) and chloro(2-methylallyl)palladium(II) dimer (7.9 mg, 20 µmol, 0.5 eq.) were dissolved in DCM (2.0 mL) and stirred for 10 min, before sodium tetrakis[3,5-bis(trifluoromethyl)phenyl]borate (35.4 mg, 40 µmol, 1.0 eq.) was added and stirred for 30 min. The reaction mixture was filtered through Celite® to yield the title complex quantitatively as two isomers (isomer A 48%; isomer B 52%).

MP: 128-130 °C. **IR** (neat): ν = 3068.1 (w), 1610.9 (w), 1504.7 (w), 1462.7 (w), 1421.6 (w), 1353.9 (s), 1273.8 (s), 1160.6 (m), 1117.5 (s), 948.6 (w), 909.9 (m), 887.1 (m), 839.0 (m), 803.0 (m), 765.5 (m), 745.1 (m), 712.4 (s), 681.5 (s), 669.7 (s), 637.1 (m) cm^{-1}. **^{1}H NMR** (500 MHz, CD_2Cl_2, 0 °C): δ (ppm) = 8.34 (dd, $^3J_{HH}$ = 8.4 Hz, $^3J_{HH}$ = 6.4 Hz, 1H, *H*3'^{A}), 8.27 (dd, $^3J_{HH}$ = 8.5 Hz, $^3J_{HH}$ = 6.4 Hz, 1H, *H*3'^{B}), 8.16 (d, $^3J_{HH}$ = 8.2 Hz, 1H, *H*5'^{B}), 8.13 (d, $^3J_{HH}$ = 8.2 Hz, 1H, *H*5'^{A}), 8.11-8.00 (m, 6H, *H*4^A/*H*4^B/*H*4'^{A}/*H*4'^{B}/*H*5^A/*H*5^B), 7.81-7.75 (m, 18H, *H*6'^{A}/*H*6'^{B}/*ortho*-BAr^F), 7.68-7.33 (m, 23H, *H*2'^{A}/*H*6^A/*H*6^B/*H*7'^{A}/*H*7'^{B}/*H*8'^{A}/*H*8'^{B}/*H*14^A/*H*14^B/*H*14'^{A}/*H*14'^{B}/*H*16^A/*H*16^B/*H*16'^{A}/*H*16'^{B}/*para*-BAr^F), 7.30-7.25 (m, 2H, *H*7^A/*H*7^B), 7.21-6.91 (m, 7H, *H*2'^{B}/*H*3^A/*H*3^B/*H*15^A/*H*15^B/*H*15'^{A}/*H*15'^{B}), 6.05 (d, $^3J_{HH}$ = 8.6 Hz, 1H, *H*8^A), 5.99 (d, $^3J_{HH}$ = 8.6 Hz, 1H, *H*8^B), 4.13 (d, $^3J_{HP}$ = 13.8 Hz, 1H, allyl-*H*t$_{anti}^A$), 3.43 (dd, $^3J_{HP}$ = 9.7 Hz, $^4J_{HH}$ = 2.4 Hz, 1H, allyl-*H*t$_{syn}^B$), 3.09 (br s, 1H, allyl-*H*c$_{syn}^B$), 3.00 (br s, 1H, allyl-*H*c$_{syn}^A$), 2.59 (br d, $^3J_{HP}$ = 9.0 Hz, 1H, allyl-*H*t$_{syn}^A$), 2.48 (d, $^3J_{HP}$ = 13.6 Hz, 1H, allyl-*H*t$_{anti}^B$), 2.35 (br s, 4H, allyl-*H*c$_{anti}^A$/aryl-C*H*$_3$), 2.31 (br s, 4H, allyl-*H*c$_{anti}^B$/aryl-C*H*$_3$), 2.11 (s, 3H, aryl-C*H*$_3$), 2.02 (s, 3H, aryl-C*H*$_3$), 1.88 (s, 3H, allyl-C*H*$_3^B$), 0.96 (s, 3H, allyl-C*H*$_3^A$). **^{11}B NMR** (160 MHz, CD_2Cl_2, 0 °C): δ (ppm) = −6.6 (s). **^{13}C{^{1}H} NMR** (126 MHz, CD_2Cl_2, 0 °C): δ (ppm) = 161.8 (q, $^1J_{CB}$ = 49.7 Hz, *ipso*-BAr^F), 147.8 (m, *C*12^A/*C*12^B/*C*12'^{A}/*C*12'^{B}), 144.1 (*overlapping*-d, *C*1^A/*C*1^B), 140.8 (d, $^2J_{CP}$ = 10.7 Hz, allyl-*C*^{B}), 138.3 (d, $^2J_{CP}$ = 10.4 Hz, allyl-*C*^{A}), 137.5 (d, $^1J_{CP}$ = 45.4 Hz, *C*2^B), 137.2 (d, $^1J_{CP}$ = 44.7 Hz, *C*2^A), 136.5 (d, $^4J_{CP}$ = 1.0 Hz, *C*10^B), 136.5 (d, $^4J_{CP}$ = 1.0 Hz, *C*10^A), 134.8 (*ortho*-BAr^F), 133.7 (*C*9'^{B}), 133.4 (*C*9'^{A}), 133.0 (d, J_{CP} = 4.6 Hz), 132.5 (d, J_{CP} = 3.2 Hz), 132.3 (d, $^3J_{CP}$ = 5.4 Hz, *C*9^B), 132.2 (d, $^3J_{CP}$ = 4.9 Hz, *C*9^A), 131.8, 131.7, 131.7, 131.2 (d, J_{CP} = 3.4 Hz), 131.0 (*C*3'^{B}), 130.8 (*C*3'^{A}), 130.7, 130.7, 130.5, 130.0, 129.8 (m), 129.7 (d, J_{CP} = 2.8 Hz), 129.6 (d, J_{CP} = 3.2 Hz), 129.5 (*C*5'^{B}), 129.4, 129.3 (*C*5'^{A}), 129.2, 129.1, 129.0, 128.9 (m), 128.8, 128.7 (m), 128.5, 128.4 (m), 128.3, 128.2 (d, J_{CP} = 10.0 Hz), 128.1 (m), 128.0, 128.0, 127.7 (d, $^3J_{CP}$ = 8.3 Hz, *C*1'^{B}), 127.5 (d, $^3J_{CP}$ = 7.7 Hz, *C*1'^{A}), 127.2, 127.1, 127.0, 126.8, 126.4, 126.1 (m), 126.0, 125.9, 125.8 (*C*8^A/*C*8^B), 125.1 (d, $^2J_{CP}$ = 10.7 Hz, *C*3^B), 124.7 (d, $^2J_{CP}$ = 7.3 Hz, *C*3^A), 124.6 (q,

$^{1}J_{CF}$ = 273 Hz, *C*F$_3$), 122.6, 122.5, 117.5 (septet, $^{3}J_{CF}$ = 3.8 Hz, *para*-BAr^F), 109.0 (*C*2'^{A}), 107.5 (*C*2'^{B}), 101.9 (d, $^{2}J_{CP}$ = 40.3 Hz, allyl-*C*t^A), 98.4 (d, $^{2}J_{CP}$ = 40.5 Hz, allyl-*C*t^B), 57.3 (d, $^{2}J_{CP}$ = 6.1 Hz, allyl-*C*c^B), 54.8 (d, $^{2}J_{CP}$ = 6.6 Hz, allyl-*C*c^A), 22.7 (allyl-*C*H$_3^B$), 21.4 (allyl-*C*H$_3^A$), 17.1 (aryl-*C*H$_3$), 16.8 (aryl-*C*H$_3$), 16.7 (aryl-*C*H$_3$), 16.6 (aryl-*C*H$_3$). **^{19}F NMR** (471 MHz, CD_2Cl_2, 0 °C): δ (ppm) = −62.7 (s). **^{31}P{^{1}H} NMR** (202 MHz, CD_2Cl_2, 0 °C): δ (ppm) = 170.1 (s, *P*^{B}), 169.5 (s, *P*^{A}). **HRMS** (NSI$^+$, DCM/MeOH + NH_4OAc): Found: *m*/*z* = 653.1194. Calculated for [M − BAr^F]$^+$: *m*/*z* = 653.1191.

2.4.19 General procedure for the asymmetric hydrosilylation of styrene derivatives

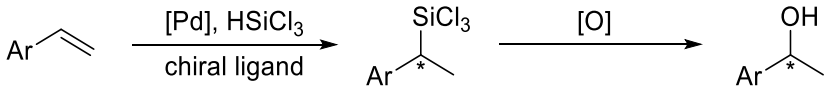

Phosphonite ligand (0.25 mol% or 0.50 mol%) and chloro(allyl)palladium(II) dimer (0.125 mol%) were dissolved in the styrene (1.0 eq.) and stirred at room temperature for 20 min; for reactions at an external temperature of 0 °C, the reaction mixture was subsequently stirred for 20 min at this temperature. Trichlorosilane (1.2 eq.) was added and the conversion of the reaction was followed by ^{1}H NMR spectroscopy. The product was purified by Kugelrohr distillation (reduced pressure; 150-180 °C).

The product (400 mg) was dissolved in methanol (30 mL) and THF (30 mL); potassium carbonate (1.40 g, 10.1 mmol), potassium fluoride (600 mg, 10.3 mmol) and hydrogen peroxide solution (35 wt. % in water, 1.8 mL) were added and the reaction mixture left to stir overnight. The suspension was filtered and the volatiles were removed *in vacuo*. The residue was dissolved in diethyl ether (50 mL) and washed with water (3 x 50 mL), dried over $MgSO_4$ and the volatiles were removed *in vacuo*. Silica gel flash chromatography (petrol/ethyl acetate, 3:1) yielded the pure alcohol products, which were all obtained as colourless oils.

The ^{1}H and ^{13}C NMR spectroscopic data matched that of commercially acquired samples or data reported in the literature,[131] and the HRMS data was in accordance with the calculated values. The enantiomeric excess was determined by chiral GC or HPLC analysis; the absolute configuration was assigned by comparison of the measured sign of the optical rotation to literature data.[125,132]

1-Phenylethanol

R_f = 0.60 (silica gel; petrol/ethyl acetate, 3:1). **^{1}H NMR** (300 MHz, $CDCl_3$): δ (ppm) = 7.44-7.26 (m, 5H), 4.91 (q, $^{3}J_{HH}$ = 6.5 Hz, 1H), 2.08 (br s, 1H), 1.52 (d, $^{3}J_{HH}$ = 6.5 Hz, 3H). **^{13}C{^{1}H} NMR** (75 MHz, $CDCl_3$): δ (ppm) = 145.9, 128.5, 127.5, 125.4, 70.4, 25.2. **HRMS** (ASAP$^+$, solid): Found: *m*/*z* = 121.0646. Calculated for [M − H]$^+$: *m*/*z* = 121.0648.

GC conditions (Supelco β-dex 225) – injection temperature: 200 °C, detection temperature: 200 °C, oven temperature: 80 °C for 45 min, then ramp to 130 °C at 10 °C/min, retention times: 51.8 min (*R*) and 52.8 min (*S*).

1-[4-(Chloro)phenyl]ethanol

R_f = 0.50 (silica gel; petrol/ethyl acetate, 3:1). **^{1}H NMR** (300 MHz, $CDCl_3$): δ (ppm) = 7.25-7.17 (m, 4H), 4.77 (q, $^3J_{HH}$ = 6.4 Hz, 1H), 2.09 (br s, 1H), 1.37 (d, $^3J_{HH}$ = 6.4 Hz, 3H). **^{13}C{^{1}H} NMR** (75 MHz, $CDCl_3$): δ (ppm) = 144.3, 133.1, 128.6, 126.8, 69.7, 25.3. **HRMS** (ASAP$^+$, solid): Found: *m*/*z* = 155.0256. Calculated for $[M - H]^+$: *m*/*z* = 155.0258.

GC conditions (Supelco β-dex 225) – injection temperature: 200 °C, detection temperature: 200 °C, oven temperature: 100 °C for 45 min, then ramp to 180 °C at 10 °C/min, retention times: 53.9 min (*R*) and 54.2 min (*S*).

1-[4-(Methoxy)phenyl]ethanol

R_f = 0.30 (silica gel; petrol/ethyl acetate, 3:1). **^{1}H NMR** (300 MHz, $CDCl_3$): δ (ppm) = 7.23 (d, $^3J_{HH}$ = 8.7 Hz, 2H), 6.81 (d, $^3J_{HH}$ = 8.7 Hz, 2H), 4.78 (q, $^3J_{HH}$ = 6.4 Hz, 1H), 3.73 (s, 3H), 1.71 (br s, 1H), 1.51 (d, $^3J_{HH}$ = 6.4 Hz, 3H). **^{13}C{^{1}H} NMR** (75 MHz, $CDCl_3$): δ (ppm) = 159.0, 138.0, 126.7, 113.9, 70.0, 55.3, 25.0. **HRMS** (ASAP$^+$, solid): Found: *m*/*z* = 151.0750. Calculated for $[M - H]^+$: *m*/*z* = 151.0754.

GC conditions (Supelco β-dex 225) – injection temperature: 200 °C, detection temperature: 200 °C, oven temperature: 100 °C for 60 min, then ramp to 180 °C at 10 °C/min, retention times: 68.7 min (R) and 69.2 min (S).

1-[4-(Dimethylamino)phenyl]ethanol

R_f = 0.25 (silica gel; petrol/ethyl acetate, 3:1). **^{1}H NMR** (300 MHz, $CDCl_3$): δ (ppm) = 7.18 (d, $^3J_{HH}$ = 8.8 Hz, 2H), 6.65 (d, $^3J_{HH}$ = 8.8 Hz, 2H), 4.74 (q, $^3J_{HH}$ = 6.4 Hz, 1H), 2.87 (s, 6H), 1.69 (br s, 1H), 1.40 (d, $^3J_{HH}$ = 6.4 Hz, 3H). **^{13}C{^{1}H} NMR** (75 MHz, $CDCl_3$): δ (ppm) = 150.2, 133.8, 126.5, 112.6, 70.2, 40.7, 24.7. **HRMS** (ASAP$^+$, solid): Found: *m*/*z* = 166.1222. Calculated for $[M - H]^+$: *m*/*z* = 166.1226.

HPLC conditions (Lux Cellulose-1) – oven temperature: 40 °C, mobile phase: hexane/2-propanol (98:2), flow rate: 0.7 mL/min, detection: 255 nm, retention times: 39.0 min (*R*) and 45.3 min (*S*). [NB Due to the highly acid-sensitive nature of the product,[125] HPLC should be ran immediately after purification].

2.5 X-ray Crystallography

Measurements were made at 150 K on an Oxford Diffraction (Agilent Technologies) Gemini A Ultra diffractometer, using CuKα radiation (1.54184 Å) for (*R*)-**28b** and MoKα radiation (λ = 0.71073 Å) for (*R*)-**29b**, (*S*)-**31a** and (*S*)-**32a**. Cell parameters were refined from the observed positions of all strong reflections. Intensities were corrected for absorption, using a semi-empirical method based on symmetry-equivalent and repeated reflections for (*R*)-**29b** and (*S*)-**31a** and analytically using a multi-faceted crystal model for (*R*)-**28b** and (*S*)-**32a**.[133] The structures were solved by direct methods and refined on F^2 values for all unique data. All non-hydrogen atoms were refined anisotropically, and H atoms were positioned with idealised geometry and the thermal parameters constrained using the riding model; $U_{(H)}$ was set at 1.2 times U_{eq} for the parent C atom. One phenyl group of one of the crystallographically independent molecules of (*R*)-**28b** and the palladium atom and 2-methylallyl ligand of one crystallographically independent molecule of (*S*)-**32a** were modeled as disordered over two positions with the use of restraints. Continuous solvent-accessible channels were observed along the crystallographic [010] direction in the structure of (*S*)-**31a**. The disordered diethyl ether molecules therein could not be modeled in a sensible way and were resolved using the Olex2 solvent mask routine, details of which can be found in the CIF. Oxford Diffraction CrysAlisPro was used for data collection and processing,[134] and Olex2[135] using SHELX[136] for structure solution, refinement, and to generate the molecular overlap figures. Crystal Impact Diamond was used to generate all other molecular graphics with displacement ellipsoids drawn at the 50% probability level.[137]

.

	(*R*)-**28b**	(*R*)-**29b**	(*S*)-**31a**	(*S*)-**32a**
Empirical formula	$C_{33}H_{25}O_3P$	$C_{33}H_{23}O_3P$	$C_{36}H_{28}O_2PClPd$	$C_{38}H_{32}O_2PClPd$
Formula weight	500.50	498.48	665.40	693.45
Temperature/K	150.0(2)	150.0(2)	150.0(2)	150.01(10)
Crystal system	monoclinic	monoclinic	orthorhombic	monoclinic
Space group	$P2_1$	$P2_1$	$P2_12_12_1$	$P2_1$
a/Å	10.57860(7)	9.5367(15)	10.0618(3)	11.4401(2)
b/Å	16.52575(9)	14.1786(15)	14.4757(4)	16.7063(3)
c/Å	14.80544(8)	9.6102(11)	25.0065(10)	16.3663(3)
α/°	90	90	90	90
β/°	95.7963(6)	107.242(14)	90	90.6112(16)
γ/°	90	90	90	90
Volume/Å^3	2575.04(3)	1241.1(3)	3642.2(2)	3127.78(10)
Z	4	2	4	4
ρ_{calc}g/cm^3	1.291	1.334	1.213	1.473
μ/mm^{-1}	1.208	0.145	0.653	0.763
F(000)	1048.0	520.0	1352.0	1416.0
Crystal size/mm^3	0.27 × 0.2 × 0.13	0.12 × 0.1 × 0.1	0.4 × 0.12 × 0.02	0.24 × 0.18 × 0.1
Radiation	CuKα (λ = 1.54184)	MoKα (λ = 0.71073)	MoKα (λ = 0.71073)	MoKα (λ = 0.71073)
2Θ range for data collection/°	6 to 133.998	5.746 to 50	5.86 to 57.234	5.544 to 58.916
Index ranges	-12 ≤ h ≤ 12, -19 ≤ k ≤ 19, -17 ≤ l ≤ 17	-11 ≤ h ≤ 11, -14 ≤ k ≤ 16, -11 ≤ l ≤ 10	-13 ≤ h ≤ 12, -17 ≤ k ≤ 17, -29 ≤ l ≤ 30	-15 ≤ h ≤ 15, -22 ≤ k ≤ 21, -22 ≤ l ≤ 22
Reflections collected	71384	5355	7676	96971
Independent reflections	9138 [R_{int} = 0.0479, R_{sigma} = 0.0227]	3452 [R_{int} = 0.0526, R_{sigma} = 0.1082]	7674 [R_{int} = 0.0000, R_{sigma} = 0.0471]	15384 [R_{int} = 0.0547, R_{sigma} = 0.0442]
Data/restraints/parameters	9138/14/687	3452/1/335	7674/0/371	15384/826/795
Goodness-of-fit on F^2	1.049	1.034	1.010	1.051
Final R indexes [I>=2σ (I)]	R_1 = 0.0273, wR_2 = 0.0645	R_1 = 0.0588, wR_2 = 0.0970	R_1 = 0.0318, wR_2 = 0.0709	R_1 = 0.0355, wR_2 = 0.0629
Final R indexes [all data]	R_1 = 0.0303, wR_2 = 0.0663	R_1 = 0.0903, wR_2 = 0.1099	R_1 = 0.0388, wR_2 = 0.0737	R_1 = 0.0560, wR_2 = 0.0708
Largest diff. peak/hole / e Å^{-3}	0.13/-0.19	0.40/-0.26	0.37/-0.49	0.79/-0.55
Flack parameter	0.001(5)	0.07(17)	-0.034(13)	-0.056(8)

2.6 Density Functional Theory Calculations

Performed with the B3LYP functional and 6-31G* basis set, using the *Spartan* program. In each case the calculations were considered to be complete and converged to a minimum on the potential energy surface after vibrational frequency analysis did not report any negative frequencies.

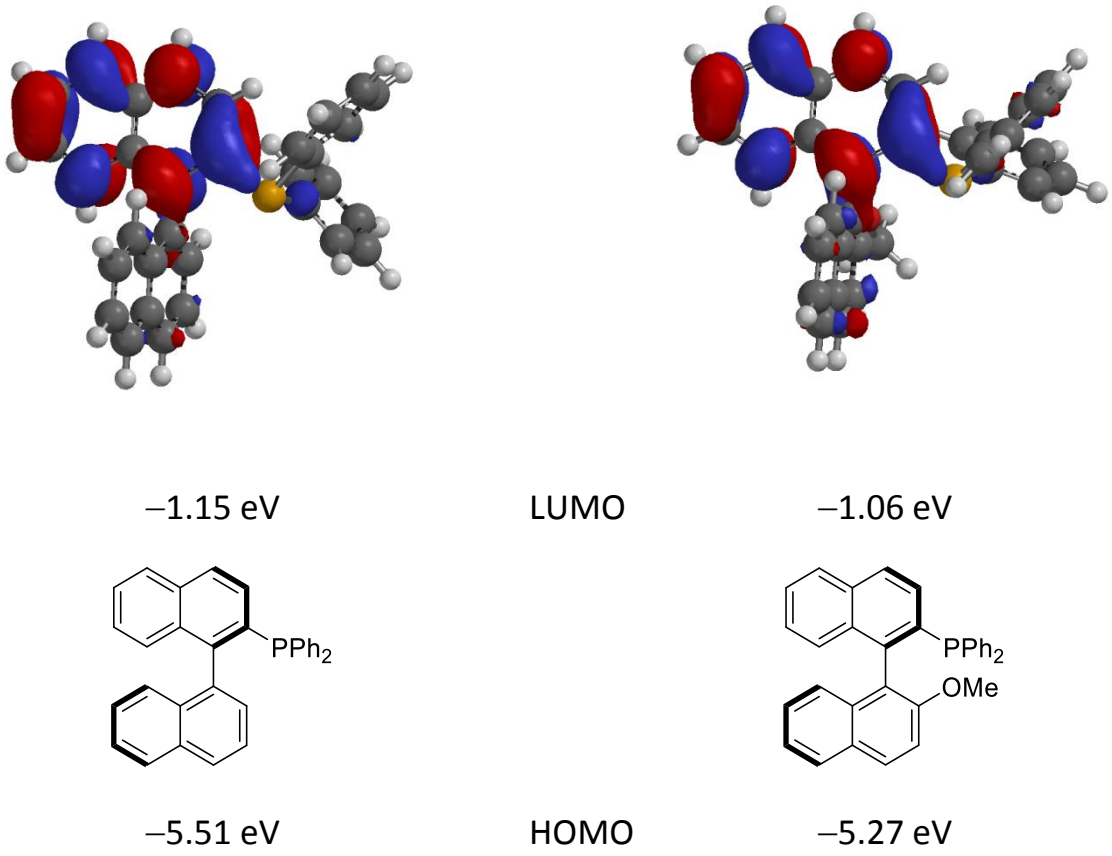

Fig. 2.8 (*S*)-H-MOP (left) and (*R*)-MeO-MOP (right).

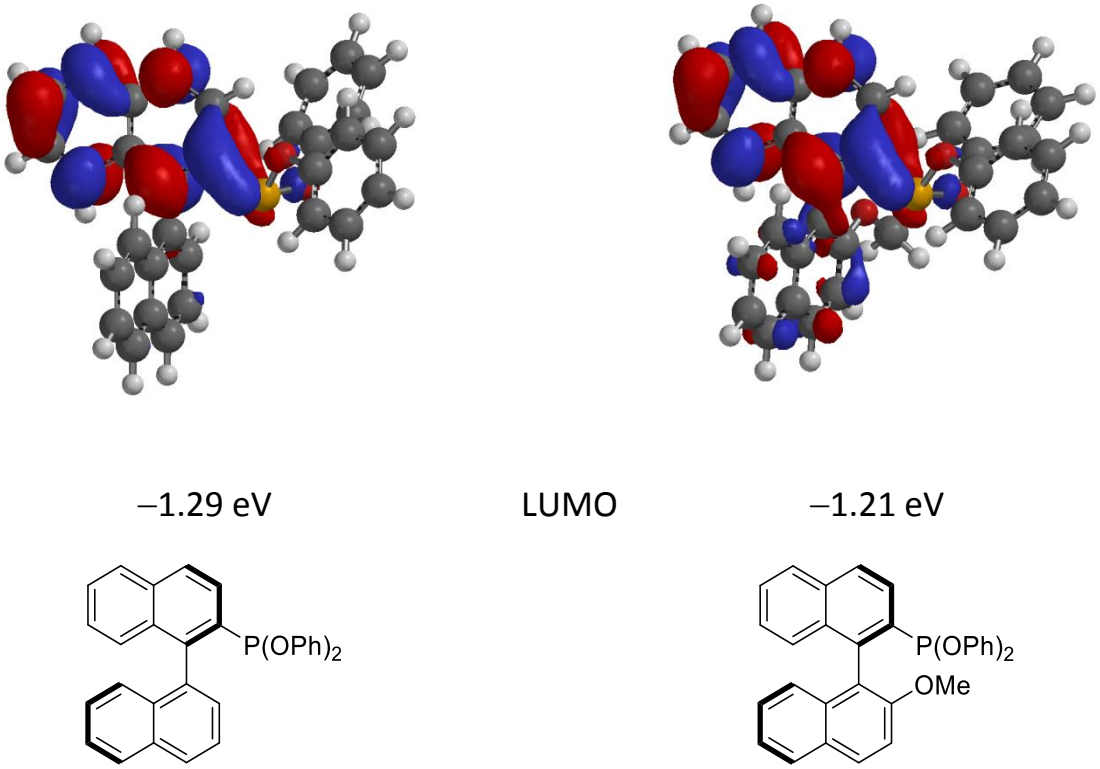

Fig. 2.9 (*S*)-**28a** (left) and (*R*)-**28b** (right).

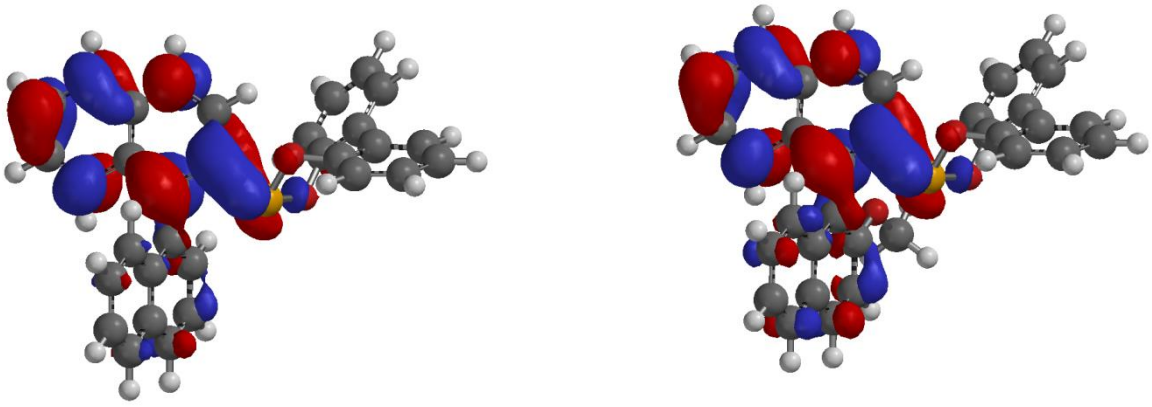

−1.33 eV LUMO −1.21 eV

−5.76 eV HOMO −5.47 eV

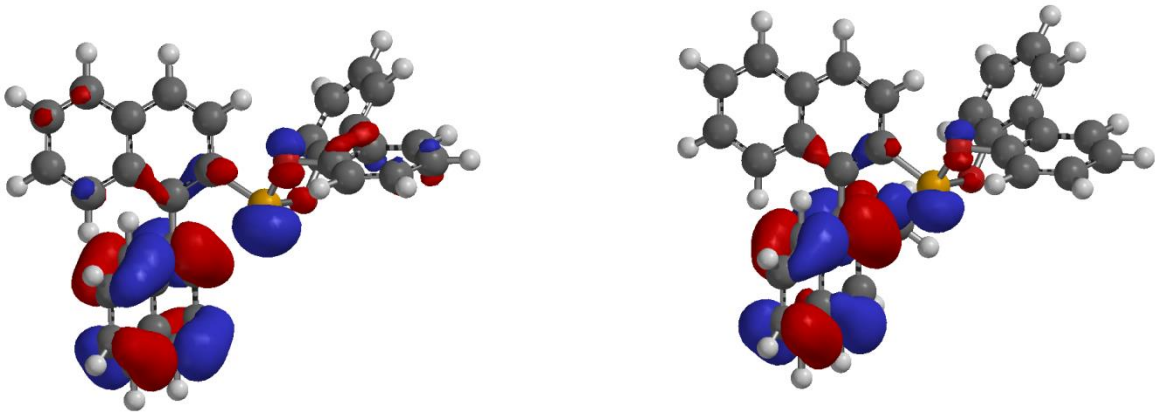

Fig. 2.10 (*S*)-**29a** (left) and (*R*)-**29b** (right).

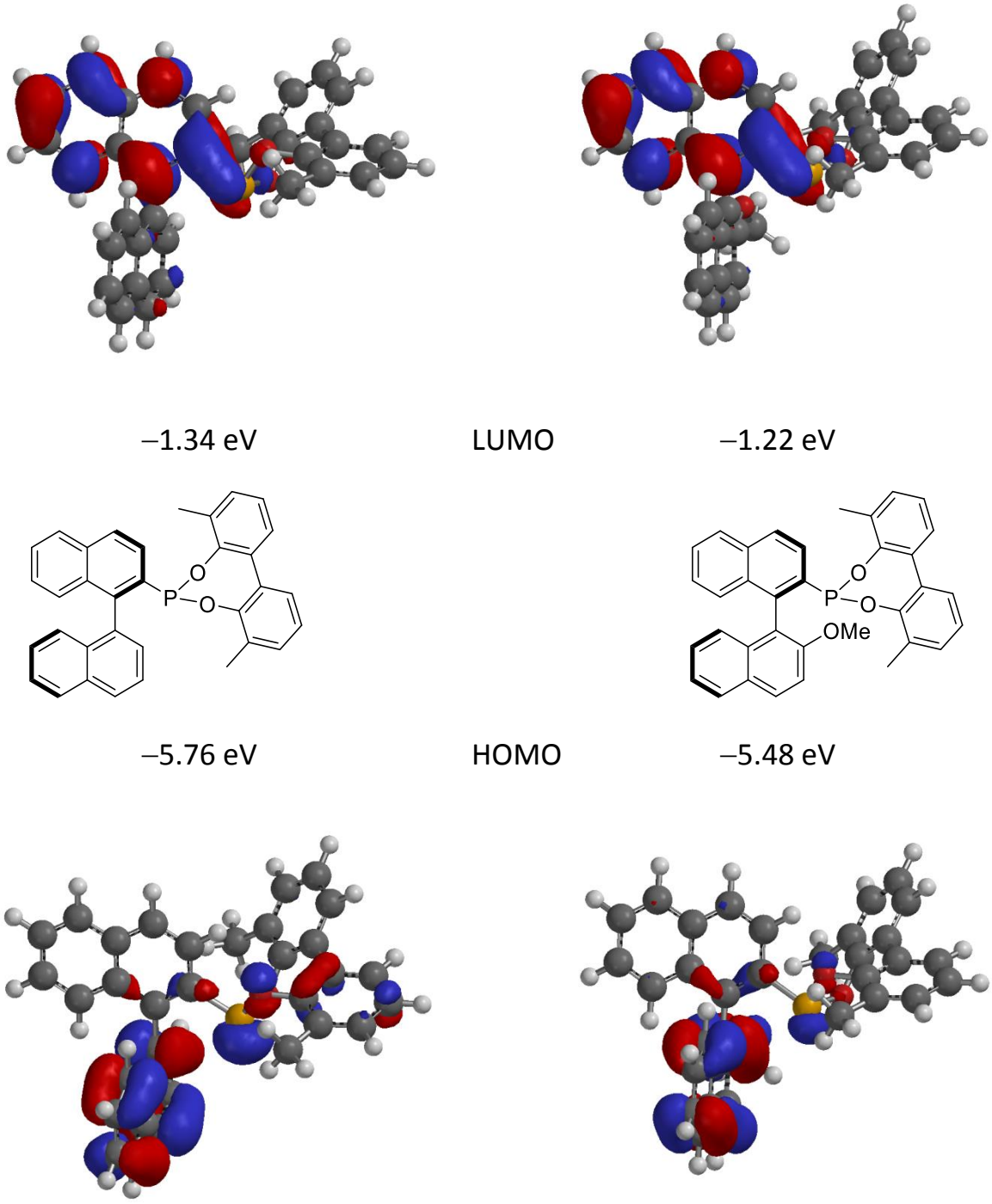

Fig. 2.11 (*S*)-**30a** (left) and (*R*)-**30b** (right).

3. A comparison of MOP-phosphonite ligands and their applications in Rh(I)- and Pd(II)-catalysed asymmetric transformations

Abstract: Six novel chiral MOP-phosphonites have been synthesised and compared via experimental and computational methods in an effort to quantify their differing structural and electronic profiles. They were found to be electron-poor ligands in comparison to their arylphosphine analogues and have a larger *trans* influence in square planar Pt(II) complexes. Four [Rh(L^P)(η^2:η^2-cod)Cl] complexes were synthesised and characterised by NMR spectroscopy, HRMS and X-ray crystallography. Two [Rh(L^P)$_2$]BF_4 complexes were prepared where one ligand acts as a chelating P,C-π-donor; detailed NMR studies demonstrated a hemilabile η^6-coordination mode, which in one case was confirmed by X-ray crystallography. Rh(I) complexes were used as catalysts in asymmetric hydrogenation and hydroformylation reactions, and in the addition of a boronic acid to an isatin. Pd(II) complexes were successfully employed in asymmetric Suzuki-Miyaura cross-coupling reactions yielding binaphthyl products. Two [Pd(L^P)$_2$$Cl_2$] complexes were synthesised and characterised by X-ray crystallography, both adopting *cis* orientations, with one of the complexes crystallising as two *pseudo*-polymorphs.

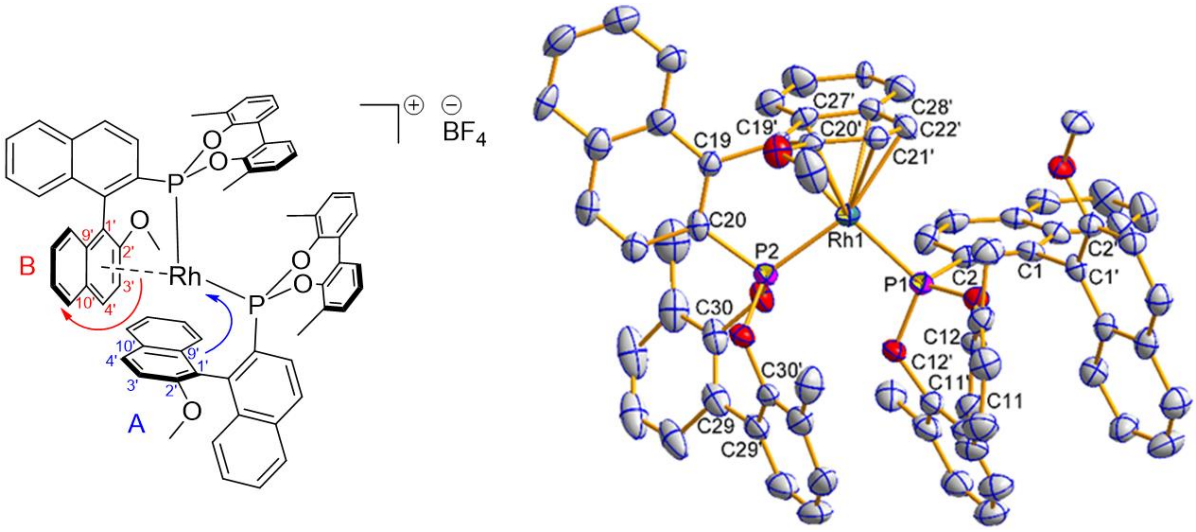

3.1 Introduction

Organophosphorus molecules are a popular choice of ligand in asymmetric homogeneous catalysis – by choosing a P-chiral ligand or one with a chiral substituent, it is possible to synthesise complexes which can catalyse reactions enantioselectively.[19] Chiral monophosphorus ligands have found applications in a variety of organometallic catalytic transformations. An important class of these ligands are Hayashi's MOP-phosphines, which have been applied in a wide range of asymmetric catalytic reactions.[47] This project aimed to employ transition metal complexes of MOP ligands, especially those with unusual functionality on the phosphorus,[92] as asymmetric catalysts.

Phosphonites are valuable phosphorus ligands used in homogeneous catalysis, with characteristic properties of being poor σ-donors but strong π-acceptors. Higham *et al*. reported a convenient synthetic route to enantiopure MOP-phosphonite ligands ((*S*,R_b)-**27a**, (*S*,S_b)-**27a**, (*R*,R_b)-**27b** and (*R*,S_b)-**27b**; Scheme 3.1), which can act in a monodentate or hemilabile fashion. Studies into the solution and solid state transition metal complexes of these ligands, and their action as P,arene-chelates to stabilise coordinatively unsaturated electron deficient metal centres were reported.[93] The MOP-phosphonite ligands were also incorporated[15b] into the ligand knowledge base for monodentate P-donors (LKB-P), developed by Fey *et al*.[14b,15] These ligands occupy a position in the database which implies that their transition metal complexes may be suitable catalysts for hydroformylation, hydrocyanation, hydrosilylation and hydrogenation reactions.[15b] Chiral phosphonite complexes are proven catalysts for a range of enantioselective reactions, including nickel-catalysed hydrocyanations,[102c] palladium-catalysed hydrovinylations[103] and rhodium-catalysed hydroformylations[106c] and hydrogenations.[107b,c,e] Furthermore, our MOP-phosphonites were shown to be effective in the palladium-catalysed asymmetric hydrosilylation of styrenes (see Chapter 2).[92-93,138]

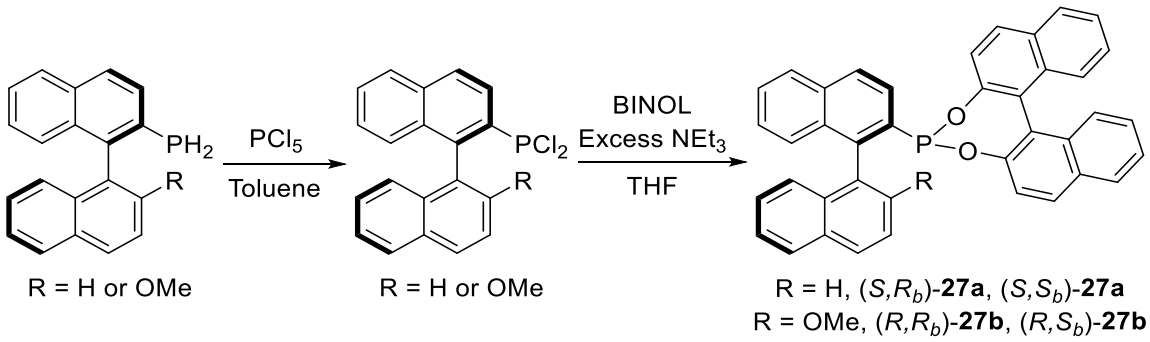

Scheme 3.1 The synthesis of MOP-phosphonite ligands with two chiral centres.

In this chapter, we investigate the synthesis of a family of novel MOP-phosphonites which contain only one chiral element – the binaphthyl backbone – and investigate the ramifications of this structural modification on the coordination chemistry and catalytic properties of the resultant transition metal complexes. Specifically, the ligands (*S*)-**28a**, (*R*)-**28b**, (*S*)-**29a**, (*R*)-**29b**, (*S*)-**30a** and (*R*)-**30b** (Chart 3.1) were prepared, as well as their corresponding selenides, and subsequent investigations allowed us to make quantitative comparisons of these donors, capturing their steric and electronic properties. We used DFT calculations to probe the frontier molecular orbitals of the ligands and also present calculations which support our experimental observations that rotation about the C–C bond in the biphenyl moiety of **29a**/**b** and **30a**/**b** is unrestricted under typical conditions.[138] The rhodium(I) and palladium(II) coordination chemistry of the ligands was then investigated in some detail by multinuclear NMR spectroscopy and X-ray crystallography. Finally, the performance of the ligands in

asymmetric hydrogenation, hydroformylation and Suzuki-Miyaura cross-coupling reactions was assessed and compared to that of the diphenylphosphine analogues MeO-MOP and H-MOP.

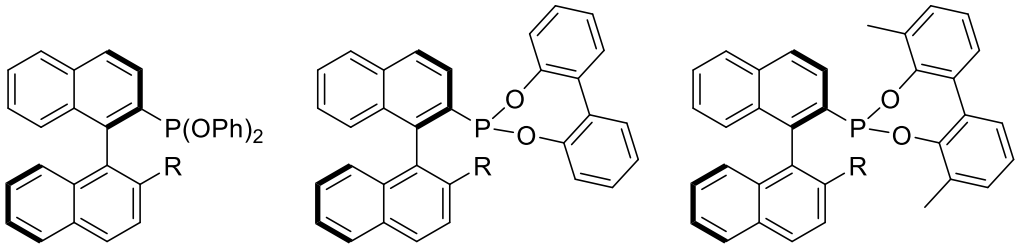

(*S*)-**28a**: R = H
(*R*)-**28b**: R = OMe

(*S*)-**29a**: R = H
(*R*)-**29b**: R = OMe

(*S*)-**30a**: R = H
(*R*)-**30b**: R = OMe

Chart 3.1 Phosphonite ligands (*S*)-**28a**, (*R*)-**28b**, (*S*)-**29a**, (*R*)-**29b**, (*S*)-**30a** and (*R*)-**30b** prepared in this study.

3.2 Results and Discussion

3.2.1 Ligand properties

Organophosphorus selenides

Compounds of the type $L^P(Se)$ were synthesised by reacting the corresponding phosphorus ligand (L^P) with an excess of potassium selenocyanate in THF at 50 °C.[92] The $^{31}P\{^1H\}$ NMR of the reaction product consists of a singlet with ^{77}Se (I = ½, natural abundance 7.6%) satellites (Table 3.1). The difference in chemical shift between $L^P(Se)$ and L^P is *ca*. 50 ppm and downfield for the arylphosphines, whereas it is larger (*ca*. 65-75 ppm) and upfield for the phosphonites.

Table 3.1 Selected $^{31}P\{^1H\}$ NMR spectroscopic data for $L^P(Se)$ compounds.

Ligand	δ ($L^P(Se)$)[c]	$^1J_{PSe}$ ($L^P(Se)$)[d]	$\Delta\delta$[e]
(*S*)-H-MOP[a]	36.6	723	+ 50.2
(*R*)-MeO-MOP[b]	38.3	720	+ 52.0
(*S*)-**28a**[a]	89.4	908	− 65.4
(*R*)-**28b**[a]	91.7	906	− 63.9
(*S*)-**29a**[a]	104.1	926	− 74.5
(*R*)-**29b**[a]	104.4	930	− 75.6
(*S*)-**30a**[a]	105.4	918	− 67.0
(*R*)-**30b**[a]	103.9	915	− 70.3

[a] NMR measurements were taken at 162 MHz in $CDCl_3$. [b] NMR measurement was taken at 202 MHz in $CDCl_3$. [c] Chemical shift in ppm. [d] Coupling constant in Hz. [e] $\Delta\delta = \delta$ ($L^P(Se)$) − δ (L^P) in ppm.

The magnitude of the ^1J (^{31}P–^{77}Se) coupling can provide an indication of the σ-donor strength of the parent phosphorus lone pair, which is inversely correlated to the coupling constant.[139] The data implies

that our MOP-phosphonites (906-930 Hz) are relatively weak σ-donors compared to their electron-rich arylphosphine analogues (720-723 Hz) due to the increased electron-withdrawing effects of the oxygen-containing substituents, which results in the phosphorus lone pair having a larger s- and lower p-character, and a decreased σ-basicity (i.e. the magnitude of the coupling-constant increases as the electron-withdrawing ability of the phosphorus substituents increases) (Table 3.1). The $^1J_{PSe}$ values for the phosphonites **28**-**30** are also larger than those reported for analogous MOP-phosphonites with two methoxy substituents bound to the phosphorus (858 Hz and 860 Hz),[92] indicating that replacing two alkyoxy functionalities with aryloxy groups results in ligands that are weaker σ-donors in this selenide series. It has been demonstrated that the presence of bulky substituents on the phosphorus can result in a lower value for the coupling constant (i.e. a decrease in the s-character of the lone pair),[140] which may explain why the bulky dimethylbiphenoxy phosphonites (*S*)-**30a** and (*R*)-**30b** have lower $^1J_{PSe}$ values than the biphenoxy phosphonites (*S*)-**29a** and (*R*)-**29b**.

Rhodium(I) Vaska-type complexes

Another indication of net-donation properties in PR_3 ligands is the carbonyl stretching frequency (ν(CO)) in the IR spectrum of *trans*-[Rh(L^P)$_2$(CO)Cl] complexes (Table 3.2).[141] The complexes are conveniently prepared by reaction of four equivalents of the corresponding phosphorus ligand with [Rh(CO)$_2$Cl]$_2$.[142] The data correlates well with the Tolman data for the related [Ni(L^P)(CO)$_3$] complexes historically used to assess the stereoelectronic profile of phosphines; however, the precursor [Ni(CO)$_4$] is highly volatile and toxic and a convenient alternative metric is preferable.[9,141] A low value for ν(CO) indicates that the phosphorus ligand is a strong electron donor, conversely, a high value indicates low net donor properties.

Table 3.2 Selected IR spectroscopic data for *trans*-[Rh(L^P)$_2$(CO)Cl] complexes.[a]

Ligand	(*S*)-H-MOP	(*R*)-MeO-MOP	(*S*)-**28a**	(*R*)-**28b**	(*S*)-**29a**	(*R*)-**29b**	(*S*)-**30a**	(*R*)-**30b**
ν(CO)[b]	1968	1974	2006	2002	2005	1997	2006	2005

[a] IR measurements were taken as solutions in DCM. [b] Symmetric carbonyl stretching frequency in cm^{-1}.

The values for our phosphonites (1997-2006 cm^{-1}) indicate overall low net-donor properties compared to the MOP-phosphine ligands (1968-1974 cm^{-1}) (Table 3.2), as would be expected for this ligand class. The reduced electron density on the rhodium atom results in less π-back-bonding with the carbonyl group, resulting in a stronger CO bond and hence an increase in ν(CO) relative to the more donating phosphines.[141b] The wavenumbers reported for analogous bimethoxy MOP-phosphonites (1996 Hz and 1999 Hz) are slightly lower than the average for the phosphonites in this series,[92]

indicating that they are generally stronger net donors. This is in agreement with the conclusion we made from the $^1J_{PSe}$ values in the organophosphorus selenide compounds (*vide supra*).

3.2.2 Platinum(II) complexes

(*S*)-H-MOP, (*R*)-MeO-MOP and each phosphonite was reacted with the platinum precursor $[Pt(PEt_3)Cl_2]_2$ in CD_2Cl_2 to generate the unsymmetrical platinum(II) complexes *trans*-[Pt((*S*)-H-MOP)(PEt_3)Cl_2] (*S*)-**34a**, *trans*-[Pt((*R*)-MeO-MOP)(PEt_3)Cl_2] (*R*)-**34b**, *trans*-[Pt((*S*)-**28a**)(PEt_3)Cl_2] (*S*)-**35a**, *trans*-[Pt((*R*)-**28b**)(PEt_3)Cl_2] (*R*)-**35b**, *trans*-[Pt((*S*)-**29a**)(PEt_3)Cl_2] (*S*)-**36a**, *trans*-[Pt((*R*)-**29b**)(PEt_3)Cl_2] (*R*)-**36b**, *trans*-[Pt((*S*)-**30a**)(PEt_3)Cl_2] (*S*)-**37a** and *trans*-[Pt((*R*)-**30b**)(PEt_3)Cl_2] (*R*)-**37b** via bridge cleavage reactions.[143] We observed exclusively the formation of the *trans* isomers in the $^{31}P\{^1H\}$ NMR spectra of the compounds (Table 3.3).[144] The value of δ (L^P) for the complexes with the phosphonite ligands was shifted *ca*. 30-50 ppm upfield compared to the resonance of the free ligand, the phenoxy derived ligands having the largest shift and the *ortho*-methyl substituted biphenoxy ligands the lowest; the phosphine ligands were shifted *ca*. 35-40 ppm downfield (Table 3.3). The values of the $^2J_{PP}$ coupling between the ligands are relatively high and characteristic of a *trans* geometry.[145] The phosphonite complexes show little variance ($^2J_{PP} \approx 620$ Hz) and the values are noticeably larger than those for the phosphine ligands ($^2J_{PP} \approx 470$ Hz).

Next we sought to determine the relative *trans* influence of our series of MOP ligands by measuring the $^1J(^{31}P–^{195}Pt)$ coupling for Pt–PEt_3 in these square-planar platinum(II) complexes (^{195}Pt, $I = ½$, natural abundance 33.8%) (Table 3.3).[143,146] The *trans* influence is defined as 'the extent to which that ligand weakens the bond *trans* to itself in the equilibrium state of a substrate'.[144a] The magnitude of the *J*-coupling corresponds well to the Pt–PEt_3 bond length. It was found that the *trans* influence of our phosphonites (2382-2519 Hz, Table 3.3, entries 3-8) is larger than that found for the arylphosphine analogues (2554-2574 Hz, Table 3.3, entries 1 and 2) – a smaller $^1J_{PPt}$ coupling for PEt_3 denotes a larger *trans* influence from L^P. The coupling constant for the *ortho*-methyl substituted biphenoxy phosphonites (Table 3.3, entries 7 and 8) was noticeably lower than that for the phenoxy and biphenoxy phosphonites (Table 3.3, entries 3-6), implying that ligands (*S*)-**30a** and (*R*)-**30b** have the largest *trans* influence in the series.

Table 3.3 Selected $^{31}P\{^{1}H\}$ NMR spectroscopic data for *trans*-[Pt(L^P)(PEt_3)Cl_2] complexes.

	Complex	δ (L^P)[c]	$^{1}J_{PPt}$ (L^P)[d]	δ (PEt_3)[c]	$^{1}J_{PPt}$ (PEt_3)[d]	$^{2}J_{PP}$[d]
1	(*S*)-**34a**[a]	21.5	2437	13.8	2574	473
2	(*R*)-**34b**[b]	25.3	2440	13.7	2554	468
3	(*S*)-**35a**[a]	111.8	3481	11.2	2495	621
4	(*R*)-**35b**[a]	108.8	3467	9.0	2519	618
5	(*S*)-**36a**[a]	140.6	3520	10.0	2490	624
6	(*R*)-**36b**[a]	140.5	3517	9.0	2503	620
7	(*S*)-**37a**[a]	140.5	3521	8.6	2398	620
8	(*R*)-**37b**[a]	142.6	3541	12.1	2382	620

[a] NMR measurements were taken at 162 MHz in CD_2Cl_2. [b] NMR measurements were taken at 202 MHz in CD_2Cl_2. [c] Chemical shift in ppm. [d] Coupling constant in Hz.

We were able to obtain single crystals suitable for X-ray crystallography for one of the platinum(II) complexes, (*R*)-**36b** (Fig. 3.1), by slow diffusion of diethyl ether into a CD_2Cl_2 solution. There is a *pseudo*-square-planar geometry around the platinum centre, both (*R*)-**29b** and PEt_3 show monodentate coordination through the phosphorus atom and are *trans* to each other with a P–Pt–P bond angle of 170.36(4)°. The Pt–PEt_3 bond length (2.3148(11) Å) is similar to that reported for an analogous phosphonite complex, containing a fluorine substituted derivative of diphenyl phenylphosphonite, which has two independent molecules in the unit cell (2.321(4) Å and 2.319(4) Å).[147] The Pt–PEt_3 bond length in (*R*)-**36b** is longer than that in the related MOP-bis(dimethylamino)phosphine and MOP-phosphirane complexes that Higham *et al*. recently reported as part of a study into the stereoelectronic profiles of a series of MOP-type ligands, which have analogous bond lengths of 2.3050(15) Å and 2.284(3) Å respectively, indicating that the phosphonite ligand has the largest *trans* influence of the three.[92]

It is cautionary to note, however, that the $^{1}J_{PPt}$ coupling for PEt_3 in (*R*)-**36b** (2503 Hz) is significantly larger than reported for the MOP-bis(dimethylamino)phosphine complex (2365 Hz),[92] which as discussed would imply that the phosphonite ligand exhibits a weaker *trans* influence – this contradiction may be due to steric effects in the solid state. We are not aware of any analogous bis(dimethylamino)phosphine complexes for comparison.

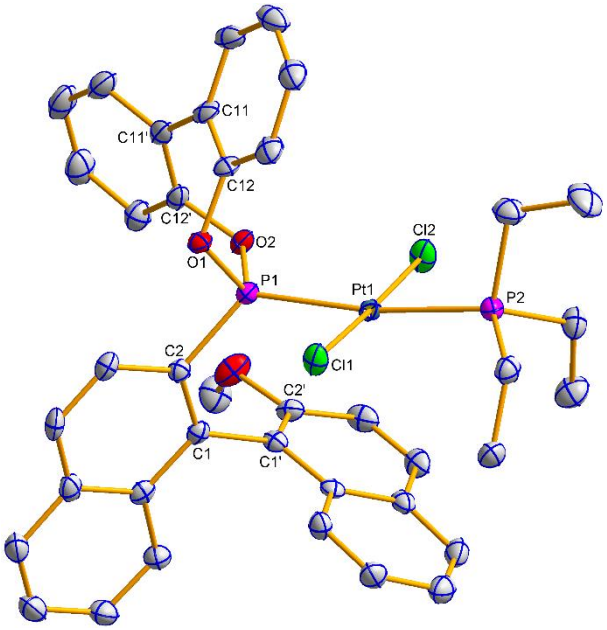

Fig. 3.1 Molecular structure of (*R*)-**36b**. Hydrogen atoms have been omitted for clarity. Selected average bond distances (Å) and angles (°): Pt1–P1 2.2703(10), Pt1–P2 2.3148(11), Pt1–Cl1 2.3203(10), Pt1–Cl2 2.2873(10), P1–C2 1.813(4), P1–O1 1.612(3), P1–O2 1.607(3); P1–Pt1–Cl1 85.72(4), P1–Pt1–P2 170.36(4), P1–Pt1–Cl2 94.02(4), C2–C1–C1'–C2' –87.6(5), C12–C11–C11'–C12' –43.2(6).

3.2.3 DFT calculations

Density Functional Theory (DFT) calculations have been performed on the optimised structures of the MOP ligands using the B3LYP functional with a 6-31G* basis set to calculate the frontier molecular orbital energies (see Chapter 2), the Highest Occupied Molecular Orbital (E_{HOMO}) and Lowest Unoccupied Molecular Orbital (E_{LUMO}) (Table 3.4).[148] These electronic descriptors can provide a useful indication of the properties of the free ligand, via a simple and direct method, rather than indirect experimental approaches such as the synthesis of organophosphorus selenides and metal complexes (*vide supra*). E_{HOMO} typically contains the phosphorus lone pair in tertiary phosphines and can be used as an indication of the ligand σ-donor strength.[18,149] The values for E_{HOMO} are invariably lower for the H-MOP molecules compared to their MeO-MOP analogues (Table 3.4), implying that the latter have stronger σ-donor properties, in agreement with calculations for related ligands previously reported.[92] The HOMO energies for the H-MOP-phosphonites are lower than their arylphosphine counterpart, and this trend also holds true for the MeO-MOP ligand family, implying the phosphonites are weaker P-ligand σ-donors in each series. However, note that the MeO-MOP-phosphonites (*R*)-**29b** and (*R*)-**30b** have a *higher* calculated HOMO energy (–5.48 eV) than the phosphine H-MOP (–5.51 eV). E_{LUMO} may be invoked in back-bonding,[148] and the lower values for the phosphonites compared to the phosphines suggests they will likely have better π-acceptor properties (Table 3.4). The H-MOP-phosphonites have lower LUMO energies than their 2'-methoxy-substituted analogues.

Table 3.4 Calculated HOMO and LUMO energies and *S*4 values for the MOP ligands discussed in this study.

Ligand	(*S*)-H-MOP	(*R*)-MeO-MOP	(*S*)-**28a**	(*R*)-**28b**	(*S*)-**29a**	(*R*)-**29b**	(*S*)-**30a**	(*R*)-**30b**
E_{LUMO}[a,b]	–1.15	–1.06	–1.29	–1.21	–1.33	–1.21	–1.34	–1.22
E_{HOMO}[a,b]	–5.51	–5.27	–5.80	–5.51	–5.76	–5.47	–5.76	–5.48
*S*4[a,c]	41	42	54	54	58	58	58	58
*S*4[c,d]	–	–	–	66/70[e]	–	60	–	–

[a] Calculated at the DFT level of theory using the B3LYP functional with a 6-31G* basis set. [b] Energies in eV. [c] Symmetric deformation coordinate in degrees. [d] Calculated from X-ray data. [e] The asymmetric unit comprises two molecules in different conformations.

One of the earliest methods for quantifying the steric effects of phosphorus ligands is the Tolman cone angle (θ), which is derived from space-filling models.[9] However, for MOP-type ligands where the substituent groups differ greatly, the values obtained may not best reflect the properties of the ligand.[13] An alternative means of evaluating the steric bulk of phosphorus ligands is the symmetric deformation coordinate (*S*4'), introduced by Orpen and co-workers using data obtained from crystal structures.[8c] *S*4' seeks to evaluate the ligands based on a geometric calculation using bond angles from species with the general formula Z–PR_3 (Z = transition-, main group- or non-metal) (see Fig. 1.3 and corresponding text). It has also been shown that *S*4' can be calculated with sufficient accuracy to the data obtained from X-ray crystallographic analysis of phosphine complexes.[150] We, therefore, used the DFT optimised structures for the series of MOP ligands in Table 3.4 to calculate a modified descriptor of *S*4' (*S*4), calculating Z to be a vector perpendicular to the plane containing the 3 substituents on the phosphorus.[151] For phosphines, small values for *S*4 can suggest substituents with increasing steric bulk. The values calculated for (*S*)-H-MOP and (*R*)-MeO-MOP (Table 3.4) are close to that calculated for PPh_3 (39.6°) by Suresh and co-workers,[151] implying that they have a similar steric profile. The *S*4 values for the MOP-phosphonite ligands are approximately 12-17° larger than their phosphine analogues and show little variation between themselves. However, it is more difficult to accurately model compounds with P–O bonds compared to P–C bonds, since the R groups in $P(OR)_3$ compounds are much further from the phosphorus than in PR_3 ligands. Therefore, the accuracy of this method may not be suitable to our MOP-phosphonites due to their conformational flexibility.[150]

We recently reported the molecular structures of (*R*)-**28b** and (*R*)-**29b** (see Chapter 2),[138] and consequently were able to calculate *S*4 from the X-ray crystallographic data and compare it to the computed structures (Table 3.4). The *S*4 value for (*R*)-**28b** is considerably larger in the X-ray structure compared to the calculated one, whereas both are similar for (*R*)-**29b**; the smaller *S*4 value for (*R*)-**29b** compared to (*R*)-**28b** is more consistent with what might be expected due to the biphenoxy group having less conformational flexibility. In order to investigate further the nature of rotation about the

biphenoxy group, we decided to calculate the approximate barrier to rotation for the ligands (*S*)-**30a** and (*R*)-**30b** (Fig. 3.2). Restricted rotations that can be frozen out on the NMR timescale, including in organophosphorus transition metal complexes, have been discussed by Orrell.[152] Substituted biphenyls display conformational enantiomorphism – the ease with which isomerisation occurs depends on the size of the *ortho*-substituents.[34,153] The peaks in the energy profile for rotation in biphenyl compounds generally occur at 0°, ±90° and 180°, when the two phenyl rings are either coplanar or orthogonal; the local minima occur near 45° either side of the secondary maxima at ±90° due to a compromise between the steric demands of the *ortho*-substituents and π-electron overlap.[154] The rotational barrier in 1,1'-biphenyl, and non-*ortho*-substituted biphenyls, are comparable at 0° and 90° (1.4-2.0 kcal/mol).[154] An activation energy barrier of approximately 23 kcal/mol is required to prevent spontaneous room temperature torsional-isomerisation of biphenyl derivatives.[34] It is important to note that, when calculating barriers to rotation, the method and basis set employed have a large impact on the optimised torsion angles.[34,153c]

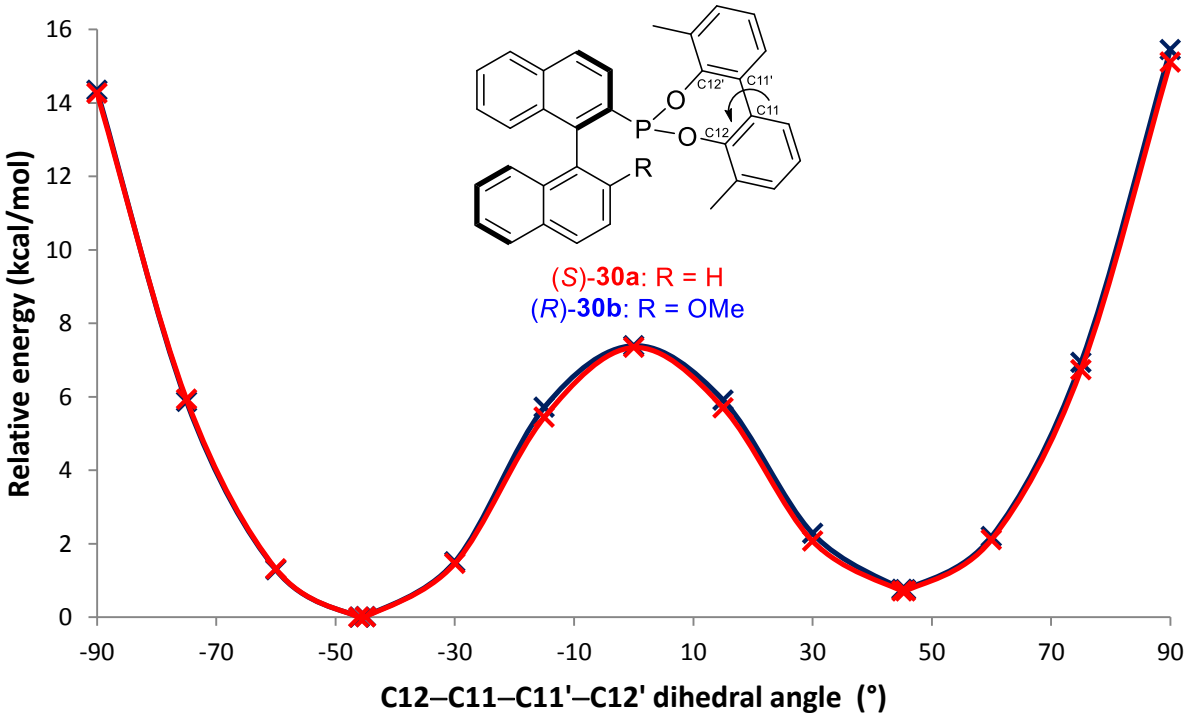

Fig. 3.2 Calculated conformational energy differences (in kcal/mol) versus dihedral angle for the ligands (S)-**30a** and (R)-**30b** (in °), relative to the energy at the optimised dihedral angle; (*S*)-**30a** (red) and (*R*)-**30b** (blue). The geometry optimisations were performed at the DFT level of theory using the B3LYP functional with a 6-31G* basis set.

In our study, the torsion angle between the planes of the two phenyl rings (C12–C11–C11'–C12') was constrained at selected values and the optimised geometry calculated. A plot of the relative energies versus the dihedral angle is shown in Fig. 3.2 (the values are provided in tabular format in Section 3.6,

Table 3.10); the curves in the graph are not mirror images of each other, as the two minima are diastereomers and hence of unequal energy. We also calculated the idealised angle for the unconstrained molecule at the two minima: −46.11° and +45.56° for (*S*)-**30a**, and −46.00° and +45.60° for (*R*)-**30b** (Table 3.10). The calculated energy profiles for both (*S*)-**30a** and (*R*)-**30b** are very similar with an energy barrier of approximately 7-8 kcal/mol when the biphenyl rings are coplanar, far below the approximate minimum free energy barrier to rotation reported for biphenyl derivatives (23 kcal/mol) (Section 1.2.4).[34] This result concurs with our experimental findings that rotation about the aryl–aryl junction is unrestricted under standard conditions (See Chapters 2 and 4).

3.2.4 Rhodium(I) complexes and catalysis

Successful examples of rhodium(I)-catalysed asymmetric transformations employing MOP-type ligands can be found in the literature. Recently Shintani, Nozaki and co-workers reported the high yielding and enantioselective synthesis of silicon-stereogenic dibenzosiloles[155] and the intramolecular alkynylsilylation of alkynes.[156] MeO-MOP and P-stereogenic phosphine derivatives have shown promise in the rhodium-catalysed asymmetric addition of phenylboronic acid to napthaldehyde.[157] Asymmetric intramolecular hydroamination of unactivated alkenes using a rhodium(I) catalyst has been described by Shen and Buchwald, who used a series of binapthyl-based monophosphine ligands to give high yields and up to 91% *ee* with the substrates tested.[158]

[Rh(L^P)(η^2:η^2-cod)Cl] complexes

To study the coordination chemistry of our ligands with rhodium(I), (*S*)-**29a**, (*R*)-**29b**, (*S*)-**30a** and (*R*)-**30b** were reacted with [Rh(η^2:η^2-cod)Cl]$_2$ in a 1:1, P:Rh ratio, to quantitatively synthesise the monophosphonite chloro(1,5-cyclooctadiene)rhodium(I) complexes [Rh((*S*)-**29a**)(η^2:η^2-cod)Cl] (*S*)-**38a**, [Rh((*R*)-**29b**)(η^2:η^2-cod)Cl] (*R*)-**38b**, [Rh((*S*)-**30a**)(η^2:η^2-cod)Cl] (*S*)-**39a** and [Rh((*R*)-**30b**)(η^2:η^2-cod)Cl] (*R*)-**39b**. The analogous reactions with (*S*)-**28a** and (*R*)-**28b** were attempted; however, the resultant complexes were very sensitive to decomposition and we were unable to isolate the complexes with sufficient purity to investigate their properties further. Three of the four rhodium complexes gave broadened $^{31}P\{^1H\}$ NMR spectral signals at room temperature. Consequently they were analysed by VT NMR spectroscopy (Figs. 3.3-3.6).

Both phosphorus and rhodium have only one naturally occurring stable isotope, ^{31}P and ^{103}Rh (I = ½, natural abundance 100%); therefore, the expected $^{31}P\{^1H\}$ NMR spectra for the complexes should consist of a doublet arising from ^{31}P–^{103}Rh spin-spin coupling. For (*S*)-**38a** a broad doublet was observed at 25 °C which became clearer upon heating to 50 °C (δ = 162.9 ppm and $^1J_{PRh}$ = 224 Hz); cooling the sample down to −55 °C resulted in the observation of two distinct species with relative intensities of

~65% (δ = 164.6 ppm and $^{1}J_{PRh}$ = 223 Hz) and ~35% (δ = 161.4 ppm and $^{1}J_{PRh}$ = 221 Hz) (Fig. 3.3). For (*R*)-**38b** a doublet was observed at 25 °C (δ = 163.3 ppm and $^{1}J_{PRh}$ = 221 Hz), and cooling down to −55 °C resulted in the appearance of an additional low intensity doublet resonance (Fig. 3.4). The two species which appear in the spectra of (*S*)-**38a** and (*R*)-**38b** at −55 °C most likely correspond to conformational isomers with the ligands exhibiting restricted rotation about the biphenyl C–C bridge. Both (*S*)-**38a** and(*R*)-**38b** were poorly soluble in $CDCl_3$ and CD_2Cl_2, which proved to be problematic when performing NMR experiments due to the high number of scans required. Presumably at low temperatures the complexes precipitate out of the solution reducing the concentration further. However, we were able to characterise the binaphthyl moiety in (*S*)-**38a** at 50 °C and (*R*)-**38b** at 25 °C, but the broadened ^{1}H and ^{13}C resonances attributed to the biphenyl moieties could not be assigned.

For the dimethylbiphenoxy phosphonite complex (*S*)-**39a**, phosphonite coordination resulted in one broad $^{31}P\{^{1}H\}$ NMR signal at 25 °C which split into a poorly resolved doublet when heated to 50 °C (Fig. 3.5). Cooling to −55 °C allowed for the resolution of three species with approximate ratios of 76% (δ = 170.2 ppm and $^{1}J_{PRh}$ = 225 Hz), 14% (δ = 169.4 ppm and $^{1}J_{PRh}$ = 224 Hz) and 10% (δ = 162.0 ppm and $^{1}J_{PRh}$ = 223 Hz). The methoxy analogue (*R*)-**39b** shows a broad doublet coupling at 25 °C whose resolution improved upon heating to 50 °C (Fig. 3.6). Cooling to −55 °C resulted in the formation of five distinct species ~13% (δ = 168.1 ppm and $^{1}J_{PRh}$ = 227 Hz), ~80% (δ = 167.5 ppm and $^{1}J_{PRh}$ = 226 Hz), ~1% (δ = 165.1 ppm and $^{1}J_{PRh}$ = 227 Hz), ~3% (δ = 163.4 ppm and $^{1}J_{PRh}$ = 224 Hz) and ~3% (δ = 162.8 ppm and $^{1}J_{PRh}$ = 223 Hz). The multiple species observed in the $^{31}P\{^{1}H\}$ NMR of (*S*)-**39a** and(*R*)-**39b** at −55 °C most likely corresponds to rotamers – restriction of rotation around the Rh–P bond or biphenyl C–C bridge torsion angle.

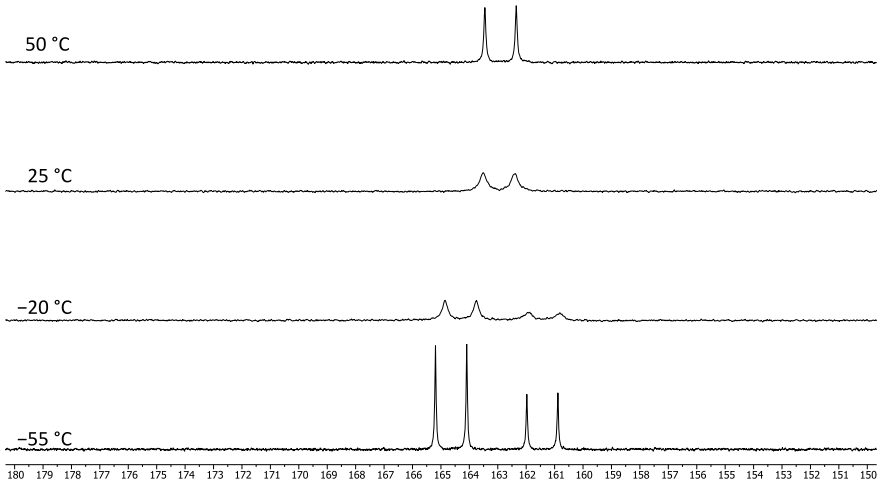

Fig. 3.3 $^{31}P\{^{1}H\}$ VT NMR of (*S*)-**38a** in $CDCl_3$.

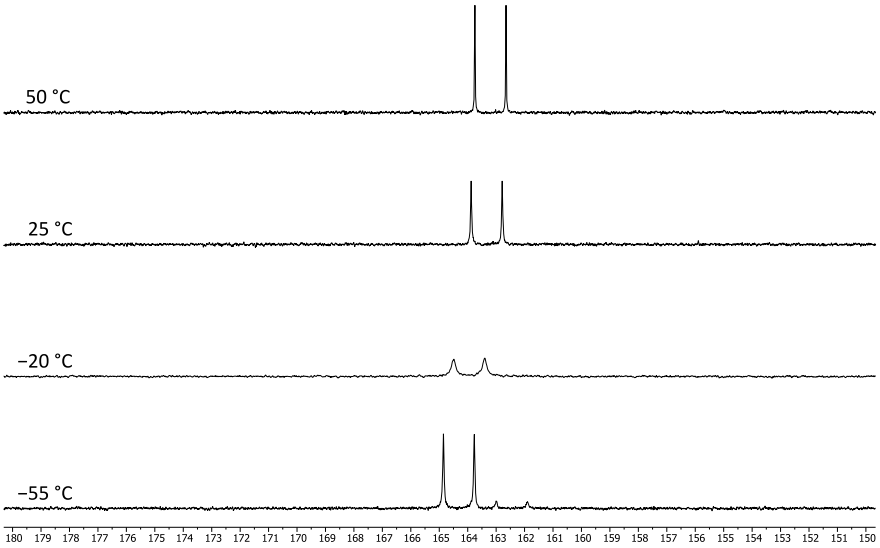

Fig. 3.4 $^{31}P\{^{1}H\}$ VT NMR of (*R*)-**38b** in $CDCl_3$.

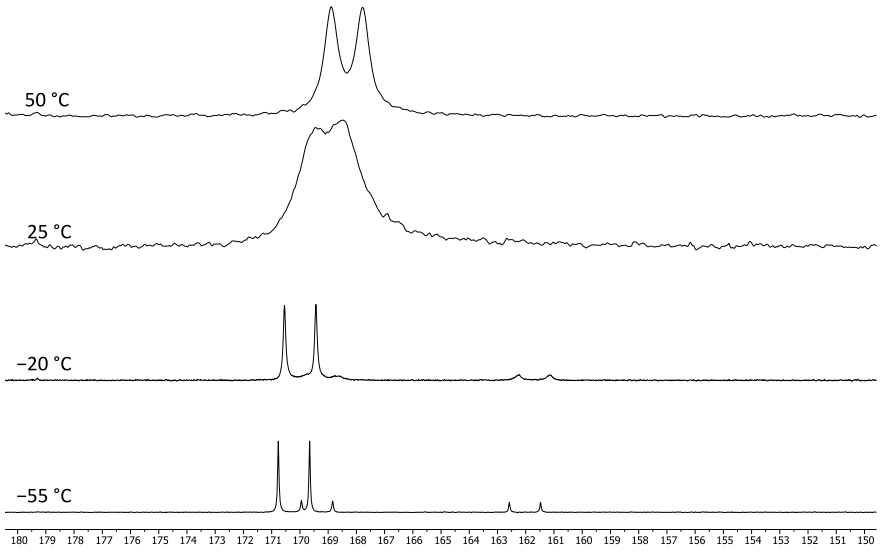

Fig. 3.5 $^{31}P\{^{1}H\}$ VT NMR of (*S*)-**39a** in $CDCl_3$.

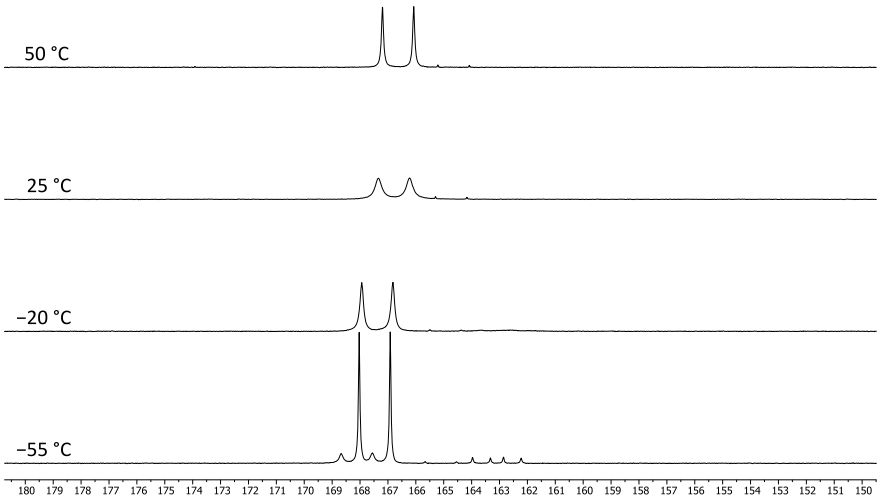

Fig. 3.6 $^{31}P\{^{1}H\}$ VT NMR of (*R*)-**39b** in $CDCl_3$.

Using 2D NMR spectroscopy, it is possible to investigate chemical and conformational exchange processes in addition to NOE effects.[159] 2D exchange spectroscopy (EXSY) has proven to be an effective method to study multisite exchange pathways under equilibrium conditions with a variety of NMR active nuclei.[160] For example, 2D phase-sensitive $^{31}P\{^{1}H\}$ EXSY NMR experiments have been used to study the mechanism for dynamic ligand exchange in chiral mercury,[161] palladium[162] and rhodium[163] phosphine complexes, as well as quantitative kinetic analysis of terminal ligand redistribution in a nickel phosphine complex.[164] We, therefore, sought to combine the low temperature $^{31}P\{^{1}H\}$ NMR study with a 2D phase-sensitive $^{31}P\{^{1}H\}$ EXSY NMR experiment to see if we could detect dynamic ligand exchange in (*S*)-**39a** and (*R*)-**39b**: measurements were recorded at −55 °C with a mixing time of 100 ms (Fig. 3.7). The absence of cross-peaks in the spectra indicates that the three distinct chemical species observed in (*S*)-**39a** and the five distinct chemical species observed in (*R*)-**39b** do not participate in dynamic exchange at this temperature. The broadening and coalescing of peaks above −55 °C (Figs. 3.5 and 3.6), suggests that this observation does not hold true at elevated temperatures.

We were able to obtain crystals suitable for X-ray crystallography for the complexes (*S*)-**38a**, (*R*)-**38b**, (*S*)-**39a** and (*R*)-**39b**, by slow diffusion of diethyl ether into a DCM solution of the respective complex (Figs. 3.8-3.11). In the asymmetric unit of both (*S*)-**39a** and (*R*)-**39b** there are two molecules in different conformations – an overlay of the crystallographically independent molecules in (*R*)-**39b** is provided to highlight that the torsion angle of the dimethyl substituted biphenyl moiety is of opposite sign in the two molecules (Fig. 3.12). The phosphonites show monodentate coordination through the phosphorus, and there is a *pseudo*-square-planar geometry around the rhodium centre. The Rh–P bond lengths range from 2.2104(13) Å in (*R*)-**38b** to 2.2428(13) Å in (*R*)-**39b**, consistent with literature values of 2.2112(7) Å for an analogous MOP-phosphonite complex reported by Higham *et al*.[93b] and 2.233(2) Å for a related complex employing a hydroxy phosphonite ligand.[106b] The Rh–Cl bond lengths are longer than the Rh–P bond lengths and range from 2.3470(13) Å in (*R*)-**39b** to 2.3757(12) Å in (*R*)-**39b** (the asymmetric unit of (*R*)-**39b** contains two different molecules) – the corresponding literature values (*vide supra*) of 2.3661(8) Å[93b] and 2.371(2) Å[106b] lie within this range. The phosphorus donor shows a stronger *trans* influence compared to the chloride in each case, hence for the alkene *trans* to the phosphorus, the C–C bond is shorter and the Rh–C bonds are longer than the alkene bound *cis* to the phosphorus atom. In (*S*)-**38a** and (*R*)-**38b** the lower naphthyl fragment of the binaphthyl backbone is face-to-face with the rhodium centre, whereas in both independent structures of (*S*)-**39a** and (*R*)-**39b** it is orientated away from the rhodium centre and faces the biphenyl moiety. As far as we are aware, (*S*)-**38a** and (*S*)-**39a** are the first crystallographically characterised examples of H-MOP type ligands coordinated to rhodium in the literature.

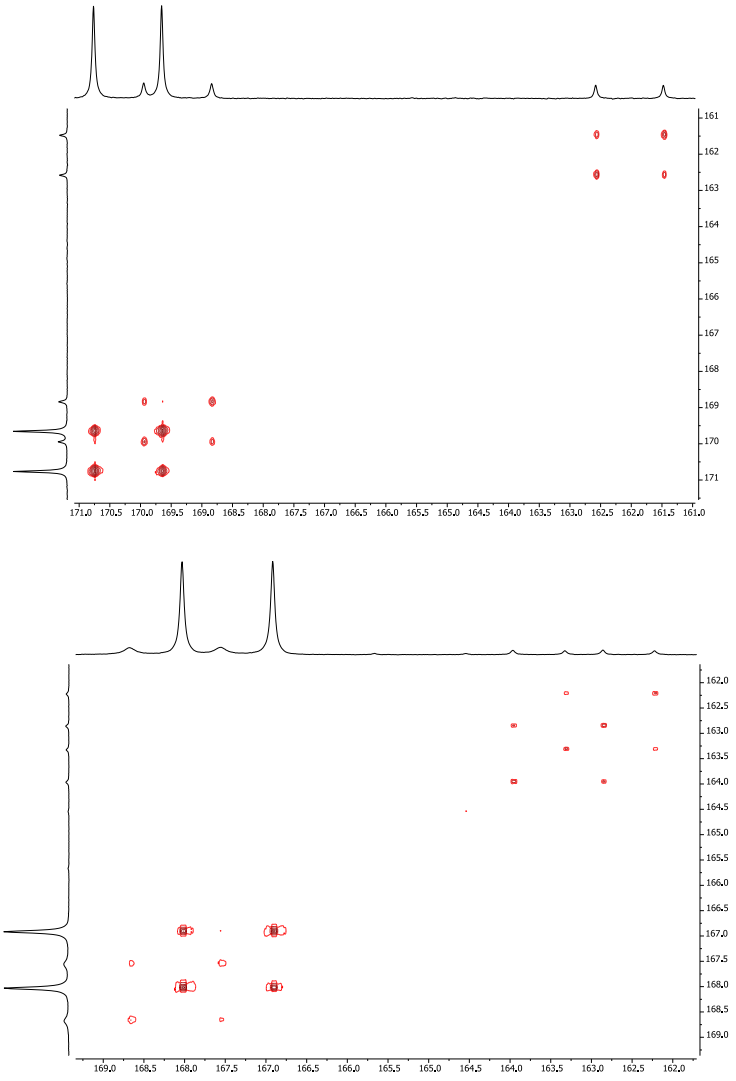

Fig. 3.7 2D phase-sensitive $^{31}P\{^{1}H\}$ EXSY NMR spectra of (*S*)-**39a** (top) and (*R*)-**39b** (bottom) in $CDCl_3$ at −55 °C, with a mixing time of 100 ms. The diagonal and exchange cross-peaks are phased positive (red).

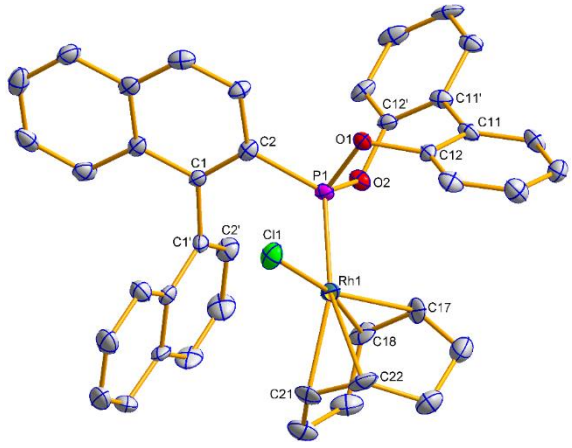

Fig. 3.8 Molecular structure of (*S*)-**38a**. Selected average bond distances (Å) and angles (°): Rh1–P1 2.211(2), Rh1–Cl1 2.364(2), Rh1–C17 2.123(8), Rh1–C18 2.116(8), Rh1–C21 2.233(8), Rh1–C22 2.265(8), P1–C2 1.812(8), P1–O1 1.621(6), P1–O2 1.619(5), C17–C18 1.426(13), C21–C22 1.358(13); P1–Rh1–Cl1 86.00(8), P1–Rh1–C17 93.0(3), P1–Rh1–C18 97.0(3), P1–Rh1–C21 162.7(2), P1–Rh1–C22 162.0(3), C2–C1–C1'–C2' −82.6(10), C12–C11–C11'–C12' −46.6(11).

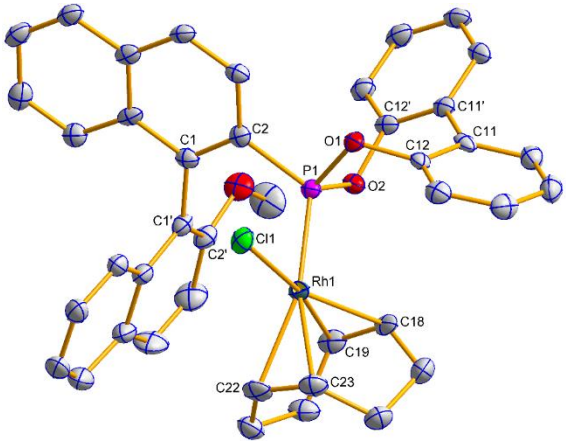

Fig. 3.9 Molecular structure of (*R*)-**38b**. Hydrogen atoms have been omitted for clarity. Selected average bond distances (Å) and angles (°): Rh1–P1 2.2104(13), Rh1–Cl1 2.3757(12), Rh1–C18 2.106(4), Rh1–C19 2.129(4), Rh1–C22 2.243(5), Rh1–C23 2.273(5), P1–C2 1.810(5), P1–O1 1.628(3), P1–O2 1.628(3), C18–C19 1.404(8), C22–C23 1.353(7); P1–Rh1–Cl1 86.00(4), P1–Rh1–C18 93.15(14), P1–Rh1–C19 96.99(14), P1–Rh1–C22 162.30(15), P1–Rh1–C23 162.61(14), C2–C1–C1'–C2' –90.9(6), C12–C11–C11'–C12' –43.3(6).

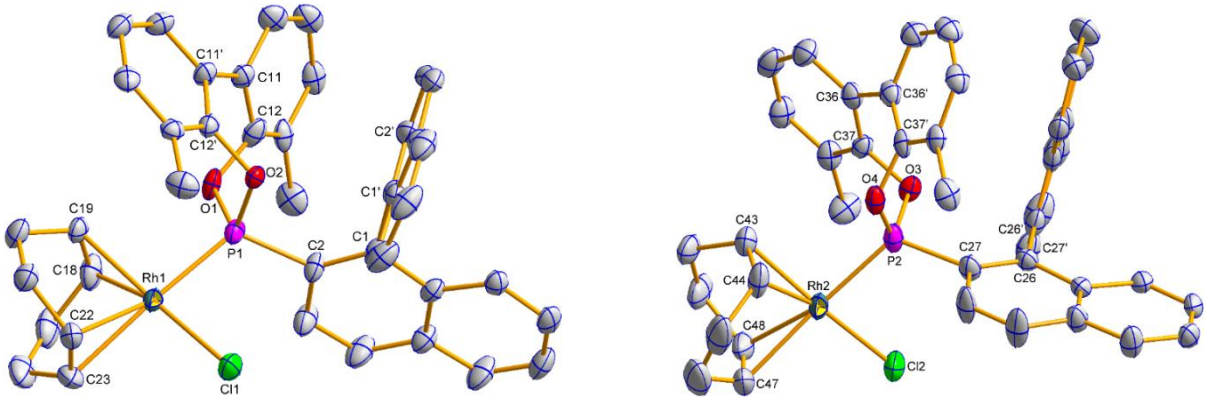

Fig. 3.10 Molecular structure of (*S*)-**39a** (the asymmetric unit comprises two molecules in different conformations). Hydrogen atoms have been omitted for clarity. Selected average bond distances (Å) and angles (°): (left) Rh1–P1 2.2139(12), Rh1–Cl1 2.3686(17), Rh1–C18 2.110(5), Rh1–C19 2.131(6), Rh1–C22 2.240(5), Rh1–C23 2.287(5), P1–C2 1.804(5), P1–O1 1.621(14), P1–O2 1.612(3), C18–C19 1.408(8), C22–C23 1.366(7); P1–Rh1–Cl1 87.72(6), P1–Rh1–C18 94.71(16), P1–Rh1–C19 93.08(15), P1–Rh1–C22 153.63(13), P1–Rh1–C23 171.16(13), C2–C1–C1'–C2' –89.0(6), C12–C11–C11'–C12' 35(2); (right) Rh2–P2 2.2173(13), Rh2–Cl2 2.353(2), Rh2–C43 2.141(7), Rh2–C44 2.122(6), Rh2–C47 2.291(6), Rh2–C48 2.248(6), P2–C27 1.816(5), P2–O3 1.611(3), P2–O4 1.550(10), C43–C44 1.408(8), C47–C48 1.322(9); P2–Rh2–Cl2 87.72(6), P2–Rh2–C43 92.83(16), P2–Rh2–C44 96.29(17), P2–Rh2–C47 173.18(18), P2–Rh2–C48 152.96(17), C27–C26–C26'–C27' –87.0(7), C37–C36–C36'–C37' –43(3).

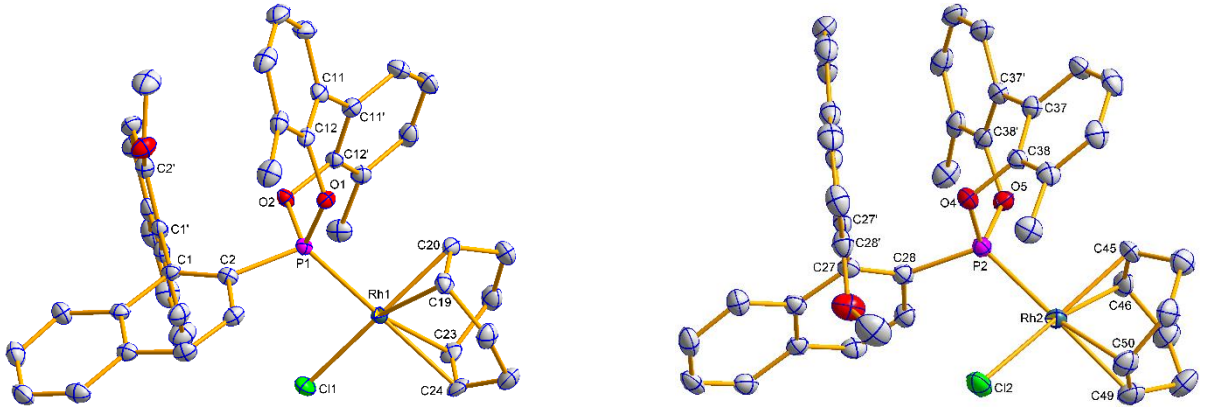

Fig. 3.11 Molecular structure of (*R*)-**39b** (the asymmetric unit comprises two molecules in different conformations). Hydrogen atoms have been omitted for clarity. Selected average bond distances (Å) and angles (°): (left) Rh2–P2 2.2428(13), Rh2–Cl2 2.3470(13), Rh2–C45 2.131(5), Rh2–C46 2.134(5), Rh2–C49 2.272(6), Rh2–C50 2.237(5), P2–C28 1.823(5), P2–O4 1.609(3), P2–O5 1.615(4), C45–C46 1.399(8), C49–C50 1.330(8); P2–Rh2–Cl2 89.62(5), P2–Rh2–C49 173.59(16), P2–Rh2–C50 152.03(16), P2–Rh2–C45 92.60(15), P2–Rh2–C46 95.98(15), C28–C27–C27'–C28' –104.6(6), C38–C37–C37'–C38' –43.3(8); (right) Rh1–P1 2.2365(11), Rh1–Cl1 2.3529(12), Rh1–C19 2.124(5), Rh1–C20 2.139(5), Rh1–C23 2.249(5), Rh1–C24 2.287(5), P1–C2 1.812(4), P1–O1 1.619(3), P1–O2 1.611(3), C19–C20 1.414(7), C23–C24 1.358(7); P1–Rh1–Cl1 91.14(4), P1–Rh1–C19 95.88(14), P1–Rh1–C20 92.01(13), P1–Rh1–C23 150.26(14), P1–Rh1–C24 174.67(14), C2–C1–C1'–C2' –82.8(6), C12–C11–C11'–C12' 44.4(7).

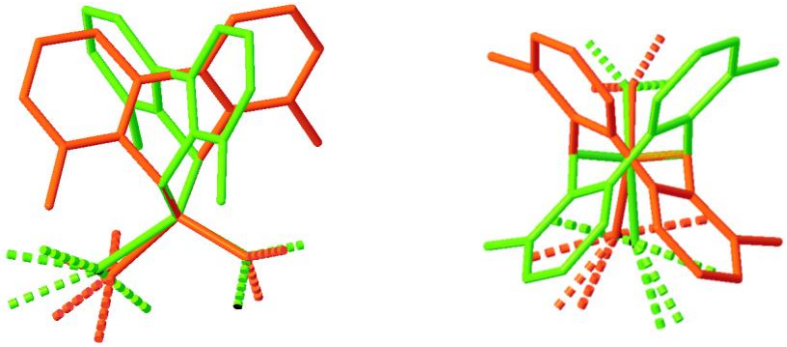

Fig. 3.12 Two views of an overlay image of the biphenyl moiety in the two independent molecules of (*R*)-**39b**.

$[Rh(L^P)_2]BF_4$ complexes

As part of our investigation into the hemilabile aryl coordination of MOP-type ligands,[92-93,138] we sought to synthesise rhodium(I) complexes of the type $[Rh(L^P)_2]^+$ using the bulky dimethylbiphenoxy ligands (*S*)-**30a** and (*R*)-**30b**. This was achieved by reacting two equivalents of the phosphonite with $[Rh(\eta^2{:}\eta^2\text{-cod}]BF_4$ in DCM; precipitation after addition of diethyl ether led to the isolation of the pure compounds $[Rh((S)\text{-}\mathbf{30a})_2]BF_4$ (*S*)-**40a** and $[Rh((R)\text{-}\mathbf{30b})_2]BF_4$ (*R*)-**40b**. (*S*)-**40a** and (*R*)-**40b** were characterised by multinuclear NMR spectroscopy, HRMS and, for (*R*)-**40b**, by X-ray crystallography. Solution state $^{31}P\{^1H\}$ VT NMR studies on (*S*)-**40a** (Fig. 3.13) and (*R*)-**40b** (Fig. 3.14) revealed that the two phosphorus nuclei are inequivalent, due to the appearance of two resonances with equal intensity, which are shifted slightly downfield compared to (*S*)-**39a** (Fig. 3.5) and (*R*)-**39b** (Fig. 3.6). We were able to measure P–P and P–Rh coupling upon cooling, which gave a doublet of doublets splitting pattern

for (*S*)-**40a** ($^{1}J_{PRh}$ = 288 Hz and 294 Hz and $^{2}J_{PP}$ = 27 Hz) and (*R*)-**40b** ($^{1}J_{PRh}$ = 283 Hz and 310 Hz and $^{2}J_{PP}$ = 32 Hz) – additional low intensity resonances were also observed.

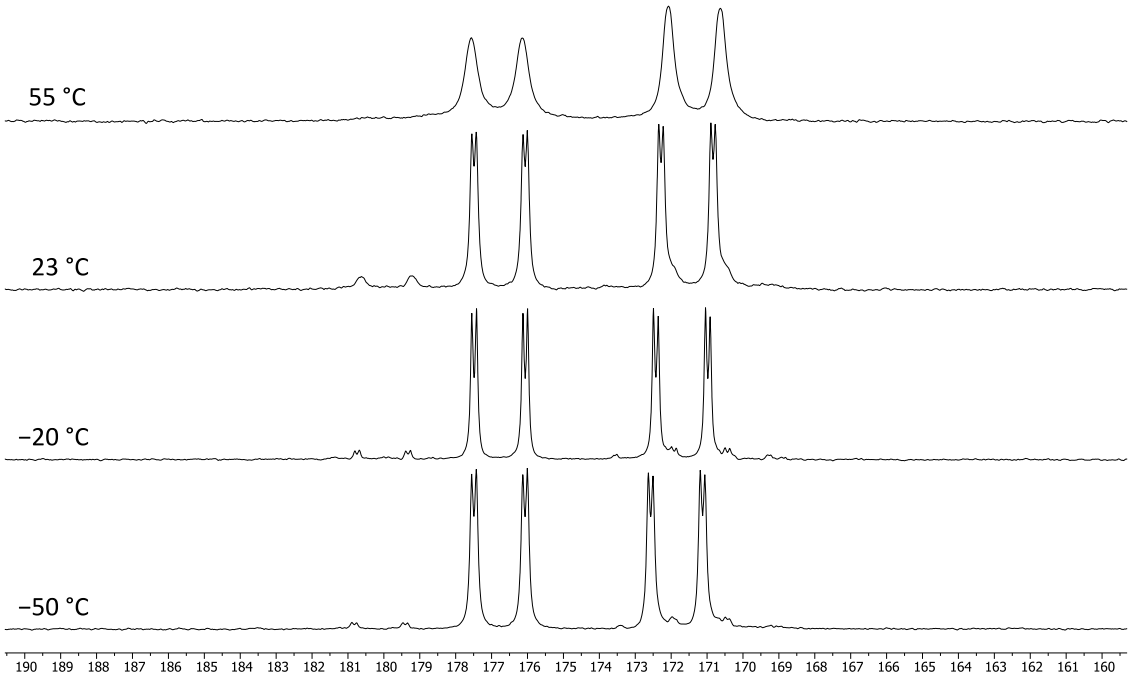

Fig. 3.13 $^{31}P\{^{1}H\}$ VT NMR of (*S*)-**40a** in $CDCl_3$.

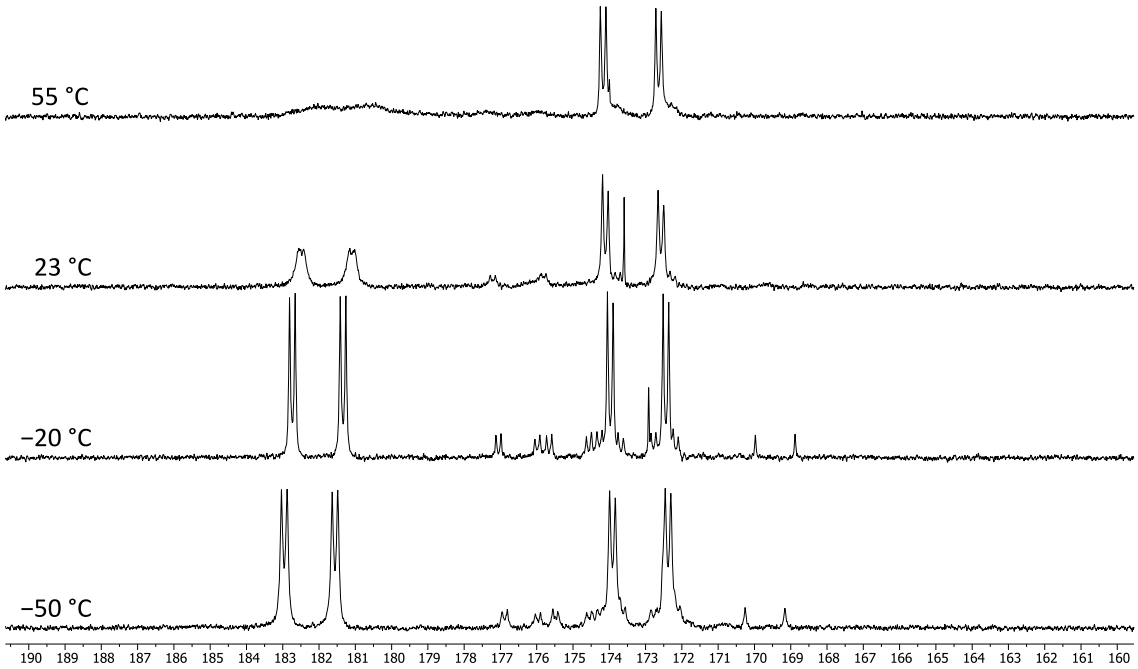

Fig. 3.14 $^{31}P\{^{1}H\}$ VT NMR of (*R*)-**40b** in $CDCl_3$.

The ^{1}H NMR resonances in the spectra of (*S*)-**40a** and (*R*)-**40b** were slightly broadened and unresolved at room temperature. However, upon cooling to 5 °C and −20 °C respectively, we were able to observe the expected number of independent aromatic resonances (38 for (*S*)-**40a** and 36 for (*R*)-**40b**) and the

4 independent methyl resonances from the biphenoxy moieties. Using 2D NMR experiments (^{1}H-COSY, ^{1}H-ROESY, HSQC and HMBC) performed at these reduced temperatures, in addition to ^{1}H, ^{1}H{^{31}P} and ^{13}C{^{1}H} NMR data, it was possible to unambiguously assign the proton and carbon resonances. The ^{13}C NMR chemical shift data for (*S*)-**40a** and (*R*)-**40b** reveal that in the solution state, one of the hemilabile MOP ligands is coordinating to the rhodium atom via an η^6-binding mode using the lower naphthyl ring, in addition to bonding through the P-atom (Fig. 3.15). The carbon atoms in the η^6-bound C_6 ring from the P,C-π-donor ligand (B) are shifted upfield compared to those in the solely P-donor ligand (A), by a magnitude of 8.9 to 26.5 ppm in (*S*)-**40a** and 6.5 to 35.7 in (*R*)-**40b** (Fig. 3.15). The resonances attributed to *C*1' and *C*4' in ligand B are the most significantly shifted and appear as doublets with *J* values of 11.3 Hz and 12.8 Hz in (*S*)-**40a**, and 15.2 Hz and 10.4 Hz in (*R*)-**40b** respectively.

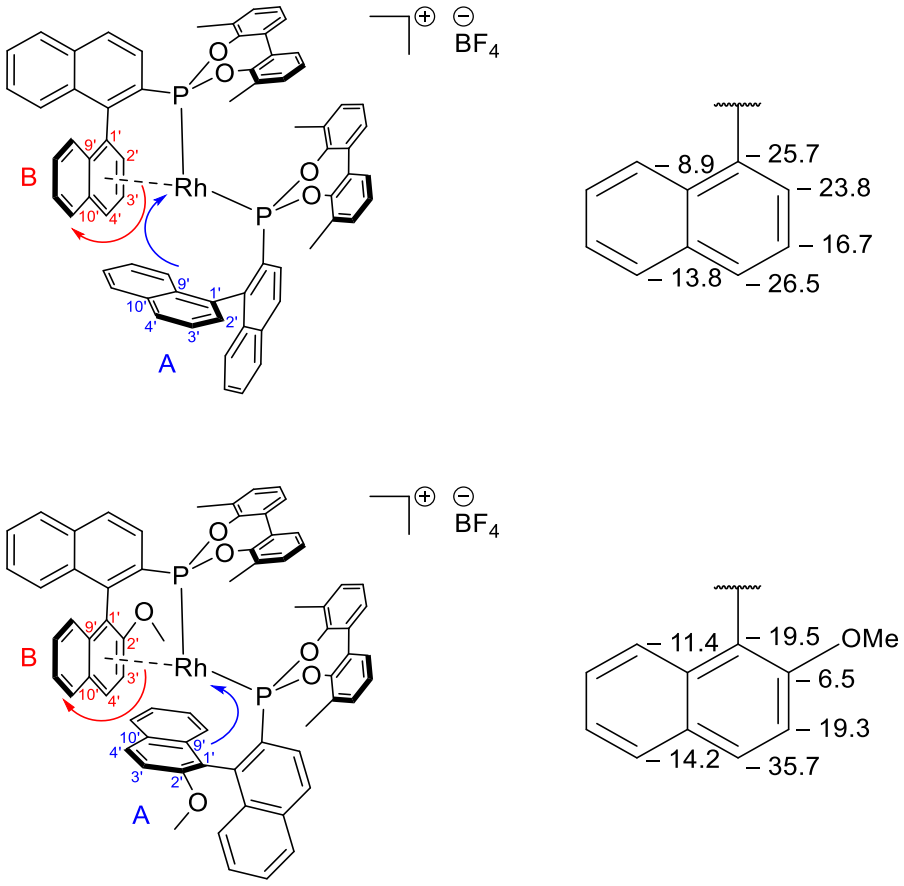

Fig. 3.15 Proposed molecular structure and a fragment showing the difference in the ^{13}C{^{1}H} NMR coordination chemical shift (ppm) of ligand B (P,C-π-donor) relative to that of ligand A (P-donor) for (*S*)-**40a** (top) and (*R*)-**40b** (bottom). NMR measurements were taken at 176 MHz in $CDCl_3$ at 5 °C for (*S*)-**40a** and at 126 MHz in $CDCl_3$ at −20 °C for (*R*)-**40b**.

The result of having a chelating P,C-π-donor is saturation of the rhodium coordination sphere (electron count of 18, counting the arene as a 6 electron donor), this may explain the increased stability we observed for the $[Rh(L^P)_2]BF_4$ complexes compared to the 16 electron $[Rh(L^P)(\eta^2{:}\eta^2\text{-cod})Cl]$ complexes, which are prone to oxidation if not handled with care, as witnessed by the presence of a phosphorus(V)

peak in the $^{31}P\{^{1}H\}$ NMR spectra of (*S*)-**29a**, (*R*)-**29b**, (*S*)-**30a** and (*R*)-**30b**. To investigate the presence of dynamic behaviour on the NMR time scale, Rotating frame Overhauser Effect Spectroscopy (ROESY) experiments were carried out on a solution of (*S*)-**40a**. The 2D phase-sensitive ^{1}H-ROESY NMR spectrum $CDCl_3$ at 0 °C and −50 °C are shown in Fig. 3.16. The ROE signals are negative (blue) and the other cross-peaks (red) are due to chemical exchange (opposite phase of a true NOE peak). It is clear that at 0 °C there is dynamic chemical exchange, this behaviour is a result of the hemilabile binding of the η^6-coordinated arene, which dissociates and is replaced by the equivalent face of the second ligand (Fig. 3.15). Upon cooling to −50 °C this dynamic behaviour ceases and cross-peaks related to chemical exchange are no longer observed.

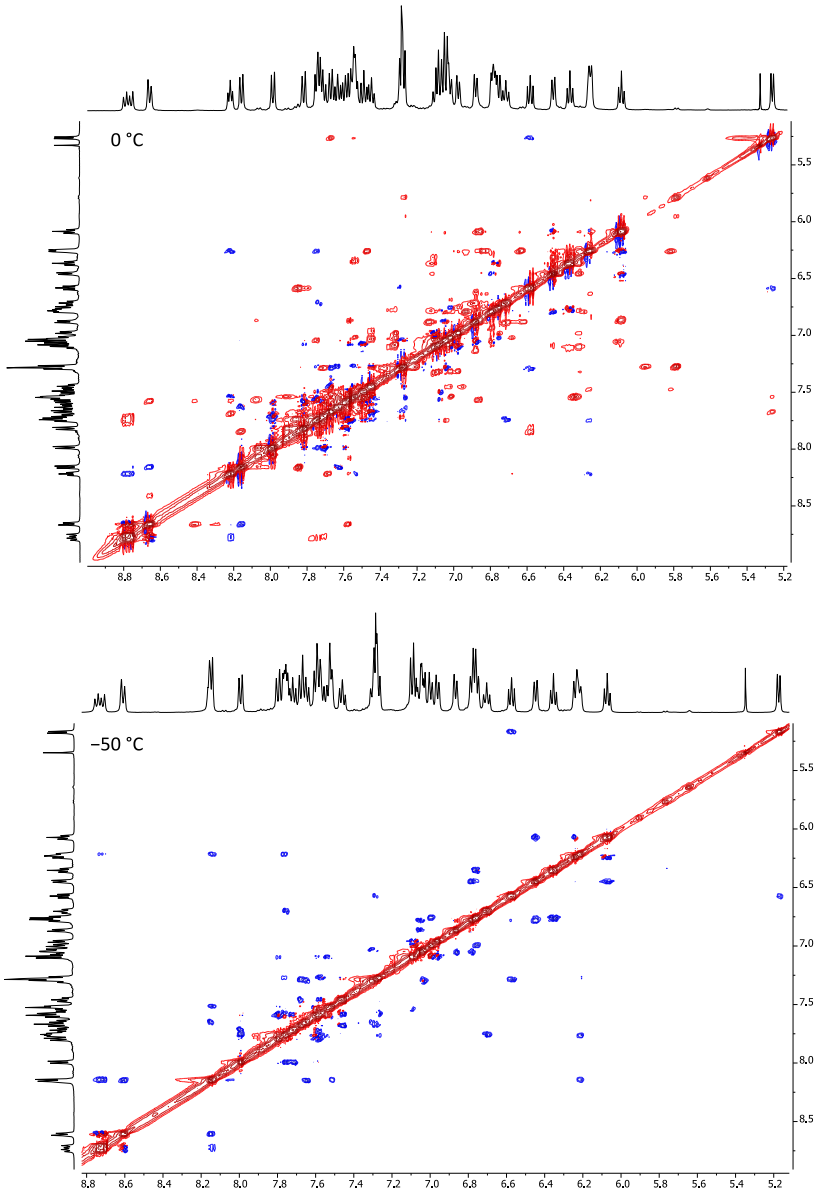

Fig. 3.16 2D phase-sensitive ^{1}H-ROESY NMR spectrum of (*S*)-**40a** in $CDCl_3$ at 0 °C (top) and −50 °C (bottom), with a mixing time of 200 ms. The diagonal and exchange cross-peaks are phased positive (red) and the ROE signals are negative (blue).

The molecular structure of (*R*)-**40b** was elucidated after growing single crystals from the slow diffusion of hexane into a $CDCl_3$ solution. There are two crystallographically independent molecules in the asymmetric unit, which comprises two cations and two BF_4 anions (Figs. 3.17 and 3.18). In the solid state, the cations of (*R*)-**40b** contain a rhodium atom with two coordinated phosphonites, both ligands coordinate via the phosphorus atom and, in each case, one ligand acts as a chelating P,C-π-donor via a second binding mode using the lower naphthyl ring (Figs. 3.17 and 3.18). The Rh–C distances suggest an η^6-binding mode, which is consistent with the conclusions drawn from the solution state NMR experiments performed on this complex, where we propose that the C_6 ring containing the *ipso*-C (which happens to be the closest contact) coordinates to the rhodium atom side-on via its π-system (*vide supra*). The solid state recognition of this bonding motif for a MOP-type ligand is rare, the only other known example we are aware of is a related MOP-phosphonite complex that Higham *et al*. previously reported with a BINOL moiety on the phosphorus atom;[93b] the Rh–C distances in both complexes are comparable. Goldberg reported η^6-bonding modes in rhodium complexes with 2-(dicyclohexylphosphino)biphenyl ligands.[165]

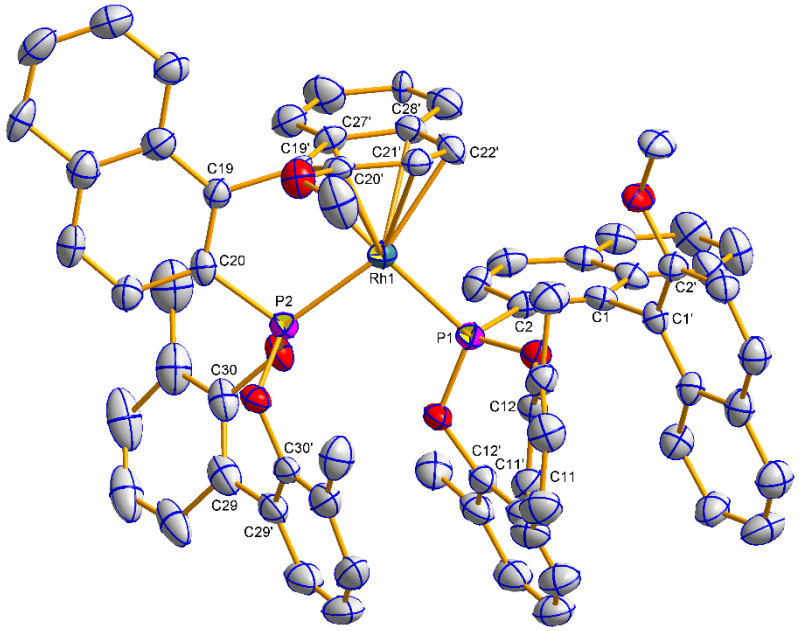

Fig. 3.17 Molecular structure of one of the cations of (*R*)-**40b** (the asymmetric unit comprises two cations and two anions in different conformations). Hydrogen atoms have been omitted for clarity. Selected average bond distances (Å) and angles (°): Rh1–P1 2.2117(16), Rh1–P2 2.2008(18), Rh1–C19' 2.200(6), Rh1–C20' 2.311(6), Rh1–C21' 2.312(6), Rh1–C22' 2.278(7), Rh1–C27' 2.445(7), Rh1–C28' 2.492(6), P1–C2 1.816(6), P2–C20 1.817(7); P1–Rh1–P2 98.62(6), Rh1–P1–C2 111.1(2), Rh1–P2–C20 105.9(2), C2–C1–C1'–C2' –84.3(8), C12–C11–C11'–C12' –37.7(11), C20–C19–C19'–C20' –92.6(8), C30–C29–C29'–C30' 40.2(10).

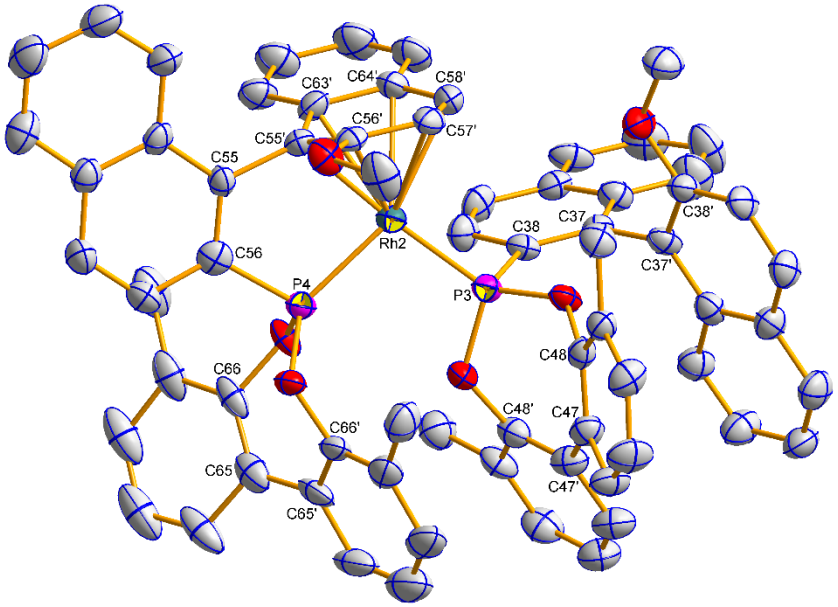

Fig. 3.18 Molecular structure of one of the cations of (*R*)-**40b** (the asymmetric unit comprises two cations and two anions in different conformations). Hydrogen atoms have been omitted for clarity. Selected average bond distances (Å) and angles (°): Rh2–P3 2.2148(18), Rh2–P4 2.1743(18), Rh2–C55' 2.174(7), Rh2–C56' 2.314(6), Rh2–C57' 2.321(6), Rh2–C58' 2.305(7), Rh2–C63' 2.474(7), Rh2–C64' 2.500(6), P3–C38 1.823(7), P4–C56 1.822(7); P3–Rh2–P4 98.97(7), Rh2–P3–C38 111.7(2), Rh2–P4–C56 105.7(2), C38–C37–C37'–C38' –84.4(8), C48–C47–C47'–C48' –34.7(12), C56–C55–C55'–C56' –92.5(8), C66–C65–C65'–C66' 38(3).

Asymmetric hydrogenation of alkenes

The rhodium-catalysed asymmetric hydrogenation (AH) of prochiral alkenes is a highly useful tool in organic chemistry, and the reaction has often played a pioneering role in the field of single-enantiomer synthesis and chiral ligand design.[166] For example, the AH of enamides is a highly useful synthetic methodology for synthesising chiral amines and amides, compounds which have important pharmaceutical applications.[167] Chiral monodentate phosphites,[168] phosphoramidites[169] and phosphonites[107b,c,e] have proven to be effective ligands in the rhodium-catalysed AH of prochiral alkenes, proving that the use of chelating ligands is not essential in order to achieve highly enantioselective catalysis. We decided to test the $[Rh(L^P)_2]BF_4$ complexes (*S*)-**40a** and (*R*)-**40b**, prepared *in situ*, in the hydrogenation of a selection of benchmark substrates, dimethyl itaconate (DMI) and the α-acetamidoacrylates methyl 2-acetamidoacrylate (MAA) and methyl (Z)-2-acetamidocinnamate (MAC) (Table 3.5). DCM was chosen as the solvent based on a report which found that both the rate and enantioselectivity were improved in the hydrogenation of MAC by a phosphoramidite complex when using nonprotic solvents.[169a] It was also considered that using anhydrous DCM would limit the risk of catalyst decomposition. In the AH of DMI we were able to obtain reasonable conversion after 48 h; however, the reaction did not proceed enantioselectively (Table 3.5, entries 1 and 2). With the substrate MAA the conversion was low (Table 3.5, entries 3 and 4) and with MAC it was negligible (Table 3.5, entries 5 and 6). Although, we did obtain a moderate *ee* for MAC

when employing (*R*)-**30b** as ligand (Table 3.5, entry 6). The low *ee*s may be due to hydrogenation of the coordinated lower naphthyl ring as suggested by Chauvin for a Rh-H-MOP catalyst,[170] who proposed that the energy barrier to binaphthyl rotation in this ligand would be lowered significantly compared to the parent H-MOP ligand, reducing the enantiocontrol of the catalyst.

Table 3.5 Rhodium-catalysed asymmetric hydrogenation of prochiral alkenes.[a]

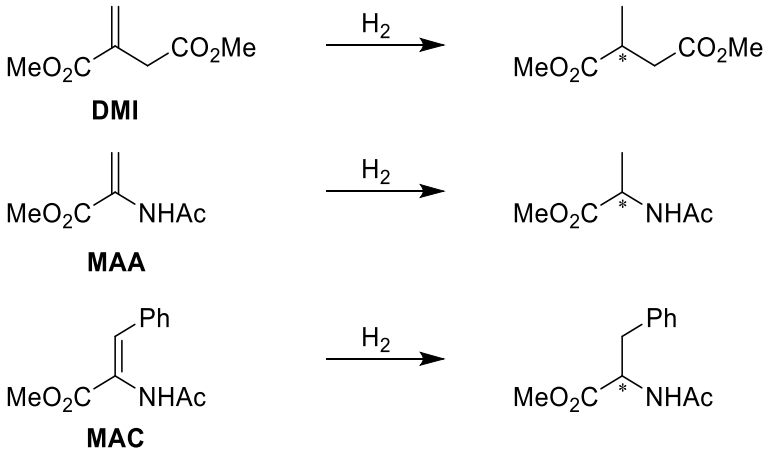

	Ligand	Substrate	Conversion[b]	*ee*[c]
1	(*S*)-**30a**	DMI	47	0[d]
2	(*R*)-**30b**	DMI	70	0[d]
3	(*S*)-**30a**	MAA	26	1 (*R*)[d]
4	(*R*)-**30b**	MAA	8	3 (*S*)[d]
5	(*S*)-**30a**	MAC	<1	–
6	(*R*)-**30b**	MAC	3	34 (*S*)[e]

[a] 0.1 mol% $[Rh(L^P)_2]BF_4$ catalyst, generated *in situ*, in DCM at room temperature and 2 bar pressure for 48 h. [b] % Conversion determined by ^1H NMR spectroscopy. [c] Absolute configuration was assigned by comparison to authentic samples. [d] % *ee* determined by chiral GC (Supelco β-dex). [e] % *ee* determined by chiral HPLC (Lux Cellulose) with hexane/2-propanol (90:10).

Asymmetric hydroformylation of styrene

Asymmetric hydroformylation (AHF) is a very atom-economic, efficient synthetic route towards chiral aldehydes, one of the most versatile organic functional groups. The reaction proceeds via the transition metal-catalysed reaction of alkenes with syngas,[171] and has many potential applications in the fine chemical and pharmaceutical industries.[172] It has long been known that rhodium complexes are able to catalyse hydroformylation reactions,[5] and that diphosphine and phosphite ligands can act as highly regio- and enantioselective ligands in AHF reactions.[173] The AHF of styrene analogues is an industrially relevant reaction due to the pharmacological importance of a number of the 2-aryl propionic acid derivatives accessible from the products of this reaction. For example, (*S*)-naproxen,

(*S*)-ibuprofen, (*R*)-flurbiprofen and (*S*)-ketoprofen are important non-steroidal anti-inflammatory drugs (NSAIDs).[171] However, the use of monodentate ligands in these transformations is underdeveloped. To the best of our knowledge, Beller and co-workers reported the best literature result for the AHF of styrene with a monodentate ligand in a rhodium-phosphepine complex (48% *ee*).[174] The poor yield for this reaction (17%) demonstrates the scope for progression in this area of research. Substitution of P–C bonds with P–O bonds in the ligand in hydroformylation catalysts often results in increased rates of reaction, as this facilitates the dissociation of CO from the metal.[171] Therefore, we speculated that our series of MOP-phosphonite ligands could be promising candidates for this transformation due to their weak σ-donor but strong π-acceptor properties. The six MOP-phosphonites and two MOP-phosphines were screened in the AHF of styrene using 0.1 mol% of a catalyst prepared *in situ* from the reaction of [Rh(acac)$(CO)_2$] with the ligand in a Rh:P ratio of 1:2. The reactions were performed at a pressure of 40 bar syngas over 16h and at a moderate temperature of 36 °C (Table 3.6).

Table 3.6 Rhodium-catalysed asymmetric hydroformylation of styrene.

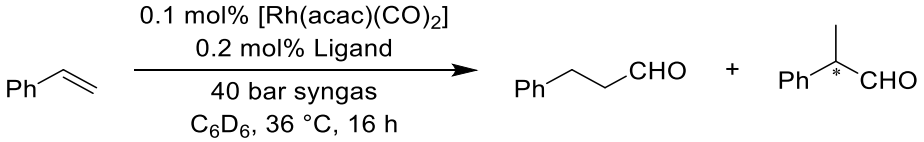

	Ligand	Conversion[a]	*Iso*/*n*[b]	*ee*[c]
1	(*S*)-H-MOP	47	19	6 (*S*)
2	(*R*)-MeO-MOP	53	24	6 (*S*)
3	(*S*)-**28a**	99	18	3 (*R*)
4	(*R*)-**28b**	>99	15	4 (*S*)
5	(*S*)-**29a**	96	16	6 (*R*)
6	(*R*)-**29b**	97	15	1 (*R*)
7	(*S*)-**30a**	98	12	1 (*S*)
8	(*R*)-**30b**	>99	16	12 (*S*)

[a] % Conversion determined by ^{1}H NMR spectroscopy. [b] Ratio determined by ^{1}H NMR spectroscopy. [c] % *ee* determined by chiral GC (Supelco β-dex); absolute configuration was assigned according to literature data.

It is clear that the phosphonite ligands (Table 3.6, entries 3-8) far outperformed their phosphine counterparts (Table 3.6, entries 1 and 2) with respect to conversion. Very high conversions were obtained in each case, and complete conversion was achieved when the MeO-MOP-phosphonites (*R*)-**28b** and (*R*)-**30b** were employed as the ligand. The product was a mixture of the linear (*n*) and branched (*iso*) isomers. The desired *iso*-aldehyde was formed in a large excess: *iso*/*n* ranged from

12-18 for the phosphonite catalysts (Table 3.6, entries 3-8) and was slightly higher (19-24) for the phosphine analogues (Table 3.6, entries 1 and 2). Unfortunately, the enantioselectivity in these reactions was found to be low, the best result being a 12% *ee* when employing the ligand (*R*)-**30b** (Table 3.6, entry 8). However, the high conversions and regioselectivity observed in these non-optimised conditions with a low catalyst loading, does indicate that modified reaction conditions[174] and further ligand development could lead to promising AHF catalysts.

Asymmetric addition of phenylboronic acid to an isatin

Hayashi and co-workers reported the rhodium-catalysed asymmetric addition of arylboronic acids to isatins, in an attempt to develop an asymmetric strategy towards the synthesis of natural products and biologically active compounds containing the 3-aryl-3-hydroxy-2-oxindole structural motif.[175] They were able to catalyse the reaction using a Rh(I)/(*R*)-MeO-MOP complex, achieving enantioselectivities of up to 91%. We, therefore, tested our series of MOP-phosphonite ligands in the addition of phenylboronic acid to 1-(*p*-methoxybenzyl)-5-chloroisatin (Table 3.7, entries 3-8). We also used the ligand (*R*)-MeO-MOP to allow us to compare our procedure to the literature data (Table 3.7, entry 2); both the conversion and the *ee* are in agreement with the literature values.[175]

Table 3.7 Rhodium-catalysed asymmetric addition of phenylboronic acid to 1-(*p*-methoxybenzyl)-5-chloroisatin.

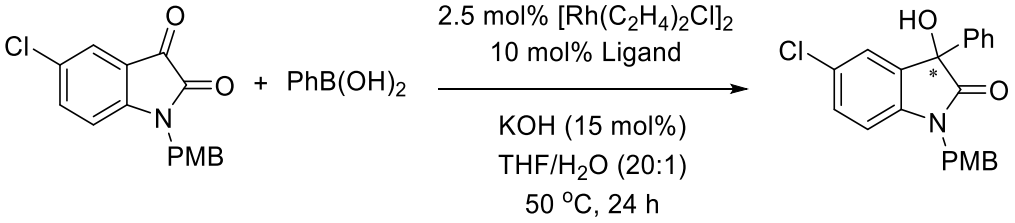

	Ligand	Conversion[a]	*ee*[b]
1	(*S*)-H-MOP	>99	70 (*S*)
2	(*R*)-MeO-MOP	83 (92)[c]	88 (*S*) (90)[c]
3	(*S*)-**28a**	0	–
4	(*R*)-**28b**	0	–
5	(*S*)-**29a**	20	32 (*S*)
6	(*R*)-**29b**	43	39 (*S*)
7	(*S*)-**30a**	41	32 (*S*)
8	(*R*)-**30b**	40	11 (*S*)

[a] % Conversion determined by ^{1}H NMR spectroscopy. [b] % *ee* determined by chiral HPLC (Lux Cellulose) with hexane/2-propanol (80:20); absolute configuration was assigned according to literature data. [c] Isolated yield and *ee* reported by Hayashi *et al*. in parenthesis.

The ligands (*S*)-**28a** and (*R*)-**28b** failed to provide any conversion, which we suspect is due to the reaction conditions that include water – both ligands have proven to be sensitive to hydrolysis during our previous studies.[138] The biphenoxy derived ligands (*R*)-**29b**, (*S*)-**30a** and (*R*)-**30b** fared better, generating conversions of between 40-43%. Ligand (*S*)-**29a** gave approximately half the conversion of (*R*)-**29b**. However, we have found that this ligand is the most sensitive to decomposition out of the biphenoxy series, and this is possibly the reason for the reduced activity. The H-MOP-phosphonites (*S*)-**29a** and (*R*)-**30a** gave matching *ee*s (Table 3.7, entries 5 and 7), whereas the MeO-MOP analogues gave very different *ee*s (Table 3.7, entries 6 and 8). Ligand (*R*)-**30b** produced a notably low value of 11%, with (*R*)-**29b** giving the highest value of 39% *ee* in this biphenoxy series. We can also report, to the best of our knowledge, the first application of a Rh(I)/(*S*)-H-MOP complex to catalyse the asymmetric addition of phenylboronic acid to 1-(*p*-methoxybenzyl)-5-chloroisatin. The reaction proceeded with complete conversion and achieved a good *ee* of 70% (Table 3.7, entry 1).

3.2.5 Palladium(II) complexes and catalysis

Palladium-mediated cross-coupling reactions are a widely used route to form C–C, C–N, C–O and C–S bonds in organic synthesis.[176] One of the most frequently applied synthetic methodologies used to form carbon–carbon bonds is the palladium-catalysed Suzuki-Miyaura cross-coupling reaction of a boronic acid with an organic halide.[177] The importance of this transformation in modern organic synthesis resulted in Suzuki being awarded a share of the 2010 Nobel Prize in Chemistry.[178] In these reactions, electron rich and bulky phosphine ligands are most often preferred.[179] However, a DFT computational study by Harvey and co-workers into phosphine donor/acceptor and steric features found that the transmetallation process in the catalytic cycle has a lower energy barrier for weak σ-donor and strong π-acceptor ligands.[180] Iwasawa and co-workers reported high yields and enantioselectivities (up to 91% and 78% respectively) in Suzuki-Miyaura cross-coupling reactions of aryl chlorides employing bulky, chiral phosphonite ligands with low catalyst loadings possible (0.1 mol%).[104] We, therefore, decided to synthesise palladium(II) dichloride complexes of our MOP-phosphonite ligands and tested their ability to catalyse the preparation of axially chiral biaryl compounds from aryl bromides and arylboronic acids, a field where a number of monophosphines have shown high activity and enantioselectivities (Tables 3.8 and 3.9).[181]

Buchwald and co-workers have shown that palladium complexes of the electron-rich binaphthyl P,N-ligand KenPhos can be applied in these reactions, with the resultant axially chiral biaryl products having high enantiomeric enrichment.[182] The enantioselective synthesis of molecules with a binaphthyl backbone from naphthalene derivatives is interesting as this can facilitate a route to chiral monophosphine ligands such as those reported in this thesis. This was demonstrated by Ma and Yang

who used a Suzuki-Miyaura cross-coupling reaction as part of their strategy to obtain optically pure H-MOP.[183] Palladium complexes using axially chiral biphenyl P,N- and P,O-ligands with a 2,4-pentanediol-tethered ether bridge have been successfully employed in the asymmetric synthesis of multifunctionalised, axially chiral biaryl phosphonates.[184] The same group subsequently reported enantiomeric excesses of up to 97% using the dicyclohexylphosphine analogue of MeO-MOP.[185] It has also been reported that MeO-MOP stabilised palladium nanoparticles can catalyse the coupling of 1-bromo-2-methoxynaphthalene and naphthalene-1-boronic acid, albeit the unoptimised reaction gave only moderate conversion (50%) and low enantioselectivity (12%).[186] However, to the best of our knowledge there are no reports of MOP-phosphonite ligands being employed in this type of reaction.

Asymmetric Suzuki-Miyaura cross-coupling reactions

We chose to test our series of MOP ligands in the palladium-catalysed reaction between 1-bromo-2-methoxynaphthalene and naphthalene-1-boronic acid in order to synthesise the axially chiral molecule 2-methoxy-1,1'-binaphthyl (Table 3.8).

Table 3.8 Asymmetric Suzuki-Miyaura coupling of naphthalene-1-boronic acid with 1-bromo-2-methoxynaphthalene.

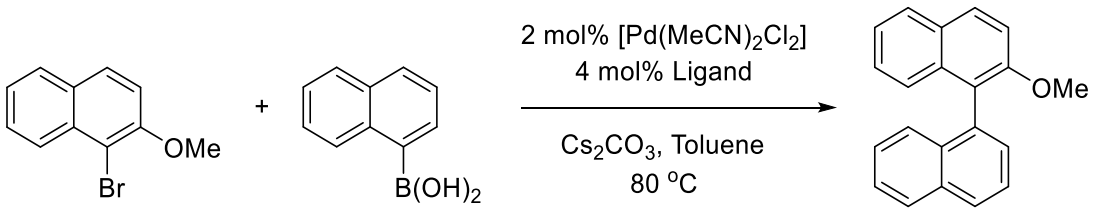

	Ligand	Conversion[a]			*ee*[b]
		30 min	1 h	16 h	
1	(*S*)-H-MOP	86	94	95	4 (*R*)
2	(*R*)-MeO-MOP	98	>99	–	8 (*R*)
3	(*S*)-**28a**	66	83	94	21 (*R*)
4	(*R*)-**28b**	>99	–	–	1 (*S*)
5	(*S*)-**29a**	42	51	75	12 (*R*)
6	(*R*)-**29b**	84	91	95	27 (*R*)
7	(*S*)-**30a**	54	65	85	11 (*S*)
8	(*R*)-**30b**	89	90	98	42 (*R*)

[a] % Conversion determined by ^{1}H NMR spectroscopy. [b] % *ee* determined by chiral HPLC (Lux Cellulose) with hexane/2-propanol (99:1); absolute configuration was assigned according to literature data.

The catalyst was generated by stirring two equivalents of the corresponding ligand with $[Pd(MeCN)_2Cl_2]$ in DCM for 2 hours at room temperature, before removing the volatiles under vacuum.

The reactions were all performed with caesium carbonate as the base, toluene as the solvent and at a temperature of 80 °C. The results of the coupling reaction with 1-bromo-2-methoxynaphthalene are given in Table 3.8. All of the MeO-MOP type ligands proceeded with almost complete conversion. The reaction was complete within 30 minutes when (*R*)-**28b** was employed as the ligand and within 1 hour with (*R*)-MeO-MOP. Longer reaction times were required to reach ≥95% conversions with (*R*)-**29b** and (*R*)-**30b** (Table 3.8, entries 2, 4, 6 and 8). The H-MOP type ligands generally had lower conversions and the reaction times were longer compared to their methoxy analogues. Although (*S*)-H-MOP had a high conversion after 1 hour, it took (*S*)-**28a** 16 hours to reach the same level; (*S*)-**29a** and (*S*)-**30a** both had lower conversions and required longer reaction times (Table 3.8, entries 1, 3, 5 and 7). There was no additional conversion observed between 16 and 24 hours reaction time. The reactions with (*R*)-MeO-MOP and (*R*)-**28b** were the quickest in the series (Table 3.8, entries 2 and 4); however, the enantioselectivity was negligible. It was markedly improved when using the biphenoxy based phosphonites (*R*)-**29b** and (*R*)-**30b** (Table 3.8, entries 6 and 8), which were the highest enantioselectivities obtained (27% and 42% respectively). The H-MOP biphenoxy phosphonite ligands (Table 3.8, entries 5 and 7) had lower values for the *ee* than their methoxy counterparts. It is noteworthy that the phenoxy derived phosphonite (*S*)-**28a** achieved the highest *ee* in the H-MOP ligands, whereas (*R*)-**30b** was the best MeO-MOP ligand.

After screening the electron donating methoxy substituted naphthalene, we were also interested in investigating the effects of replacing the functional group with a weakly donating methyl moiety. The results of the coupling reactions of 1-bromo-2-methylnaphthalene with naphthalene-1-boronic acid to synthesise 2-methyl-1,1'-binaphthyl are given in Table 3.9. In comparison to the results obtained with the methoxy substituted substrate, the conversions obtained are significantly lower in all cases and, with the exception of (*S*)-**28a** and (*S*)-**30a** (Table 3.9, entries 3 and 7), only a minor improvement to the conversion is made by leaving the reactions longer than 30 minutes. As with the methoxy substituted substrate, there was no additional conversion between 16 and 24 hours reaction times. The *ee*s improved using 1-bromo-2-methylnaphthalene compared to 1-bromo-2-methoxynaphthalene – the value of the *ee* increased for every ligand used in the screening (Tables 3.8 and 3.9). There is no significant variation in the conversion observed between analogous ligands in the H-MOP and MeO-MOP series (Table 3.9). However, there is a consistent pattern of the *ee* being higher for the MeO-MOP ligands in each case. The enantioselectivity for the diphenoxy ((*S*)-**28a**) and dimethylbiphenoxy ((*S*)-**30a**) phosphonites was similar (Table 3.9, entries 3 and 7), whereas it was noticeably lower for the biphenoxy ligand (*S*)-**29a**, which had an *ee* close to that obtained with the parent phosphine (*S*)-H-MOP (Table 3.9, entries 1 and 5). For the MeO-MOP series, the *ee* doubled upon changing the ligand from (*R*)-MeO-MOP to (*R*)-**28b**. However, this was accompanied by a ~50%

reduction in the conversion (Table 3.9, entries 2 and 4). The ligands (*R*)-**29b** and (*R*)-**30b** achieved higher conversions than (*R*)-**28b** (Table 3.9, entries 4, 6 and 8), with (*R*)-**29b** affording an *ee* similar to that of (*R*)-**28b**. Out of all the ligands tested, (*R*)-**30b** achieved the highest *ee* of all (49%).

Table 3.9 Asymmetric Suzuki-Miyaura coupling of naphthalene-1-boronic acid with 1-bromo-2-methylnaphthalene.

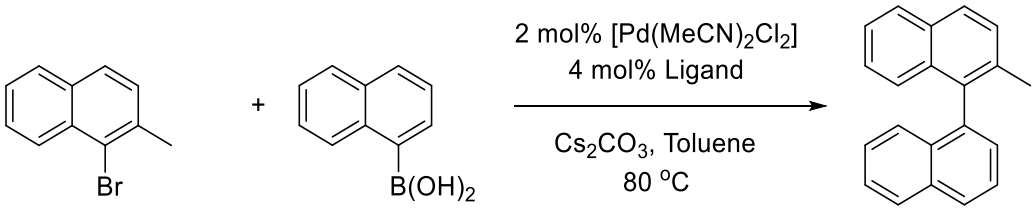

	Ligand	Conversion[a]			*ee*[b]
		30 min	1 h	16 h	
1	(*S*)-H-MOP	50	52	55	19 (*S*)
2	(*R*)-MeO-MOP	47	48	53	21 (*S*)
3	(*S*)-**28a**	26	31	38	30 (*S*)
4	(*R*)-**28b**	24	25	26	42 (*S*)
5	(*S*)-**29a**	32	33	40	17 (*S*)
6	(*R*)-**29b**	32	34	38	43 (*S*)
7	(*S*)-**30a**	27	38	46	32 (*S*)
8	(*R*)-**30b**	41	42	47	49 (*S*)

[a] % Conversion determined by ^{1}H NMR spectroscopy. [b] % *ee* determined by chiral HPLC (Lux Cellulose) with hexane/2-propanol (99:1); absolute configuration was assigned according to literature data.

$[Pd(L^P)_2Cl_2]$ complexes

In an effort to investigate the solution and solid state properties of our Suzuki-Miyaura catalysts, the complexes $[Pd((S)\text{-}\mathbf{30a})_2Cl_2]$ (*S*)-**41a** and $[Pd((R)\text{-}\mathbf{30b})_2Cl_2]$ (*R*)-**41b** were synthesised by reacting $[Pd(MeCN)_2Cl_2]$ with two equivalents of the corresponding phosphonite ligand in DCM. We were able to able to obtain single crystals of (*S*)-**41a** and (*R*)-**41b** suitable for X-ray crystallographic analysis, from $CDCl_3$/hexane and DCM/diethyl ether respectively. (*S*)-**41a** crystallised as two *pseudo*-polymorphs. One is in a monoclinic space group as a solvate with three chloroform molecules (Fig. 3.19), whereas the second *pseudo*-polymorph is the same main molecule but in an orthorhombic space group with one chloroform molecule (Fig. 3.20); an overlay image of the two *pseudo*-polymorphs has been provided (Fig. 3.21). (*R*)-**41b** crystallised in a monoclinic space group and the asymmetric unit contains two disordered molecules of DCM in multiple orientations (Fig. 3.22). Both *pseudo*-polymorphs of (*S*)-**41a** and (*R*)-**41b** have a square-planar geometry about the palladium centre and the phosphonite

ligands are in a *cis* orientation. The P–Pd–P bond angles are 99.79(5)° and 101.16(3)° for (*S*)-**41a** and 100.73(4)° for (*R*)-**41b**. The Pd–P bond lengths range from 2.2234(9) to 2.2331(15) Å in (*S*)-**41a** and are 2.2329(11) Å and 2.2354(11) Å in (*R*)-**41b,** and the Pd–Cl bond lengths range from 2.3302(9) to 2.3485(15) Å in (*S*)-**41a** and are 2.3359(11) Å and 2.3379(11) Å in (*R*)-**41b**.

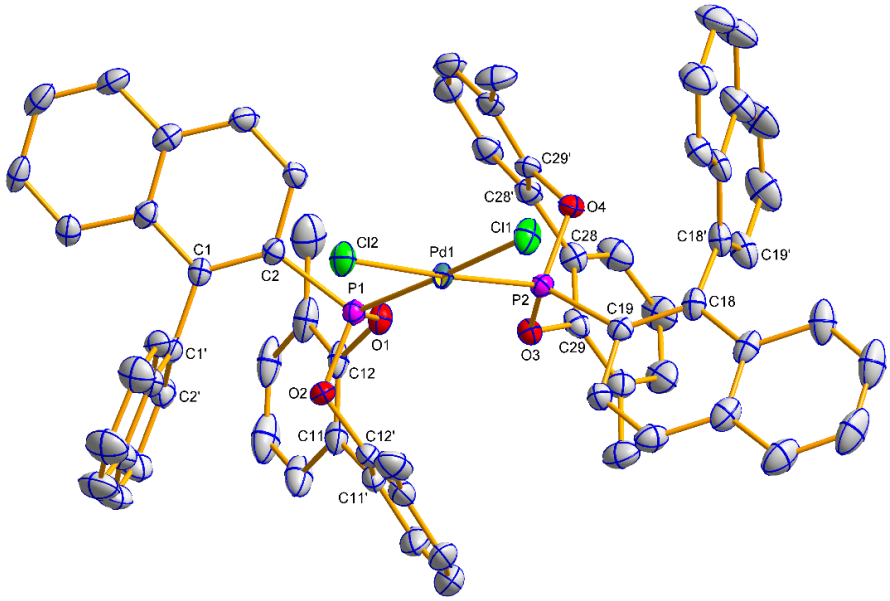

Fig. 3.19 Molecular structure of (*S*)-**41a**, *pseudo*-polymorph 1. Hydrogen atoms have been omitted for clarity. Selected average bond distances (Å) and angles (°): Pd1–P1 2.2246(14), Pd1–P2 2.2331(15), Pd1–Cl1 2.3372(15), Pd1–Cl2 2.3485(15), P1–C2 1.811(6), P1–O1 1.596(4), P1–O2 1.597(4), P2–C19 1.807(6), P2–O3 1.594(4), P2–O4 1.598(4); P1–Pd1–P2 99.79(5), P1–Pd1–Cl1 175.23(6), P1–Pd1–Cl2 84.30(5), C2–C1–C1'–C2' –94.3(7), C12–C11–C11'–C12' 45.6(9), C19–C18–C18'–C19' –87.6(7), C29–C28–C28'–C29' 44.1(8).

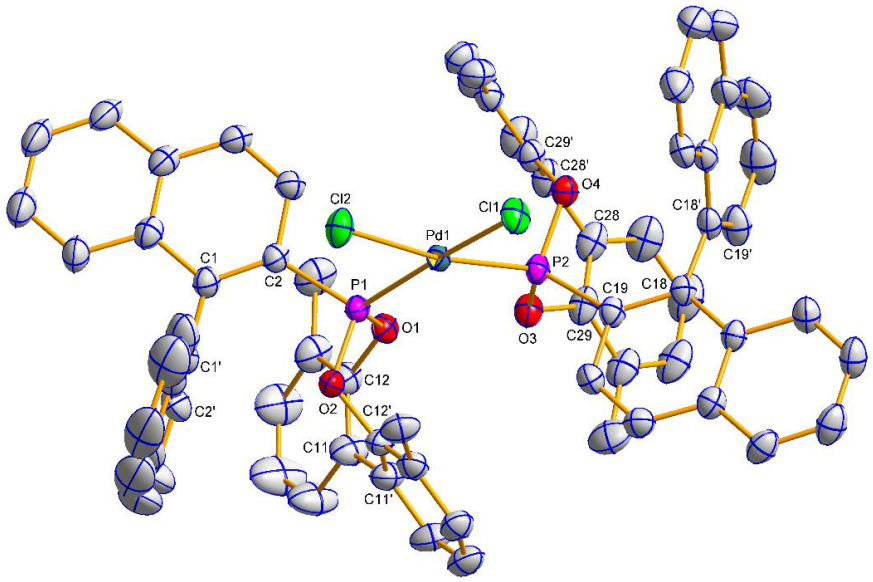

Fig. 3.20 Molecular structure of (*S*)-**41a**, *pseudo*-polymorph 2. Hydrogen atoms have been omitted for clarity. Selected average bond distances (Å) and angles (°): Pd1–P1 2.2234(9), Pd1–P2 2.2302(10), Pd1–Cl1 2.3411(9), Pd1–Cl2 2.3302(9), P1–C2 1.807(4), P1–O1 1.598(3), P1–O2 1.596(3), P2–C19 1.803(4), P2–O3 1.599(3), P2–O4 1.597(3); P1–Pd1–P2 101.16(3), P1–Pd1–Cl1 170.96(4), P1–Pd1–Cl2 84.57(4), C2–C1–C1'–C2' –89.9(5), C12–C11–C11'–C12' 47.1(7), C19–C18–C18'–C19' –93.0(5), C29–C28–C28'–C29' 45.4(6).

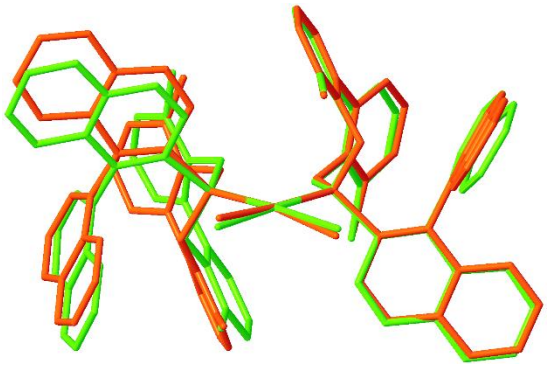

Fig. 3.21 An overlay image of the two *pseudo*-polymorphs of (*S*)-**41a**.

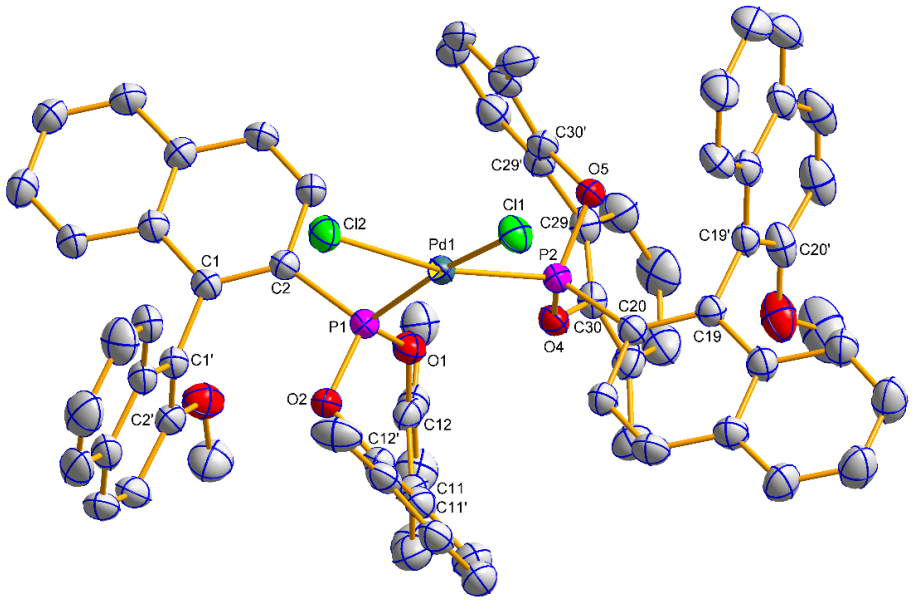

Fig. 3.22 Molecular structure of (*R*)-**41b**. Hydrogen atoms have been omitted for clarity. Selected average bond distances (Å) and angles (°): Pd1–P1 2.2354(11), Pd1–P2 2.2329(11), Pd1–Cl1 2.3359(11), Pd1–Cl2 2.3379(11), P1–C2 1.793(4), P1–O1 1.605(3), P1–O2 1.593(3), P2–C20 1.806(4), P2–O4 1.586(3), P2–O5 1.595(3); P1–Pd1–P2 100.73(4), P1–Pd1–Cl1 169.34(4), P1–Pd1–Cl2 84.88(4), C2–C1–C1'–C2' –89.5(6), C12–C11–C11'–C12' 44.0(7), C20–C19–C19'–C20' –96.0(5), C30–C29–C29'–C30' 45.0(7).

The X-ray structure of the complex [Pd((*R*)-MeO-MOP)$_2$Cl$_2$] was reported by Hayashi *et al*. and reveals that the MOP-phosphine ligands are in a *trans* orientation, unlike that seen for our MOP-phosphonite ligands: the Pd–P bond lengths in *trans*-[Pd((*R*)-MeO-MOP)$_2$Cl$_2$] are 2.339(2) Å and 2.344(15) Å and the P–Pd–P bond angle is 174.95(8)°.[113] The X-ray structure of a related complex with the chloride atoms replaced by fumaronitrile (*trans*-1,2-dicyanoethylene) and where the palladium is in a zero oxidation state, [Pd((*S*)-MeO-MOP)$_2$(fumaronitrile)], was reported by Pregosin. The molecule lies on a C2 axis and the MOP-phosphine ligands are in a *cis* orientation, the P–Pd–P bond angle is 114.11(3)° and the Pd–P bond length is 2.3588(8) Å.[187] The Pd–P bond lengths in these MeO-MOP-phosphine complexes are significantly longer than those found in our MOP-phosphonite complexes. A phosphonite complex analogous to (*S*)-**41a** and (*R*)-**41b**, *cis*-[Pd(P(OMe)$_2$Ph)$_2$Cl$_2$], which has a crystallographic twofold

rotation axis, has a Pd–P bond length of 2.2300(16) Å and a P–Pd–P bond angle of 100.88(2)°, values which are very similar to those found in (*S*)-**41a** and (*R*)-**41b**.[188]

(*S*)-**41a** and (*R*)-**41b** were analysed in the solution state through multinuclear NMR spectroscopy (Figs. 3.23 and 3.24). For (*S*)-**41a** two broad peaks in the $^{31}P\{^{1}H\}$ NMR spectrum were observed at 25 °C, a large peak at 144.3 ppm and a smaller peak at 142.8 ppm, which correspond to the *cis* and *trans* isomers (Fig. 3.23). We also observed a broad multiplet of low intensity over the range 146-147 ppm; upon cooling the solution we began to observe a sharpening of these peaks, and at −40 °C two doublets centred at 145.9 ppm and 147.0 ppm with a $^{2}J_{PP}$ value of 73.0 Hz were resolved (see expansion, Fig. 3.23). The inequivalence of these two phosphorus nuclei may be a result of rotamers, presumably due to restricted rotation about the biphenyl C–C bridge or rotation about the Pd–P bonds. For (*R*)-**41b** one broad peak was observed in the $^{31}P\{^{1}H\}$ NMR spectrum at room temperature. As the temperature was lowered, the peak width decreased and a new small peak was observed, shifted ~0.1 ppm upfield from the main peak – again this could indicate the presence of *cis* and *trans* isomers (Fig. 3.24). Two very low intensity doublets shifted ~7 ppm downfield from the main peak were observed with a *J* value of ~72 Hz (see expansion, Fig. 3.24), similar to that seen in (*S*)-**41a** and again indicative of rotamers.

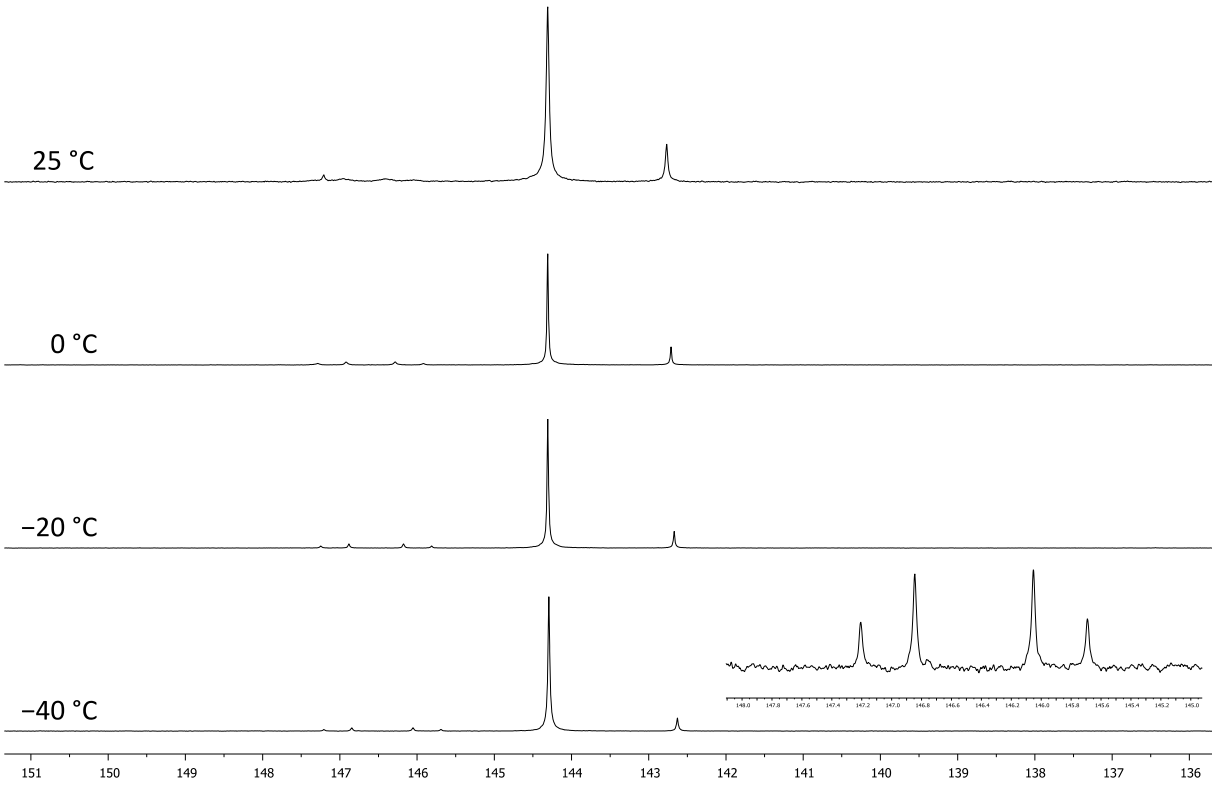

Fig. 3.23 $^{31}P\{^{1}H\}$ VT NMR of (*S*)-**41a** in $CDCl_3$. An expansion of the region 145-148 ppm is provided for the NMR spectrum obtained at −40 °C.

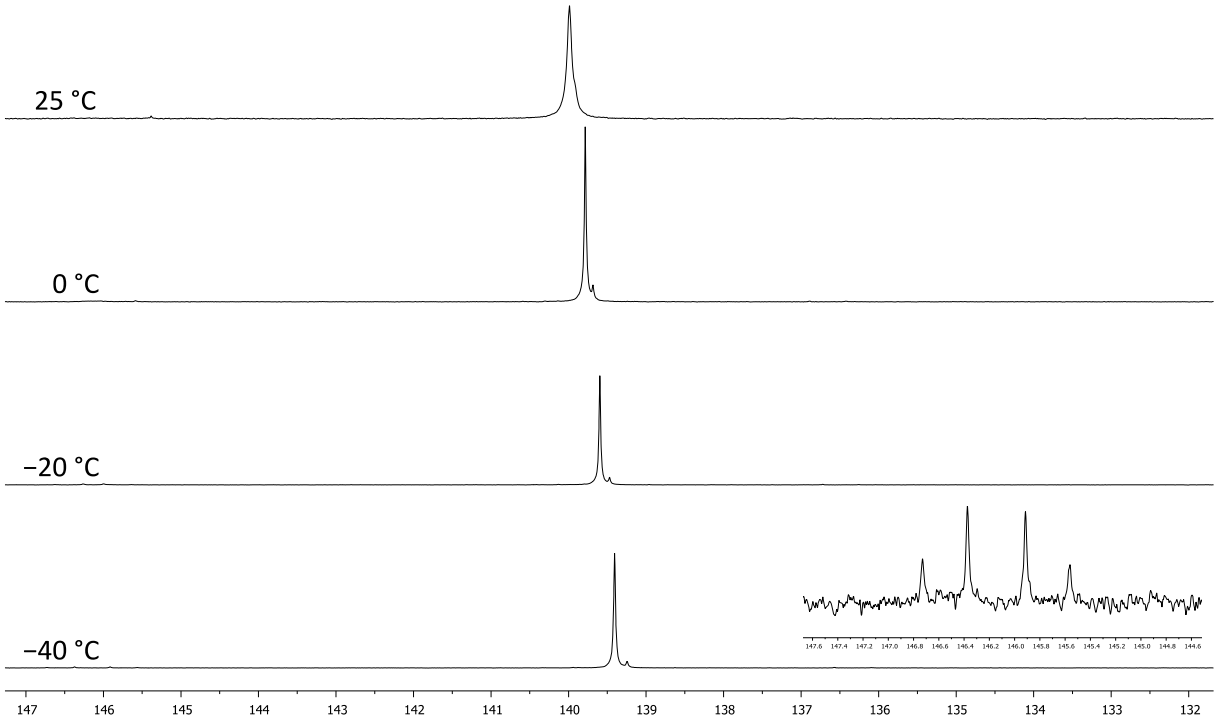

Fig. 3.24 $^{31}P\{^{1}H\}$ VT NMR of (*R*)-**41b** in $CDCl_3$. An expansion of the region 144-148 ppm is provided for the NMR spectrum obtained at −40 °C.

3.3 Summary

We have presented a series of reactions that were performed in order to further our research into finding applications for enantiopure MOP-phosphonite ligands in asymmetric catalysis. The experimental and computational data has been used to quantify the steric and electronic donor properties within a ligand series we have designed, and used DFT calculations to explain previously reported findings that rotation about the aryl–aryl junction in the biphenyl moiety of (*S*)-**29a**, (*R*)-**29b**, (*S*)-**30a** and (*R*)-**30b** is unrestricted under standard conditions. Rhodium(I) complexes of chiral MOP-phosphonites were prepared and detailed NMR and X-ray crystallographic analyses of these compounds were presented, both of which have supported the existence of M–π interactions in complexes of the type $[Rh(L^{P})_2]^+$ with one ligand acting as a chelating P,C-π-donor. In the rhodium-catalysed asymmetric hydroformylation reaction of styrene, the MOP-phosphonite ligands proved to be high yielding and regioselective for the branched isomer with low catalyst loadings. The synthesis of palladium dichloride complexes of MOP ligands and their application as catalysts in asymmetric Suzuki-Miyaura cross-coupling reactions has been reported, with enantioselectivities of up to 49% achieved using unoptimised reaction conditions. It was demonstrated that is possible to tune the electron donor and steric properties of our MOP-phosphonite ligands. In future work we aim to tailor the biphenyl moiety, to investigate the consequences of increased steric bulk and hindrance to rotation about the aryl–aryl junction on the selectivity of the next generation ligands in asymmetric catalytic transformations.

3.4 Experimental Procedures

All air- and/or water-sensitive reactions were performed under a nitrogen atmosphere using standard Schlenk line techniques in oven dried glassware. Solvents were freshly distilled prior to use; toluene was dried over sodium, tetrahydrofuran and diethyl ether were dried over sodium/benzophenone and dichloromethane was dried over calcium hydride. Hexane was dried over sodium/benzophenone and *d*-chloroform was dried over phosphorus pentoxide, prior to distillation and storage over molecular sieves. (*S*)-H-MOP,[126] (*R*)-MeO-MOP,[127] platinum(II) dichloride triethylphosphine,[145] chloro(1,5-cyclooctadiene)rhodium(I),[189] bis(1,5-cyclooctadiene)rhodium(I) tetrafluoroborate,[190] MAC,[191] chlorobis(ethylene)rhodium(I),[192] 1-(*p*-methoxybenzyl)-5-chloroisatin,[175] bis(acetonitrile) dichloropalladium(II)[193] and 1-bromo-2-methoxynaphthalene[194] were prepared according to literature procedures. All other chemicals were used as received without further purification. Flash chromatography was performed on silica gel (Fluorochem, 60A, 40-63 µm). Thin-layer chromatography was performed on Merck silica gel coated aluminium sheets with fluorescent indicator (UV_{254}), UV light was used for indicating. Melting points were determined in open glass capillary tubes on a Stuart SMP3 melting point apparatus. Optical rotation values were determined on an Optical Activity Polaar 2001 device. Infrared spectra were measured on a Varian 800 FT-IR Scimitar Series spectrometer. ^{1}H, $^{13}C\{^{1}H\}$ and $^{31}P\{^{1}H\}$ NMR spectra were recorded on a Bruker 700 (^{1}H 700.13 MHz), Bruker 500 (^{1}H 500.15 MHz), JEOL 400 (^{1}H 399.78 MHz) or Bruker 300 (^{1}H 300.13 MHz) spectrometer at room temperature (21-25 °C) if not otherwise stated, using the indicated solvent as internal reference. 2D NMR experiments (^{1}H-^{1}H COSY, ^{1}H-^{1}H ROESY, HSQC and HMBC) were used for the assignment of proton and carbon resonances, the numbering scheme is given in Fig. 3.25. High-resolution mass spectrometry was carried out by the EPSRC National Mass Spectrometry Facility, Swansea. Analytical gas chromatography was performed on a Shimadzu GC2014 instrument with a flame ionisation detector, using a Supelco β-dex™ 225 capillary column (L = 30 m, I.D. = 0.25 mm, d_f = 0.25 µm) and helium (purge flow 3 ml/min) as the carrier gas. High-performance liquid chromatography was performed on a Shimadzu Prominence UFLC instrument with a UV-Vis absorbance detector, using a Lux® 5µ Cellulose-1 or Lux® 5µ Cellulose-3 column (250 × 4.6 mm).

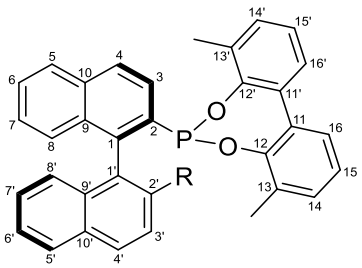

Fig. 3.25 Numbering scheme used to assign proton and carbon resonances in the NMR spectra.

3.4.1 Ligand properties

General procedure for the synthesis of L^P(Se).

The ligand (50.0 µmol, 1.0 eq.) and potassium selenocyanate (14.4 mg, 100 µmol, 2.0 eq.) were dissolved in THF (1.0 mL) and stirred at 50 °C for 2 h, after which the volatiles were removed *in vacuo*. The residue was dissolved in $CDCl_3$, filtered through Celite® and the solution was analysed by $^{31}P\{^1H\}$ NMR spectroscopy.

General procedure for the synthesis of *trans*-[Rh(L^P)$_2$(CO)Cl] complexes.

The ligand (12.4 µmol, 1.0 eq.) and rhodium(I) dicarbonyl chloride dimer (1.2 mg, 3.1 µmol, 0.25 eq.) were dissolved in DCM (0.5 mL) and stirred at room temperature for 15 min, after which the solution was concentrated and analysed by IR spectroscopy.

General procedure for the synthesis of [Pt(L^P)(PEt_3)Cl_2] complexes.

The ligand (50.0 µmol, 1.0 eq.) and platinum(II) dichloride triethylphosphine dimer (19.2 mg, 25.0 µmol, 0.5 eq.) were dissolved in CD_2Cl_2 (0.6 mL) and stirred at room temperature for 30 min, after which the solution was analysed by $^{31}P\{^1H\}$ NMR spectroscopy.

3.4.2 General procedure for the synthesis of [Rh(L^P)(η^2:η^2-cod)Cl] complexes.

The phosphonite ligand (40.0 µmol, 1.0 eq.) and chloro(1,5-cyclooctadiene)rhodium(I) dimer (9.9 mg, 20 µmol, 1.0 eq.) were dissolved in DCM (0.5 mL) and stirred at room temperature for 10 min, after which the $^{31}P\{^1H\}$ NMR spectrum showed no free ligand resonance. To remove small quantities of a phosphorus(V) impurity, the solution was diluted with diethyl ether/hexane and cooled in a salt/ice bath until the pure title compound precipitated as a yellow solid.

3.4.3 [Rh((*S*)-**29a**)(η^2:η^2-cod)Cl] (*S*)-**38a**

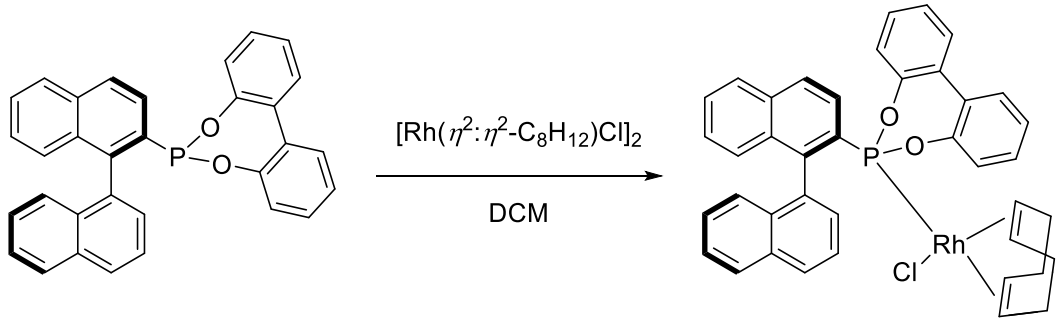

Single crystals were grown by slow diffusion of diethyl ether into a DCM solution.

MP: 206-208 °C (decomp.). **IR** (neat): ν = 3064.4 (w), 2918.2 (m), 1495.1 (m), 1472.2 (m), 1434.7 (s), 1368.4 (w), 1244.9 (m), 1197.8 (s), 1094.6 (s), 1015.9 (m), 953.0 (w), 895.2 (s), 869.4 (s), 820.2 (w), 781.8 (s), 748.0 (s), 674.4 (m), 633.8 (m) cm^{-1}. **^{1}H NMR** (500 MHz, $CDCl_3$, 50 °C): δ (ppm) = 8.14 (d, $^3J_{HH}$ = 8.3 Hz, 1H, *H*4), 8.05 (d, $^3J_{HH}$ = 8.2 Hz, 1H, *H*5), 8.02-7.98 (m, 2H, *H*6'), 7.88 (d, $^3J_{HH}$ = 8.2 Hz, 1H), 7.83 (d, $^3J_{HH}$ = 8.7 Hz, 1H, *H*5'), 7.79 (*apparent*-t (dd), *J* = 7.6 Hz, 1H, *H*3), 7.56 (ddd, $^3J_{HH}$ = 8.2 Hz, $^3J_{HH}$ = 6.8 Hz, $^4J_{HH}$ = 1.2 Hz, 1H, *H*6), 7.54-7.48 (m, 4H, *H*4'), 7.41 (ddd, $^3J_{HH}$ = 8.4 Hz, $^3J_{HH}$ = 6.8 Hz, $^4J_{HH}$ = 1.3 Hz, 1H, *H*7), 7.39-7.29 (m, 6H, *H*7/*H*8), 6.76 (ddd, $^3J_{HH}$ = 8.6 Hz, $^3J_{HH}$ = 6.8 Hz, *J* = 1.2 Hz, 1H, *H*3'), 7.00 (d, $^3J_{HH}$ = 8.6 Hz, 1H, *H*2'), 5.35 (br s, 1H, cod-C*H*), 5.01 (br s, 1H, cod-C*H*), 2.61 (br s, 2H, cod-C*H*), 2.09-1.99 (m, 1H, cod-CH_2), 1.73-1.56 (m, 5H, cod-CH_2), 1.43-1.37 (m, 2H, cod-CH_2). **^{13}C{^{1}H} NMR** (126 MHz, $CDCl_3$, 50 °C): δ (ppm) = 151.1 (*overlapping*-d, *C*12/*C*12'), 143.1 (d, $^2J_{CP}$ = 24.6 Hz, *C*1), 135.5 (d, $^1J_{CP}$ = 8.0 Hz, *C*2), 133.4 (d, $^4J_{CP}$ = 1.5 Hz, *C*9'), 133.9 (*C*9), 133.6 (*C*10), 133.6 (d, $^3J_{CP}$ = 11.0 Hz, *C*1'), 131.2 (*C*6'), 130.9, 129.8, 129.5, 129.2 (m, *C*8), 129.0 (*C*4), 128.0 (*C*10'), 127.7 (*C*5), 127.5 (*C*4'), 127.2 (m, *C*2'/*C*5'), 126.4 (*C*3'), 126.2 (*C*6), 126.0 (*C*7), 125.6 (d, J_{CP} = 3.1 Hz), 125.4, 125.1 (*C*3), 123.4, 122.5, 111.4 (dd, *J* = 14.3 Hz, *J* = 5.8 Hz, cod-*C*H), 109.8 (m, cod-*C*H), 70.8 (m, cod-*C*H), 70.1 (m, cod-*C*H), 32.9 (cod-*C*H_2), 31.7 (cod-*C*H_2), 27.6 (cod-*C*H_2), 27.1 (cod-*C*H_2). **^{31}P{^{1}H} NMR** (202 MHz, $CDCl_3$, 50 °C): δ (ppm) = 162.9 (d, $^1J_{PRh}$ = 224 Hz). **HRMS** (NSI^+, DCM/MeOH + NH_4OAc): Found: *m*/*z* = 571.0319. Calculated for $[M - (Cl + cod)]^+$: *m*/*z* = 571.0329.

3.4.4 [Rh((*R*)-**29b**)(η^2:η^2-cod)Cl] (*R*)-**38b**

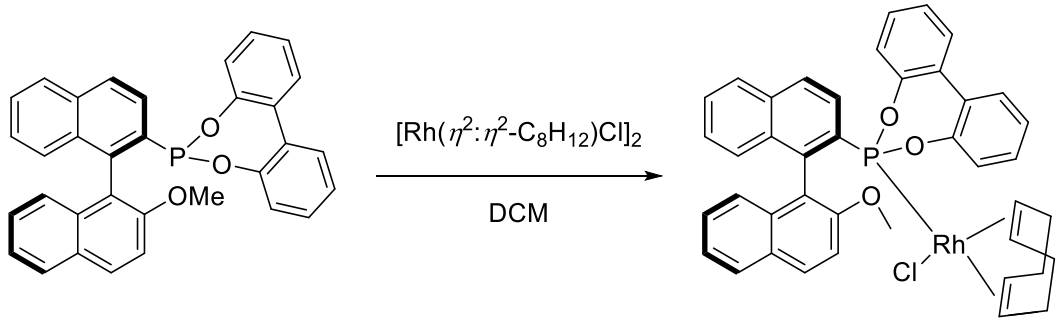

Single crystals were grown by slow diffusion of diethyl ether into a DCM solution.

MP: 236-238 °C (decomp.). **IR** (neat): ν = 3054.8 (w), 1593.1 (w), 1495.7 (m), 1471.0 (m), 1434.5 (s), 1195.5 (s), 1124.6 (w), 1092.5 (m), 1050.3 (m), 961.9 (w), 894.0 (s), 873.9 (s), 817.9 (m), 779.2 (s), 747.5 (m), 743.2 (s), 673.8 (s), 637.0 (s) cm^{-1}. **^{1}H NMR** (500 MHz, $CDCl_3$, 25 °C): δ (ppm) = 8.21 (d, $^3J_{HH}$ = 9.1 Hz, 1H, *H*4'), 7.98 (d, $^3J_{HH}$ = 8.2 Hz, 1H, *H*5'), 7.95 (dd, $^3J_{HH}$ = 8.7 Hz, $^3J_{HP}$ = 6.2 Hz, 1H, *H*3), 7.89 (d, $^3J_{HH}$ = 8.2 Hz, 1H, *H*5), 7.86-7.77 (br s, 1H), 7.80 (d, $^3J_{HH}$ = 8.7 Hz, 1H, *H*4), 7.56 (d, $^3J_{HH}$ = 9.1 Hz, 1H, *H*3'), 7.55-7.45 (m, 4H, *H*6), 7.42 (ddd, $^3J_{HH}$ = 8.2 Hz, $^3J_{HH}$ = 6.2 Hz, $^4J_{HH}$ = 1.8 Hz, 1H, *H*6'), 7.39-7.32 (m, 3H, *H*7'/*H*8'), 7.27-7.21 (m, 2H, *H*7), 7.20-7.08 (m, 2H), 7.01 (d, $^3J_{HH}$ = 8.6 Hz, 1H, *H*8), 5.30 (br s, 1H, cod-C*H*), 4.59 (br s, 1H, cod-C*H*), 3.88 (s, 3H, OCH_3), 2.85 (br s, 1H, cod-C*H*), 2.55 (br s, 1H, cod-C*H*), 1.95-1.86 (m, 1H, cod-CH_2), 1.63-1.57 (m, 3H, cod-CH_2), 1.51-1.45 (m, 3H, cod-CH_2), 1.45-1.38 (m, 1H, cod-CH_2). **^{13}C{^{1}H} NMR** (126 MHz, $CDCl_3$, 25 °C): δ (ppm) = 155.7 (*C*2'), 151.3 (*overlapping*-d, *C*12/*C*12'), 140.1 (d, $^2J_{CP}$ = 24.9 Hz, *C*1), 135.1 (*C*10), 134.7 (*C*9'), 133.2 (d, $^1J_{CP}$ = 11.1 Hz, *C*2), 131.4, 131.1 (*C*4'), 130.8, 129.8, 129.2, 129.0 (m, *C*6/*C*10'), 128.1 (*C*5), 127.6, 127.2 (*C*5'), 127.0 (d, $^3J_{CP}$ = 5.9 Hz, *C*4), 126.7 (*C*7'), 126.6 (*C*8), 126.4 (*C*7), 125.7 (d, $^2J_{CP}$ = 2.1 Hz, *C*3), 125.6 (*C*8'), 125.1, 124.4, 124.2 (*C*6'), 122.7, 120.1 (d, $^3J_{CP}$ = 7.9 Hz, *C*1'), 112.8 (*C*3'), 110.9 (m, cod-*C*H), 110.0 (m, cod-*C*H), 56.1 (O*C*H_3), 33.1 (cod-*C*H_2), 31.8 (cod-*C*H_2), 27.2 (cod-*C*H_2), 27.2 (cod-*C*H_2); resonances for *C*9 and two cod-*C*H were obscured. **^{31}P{^{1}H} NMR** (202 MHz, $CDCl_3$, 25 °C): δ (ppm) = 163.3 (d, $^1J_{PRh}$ = 221 Hz). **HRMS** (NSI$^+$, DCM/MeOH + NH_4OAc): Found: *m*/*z* = 601.0427. Calculated for [M − (Cl + cod)]$^+$: *m*/*z* = 601.0434.

3.4.5 [Rh((*S*)-**30a**)(η^2:η^2-cod)Cl] (*S*)-**39a**

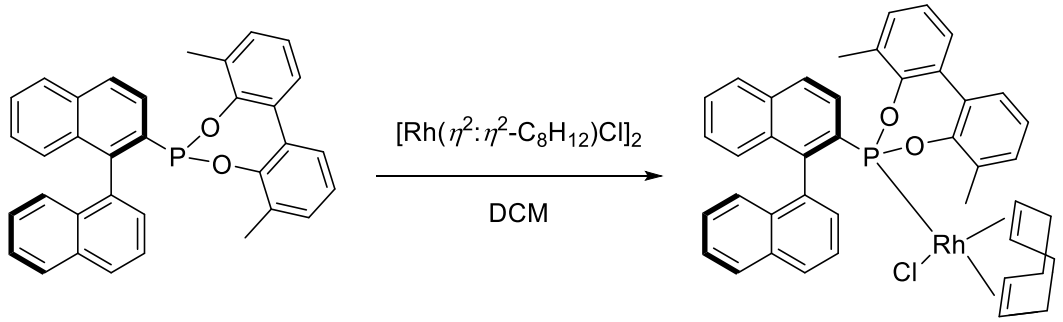

Single crystals were grown by slow diffusion of diethyl ether into a DCM solution. Three isomers were observed in the solution NMR spectra at −55 °C (approximate ratios: isomer A 76%; isomer B 14%; isomer C 10%), the ^{1}H and ^{13}C assignments correspond to the major isomer.

MP: 218-220 °C (decomp.). **IR** (neat): ν = 3048.6 (w), 2922.6 (m), 2875.2 (w), 1557.7 (w), 1453.3 (m), 1418.4 (m), 1367.6 (w), 1308.3 (w), 1260.1 (m), 1188.6 (s), 1085.4 (s), 1018.1 (m), 886.5 (s), 800.3 (s), 769.7 (s), 690.3 (s), 634.9 (s), 614.5 (s) cm^{-1}. **^{1}H NMR** (500 MHz, $CDCl_3$, −55 °C): δ (ppm) = 8.77 (dd, $^{3}J_{HP}$ = 17.1 Hz, $^{3}J_{HH}$ = 8.6 Hz, 1H, *H*3), 8.21 (d, $^{3}J_{HH}$ = 8.6 Hz, 1H, *H*4), 7.98 (d, $^{3}J_{HH}$ = 8.4 Hz, 1H, *H*5), 7.70-7.66 (m, 2H, *H*5'/*H*6'), 7.55 (*apparent*-t (dd), $^{3}J_{HH}$ = 7.5 Hz, 1H, *H*6), 7.48 (d, $^{3}J_{HH}$ = 8.2 Hz, 1H, *H*4'), 7.40-7.33 (m, 2H, *H*7'/*H*8'), 7.25-7.21 (m, 2H, *H*7/*H*16), 7.11-7.03 (m, 6H, *H*8/*H*14/*H*14'/*H*15/*H*15'/*H*16'), 6.76 (dd, $^{3}J_{HH}$ = 8.2 Hz, $^{3}J_{HH}$ = 7.0 Hz, 1H, *H*3'), 5.68 (br s, 1H, cod-C*H*), 5.64 (br s, 1H, cod-C*H*), 5.58 (d, $^{3}J_{HH}$ = 7.0 Hz, 1H, *H*2'), 4.15 (br s, 1H, cod-C*H*), 2.89 (br s, 1H, cod-C*H*), 2.59-2.55 (m, 1H, cod-CH_2), 2.51-2.44 (m, 1H, cod-CH_2), 2.18-1.98 (m, 4H, cod-CH_2), 1.88 (s, 3H, CH_3'), 1.84-1.78 (m, 1H, cod-CH_2), 1.69-1.64 (m, 1H, cod-CH_2), 1.63 (s, 3H, CH_3). **^{13}C{^{1}H} NMR** (126 MHz, $CDCl_3$, −55 °C): δ (ppm) = 148.9 (d, $^{2}J_{CP}$ = 13.8 Hz, *C*12), 147.2 (d, $^{2}J_{CP}$ = 6.8 Hz, *C*12'), 141.3 (*C*1), 136.6 (*C*1'), 134.5 (*C*10), 133.4 (*C*9'), 133.0 (d, $^{3}J_{CP}$ = 6.7 Hz, *C*9), 132.0 (*C*10'), 131.3 (*C*13'), 131.1 (*C*11 or *C*11'), 130.7 (*C*14), 130.5 (*obscured*-d, *C*2), 130.4 (m, *C*3/*C*14'), 130.4 (*C*13), 129.6 (*C*11 or *C*11'), 128.8 (*C*16'), 128.3 (*C*8), 128.2 (*C*5/*C*6'), 128.1 (*C*6), 127.5 (d, $^{3}J_{CP}$ = 19.0 Hz, *C*4), 127.4 (*C*15 or *C*15'), 127.2 (*C*5'), 126.9 (*C*7), 126.8 (*C*4'), 126.0 (*C*2'), 125.9 (*C*7' or *C*8'), 125.6 (*C*7' or *C*8'), 125.2 (*C*15 or *C*15'), 125.2 (*C*16), 124.4 (*C*3'), 113.0 (br d, *J* = 13.5 Hz, cod-*C*H), 112.3 (br d, *J* = 14.3 Hz, cod-*C*H), 71.3 (d, *J* = 12.6 Hz, cod-*C*H), 70.4 (d, *J* = 11.8 Hz, cod-*C*H), 33.4 (cod-*C*H_2), 32.9 (cod-*C*H_2), 28.5 (cod-*C*H_2), 28.2 (cod-*C*H_2), 17.9 (*C*H_3'), 17.0 (*C*H_3). **^{31}P{^{1}H} NMR** (202 MHz, $CDCl_3$, −55 °C): δ (ppm) = 170.2 (d, $^{1}J_{PRh}$ = 225 Hz, P^{A}), 169.4 (d, $^{1}J_{PRh}$ = 224 Hz, P^{B}), 162.0 (d, $^{1}J_{PRh}$ = 223 Hz, P^{C}). **HRMS** (ASAP^{+}, solid): Found: *m*/*z* = 707.1570. Calculated for [M − Cl]$^{+}$: *m*/*z* = 707.1581.

3.4.6 [Rh((*R*)-**30b**)(η^2:η^2-cod)Cl] (*R*)-**39b**

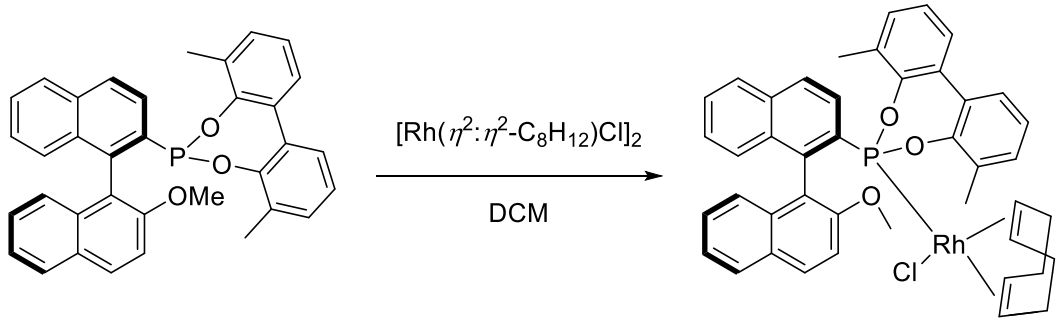

Single crystals were grown by slow diffusion of diethyl ether into a DCM solution. Five isomers were observed in the solution NMR spectra at −55 °C (approximate ratios: isomer A 13%; isomer B 80%; isomer C 1%; isomer D 3%; isomer E 3%), the ^{1}H and ^{13}C assignments correspond to the major isomer.

MP: 230-232 °C (decomp.). **IR** (neat): ν = 2925.4 (w), 2832.5 (w), 1622.4 (w), 1593.6 (w), 1557.8 (w), 1510.6 (m), 1453.6 (m), 1418.0 (m), 1334.8 (w), 1251.2 (s), 1189.5 (s), 1081.6 (s), 1021.0 (m), 965.5 (w), 896.7 (s), 806.6 (s), 771.3 (s), 744.6 (s), 687.7 (s), 637.4 (s) cm^{-1}. **^{1}H NMR** (500 MHz, $CDCl_3$, −55 °C): δ (ppm) = 8.68 (dd, $^{3}J_{HP}$ = 16.9 Hz, $^{3}J_{HH}$ = 8.6 Hz, 1H, *H*3), 8.21 (d, $^{3}J_{HH}$ = 8.6 Hz, 1H, *H*4), 7.98 (d, $^{3}J_{HH}$ = 8.3 Hz, 1H, *H*5), 7.76 (d, $^{3}J_{HH}$ = 8.4 Hz, 1H, *H*8'), 7.70 (d, $^{3}J_{HH}$ = 8.0 Hz, 1H, *H*5'), 7.66 (d, $^{3}J_{HH}$ = 9.1 Hz, 1H, *H*4'), 7.55 (*apparent*-t (dd), $^{3}J_{HH}$ = 7.5 Hz, 1H, *H*6), 7.35-7.31 (m, 1H, *H*7'), 7.30-7.26 (m, 1H, *H*6'), 7.25-7.20 (m, 1H, *H*7), 7.15 (d, $^{3}J_{HH}$ = 8.6 Hz, 1H, *H*8), 7.13-7.05 (m, 6H, *H*14/*H*14'/*H*15/*H*15'/*H*16/*H*16'), 6.79 (d, $^{3}J_{HH}$ = 9.1 Hz, 1H, *H*3'), 5.69 (br s, 1H, cod-C*H*), 5.50 (br s, 1H, cod-C*H*), 4.19 (br s, 1H, cod-C*H*), 2.92 (s, 3H, OCH_3), 2.64-2.54 (m, 2H, cod-C*H*/cod-CH_2), 2.38-2.29 (m, 1H, cod-CH_2), 2.13-1.96 (m, 4H, cod-CH_2), 1.81 (s, 3H, CH_3'), 1.72 (s, 3H, CH_3), 1.70-1.65 (m, 1H, cod-CH_2), 1.50-1.40 (m, 1H, cod-CH_2). **^{13}C{^{1}H} NMR** (126 MHz, $CDCl_3$, −55 °C): δ (ppm) = 153.3 (*C*2'), 149.4 (d, $^{2}J_{CP}$ = 14.8 Hz, *C*12'), 148.0 (d, $^{2}J_{CP}$ = 6.3 Hz, *C*12), 137.8 (*C*1), 134.5 (*C*10), 134.3 (*C*9'), 132.4 (d, $^{3}J_{CP}$ = 7.3 Hz, *C*9), 132.1 (d, $^{1}J_{CP}$ = 41.7 Hz, *C*2), 132.0 (*C*13 or *C*13'), 131.0 (*C*13 or *C*13'), 130.7 (*C*14 or *C*14'), 130.5 (*C*14 or *C*14'), 130.1 (*obscured*-d, *C*3), 130.0 (*C*11 or *C*11'), 129.4 (*C*11 or *C*11'), 129.3 (*C*4'), 128.2 (*C*5), 128.0 (*C*6), 127.9 (*C*8'), 127.8 (*C*16 or *C*16'), 127.7 (*C*16 or *C*16'), 127.6 (*C*10'), 127.5 (*C*8), 127.3 (d, $^{3}J_{CP}$ = 18.1 Hz, *C*4), 126.9 (*C*7), 126.8 (*C*5'), 126.3 (*C*7'), 125.4 (*C*15 or *C*15'), 124.7 (*C*15 or *C*15'), 123.3 (*C*6'), 120.2 (*C*1'), 113.0 (br d, *J* = 14.0 Hz, cod-*C*H), 111.5 (br d, *J* = 15.0 Hz, cod-*C*H), 110.9 (*C*3'), 72.8 (d, *J* = 11.7 Hz, cod-*C*H), 70.0 (d, *J* = 11.5 Hz, cod-*C*H), 56.1 (OCH_3), 34.0 (cod-CH_2), 32.2 (cod-CH_2), 29.0 (cod-CH_2), 27.5 (cod-CH_2), 17.6 (CH_3'), 17.5 (CH_3). **^{31}P{^{1}H} NMR** (202 MHz, $CDCl_3$, −55 °C): δ (ppm) = 168.1 (d, $^{1}J_{PRh}$ = 227 Hz, P^{A}), 167.5 (d, $^{1}J_{PRh}$ = 226 Hz, P^{B}), 165.1 (d, $^{1}J_{PRh}$ = 227 Hz, P^{C}), 163.4 (d, $^{1}J_{PRh}$ = 224 Hz, P^{D}), 162.8 (d, $^{1}J_{PRh}$ = 223 Hz, P^{E}). **HRMS** (ASAP^{+}, solid): Found: *m*/*z* = 737.1686. Calculated for [M − Cl]$^{+}$: *m*/*z* = 737.1686.

3.4.7 General procedure for the synthesis of $[Rh(L^P)_2]BF_4$ complexes.

The phosphonite ligand (40.0 µmol, 1.0 eq.) and bis(1,5-cyclooctadiene)rhodium(I) tetrafluoroborate (8.1 mg, 20 µmol, 1.0 eq.) were dissolved in DCM (1.0 mL) and stirred at room temperature for 10 min, after which the $^{31}P\{^1H\}$ NMR spectrum showed no free ligand resonance. To remove small quantities of a phosphorus(V) impurity, the solution was diluted with diethyl ether and cooled in a salt/ice bath until the pure title compound precipitated as an orange solid.

3.4.8 $[Rh((S)\text{-}\mathbf{30a})_2]BF_4$ (*S*)-**40a**

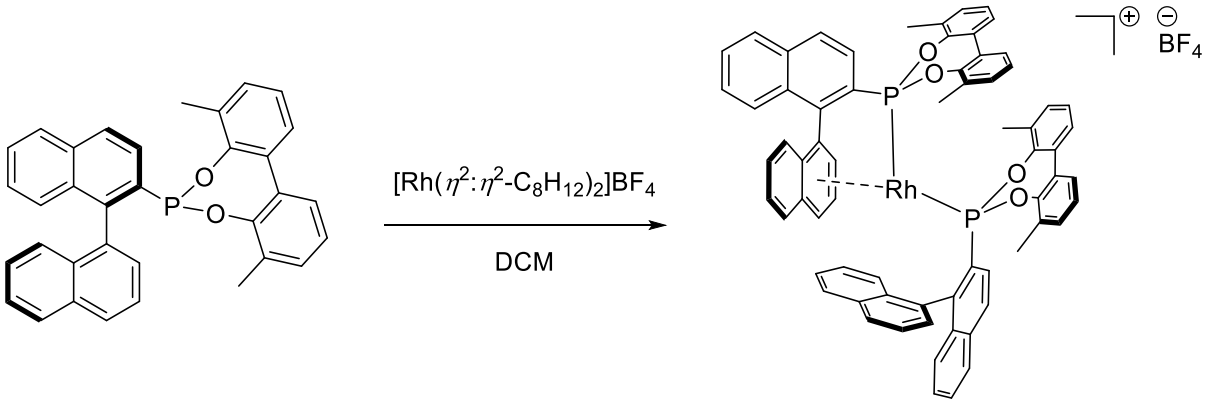

MP: 260-262 °C (decomp.). **IR** (neat): ν = 1485.1 (w), 1436.2 (m), 1418.7 (m), 1365.0 (w), 1249.9 (m), 1188.7 (s), 1052.4 (s), 910.3 (s), 761.7 (s), 726.8 (m), 688.8 (s), 632.5 (s) cm^{-1}. **^{1}H NMR** (700 MHz, $CDCl_3$, 5 °C): *δ* (ppm) = 8.78 (dd, $^3J_{HP}$ = 16.6 Hz, $^3J_{HH}$ = 8.6 Hz, 1H, *H*3^A), 8.67 (d, $^3J_{HH}$ = 8.6 Hz, 1H, *H*4^A), 8.24 (*apparent*-t (dd), $^3J_{HH}$ = 6.3 Hz, 1H, *H*3'^{B}), 8.16 (d, $^3J_{HH}$ = 8.4 Hz, 1H, *H*5^A), 7.99 (d, $^3J_{HH}$ = 8.3 Hz, 1H, *H*5^B), 7.82 (d, $^3J_{HH}$ = 8.6 Hz, 1H, *H*8^B), 7.70-7.76 (m, 3H, *H*4^B/*H*5'^{B}/*H*6^B), 7.67 (d, $^3J_{HH}$ = 8.2 Hz, 1H, *H*5'^{A}), 7.63 (*apparent*-t (dd), $^3J_{HH}$ = 7.6 Hz, 1H, *H*6^A), 7.59 (*apparent*-t (dd), $^3J_{HH}$ = 7.8 Hz, 1H, *H*7^B), 7.57-7.52 (m, 3H, *H*2'^{B}/*H*6'^{B}/*H*7'^{A}), 7.48 (*apparent*-t (dd), $^3J_{HH}$ = 7.6 Hz, 1H, *H*7'^{B}), 7.45 (*apparent*-t (dd), $^3J_{HH}$ = 7.5 Hz, 1H, *H*6'^{A}), 7.30-7.26 (m, 3H, *H*4'^{A}/*H*7^A/*H*8'^{A}), 7.11-7.01 (m, 5H, *H*8^A/*H*8'^{B}/*H*15^A/*H*15^B/*H*16^B), 6.98 (d, $^3J_{HH}$ = 7.4 Hz, 1H, *H*14^B), 6.88 (d, $^3J_{HH}$ = 7.4 Hz, 1H, *H*14^A), 6.80-6.77 (m, 2H, *H*14'^{B}/*H*16^A), 6.75 (d, $^3J_{HH}$ = 7.6 Hz, 1H, *H*16'^{B}), 6.72 (*apparent*-t (dd), *J* = 7.8 Hz, 1H, *H*3^B), 6.58 (*apparent*-t (dd), $^3J_{HH}$ = 7.6 Hz, 1H, *H*3'^{A}), 6.46 (d, $^3J_{HH}$ = 7.5 Hz, 1H, *H*16'^{A}), 6.37 (*apparent*-t (dd), $^3J_{HH}$ = 7.5 Hz, 1H, *H*15'^{B}), 6.27-6.24 (m, 2H, *H*4'^{B}/*H*14'^{A}), 6.09 (*apparent*-t (dd), $^3J_{HH}$ = 7.5 Hz, 1H, *H*15'^{A}), 5.27 (d, $^3J_{HH}$ = 6.9 Hz, 1H, *H*2'^{A}), 2.57 (s, 3H, C*H*$_3$'^{B}), 1.66 (s, 3H, C*H*$_3$^{A}), 1.37 (s, 3H, C*H*$_3$^{B}), 0.09 (s, 3H, C*H*$_3$'^{A}). **^{13}C{^{1}H} NMR** (176 MHz, $CDCl_3$, 5 °C): *δ* (ppm) = 149.5 (d, $^1J_{CP}$ = 58.9 Hz, *C*2^B), 148.7 (d, $^2J_{CP}$ = 15.5 Hz, *C*12^B), 148.2 (d, $^2J_{CP}$ = 14.5 Hz, *C*12^A), 147.7 (d, $^2J_{CP}$ = 7.9 Hz, *C*12'^{B}), 146.6 (d, $^2J_{CP}$ = 7.5 Hz, *C*12'^{A}), 140.1 (*C*1^A), 140.0 (d, $^2J_{CP}$ = 32.1 Hz, *C*1^B), 136.2 (*C*1'^{A}), 135.1 (*C*10^B), 134.9 (*C*10^A), 133.5 (d, $^1J_{CP}$ = 45.8 Hz, *C*2^A), 132.9 (*C*9'^{A}), 132.4 (*C*9^A/*C*10'^{A}), 131.4 (*C*11'^{B}), 131.2 (*C*11^A), 131.1 (*C*7'^{B}), 130.9 (*C*6'^{B}), 130.9 (d, $^2J_{CP}$ = 36.6 Hz, *C*3^A), 130.5 (*obscured*-d, *C*9^B), 130.4 (*C*14^A/*C*14^B/*C*14'^{B}), 130.3 (*C*4^B), 130.1 (*C*13^A), 129.7 (*C*6^B), 129.2 (d, $^3J_{CP}$ = 17.1 Hz, *C*4^A), 129.0 (*C*11'^{A}/*C*13^B/*C*14'^{A}), 128.9 (*C*7^B/*C*16^A/*C*16^B), 128.8 (*C*11^B), 128.7 (*C*5^A), 128.7

($C6^A$), 128.6 ($C5^B$), 128.3 ($C8^A$), 128.2 ($C5'^A$), 127.7 ($C13'^A$), 127.6 ($C13'^B$), 127.4 ($C7^A$), 127.0 ($C2'^A$), 126.8 ($C4'^A$/$C5'^B$/$C16'^B$), 126.5 ($C16'^A$), 126.4 ($C8^B$), 125.8 ($C7'^A$), 125.8 ($C8'^A$), 125.5 ($C15^B$), 125.2 ($C6'^A$), 125.0 ($C15^A$), 124.6 ($C3'^A$), 124.5 ($C15'^B$), 124.0 ($C9'^B$), 123.9 ($C15'^A$), 123.6 ($C3^B$), 123.4 ($C8'^B$), 118.6 ($C10'^B$), 110.5 (d, J = 11.3 Hz, $C1'^B$), 107.9 ($C3'^B$), 103.2 ($C2'^B$), 100.3 (d, J = 12.8 Hz, $C4'^B$), 18.4 ($CH_3'^B$), 16.7 (CH_3^A), 15.9 (CH_3^B), 14.1 ($CH_3'^A$). **^{31}P{^{1}H} NMR** (202 MHz, $CDCl_3$, 5 °C): δ (ppm) = 176.8 (dd, $^1J_{PRh}$ = 288 Hz, $^2J_{PP}$ = 27 Hz, P^A), 171.7 (dd, $^1J_{PRh}$ = 294 Hz, $^2J_{PP}$ = 27 Hz, P^B). **HRMS** (NSI^+, DCM/MeOH): Found: m/z = 1095.2221. Calculated for $[M - BF_4]^+$: m/z = 1095.2234.

3.4.9 $[Rh((R)\text{-}\mathbf{30b})_2]BF_4$ (*R*)-**40b**

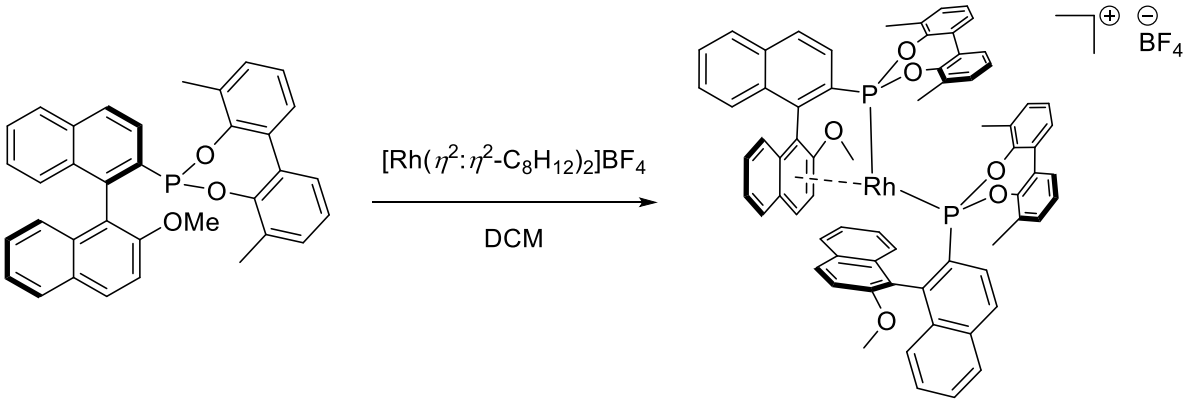

MP: 280-282 °C (decomp.). **IR** (neat): ν = 1623.3 (w), 1595.9 (w), 1452.7 (m), 1416.5 (m), 1278.8 (w), 1249.1 (s), 1193.3 (s), 1047.9 (s), 925.3 (s), 869.1 (m), 804.1 (m), 759.8 (s), 709.7 (m), 682.8 (m), 633.0 (s) cm^{-1}. **^{1}H NMR** (500 MHz, $CDCl_3$, −20 °C): δ (ppm) = 8.06 (d, $^3J_{HH}$ = 8.3 Hz, 1H, $H5^B$), 7.91 (d, $^3J_{HH}$ = 8.4 Hz, 1H, $H8^B$), 7.84 (d, $^3J_{HH}$ = 8.7 Hz, 1H, $H4^B$), 7.83 (d, $^3J_{HH}$ = 8.0 Hz, 1H, $H5^A$), 7.80-7.75 (m, 2H, $H3'^B$/$H6^B$), 7.71 (d, $^3J_{HH}$ = 9.0 Hz, 1H, $H4'^A$), 7.66 (*apparent*-t (dd), $^3J_{HH}$ = 7.7 Hz, 1H, $H7^B$), 7.60 (dd, $^3J_{HP}$ = 16.5 Hz, $^3J_{HH}$ = 8.8 Hz, 1H, $H3^A$), 7.57-7.49 (m, 4H, $H3'^A$/$H4^A$/$H6^A$/$H7'^B$), 7.44 (d, $^3J_{HH}$ = 8.1 Hz, 1H, $H5'^A$), 7.32-7.28 (m, 4H, $H4'^B$/$H14^B$/$H15^B$/$H16^B$), 7.24 (*apparent*-t (dd), $^3J_{HH}$ = 7.7 Hz, 1H, $H7^A$), 7.21 (d, $^3J_{HH}$ = 7.5 Hz, 1H, $H14^A$), 7.11 (*apparent*-t (dd), $^3J_{HH}$ = 7.7 Hz, 1H, $H15^A$), 7.07 (*overlapping*-d, $^3J_{HH}$ = 8.5 Hz, 2H, $H8^A$/$H8'^B$), 6.94 (d, $^3J_{HH}$ = 7.8 Hz, 1H, $H16^A$), 6.91 (*apparent*-t (dd), J = 8.0 Hz, 1H, $H3^B$), 6.87 (*apparent*-t (dd), $^3J_{HH}$ = 7.5 Hz, 1H, $H6'^A$), 7.83-7.76 (m, 4H, $H5'^B$/$H6'^B$/H15'^{B}/H16'^{A}), 6.60 (d, $^3J_{HH}$ = 7.2 Hz, 1H, H14'^{B}), 6.46 (d, $^3J_{HH}$ = 7.2 Hz, 1H, H14'^{A}), 6.31 (d, $^3J_{HH}$ = 7.8 Hz, 1H, H16'^{B}), 6.26 (*apparent*-t (dd), $^3J_{HH}$ = 7.6 Hz, 1H, H15'^{A}), 6.21 (*apparent*-t (dd), $^3J_{HH}$ = 7.7 Hz, 1H, $H7'^A$), 5.53 (d, $^3J_{HH}$ = 8.6 Hz, 1H, $H8'^A$), 4.28 (s, 3H, OCH_3^A), 3.84 (s, 3H, OCH_3^B), 2.46 (s, 3H, CH_3^A), 1.93 (s, 3H, CH_3^B), 1.37 (s, 3H, $CH_3'^B$), 1.25 (s, 3H, $CH_3'^A$). **^{13}C{^{1}H} NMR** (126 MHz, $CDCl_3$, −20 °C): δ (ppm) = 153.3 ($C2'^A$), 149.5 (d, $^1J_{CP}$ = 57.0 Hz, $C2^B$), 148.4 (*overlapping*-d, $C12^B$/$C12'^B$), 147.7 (d, $^2J_{CP}$ = 8.3 Hz, $C12'^A$), 146.8 ($C2'^B$), 146.2 (d, $^2J_{CP}$ = 8.2 Hz, $C12^A$), 138.0 (d, $^2J_{CP}$ = 32.4 Hz, $C1^B$), 135.9 (d, $^1J_{CP}$ = 47.2 Hz, $C2^A$), 135.3 ($C10^B$), 134.9 ($C10^A$), 133.9 ($C9'^A$), 133.6 ($C1^A$), 131.9 (d, $^3J_{CP}$ = 8.4 Hz, $C9^A$), 131.2 ($C14'^A$), 131.1 (*obscured*-d, $C9^B$), 131.0 ($C14^B$), 130.8 ($C14^A$), 130.7 ($C7'^B$), 130.5 ($C6'^B$), 130.2 ($C4^B$/$C13^B$), 130.1 ($C13^A$),

130.1 (*C*13'^{A}), 129.9 (*C*14'^{B}), 129.7 (*C*6^{B}/*C*11'^{B}), 129.4 (*C*4'^{A}), 129.2 (*C*11^{A}/*C*11^{B}), 129.2 (*C*16^{B}), 129.0 (*C*13'^{B}), 128.8 (*C*7^{B}), 128.7 (*C*5^{B}), 128.5 (*C*6^{A}/*C*16^{A}), 128.0 (*C*11'^{A}), 127.8 (*C*16'^{B}), 127.8 (*obscured*-d, *C*3^{A}), 127.8 (*C*8^{A}), 127.6 (*C*10'^{A}), 127.5 (*C*5^{A}), 127.3 (*C*7^{A}), 127.2 (*C*5'^{A}), 127.0 (*C*16'^{A}), 126.6 (*obscured*-d, *C*4^{A}), 126.6 (*C*8^{B}), 126.3 (*C*7'^{A}), 126.2 (*C*15^{B}), 125.4 (*C*15'^{B}), 125.0 (*C*15^{A}), 124.9 (*C*5'^{B}), 124.3 (*C*3^{B}), 124.1 (*C*15'^{A}), 122.6 (*C*8'^{A}), 122.5 (*C*9'^{B}), 122.3 (*C*8'^{B}), 122.1 (*C*6'^{A}), 120.8 (*C*1'^{A}), 113.4 (*C*10'^{B}), 112.7 (*C*3'^{A}), 101.3 (d, *J* = 15.2 Hz, *C*1'^{B}), 93.7 (d, *J* = 10.4 Hz, *C*4'^{B}), 93.4 (*C*3'^{B}), 57.9 (O*C*H$_3$^{B}), 57.1 (O*C*H$_3$^{A}), 16.9 (*C*H$_3$^{B}), 16.6 (*C*H$_3$^{A}/ *C*H$_3$'^{B}), 14.9 (*C*H$_3$'^{A}). **^{31}P{^{1}H} NMR** (202 MHz, $CDCl_3$, −20 °C): δ (ppm) = 182.0 (dd, $^{1}J_{PRh}$ = 283 Hz, $^{2}J_{PP}$ = 32 Hz, *P*^{A}), 173.2 (dd, $^{1}J_{PRh}$ = 310 Hz, $^{2}J_{PP}$ = 32 Hz, *P*^{B}). **HRMS** (NSI^{+}, DCM/MeOH): Found: *m*/*z* = 1155.2423. Calculated for $[M - BF_4]^+$: *m*/*z* = 1155.2445.

3.4.10 General procedure for the asymmetric hydrogenation of alkenes

The alkene substrate (3.70 mmol, 1.0 eq.) was dissolved in DCM (6 mL) in an autoclave vessel at room temperature. MOP ligand (15 µmol, 0.004 eq.) and bis(1,5-cyclooctadiene)rhodium(I) tetrafluoroborate (3.0 mg, 7.4 µmol, 0.002 eq.) were dissolved in DCM (2 mL) and stirred at room temperature for 30 min, after which the solution was transferred to the autoclave vessel and pressurised to 2 bar with hydrogen gas. The reaction mixture was stirred for 48h, after which the conversion was obtained by ^{1}H NMR spectroscopy. The reaction mixture was filtered through silica with rinsing by DCM, the volatiles were removed *in vacuo* and the enantiomeric excess determined.

Dimethyl methylsuccinate

The ^{1}H spectroscopic data matched that of a commercially acquired sample. The enantiomeric excess was determined by chiral GC analysis; the absolute configuration was assigned by comparison to an enantiopure, commercially acquired sample.

GC conditions (Supelco β-dex 225) − injection temperature: 220 °C, detection temperature: 200 °C, oven temperature: 70 °C for 40 min, then ramp to 180 °C at 10 °C/min, retention times: 45.2 min (*S*) and 45.7 min (*R*).

Methyl *N*-acetylalaninate

The ^{1}H spectroscopic data matched that of an authentic sample, which was prepared via a literature procedure from *N*-acetyl-L-alanine.[195] The ^{1}H and ^{13}C NMR spectroscopic data matched that of data reported in the literature,[196] and the HRMS data was in accordance with the calculated values. The enantiomeric excess was determined by chiral GC analysis; the absolute configuration was assigned by comparison to the enantiopure, authentically prepared sample.

^{1}H NMR (300 MHz, $CDCl_3$): δ (ppm) = 6.12 (br s, 1H), 4.53 (apparent quintet (dq), $^3J_{HH}$ = 7.2 Hz, 1H), 3.69 (s, 3H), 1.95 (s, 3H), 1.34 (d, $^3J_{HH}$ = 7.2 Hz, 3H). **^{13}C{^{1}H} NMR** (75 MHz, $CDCl_3$): δ (ppm) = 173.7, 169.7, 52.5, 48.0, 23.1, 18.5. **HRMS** (NSI^+, DCM/MeOH + NH_4OAc): Found: m/z = 146.0808. Calculated for $[M + H]^+$: m/z = 146.0812.

GC conditions (Supelco β-dex 225) – injection temperature: 220 °C, detection temperature: 200 °C, oven temperature: 100 °C for 5 min, then ramp to 180 °C at 10 °C/min, retention times: 12.6 min (*R*) and 13.0 min (*S*).

Methyl *N*-acetylphenylalaninate

The ^{1}H spectroscopic data matched that of an authentic sample, which was prepared via a literature procedure from *N*-acetyl-L-phenylalanine.[195] The ^{1}H and ^{13}C NMR spectroscopic data matched that of data reported in the literature,[196] and the HRMS data was in accordance with the calculated values. The enantiomeric excess was determined by chiral HPLC analysis; the absolute configuration was assigned by comparison to the enantiopure, authentically prepared sample.

^{1}H NMR (300 MHz, $CDCl_3$): δ (ppm) = 7.25-7.16 (m, 3H), 7.04-7.00 (m, 2H), 5.94 (br d, 1H), 4.81 (dt, $^3J_{HH}$ = 7.9 Hz, $^3J_{HH}$ = 5.8 Hz, 1H), 3.65 (s, 3H), 3.12-2.97 (m, 2H), 1.91 (s, 3H). **^{13}C{^{1}H} NMR** (75 MHz, $CDCl_3$): δ (ppm) = 172.1, 169.7, 135.9, 129.2, 128.6, 127.1, 53.1, 52.3, 37.9, 23.1. **HRMS** (NSI^+, DCM/MeOH + NH_4OAc): Found: m/z = 222.1122. Calculated for $[M + H]^+$: m/z = 222.1125.

HPLC conditions (Lux Cellulose-1) – oven temperature: 40 °C, mobile phase: hexane/2-propanol (90:10), flow rate: 0.5 mL/min, detection: 216 nm, retention times: 24.9 min (*R*) and 32.9 min (*S*).

3.4.11 General procedure for the asymmetric hydroformylation of styrene

The MOP ligand (38 µmol, 0.004 eq.) and (acetylacetonato)dicarbonylrhodium(I) (5.0 mg, 19 µmol, 0.002 eq.) were dissolved in C_6D_6 (1 mL) and stirred at room temperature for 10 min, after which the solution was transferred to an autoclave vessel at 36 °C and pressurised to 40 bar with syngas and stirred for 1h. The vessel was depressurised before styrene (1.1 mL, 1.0 g, 9.6 mmol, 1.0 eq.) was added, the vessel was subsequently re-pressurised to 40 bar with syngas and left to stir for 16 h, after which the conversion was obtained by ^{1}H NMR spectroscopy; the ^{1}H spectroscopic data matched that of commercially acquired samples of 2-phenylpropionaldehyde and 3-phenylpropionaldehyde. The reaction mixture was filtered through silica with rinsing by DCM, the volatiles were removed *in vacuo* and the enantiomeric excess of 2-phenylpropionaldehyde determined immediately by chiral GC analysis; the absolute configuration was assigned by comparison to literature data.[197]

GC conditions (Supelco β-dex 225) – injection temperature: 200 °C, detection temperature: 200 °C, oven temperature: 100 °C, retention times: 20.0 min (*S*) and 21.0 min (*R*).

3.4.12 General procedure for the asymmetric addition of phenylboronic acid to 1-(*p*-methoxybenzyl)-5-chloroisatin

The MOP ligand (20.0 µmol, 0.1 eq.) and chlorobis(ethylene)rhodium(I) dimer (1.9 mg, 5.0 µmol, 0.025 eq.) were dissolved in THF (1.0 mL) and stirred at room temperature for 10 min, after which 1-(*p*-methoxybenzyl)-5-chloroisatin (60.3 mg, 200 µmol, 1.0 eq.), phenylboronic acid (48.8 mg, 400 µmol, 2.0 eq.), THF (1.0 mL) and potassium hydroxide (0.1 mL, 0.3 M (aq.), 0.3 mmol) were added sequentially. The reaction mixture was heated to 50 °C and left to stir for 24 h, after which the conversion was obtained by ^{1}H NMR spectroscopy. Filtration through silica with rinsing by ethyl acetate, removal of the volatiles *in vacuo* and silica gel column chromatography (ethyl acetate/chloroform, 95:5) yielded the pure product as a white solid. The ^{1}H and ^{13}C NMR spectroscopic data matched that of data reported in the literature,[175] and the HRMS data was in accordance with the calculated values. The enantiomeric excess of 5-chloro-3-hydroxy-1-(4-methoxybenzyl)-3-phenylindolin-2-one was determined by chiral HPLC analysis; the absolute configuration was assigned by comparison to literature data.[175]

R_f = 0.21 (silica gel; ethyl acetate/chloroform, 95:5). **^{1}H NMR** (300 MHz, $CDCl_3$): δ (ppm) = 7.30-7.22 (m, 5H), 7.16-7.07 (m, 4H), 6.79-6.73 (m, 2H), 6.62 (d, $^{3}J_{HH}$ = 8.3 Hz, 1H), 4.85 (d, $^{2}J_{HH}$ = 15.4 Hz, 1H), 4.65 (d, $^{2}J_{HH}$ = 15.4 Hz, 1H), 4.04 (br s, 1H), 3.69 (s, 3H). **^{13}C{^{1}H} NMR** (75 MHz, $CDCl_3$): δ (ppm) = 177.4, 159.3, 141.1, 139.7, 133.5, 129.6, 129.0, 128.8, 128.7, 128.6, 127.0, 125.5, 125.2, 114.4, 110.8, 78.0, 55.3, 43.7. **HRMS** (NSI^+, DCM/MeOH + NH_4OAc): Found: *m*/*z* = 380.1047. Calculated for $[M + H]^+$: *m*/*z* = 380.1048.

HPLC conditions (Lux Cellulose-1) – oven temperature: 40 °C, mobile phase: hexane/2-propanol (80:20), flow rate: 0.5 mL/min, detection: 264 nm, retention times: 23.1 min (*S*) and 27.2 min (*R*).

3.4.13 General procedure for the asymmetric Suzuki-Miyaura cross-coupling reactions

The MOP ligand (20.0 µmol, 0.04 eq.) and bis(acetonitrile)dichloropalladium(II) (2.6 mg, 10 µmol, 0.02 eq.) were dissolved in DCM (2.0 mL) and stirred at room temperature for 2 h, after which the volatiles were removed *in vacuo*. Subsequently, the 1-bromo-naphthalene derivative (500 µmol, 1.0 eq.), naphthalene-1-boronic acid (112 mg, 650 µmol, 1.3 eq.), caesium carbonate (277 mg, 850 µmol, 1.7 eq.) and toluene (2.0 mL) were added. The reaction mixture was heated to 80 °C with stirring, and the conversion was monitored by ^{1}H NMR spectroscopy.

2-Methoxy-1,1'-binaphthyl

Silica gel column chromatography (petrol) yielded the pure product as a white solid. The ^{1}H and ^{13}C NMR spectroscopic data matched that of data reported in the literature,[198] and the HRMS data was in accordance with the calculated values. The enantiomeric excess was determined by chiral HPLC analysis; the absolute configuration was assigned by comparison to literature data.[199]

R_f = 0.07 (silica gel; petrol). **^{1}H NMR** (300 MHz, $CDCl_3$): δ (ppm) = 7.93-7.84 (m, 3H), 7.80 (d, $^{3}J_{HH}$ = 8.2 Hz, 1H), 7.54 (dd, $^{3}J_{HH}$ = 8.2 Hz, $^{3}J_{HH}$ = 7.0 Hz, 1H), 7.42-7.34 (m, 3H), 7.28-7.05 (m, 5H), 3.69 (s, 3H). **^{13}C{^{1}H} NMR** (75 MHz, $CDCl_3$): δ (ppm) = 154.6, 134.6, 134.3, 133.7, 133.0, 129.5, 129.0, 128.4, 128.2, 127.8, 127.7, 126.4, 126.2, 125.9, 125.7, 125.6, 125.5, 123.6, 123.3, 113.9, 56.8. **HRMS** (ASAP$^+$, solid): Found: *m*/*z* = 285.1276. Calculated for $[M + H]^+$: *m*/*z* = 285.1274.

HPLC conditions (Lux Cellulose-3) – oven temperature: 40 °C, mobile phase: hexane/2-propanol (99:1), flow rate: 0.5 mL/min, detection: 221 nm, retention times: 17.3 min (*S*) and 21.6 min (*R*).

2-Methyl-1,1'-binaphthyl

Silica gel column chromatography (petrol) yielded the product as a white solid, which contained a small amount of the inseparable homocoupling side product 1,1'-binaphthyl.[200] The ^{1}H and ^{13}C NMR spectroscopic data matched that of data reported in the literature,[198] and the HRMS data was in accordance with the calculated values. The enantiomeric excess was determined by chiral HPLC analysis; the absolute configuration was assigned by comparison to literature data.[199]

R_f = 0.28 (silica gel; petrol). **^{1}H NMR** (300 MHz, $CDCl_3$): δ (ppm) = 7.88 (*overlapping*-d, $^{3}J_{HH}$ = 8.3 Hz, 2H), 7.83-7.78 (m, 2H), 7.54 (dd, $^{3}J_{HH}$ = 8.3 Hz, $^{3}J_{HH}$ = 7.0 Hz, 1H), 7.44-7.36 (m, 2H), 7.34-7.28 (m, 2H), 7.23-7.04 (m, 4H), 2.04 (s, 3H). **^{13}C{^{1}H} NMR** (75 MHz, $CDCl_3$): δ (ppm) = 137.5, 136.1, 134.4, 133.8, 133.5, 132.6, 132.0, 128.6, 128.3, 127.8, 127.8, 127.6, 127.6, 126.3, 126.1, 126.0, 125.9, 125.9, 125.7, 124.8, 20.5. **HRMS** (ASAP$^+$, solid): Found: *m*/*z* = 269.1326. Calculated for $[M + H]^+$: *m*/*z* = 269.1325.

HPLC conditions (Lux Cellulose-3) – oven temperature: 40 °C, mobile phase: hexane/2-propanol (99:1), flow rate: 0.1 mL/min, detection: 217 nm, retention times: 59.6 min (*R*) and 71.0 min (*S*).

3.4.14 General procedure for the synthesis of $[Pd(L^P)_2Cl_2]$ complexes.

The phosphonite ligand (40.0 µmol, 1.0 eq.) and bis(acetonitrile)dichloropalladium(II) (5.2 mg, 20 µmol, 1.0 eq.) were dissolved in DCM (2.0 mL) and stirred at room temperature for 2 h, after which the volatiles were removed *in vacuo*. The residue was washed with diethyl ether and dried *in vacuo*, to yield the pure title compound quantitatively as an off-white solid.

3.4.15 [Pd((*S*)-**30a**)$_2$Cl$_2$] (*S*)-**41a**

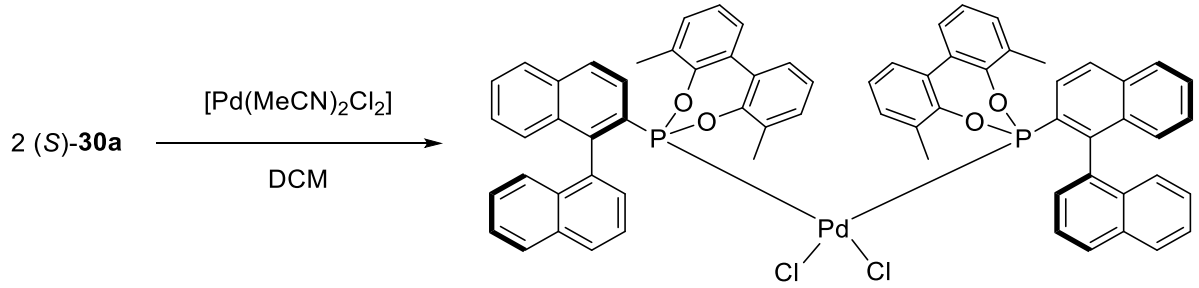

Single crystals were grown by slow diffusion of hexane into a $CDCl_3$ solution.

MP: 255-257 °C (decomp.). **IR** (neat): ν = 3046.2 (w), 2360.3 (m), 1557.7 (w), 1452.7 (m), 1416.3 (m), 1249.8 (m), 1185.6 (s), 1087.4 (m), 912.0 (s), 873.0 (w), 800.6 (m), 771.3 (s), 745.1 (m), 690.1 (s), 634.8 (s), 613.0 (m) cm^{-1}. **^{1}H NMR** (500 MHz, $CDCl_3$, −40 °C): δ (ppm) = 7.96 (d, $^3J_{HH}$ = 8.7 Hz, 1H, *H*4), 7.89 (d, $^3J_{HH}$ = 8.3 Hz, 1H, *H*5), 7.85 (d, $^3J_{HH}$ = 8.2 Hz, 1H, *H*5'), 7.70-7.66 (m, 2H, *H*3/*H*8'), 7.53 (*apparent*-t (dd), $^3J_{HH}$ = 7.6 Hz, 1H, *H*6), 7.46 (d, $^3J_{HH}$ = 8.3 Hz, 1H, *H*4'), 7.40 (*apparent*-t (dd), $^3J_{HH}$ = 7.4 Hz, 1H, *H*6'), 7.38-7.32 (m, 2H, *H*7'/*H*14'), 7.22-7.16 (m, 2H, *H*7/H15'), 7.15 (*apparent*-t (dd), $^3J_{HH}$ = 7.5 Hz, 1H, *H*15), 7.04-6.98 (m, 3H, *H*8/*H*16/*H*16'), 6.88 (d, $^3J_{HH}$ = 7.2 Hz, 1H, *H*14), 6.66 (*apparent*-t (dd), $^3J_{HH}$ = 7.5 Hz, 1H, *H*3'), 5.34 (d, $^3J_{HH}$ = 6.9 Hz, 1H, *H*2'), 2.09 (s, 3H, CH_3'), 0.84 (s, 3H, CH_3). **^{13}C{^{1}H} NMR** (126 MHz, $CDCl_3$, −40 °C): δ (ppm) = 148.4 (*apparent*-t, J_{CP} = 6.6 Hz, *C*12), 146.5 (*apparent*-t, J_{CP} = 3.6 Hz, *C*12'), 141.5 (*C*1), 135.7 (*C*1'), 134.4 (*C*10), 133.1 (*C*9'), 132.7 (*apparent*-t, J_{CP} = 4.8 Hz, *C*9), 132.0 (*C*10'), 131.0 (*C*11'/*C*14/*C*14'), 130.3 (*C*13), 130.2 (*obscured*-m, *C*2), 130.2 (*C*11), 130.0 (*C*13'), 129.1 (*C*16), 128.9 (*C*5'), 128.5 (*C*6), 128.3 (*C*8), 128.0 (m, *C*3/*C*5), 127.7 (*C*4/*C*16'), 127.2 (*C*7), 127.1 (*C*4'), 127.0 (*C*8'), 126.4 (*C*15'), 126.1 (*C*7'), 126.0 (*C*2'), 125.8 (*C*6'), 125.4 (*C*15), 124.1 (*C*3'), 17.8 (*C*H$_3$'), 16.0 (*C*H$_3$). **^{31}P{^{1}H} NMR** (202 MHz, $CDCl_3$, −40 °C): δ (ppm) = 144.3 (s). **LRMS** (MALDI$^+$): Found: *m*/*z* = 1131.1. Calculated for [M − Cl]$^+$: *m*/*z* = 1131.2.

3.4.16 [Pd((*R*)-**30b**)$_2$Cl$_2$] (*R*)-**41b**

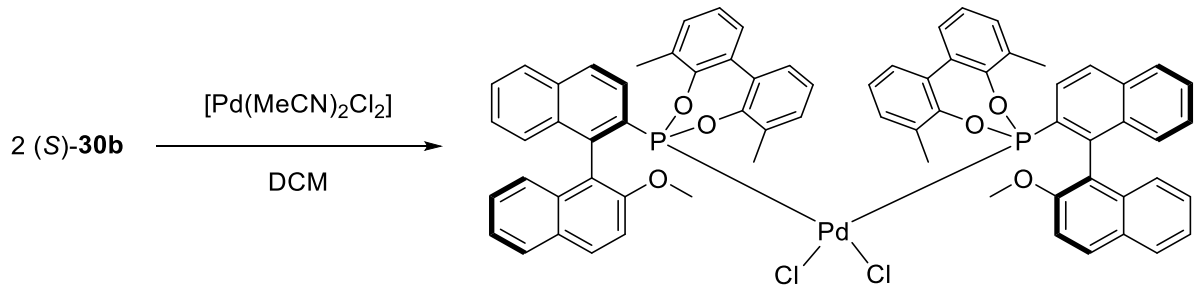

Single crystals were grown by slow diffusion of diethyl ether into a DCM solution.

MP: 247-249 °C (decomp.). **IR** (neat): ν = 2968.9 (w), 2361.2 (m), 1591.3 (w), 1486.3 (m), 1456.0 (m), 1250.7 (m), 1184.6 (m), 1081.1 (m), 963.3 (m), 915.5 (s), 806.1 (s), 773.2 (s), 745.9 (s), 685.4 (m), 638.2

(s), 617.4 (m) cm^{-1}. **^{1}H NMR** (500 MHz, $CDCl_3$, −40 °C): δ (ppm) = 7.88 (d, $^3J_{HH}$ = 8.4 Hz, 1H, *H*5), 7.75 (d, $^3J_{HH}$ = 8.7 Hz, 1H, *H*4), 7.70-7.65 (m, 2H, *H*4'/*H*5'), 7.57 (d, $^3J_{HH}$ = 8.2 Hz, 1H, *H*8'), 7.53-7.46 (m, 2H, *H*6/*H*15'), 7.42 (d, $^3J_{HH}$ = 7.3 Hz, 1H, *H*14'), 7.31-7.25 (m, 3H, *H*6'/*H*7'/*H*16'), 7.21-7.17 (m, 1H, *H*7), 7.10 (d, $^3J_{HH}$ = 8.5 Hz, 1H, *H*8), 7.05 (d, $^3J_{HH}$ = 7.8 Hz, 1H, *H*16), 6.92 (*apparent*-t (dd), $^3J_{HH}$ = 7.5 Hz, 1H, *H*15), 6.75 (d, $^3J_{HH}$ = 7.2 Hz, 1H, *H*14), 6.68 (d, $^3J_{HH}$ = 9.1 Hz, 1H, *H*3'), 6.60-6.52 (m, 1H, *H*3), 2.73 (s, 3H, OCH_3), 1.69 (s, 3H, CH_3'), 1.13 (s, 3H, CH_3). **^{13}C{^{1}H} NMR** (126 MHz, $CDCl_3$, −40 °C): δ (ppm) = 153.4 (*C*2'), 149.1 (*apparent*-t, J_{CP} = 7.2 Hz, *C*12), 148.3 (*apparent*-t, J_{CP} = 3.0 Hz, *C*12'), 136.8 (*C*1), 134.4 (*C*10), 134.0 (*C*9'), 132.8 (*C*13'), 132.4 (*apparent*-t, J_{CP} = 4.8 Hz, *C*9), 132.2 (*apparent*-t, J_{CP} = 34.8 Hz, *C*2), 131.5 (*C*14'), 130.8 (*C*11'), 130.4 (*C*13/*C*14), 129.7 (*C*4'), 128.6 (*C*16'), 128.4 (*C*16), 128.2 (*C*6), 128.0 (m, *C*4/*C*5/*C*8'), 127.7 (*C*10'), 127.5 (*C*8), 127.0 (m, *C*3/*C*7), 126.9 (*C*11), 126.7 (*C*5'), 126.5 (*C*7'), 126.4 (*C*15'), 124.1 (*C*15), 123.6 (*C*6'), 119.3 (*C*1'), 110.8 (*C*3'), 55.2 (O*C*H$_3$), 17.4 (*C*H$_3$'), 16.3 (*C*H$_3$). **^{31}P{^{1}H} NMR** (202 MHz, $CDCl_3$, −40 °C): δ (ppm) = 139.4 (s). **LRMS** (MALDI$^+$): Found: *m*/*z* = 1191.3. Calculated for $[M - Cl]^+$: *m*/*z* = 1191.2.

3.5 X-ray Crystallography

Measurements were made at 150 K on an Oxford Diffraction (Agilent Technologies) Gemini A Ultra diffractometer, using CuKα radiation (λ =1.54184 Å) for (*R*)-**40b**, (*S*)-**41a** (*pseudo*-polymorph 2) and (*R*)-**41b** and MoKα radiation (λ = 0.71073 Å) for (*R*)-**36b**, (*S*)-**38a**, (*R*)-**38b**, (*S*)-**39a**, (*R*)-**39b** and (*S*)-**41a** (*pseudo*-polymorph 1). Cell parameters were refined from the observed positions of all strong reflections. Intensities were corrected for absorption, using a semi-empirical method based on symmetry-equivalent and repeated reflections for (*S*)-**38a** and (*R*)-**38b** and analytically using a multi-faceted crystal model for (*R*)-**36b**, (*S*)-**39a**, (*R*)-**39b**, (*R*)-**40b**, (*S*)-**41a** (*pseudo*-polymorphs 1 and 2) and (*R*)-**41b**.[133] The structures were solved by direct methods and refined on F^2 values for all unique data. All non-hydrogen atoms were refined anisotropically, and H atoms were positioned with idealised geometry and their thermal parameters constrained using the riding model; $U_{(H)}$ was set at 1.2 times U_{eq} for the parent C atom. Oxford Diffraction CrysAlisPro was used for data collection and processing,[134] and Olex2[135] using SHELX[136] for structure solution, refinement, and to generate the molecular overlap figures. Crystal Impact Diamond was used to generate all other molecular graphics with displacement ellipsoids drawn at the 50% probability level.[137]

	(*R*)-**36b**	(*S*)-**38a**	(*S*)-**38b**
Empirical formula	$C_{39}H_{38}O_3P_2Cl_2Pt$	$C_{40}H_{33}O_2PClRh$	$C_{41}H_{35}O_3PClRh$
Formula weight	882.62	714.99	745.02
Temperature/K	150.00(10)	150.0(2)	150.0(2)
Crystal system	trigonal	hexagonal	trigonal
Space group	$P3_2$	$P6_5$	$P3_2$
a/Å	11.52064(15)	10.4774(2)	10.6324(3)
b/Å	11.52064(15)	10.4774(2)	10.6324(3)
c/Å	22.9152(3)	49.1495(16)	24.9502(8)
α/°	90	90	90
β/°	90	90	90
γ/°	120	120	120
Volume/Å^3	2633.95(8)	4672.6(2)	2442.68(16)
Z	3	6	3
ρ_{calc}g/cm^3	1.669	1.525	1.519
μ/mm^{-1}	4.276	0.722	0.696
F(000)	1314.0	2196.0	1146.0
Crystal size/mm^3	0.21 × 0.17 × 0.11	0.3 × 0.3 × 0.2	0.24 × 0.2 × 0.1
Radiation	MoKα (λ = 0.71073)	MoKα (λ = 0.71073)	MoKα (λ = 0.71073)
2Θ range for data collection/°	5.414 to 56.796	5.582 to 56.418	6.602 to 56.85
Index ranges	-15 ≤ h ≤ 15, -15 ≤ k ≤ 15, -30 ≤ l ≤ 30	-13 ≤ h ≤ 13, -13 ≤ k ≤ 12, -64 ≤ l ≤ 59	-14 ≤ h ≤ 10, -11 ≤ k ≤ 12, -31 ≤ l ≤ 32
Reflections collected	83576	31490	15538
Independent reflections	8250 [R_{int} = 0.0495, R_{sigma} = 0.0282]	6807 [R_{int} = 0.0613, R_{sigma} = 0.0456]	6762 [R_{int} = 0.0369, R_{sigma} = 0.0556]
Data/restraints/parameters	8250/400/428	6807/1/406	6762/1/425
Goodness-of-fit on F^2	1.048	1.220	1.068
Final R indexes [I>=2σ (I)]	R_1 = 0.0200, wR_2 = 0.0353	R_1 = 0.0574, wR_2 = 0.1080	R_1 = 0.0351, wR_2 = 0.0638
Final R indexes [all data]	R_1 = 0.0227, wR_2 = 0.0363	R_1 = 0.0591, wR_2 = 0.1090	R_1 = 0.0413, wR_2 = 0.0680
Largest diff. peak/hole / e Å^{-3}	0.99/-0.44	0.66/-1.67	0.55/-0.45
Flack parameter	-0.0247(18)	0.065(15)	-0.059(15)

	(*R*)-**39a**	(*S*)-**39b**	(*S*)-**40b**
Empirical formula	$C_{42}H_{37}O_2PClRh$	$C_{43}H_{39}O_3PClRh$	$C_{70}H_{54}O_6P_2Rh^+ \cdot BF_4^-$
Formula weight	743.04	773.07	1242.79
Temperature/K	150.0(2)	150.0(2)	150.0(2)
Crystal system	monoclinic	monoclinic	triclinic
Space group	$P2_1$	$P2_1$	P1
a/Å	10.46454(10)	9.69170(6)	11.7059(2)
b/Å	18.62602(18)	17.44304(12)	16.9283(3)
c/Å	18.5228(2)	20.04701(13)	17.9950(4)
α/°	90	90	73.4211(18)
β/°	92.0930(9)	90.6504(6)	73.7906(17)
γ/°	90	90	89.1816(15)
Volume/Å^3	3607.92(6)	3388.78(4)	3273.51(11)
Z	4	4	2
ρ_{calc}g/cm^3	1.368	1.515	1.261
μ/mm^{-1}	0.626	0.672	3.070
F(000)	1528.0	1592.0	1276.0
Crystal size/mm^3	0.22 × 0.19 × 0.13	0.32 × 0.17 × 0.11	0.19 × 0.11 × 0.08
Radiation	MoKα (λ = 0.71073)	MoKα (λ = 0.71073)	CuKα (λ = 1.54184)
2Θ range for data collection/°	6.604 to 56.462	6.59 to 55.754	5.35 to 133.952
Index ranges	-13 ≤ h ≤ 13, -24 ≤ k ≤ 24, -24 ≤ l ≤ 24	-12 ≤ h ≤ 12, -22 ≤ k ≤ 22, -26 ≤ l ≤ 26	-13 ≤ h ≤ 13, -20 ≤ k ≤ 20, -20 ≤ l ≤ 21
Reflections collected	115490	107785	89533
Independent reflections	16266 [R_{int} = 0.0501, R_{sigma} = 0.0350]	15240 [R_{int} = 0.0451, R_{sigma} = 0.0327]	22461 [R_{int} = 0.0631, R_{sigma} = 0.0517]
Data/restraints/parameters	16266/1097/889	15240/1/889	22461/292/1574
Goodness-of-fit on F^2	1.060	1.059	1.053
Final R indexes [I>=2σ (I)]	R_1 = 0.0340, wR_2 = 0.0763	R_1 = 0.0344, wR_2 = 0.0845	R_1 = 0.0455, wR_2 = 0.1105
Final R indexes [all data]	R_1 = 0.0439, wR_2 = 0.0802	R_1 = 0.0401, wR_2 = 0.0877	R_1 = 0.0539, wR_2 = 0.1155
Largest diff. peak/hole / e Å^{-3}	0.44/-0.89	0.62/-1.14	1.81/-0.84
Flack parameter	-0.013(12)	-0.028(6)	-0.026(3)

	(*R*)-**41a**, *pseudo*-polymorph 1	(*S*)-**41a**, *pseudo*-polymorph 2	(*S*)-**41b**
Empirical formula	$C_{68}H_{50}O_4P_2Cl_2Pd \cdot 3CHCl_3$	$C_{68}H_{50}O_4P_2Cl_2Pd \cdot CHCl_3$	$C_{70}H_{54}O_6P_2Cl_2Pd$
Formula weight	1528.42	1289.69	1230.37
Temperature/K	150.00(10)	150.01(10)	150.0(2)
Crystal system	monoclinic	orthorhombic	monoclinic
Space group	$P2_1$	$P2_12_12_1$	$P2_1$
a/Å	11.5925(9)	11.54920(12)	11.28960(10)
b/Å	21.8177(11)	17.81230(17)	20.94262(17)
c/Å	14.4054(11)	29.1165(3)	14.09792(13)
α/°	90	90	90
β/°	111.477(8)	90	101.7126(8)
γ/°	90	90	90
Volume/Å^3	3390.4(4)	5989.78(11)	3263.82(5)
Z	2	4	2
ρ_{calc}g/cm^3	1.497	1.430	1.252
μ/mm^{-1}	0.803	5.450	3.897
F(000)	1548.0	2632.0	1264.0
Crystal size/mm^3	0.27 × 0.17 × 0.11	0.13 × 0.12 × 0.11	0.19 × 0.16 × 0.11
Radiation	MoKα (λ = 0.71073)	CuKα (λ = 1.54184)	CuKα (λ = 1.54184)
2Θ range for data collection/°	5.864 to 57.792	5.816 to 132.694	6.402 to 133.838
Index ranges	-14 ≤ h ≤ 14, -28 ≤ k ≤ 29, -19 ≤ l ≤ 19	-13 ≤ h ≤ 13, -16 ≤ k ≤ 21, -34 ≤ l ≤ 33	-13 ≤ h ≤ 13, -25 ≤ k ≤ 24, -16 ≤ l ≤ 16
Reflections collected	22655	52298	43167
Independent reflections	13225 [R_{int} = 0.0402, R_{sigma} = 0.0727]	10465 [R_{int} = 0.0385, R_{sigma} = 0.0294]	11588 [R_{int} = 0.0448, R_{sigma} = 0.0382]
Data/restraints/parameters	13225/787/831	10465/702/734	11588/1/736
Goodness-of-fit on F^2	1.033	1.048	1.035
Final R indexes [I>=2σ (I)]	R_1 = 0.0455, wR_2 = 0.0810	R_1 = 0.0266, wR_2 = 0.0627	R_1 = 0.0293, wR_2 = 0.0690
Final R indexes [all data]	R_1 = 0.0608, wR_2 = 0.0892	R_1 = 0.0289, wR_2 = 0.0643	R_1 = 0.0329, wR_2 = 0.0710
Largest diff. peak/hole / e Å^{-3}	0.66/-0.64	0.59/-0.47	0.26/-0.27
Flack parameter	-0.052(15)	-0.024(2)	-0.016(4)

3.6 Density Functional Theory Calculations

Performed with the B3LYP functional and 6-31G* basis set, using the *Spartan* program. In each case the calculations were considered to be complete and converged to a minimum on the potential energy surface after vibrational frequency analysis did not report any negative frequencies.

Table 3.10 Calculated conformational energy differences versus dihedral angle for the ligands (*S*)-**30a** and (*R*)-**30b**, relative to the energy at the optimised dihedral angle.

Dihedral angle[a]	Relative energy[b]	
	(*S*)-**30a**	(*R*)-**30b**
−90.00	14.26	14.34
−75.00	5.93	5.87
−60.00	1.31	1.29
−46.11	0.00	–
−46.00	–	0.00
−45.00	0.01	0.02
−30.00	1.46	1.15
−15.00	5.44	5.71
0.00	7.34	7.39
15.00	5.70	5.91
30.00	2.07	2.28
45.00	0.71	0.76
45.56	0.71	–
45.60	–	0.75
60.00	2.11	2.19
75.00	6.73	6.93
90.00	15.11	15.45

[a] C12–C11–C11'–C12' (°). [b] Optimised ligand geometry (kcal/mol).

4. Coinage Metal Complexes of MOP-Phosphonites

Abstract: Chiral MOP-phosphonites containing two phenoxy substituents (*S*)-**28a** and (*R*)-**28b**, a biphenoxy group (*S*)-**29a** and (*R*)-**29b** or the 3,3'-dimethylbiphenoxy group (*S*)-**30a** and (*R*)-**30b**, have been coordinated to the coinage metals. Six [Au(L^P)Cl] complexes have been prepared and five characterised by X-ray crystallography, as has the related complex [Au((*S*)-**30a**)$_2$]SbF_6. Six [Ag(L^P)OTf] complexes were synthesised, studied by VT NMR and, in one case, by X-ray crystallography. Six [Cu(L^P)(MeCN)$_2$]PF_6 complexes were also prepared, one example was characterised crystallographically, as was the decomposition product [Cu((*S*)-**28a**)(O_2PF_2)]$_2$.

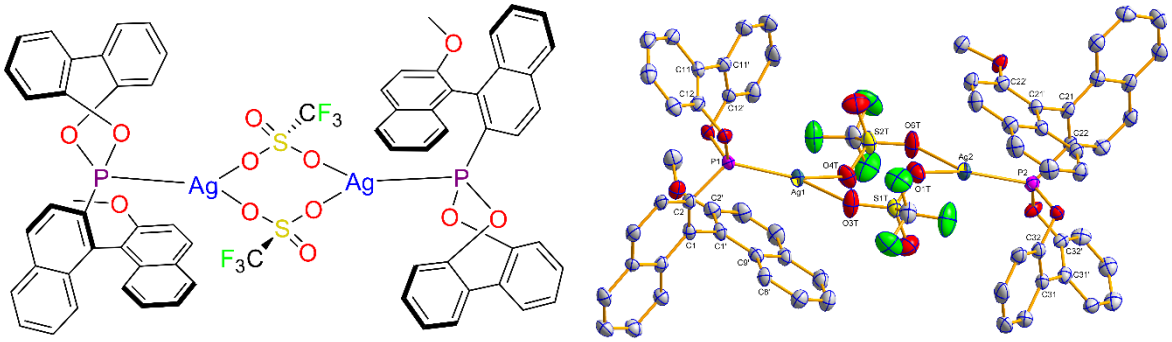

4.1 Introduction

Chiral phosphonites are ligands with good π-acceptor properties which have proven to be effective in nickel-catalysed hydrocyanations,[102c] and rhodium-catalysed hydroformylations[106c] and hydrogenations.[107b,c] We have demonstrated that atropisomeric monophosphonites with a binaphthyl backbone are particularly successful in the palladium-catalysed asymmetric hydrosilylation of alkenes, capable of transforming methoxy-substituted styrenes with greater enantioselectivity than the parent phosphine (*S*)-H-MOP (see Chapter 2).[138] They possess a phosphorus donor bound directly to a binaphthyl backbone – the **a** series has a hydrogen in the 2' position of the lower naphthyl ring, whilst a methoxy group occupies that site in the **b** series (ligands **28**-**30**, Chart 4.1).

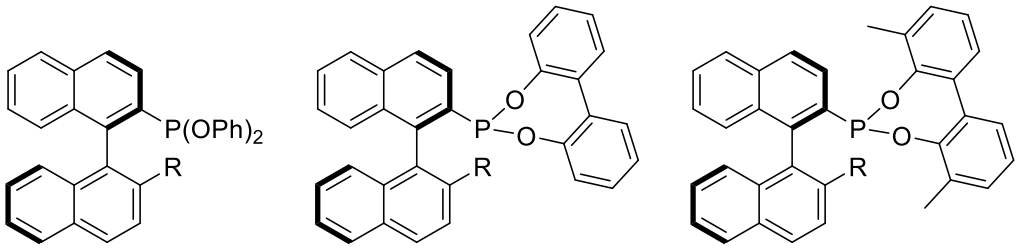

(*S*)-**28a**: R = H
(*R*)-**28b**: R = OMe

(*S*)-**29a**: R = H
(*R*)-**29b**: R = OMe

(*S*)-**30a**: R = H
(*R*)-**30b**: R = OMe

Chart 4.1 Phosphonite ligands (*S*)-**28a**, (*R*)-**28b**, (*S*)-**29a**, (*R*)-**29b**, (*S*)-**30a** and (*R*)-**30b** prepared in this study.

This difference has profound implications for the catalytic performance of the parent (*S*)-H-MOP and (*R*)-MeO-MOP ligands.[122] However, despite the fact that gold catalysis is a very active research area,[201] reports of coinage metal (group 11) MOP complexes are rare. A gold catalyst prepared from [Au((*R*)-MeO-MOP)Cl] was used in the alkoxycyclisation of an enyne, albeit affording negligible enantioselectivity,[202] whilst analogous complexes containing a MOP-phosphine bearing a phenyl ((*S*)-Ph-MOP) or hydroxy group ((*S*)-HO-MOP) in the 2' position were used in the intramolecular hydroamination of an alkene, achieving a maximum *ee* of 29% (Scheme 4.1).[203] In the latter article, the authors describe a weak Au–π interaction with the ligand backbone. [Au((*R*)-MeO-MOP)Cl] was also used to effect the enantioselective gold(I)-catalysed [4+2] cyclisation of a 1,6-enyne in good yields, but with *ee*s capped at 25% (Scheme 4.2).[204] Air-stable vinyl gold complexes were prepared from a MOP ligand bearing two phosphorus-bound *tert*-butyl substituents and a hydrogen in the 2' position.[205] These complexes reacted further in palladium-catalysed aryl cross-coupling reactions and C(sp^3)–C(sp^2) bond formations using electrophilic reagents, to give polycyclic natural product derivatives.[205] The same ligand was used in the synthesis of dihydroisocoumarins; the authors assert that the highly effective nature of the catalyst may result from stabilisation of the Au(I) centre in the transition state by a side-on π–arene interaction with the ligand.[206] The subject of Au–arene π-bonding to biphenyl phosphines has also been investigated theoretically.[207] Echavarren and co-workers published their study on M–π interactions for group 11 metal complexes containing ligated biphenylphosphine ligands, noting a stronger bonding for the Cu and Ag analogues compared to Au.[208]

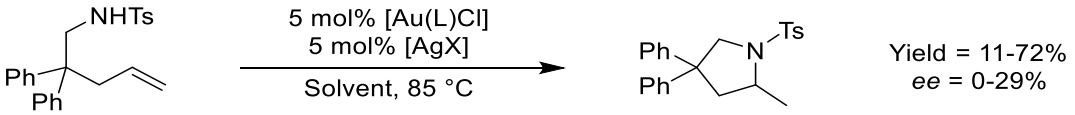

Scheme 4.1 Au(I)-catalysed asymmetric intramolecular hydroamination of an alkene. L = (*S*)-Ph-MOP or (*S*)-HO-MOP; X = OTf, OTs, CF_3CO_2, BF_4 or NTf_2; solvent = acetonitrile, DCE or toluene.[203]

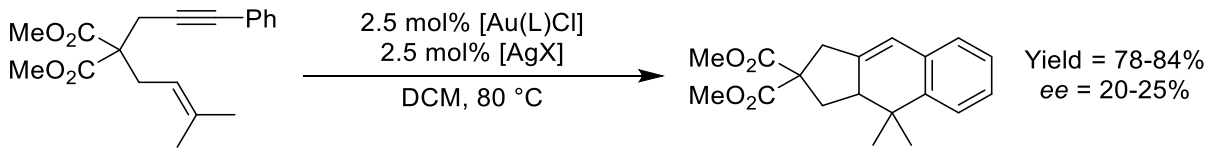

Scheme 4.2 Au(I)-catalysed asymmetric [4+2] cyclisation of a 1,6-enyne. L = (*R*)-MeO-MOP; X = PF_6 or SbF_6.[204]

MOP ligands with benzyl substituents in the 2' position are effective in silver-catalysed chiral vinylogous Mannich reactions,[209] where weak Ag–π/π–π stacking was invoked as a possible explanation for the diastereoselective nucleophilic addition of siloxyfuran to the imine. Ag–MOP catalysts have shown high reactivity and encouraging enantioselectivity in the allylation of aldimines.[210] A silver

acetate complex bound to (*S*)-HO-MOP was found to be effective in the asymmetric formal [3+2] cycloaddition of isocyanoesters to 2-oxobutenoate esters in high yields and *ee*s (Scheme 4.3).[211]

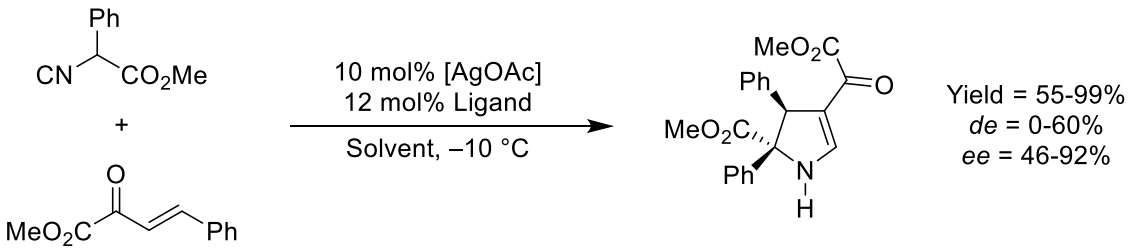

Scheme 4.3 Ag(I)-catalysed asymmetric [3+2] cycloaddition of methyl 2-cyano-2-phenylacetate to methyl 2-oxo-4-phenylbut-3-enoate. Solvent = acetonitrile, carbon tetrachloride, chloroform, DCE, DCM, toluene or THF.[211]

(*R*)-MeO-MOP was effective in the copper-catalysed propargylic amination of propargyl acetate with *N*-methylaniline,[212] although the *ee* was found to be low. H-MOP and MeO-MOP backbones with two methyl groups on the phosphorus have been prepared, but their copper(I) hydride complexes did not perform as ketone hydrogenation catalysts.[213] (*R*)-MeO-MOP gave a low yield but moderate enantioselectivity in the copper(I)-catalysed hydroboration of a cyclopropane (Scheme 4.4).[214] The *S* enantiomer of the same ligand gave low yields and *ee*s in copper-catalysed azide-alkyne cycloadditions.[215] However, no coordination chemistry of the MOP-copper complexes was reported.

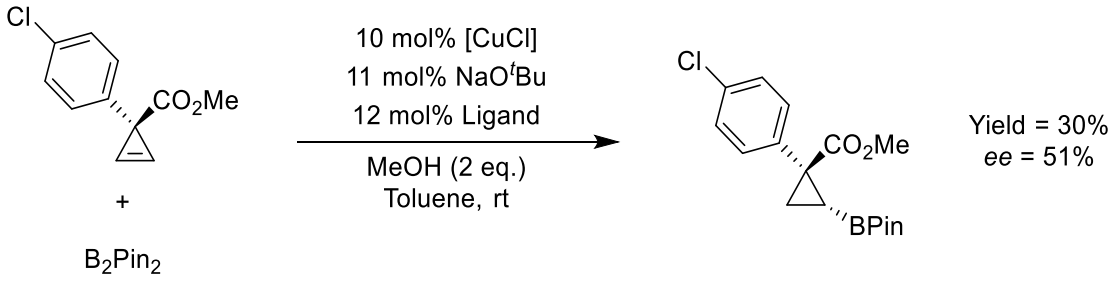

Scheme 4.4 Cu(I)-catalysed hydroboration of a cyclopropane. B_2Pin_2 = bis(pinacolato)diboron.

We have noted the ramifications of π-interactions between palladium and the lower naphthyl ring of our MOP ligands in affecting the outcome of asymmetric hydrosilylations (see Chapter 2).[93a,138] In this chapter, we report for the first time the coordination chemistry of all the group 11 metals with one uniform set of chiral phosphonite ligands.

4.2 Results and Discussion

4.2.1 Gold coordination chemistry

Each phosphonite (Chart 4.1) was reacted with the gold precursor [Au(tht)Cl], to generate the corresponding phosphonite gold chloride complexes [Au((*S*)-**28a**)Cl] (*S*)-**42a**, [Au((*R*)-**28b**)Cl] (*R*)-**42b**, [Au((*S*)-**29a**)Cl] (*S*)-**43a**, [Au((*R*)-**29b**)Cl] (*R*)-**43b**, [Au((*S*)-**30a**)Cl] (*S*)-**44a** and [Au((*R*)-**30b**)Cl] (*R*)-**44b**,

which were fully characterised by multinuclear NMR spectroscopy, HRMS, and in each case, with the exception of (*R*)-**44b**, by X-ray crystallography (Figs. 4.1-4.5). The complexes all share a slightly distorted linear geometry, with P–Au–Cl bond angles ranging from 174.27(5)° in (*S*)-**44a** to 178.67(10)° in (*S*)-**43a**. The Au–P bond lengths vary from 2.1932(11) Å in (*R*)-**43b** to 2.209(2) Å in (*R*)-**42b**, whilst the Au–Cl bond lengths lie in the range 2.270(2) Å in (*R*)-**42b** to 2.287(3) Å in (*S*)-**43a**. Hashmi *et al*. reported bond distance ranges of 2.22 to 2.25 Å for Au–P and 2.28 to 2.30 Å for Au–Cl in their study into Au–biarylphosphine complexes.[206] When the torsion angles for the 2,2'-biphenoxy groups in (*S*)-**43a** and (*R*)-**43b** are compared, it can be deduced that there is free rotation about the C11–C11' bond. In the asymmetric unit of (*S*)-**43a** there are two molecules with different conformations which have angles of 43.6(15)° and −42.0(14)°, and in (*R*)-**43b** the angle is −44.0(6)°.

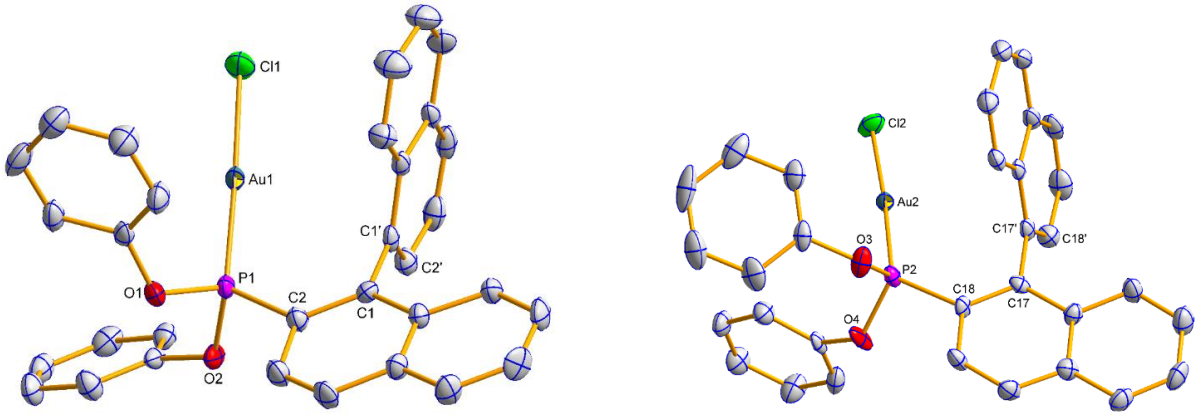

Fig. 4.1 Molecular structure of (*S*)-**42a** (the asymmetric unit comprises two molecules in different conformations). Hydrogen atoms have been omitted for clarity. Selected average bond distances (Å) and angles (°): (left) P1–Au1 2.2026(18), P1–C2 1.790(6), P1–O1 1.617(4), P1–O2 1.601(4), Au1–Cl1 2.2791(17); P1–Au1–Cl1 177.72(8), Au1–P1–C2 119.6(2), Au1–P1–O1 112.14(15), Au1–P1–O2 119.29(16), C2–C1–C1'–C2' –76.6(6); (right) P2–Au2 2.2057(18), P2–C18 1.787(5), P2–O3 1.611(4), P2–O4 1.603(4), Au2–Cl2 2.2776(16); P2–Au2–Cl2 176.71(8), Au2–P2–C18 124.5(2), Au2–P2–O3 114.74(17), Au2–P2–O4 112.96(15), C18–C17–C17'–C18' –108.7(6).

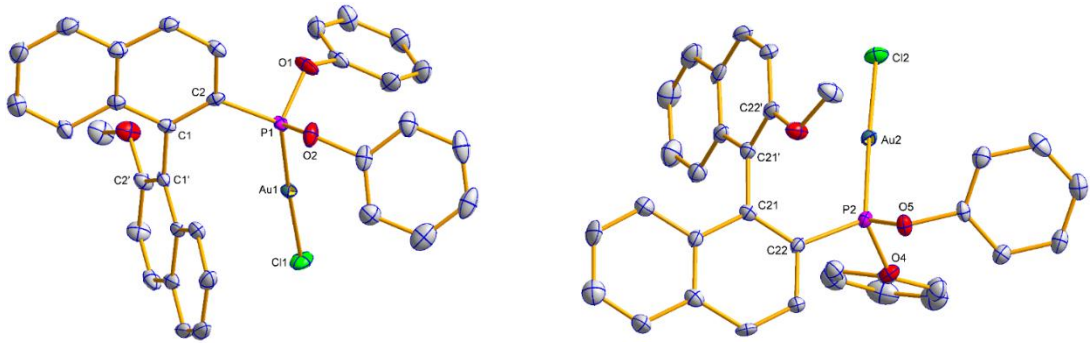

Fig. 4.2 Molecular structure of (*R*)-**42b** (the asymmetric unit comprises two molecules in different conformations). Hydrogen atoms have been omitted for clarity. Selected average bond distances (Å) and angles (°): (left) P1–Au1 2.195(2), P1–C2 1.794(7), P1–O1 1.603(5), P1–O2 1.622(6), Au1–Cl1 2.285(2); P1–Au1–Cl1 177.43(10), Au1–P1–C2 124.0(3), Au1–P1–O1 113.9(2), Au1–P1–O2 114.7(2), C2–C1–C1'–C2' –106.4(8); (right) P2–Au2 2.209(2), P2–C22 1.793(7), P2–O4 1.622(5), P2–O5 1.588(5), Au2–Cl2 2.270(2); P2–Au2–Cl2 177.64(10), Au2–P2–C22 120.0(2), Au2–P2–O4 112.6(2), Au2–P2–O5 117.6(2), C22–C21–C21'–C22' –74.5(10).

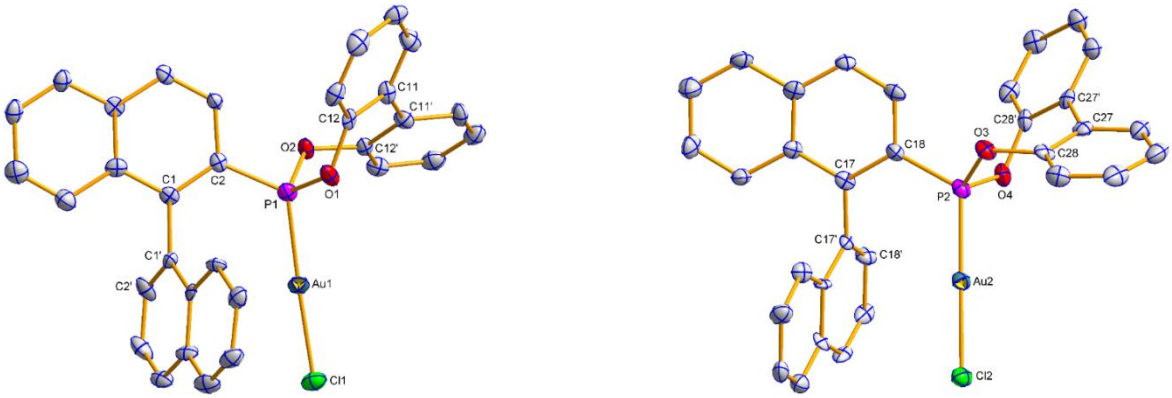

Fig. 4.3 Molecular structure of (*S*)-**43a** (the asymmetric unit comprises two molecules in different conformations). Hydrogen atoms have been omitted for clarity. Selected average bond distances (Å) and angles (°): (left) P1–Au1 2.200(3), P1–C2 1.789(10), P1–O1 1.602(7), P1–O2 1.603(7), Au1–Cl1 2.287(3); P1–Au1–Cl1 177.46(11), Au1–P1–C2 121.4(3), Au1–P1–O1 106.1(3), Au1–P1–O2 119.0(3), C2–C1–C1'–C2' –106.5(11), C12–C11–C11'–C12' 43.6(15); (right) P2–Au2 2.200(3), P2–C18 1.789(11), P2–O3 1.598(7), P2–O4 1.603(7), Au2–Cl2 2.277(3); P2–Au2–Cl2 178.67(10), Au2–P2–C18 119.6(3), Au2–P2–O3 117.2(3), Au2–P2–O4 108.2(3), C18–C17–C17'–C18' –76.1(12), C28–C27–C27'–C28' –42.0(14).

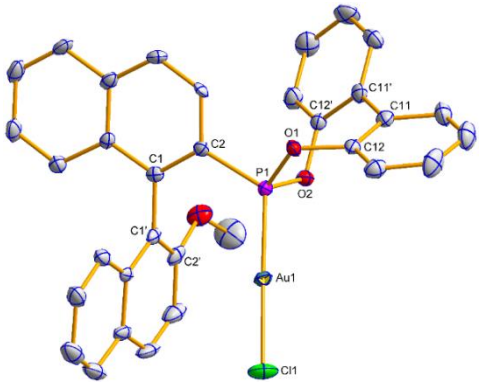

Fig. 4.4 Molecular structure of (*R*)-**43b**. Hydrogen atoms have been omitted for clarity. Selected bond distances (Å) and angles (°): P1–Au1 2.1932(11), P1–C2 1.798(4), P1–O1 1.608(3), P1–O2 1.616(3), Au1–Cl1 2.2737(11); P1–Au1–Cl1 177.18(5), Au1–P1–C2 121.50(14), Au1–P1–O1 115.11(13), Au1–P1–O2 110.10(11), C2–C1–C1'–C2' –85.4(6), C12–C11–C11'–C12' –44.0(6).

Of particular interest to us was the distance separating the gold centre from the nearest carbon and corresponding aryl group (Table 4.1). Hashmi's aforementioned biarylphosphine complexes have Au–C_{ipso} distances of 2.96 to 3.26 Å; for the H-MOP ligand bearing two phosphorus-bound *tert*-butyl substituents, Au–C_{ipso} is 3.052Å. The authors state that the sum of the van der Waals radii is 3.36 Å, and suggest a gold–arene interaction in these complexes.[206,216] By this metric, our gold phosphonite complexes have a degree of arene interaction (Table 4.1). For the complex [Au((*S*)-HO-MOP)Cl], the Au–centroid^{Ar} separation was reported to be 3.3 Å.[203] Echavarren *et al.* reported Au–biphenylphosphine distances of 3.0–3.3 Å in their series of complexes; however, in this publication the authors argue that 2.95 Å is the limit for significant gold–arene bonding.[208] An inspection of the Au–arene separations in our series of gold phosphonites shows that, by this metric, there appears to

be little interaction, with Au–C_{ipso} distances ranging from 3.131(10) Å in (*S*)-**43a** to 3.296(5) Å for (*S*)-**44a**; the distances to the centroid of the C_6 ring containing C_{ipso} are all above 3.26 Å (Table 4.1).

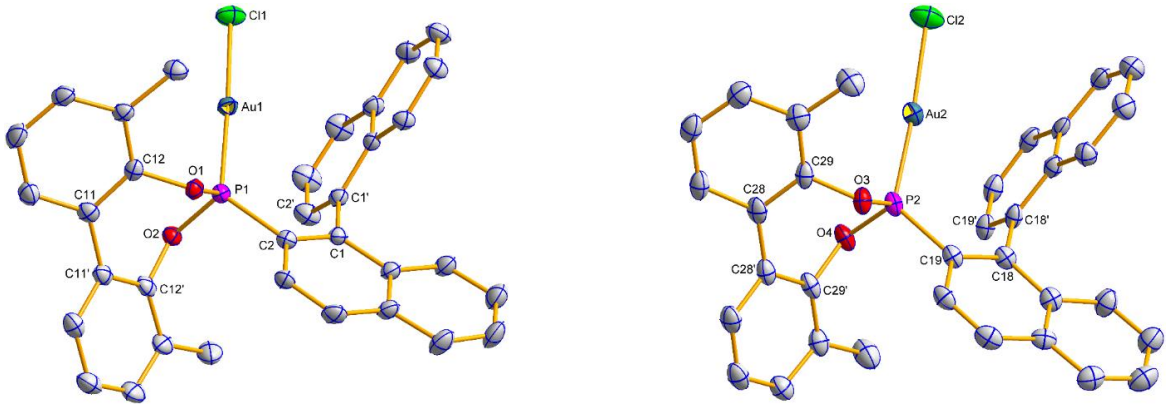

Fig. 4.5 Molecular structure of (*S*)-**44a** (the asymmetric unit comprises two molecules in different conformations). Hydrogen atoms have been omitted for clarity. Selected average bond distances (Å) and angles (°): (left) P1–Au1 2.1985(11), P1–C2 1.796(5), P1–O1 1.607(3), P1–O2 1.615(3), Au1–Cl1 2.2724(11); P1–Au1–Cl1 177.90(5), Au1–P1–C2 122.20(15), Au1–P1–O1 115.23(13), Au1–P1–O2 108.85(12), C2–C1–C1'–C2' –72.9(6), C12–C11–C11'–C12' –45.0(6); (right) P2–Au2 2.1998(13), P2–C19 1.798(5), P2–O3 1.614(3), P2–O4 1.602(3), Au2–Cl2 2.2705(14); P2–Au2–Cl2 174.27(5), Au2–P2–C19 121.78(15), Au2–P2–O3 111.59(14), Au2–P2–O4 110.97(13), C19–C18–C18'–C19' –76.3(6), C29–C28–C28'–C29' –48.4(7).

Table 4.1 Selected distances for [Au(L^P)Cl] complexes.[a]

Complex[b]	Au–C^{Ar} (Å)[c]	Au–centroid^{Ar} (Å)[d]
(*S*)-**42a**	3.218(4)	3.389(2)
	3.289(5)	3.432(2)
(*R*)-**42b**	3.245(9)	3.346(3)
	3.168(6)	3.261(3)
(*S*)-**43a**	3.165(10)	3.305(4)
	3.131(10)	3.279(4)
(*R*)-**43b**	3.261(5)	3.381(2)
(*S*)-**44a**	3.215(3)	3.267(2)
	3.296(5)	3.387(2)

[a] Experimental values (X-ray data). [b] (*S*)-**42a**, (*R*)-**42b**, (*S*)-**43a** and (*S*)-**44a** contain two independent molecules in the asymmetric unit. [c] *ipso*-C of the lower naphthyl ring. [d] Centroid of the C_6 ring containing the *ipso*-C.

We then synthesised the complex [Au((*S*)-**30a**)$_2$]SbF_6 (*S*)-**45a** by treating (*S*)-**44a** (prepared *in situ*) with silver(I) hexafluoroantimonate and an additional equivalent of (*S*)-**30a**. Single crystals of (*S*)-**45a**, suitable for X-ray crystallographic analysis, were obtained by layering a DCM solution of the complex with hexane (Fig. 4.6 and Fig. 4.7).

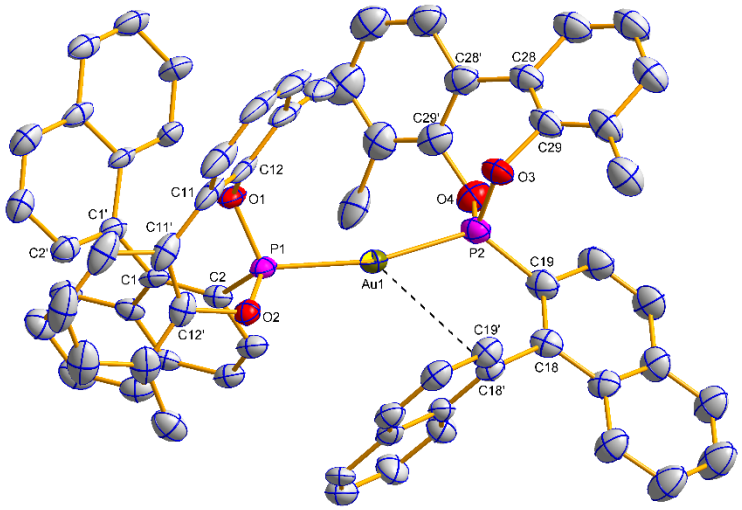

Fig. 4.6 Molecular structure of one of the two independent cations of (*S*)-**45a** (the asymmetric unit comprises two cations in different conformations and two anions). Hydrogen atoms have been omitted for clarity. Selected average bond distances (Å) and angles (°): P1–Au1 2.284(3), P2–Au1 2.290(3), P1–C2 1.791(11), P2–C19 1.770(14); P1–Au1–P2 164.78(11), Au1–P1–C2 111.7(4), Au1–P1–O1 112.2(3), Au1–P1–O2 112.7(3), Au1–P2–C19 124.7(4), Au1–P2–O3 105.2(3), Au1–P2–O4 112.8(4), C2–C1–C1'–C2' –99.5(14), C12–C11–C11'–C12' 45.2(19), C19–C18–C18'–C19' –90.3(14), C29–C28–C28'–C29' –42.7(19).

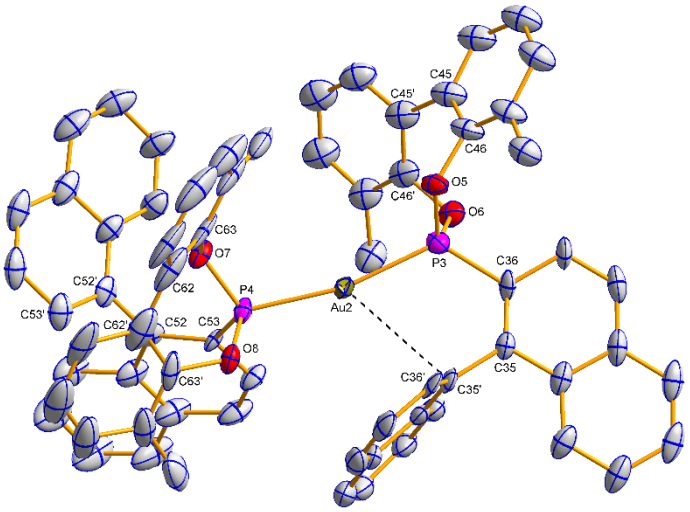

Fig. 4.7 Molecular structure of one of the two independent cations of (*S*)-**45a** (the asymmetric unit comprises two cations in different conformations and two anions). Hydrogen atoms have been omitted for clarity. Selected average bond distances (Å) and angles (°): P3–Au2 2.291(3), P4–Au2 2.279(3), P3–C36 1.803(11), P4–C53 1.813(9); P3–Au2–P4 166.91(10), Au2–P3–C36 122.1(4), Au2–P3–O5 106.7(3), Au2–P3–O6 111.9(3), Au2–P4–C53 116.1(3), Au2–P4–O7 113.0(3), Au2–P4–O8 108.0(3), C36–C35–C35'–C36' –91.3(13), C46–C45–C45'–C46' –45(2), C53–C52–C52'–C53' –107.0(13), C63–C62–C62'–C63' 48(2).

As seen previously for the [Au(L^P)Cl] complexes, (*S*)-**45a** has two crystallographically independent molecules in the asymmetric unit, which comprises two cations and two anions. The Au–P bond lengths range from 2.279(3) to 2.291(3) Å and the P–Au–P bond angles were determined to be 164.78(11)° and 166.91(10)°. Thus, they are contracted from the ideal linear geometry. The related phosphine complex [Au(PPh_3)$_2$]PF_6 has Au–P bond lengths of 2.314(2) Å and 2.309(2) Å and a P–Au–P bond angle of 177.4(1)°; for [Au(PPh_3)$_2$]NO_3 the corresponding values are 2.312(4) Å and 2.311(2) Å, and

171.1(2)°.[217] Thus, the gold-phosphonite bond lengths are shorter than in the related arylphosphine complexes, and the smaller P–Au–P bond angle is perhaps a consequence of the bulky 3,3'-dimethylbiphenoxy moiety of the ligand, although for $[Au(PPh_3)_2]BF_4$ the value is 167.3(1)°,[218] so care must be taken when drawing conclusions. Again, there appears to be no significant metal–arene interaction, as the distances are above Echavarren's limiting value of 2.95 Å.[208] The closest contact is the *ipso*-C of the lower naphthyl: Au1–C18' 3.267(11) Å, Au1–centroid 3.267(2) Å (Fig. 4.6), Au2–C35' 3.174(10) Å and Au2–centroid 3.376(5) Å (Fig. 4.7).

4.2.2 Silver coordination chemistry

In this section, the fluxionality of silver phosphonite complexes is studied by $^{31}P\{^1H\}$ NMR spectroscopy, and the results are compared to the phosphine analogues. Metal–arene distances in the solid state are also investigated by X-ray crystallography. Thus, the silver complexes $[Ag(L^P)OTf]$ were synthesised by the reaction of one equivalent of the pertinent phosphonite with silver(I) trifluoromethanesulfonate, to generate [Ag((*S*)-**28a**)OTf] (*S*)-**46a**, [Ag((*R*)-**28b**)OTf] (*R*)-**46b**, [Ag((*S*)-**29a**)OTf] (*S*)-**47a**, [Ag((*R*)-**29b**)OTf] (*R*)-**47b**, [Ag((*S*)-**30a**)OTf] (*S*)-**48a** and [Ag((*R*)-**30b**)OTf] (*R*)-**48b**. For comparison, the phosphine complexes [Ag((*S*)-H-MOP)OTf] and [Ag((*R*)-MeO-MOP)OTf] were also prepared. We were able to obtain single crystals of (*R*)-**47b** suitable for X-ray analysis, by slow diffusion of diethyl ether into a solution of the complex in DCM (Fig. 4.8). In the solid state the compound exists as a dimer, $[Ag((R)\text{-}\mathbf{29b})OTf]_2$. The silver atoms are three-coordinate and in a trigonal planar geometry, the phosphonite ligand is bound as a monodentate P-donor, and there are two bridging triflate groups, as reported for related ligands;[219] it is also worth noting that $[Ag(PPh_3)OTf]$ crystallises as a trimer.[220] For (*R*)-**47b**, there appears to be no significant metal–arene interaction as the interatomic distances are above the limiting value of 3.03 Å, as determined by Echavarren for Ag–arene bonding.[208] The ligand bound to Ag1 shows a closest contact of 3.187(6) Å to one of the internal quaternary carbons of the lower naphthyl ring (C9'), whereas the closest contact for the ligand bound to Ag2 is 3.251(7) Å to the carbon of the lower naphthyl ring bearing the methoxy substituent (C22'). Interestingly, the ligand bound to Ag1 shows a shorter distance to a C_6 ring centroid for the ring containing C8' rather than the *ipso*-C (C1'), in contrast to that seen for the ligand bound to Ag2 and all of the Au complexes discussed earlier: Ag1–centroid (containing C1') 3.550(3) Å, Ag1–centroid (containing C8') 3.518(3) Å and Ag2–centroid 3.327(3) Å (containing C21'). The Ag–P bond lengths are 2.3769(17) Å and 2.3678(17) Å, consistent with those of other silver phosphonite complexes, although X-ray crystal structure determinations appear rare (Fig. 4.8).[98] For Ag1, the 2,2'-biphenoxy moiety features a torsion angle C12–C11–C11'–C12' of 43.5(10)°, whereas for Ag2 the angle C32–C31–C31'–C32' is −44.7(9)°, indicating again that rotation about those aryl–aryl junctions is unrestricted.

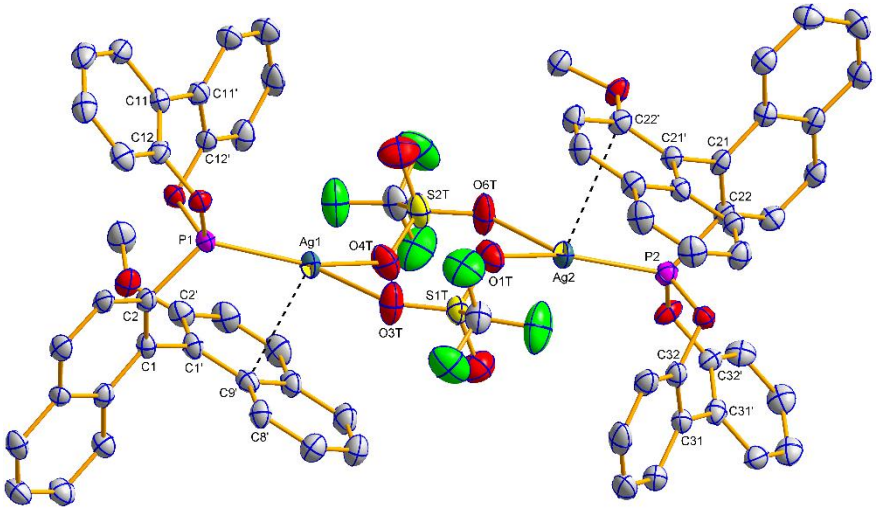

Fig. 4.8 Molecular structure of (*R*)-**47b**. Hydrogen atoms have been omitted for clarity. Selected average bond distances (Å) and angles (°): P1–Ag1 2.3769(17), P2–Ag2 2.3678(17), P1–C2 1.820(7), P2–C22 1.820(7), Ag1–O3T 2.318(6), Ag1–O4T 2.356(6), Ag2–O1T 2.308(5), Ag2–O6T 2.340(6); P1–Ag1–O3T 134.62(15), P1–Ag1–O4T 142.65(17), O3T–Ag1–O4T 82.7(2), P2–Ag2–O1T 147.43(17), P2–Ag2–O6T 127.89(14), O1T–Ag2–O6T 84.6(2), Ag1–P1–C2 122.3(2), Ag2–P2–C22 123.5(2), O1T–S1T–O3T 115.1(4), O4T–S2T–O6T 119.1(4), C2–C1–C1'–C2' –88.1(8), C12–C11–C11'–C12' 43.5(10), C22–C21–C21'–C22' –101.3(7), C32–C31–C31'–C32' –44.7(9).

The silver phosphonite complexes were characterised by NMR spectroscopy (Figs. 4.9-4.16). Silver has two NMR-active isotopes, ^{107}Ag (I = ½, natural abundance 51.8%) and ^{109}Ag (I = ½, natural abundance 48.2%); therefore, the expected ^{31}P{^{1}H} NMR spectra for the complexes should consist of two doublets arising from ^{107}Ag–P and ^{109}Ag–P spin-spin coupling. For the phosphine complexes [Ag((*S*)-H-MOP)OTf] and [Ag((*R*)-MeO-MOP)OTf], phosphine coordination resulted in one broad ^{31}P{^{1}H} NMR signal at δ 5.1 ppm for the (*S*)-H-MOP complex (Fig. 4.9) at 25 °C and two broad peaks at δ 3.8 ppm and 7.8 ppm for the (*R*)-MeO-MOP analogue, at 23 °C (Fig. 4.10). This broadening is likely due to rapid phosphine exchange.[221] Cooling to −40 °C was necessary to observe the formation of the expected doublets, with the ^{107}Ag–P and ^{109}Ag–P coupling constants measured at −60 °C (Table 4.2). The magnitude of these couplings are J^{107}Ag–P = 755 Hz and J^{109}Ag–P = 858 Hz for [Ag((*S*)-H-MOP)OTf] and J^{107}Ag–P = 743 Hz and J^{109}Ag–P = 857 Hz for [Ag((*R*)-MeO-MOP)OTf], and are consistent with complexes containing one bound phosphine ligand.[222] [Ag(PPh_3)OTf] gave a doublet of 746 Hz and 860 Hz for J^{107}Ag–P and J^{109}Ag–P coupling respectively.[220b] Much smaller couplings are consistent with species containing more than one bound phosphine, silver phosphine complexes are known to form a series of complexes of the type [Ag(L^P)$_n$X] (n = 1-4) in which the ligands can be labile.[220b,221-222] When the solution of [Ag((*S*)-H-MOP)OTf] was cooled to −40 °C, two additional doublets of very low intensity were observed in the NMR, at 3.5 ppm and 7.4 ppm, which by virtue of the magnitude of the couplings (J^{107}Ag–P = 741 Hz and J^{109}Ag–P = 856 Hz) indicates the presence of species with the same nuclearity. The phosphonite ligands appear downfield from their phosphine analogues: (*S*)-**28a**, 154.8 ppm; (*R*)-**28b**, 155.6 ppm; (*S*)-**29a**, 177.7 ppm; (*R*)-**29b**, 180.0 ppm; (*S*)-**30a**, 172.4 ppm and (*R*)-**30b**, 174.2 ppm.[138]

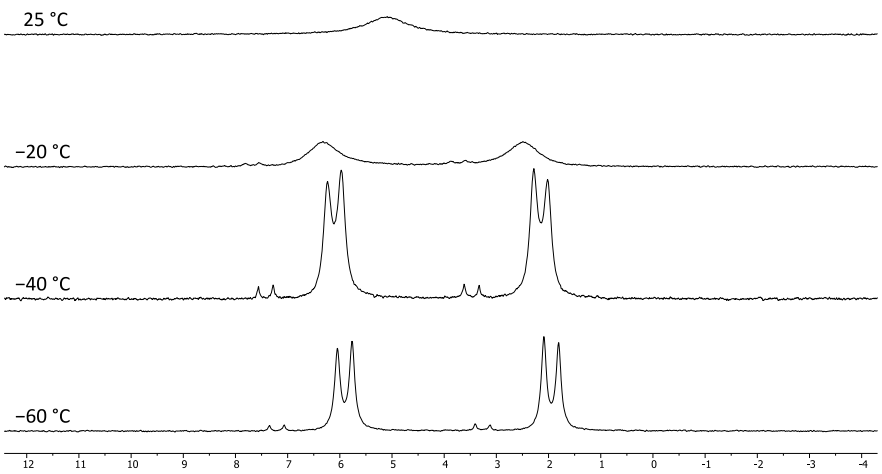

Fig. 4.9 $^{31}P\{^{1}H\}$ VT NMR of [Ag((*S*)-H-MOP)OTf] in CD_2Cl_2.

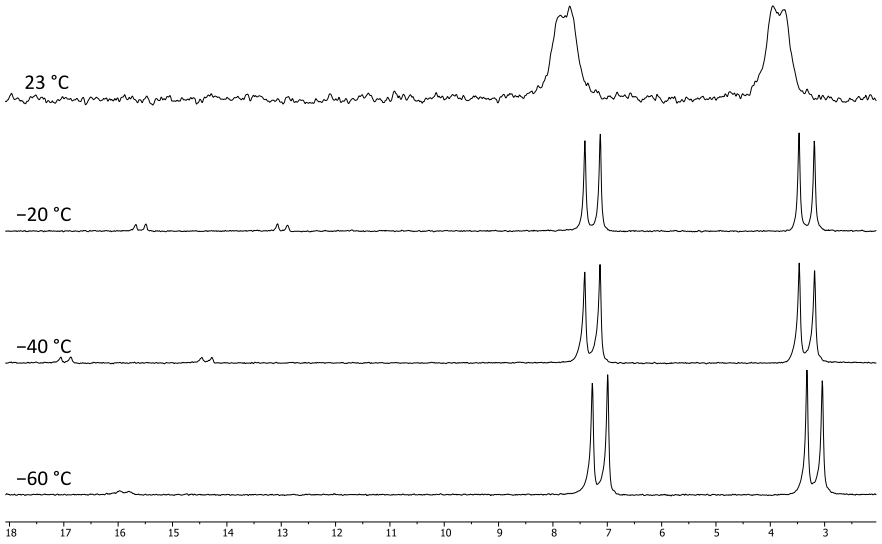

Fig. 4.10 $^{31}P\{^{1}H\}$ VT NMR of [Ag((*R*)-MeO-MOP)OTf] in CD_2Cl_2.

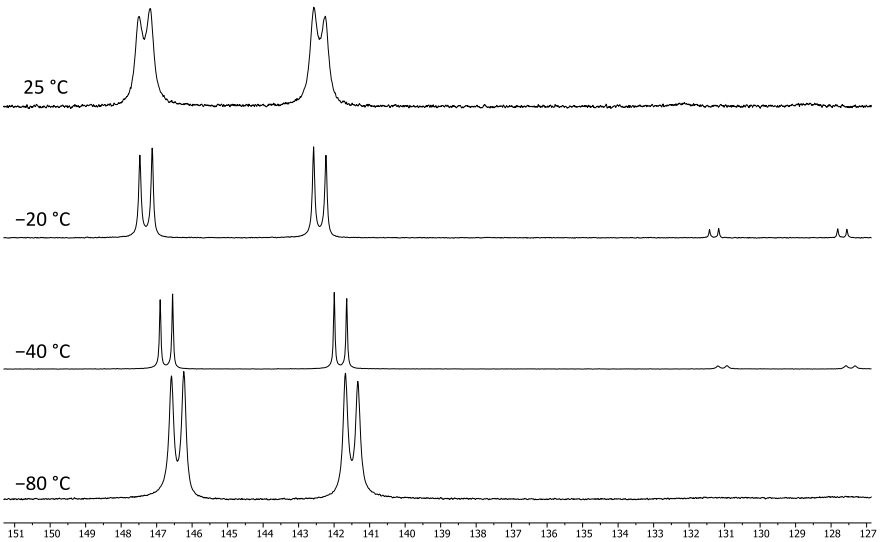

Fig. 4.11 $^{31}P\{^{1}H\}$ VT NMR of (*S*)-**46a** in CD_2Cl_2.

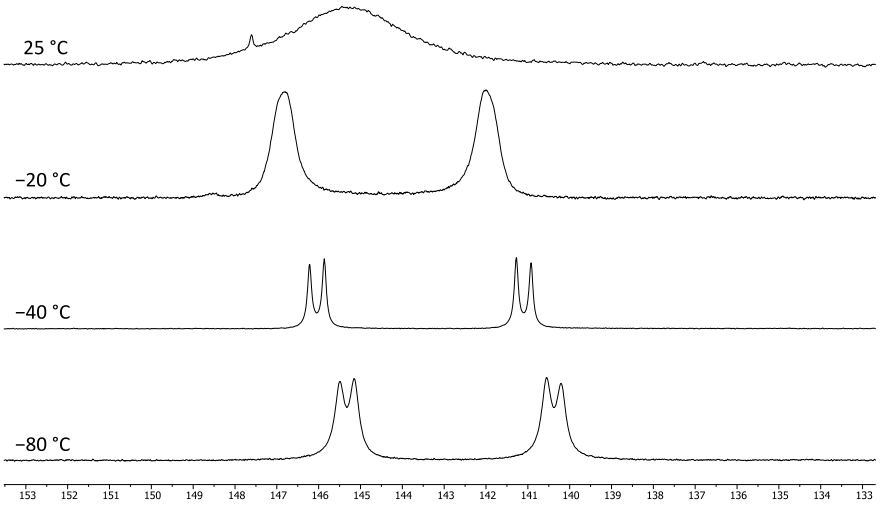

Fig. 4.12 $^{31}P\{^{1}H\}$ VT NMR of (*R*)-**46b** in CD_2Cl_2.

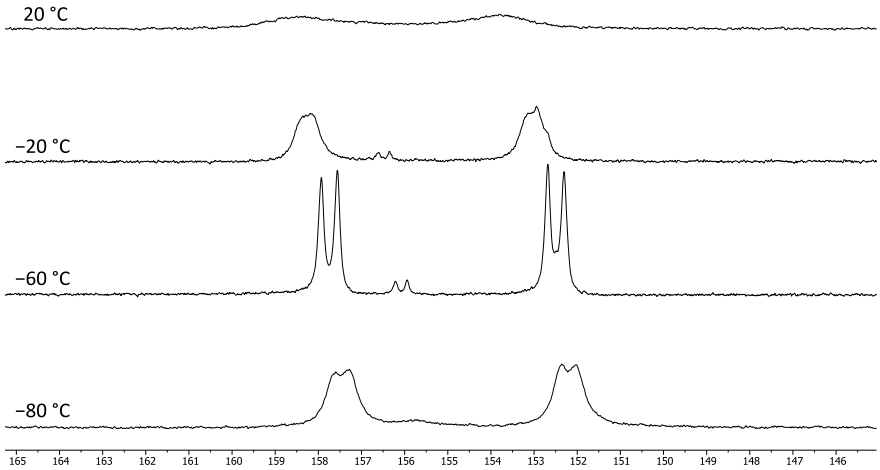

Fig. 4.13 $^{31}P\{^{1}H\}$ VT NMR of (*S*)-**47a** in CD_2Cl_2.

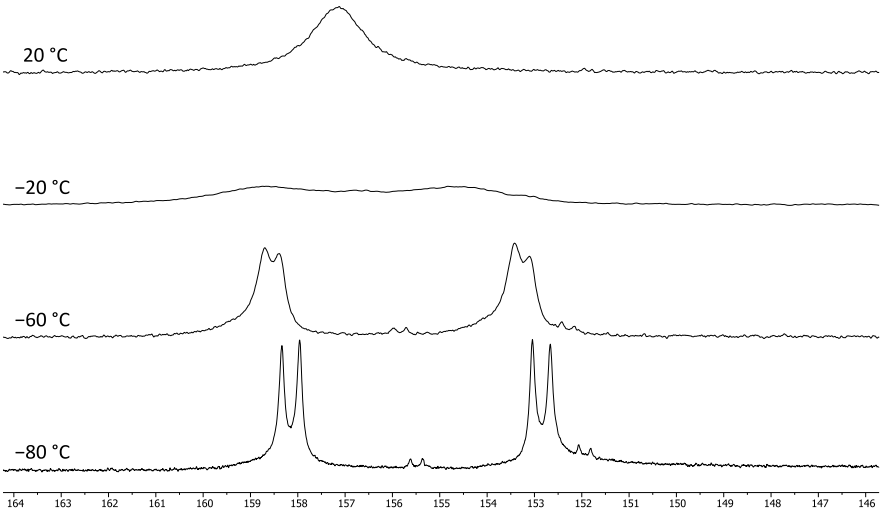

Fig. 4.14 $^{31}P\{^{1}H\}$ VT NMR of (*R*)-**47b** in CD_2Cl_2.

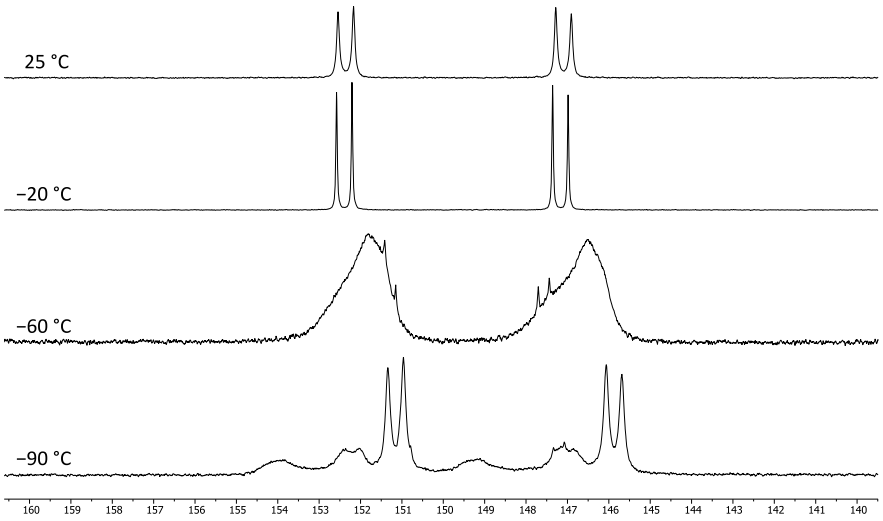

Fig. 4.15 $^{31}P\{^{1}H\}$ VT NMR of (*S*)-**48a** in CD_2Cl_2.

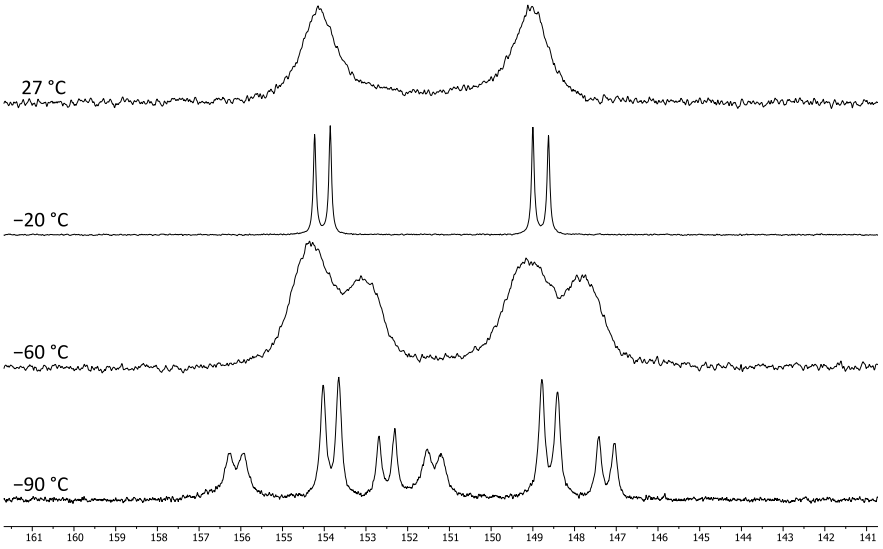

Fig. 4.16 $^{31}P\{^{1}H\}$ VT NMR of (*R*)-**48b** in CD_2Cl_2.

The $^{31}P\{^{1}H\}$ NMR spectra of their silver complexes echo the general behaviour of the aforementioned phosphine analogues (Figs. 4.11-4.16), albeit with some notable differences. As expected, the chemical shifts of the phosphonite complexes are shifted upfield relative to the free ligands, and appear over the range δ 140 to 160 ppm. With the exception of (*S*)-**46a** (Fig. 4.11) and (*S*)-**48a** (Fig. 4.15), cooling was again required to resolve the $^{107}Ag–P$ and $^{109}Ag–P$ couplings. The observation of coupling at room temperature is unusual, and is normally associated with bulky or chelating phosphines,[220b,223] but there does not appear to be a particular trend for our phosphonites, although the **b** series of ligands form complexes that always give broad signals at room temperature. For the bulky dimethylbiphenoxy complexes, (*S*)-**48a** and (*R*)-**48b**, several additional resonances appeared as the samples were cooled to −90 °C which, given their absence for the other ligands, probably correspond to rotamers (Figs. 4.15 and 4.16). From Table 4.2 it is apparent that Ag–P couplings are significantly increased for the

phosphonite complexes, compared to the phosphine analogues: J^{107}Ag–P increases by approximately 200 Hz and J^{109}Ag–P by 200 to 300 Hz.

Table 4.2 $^{31}P\{^{1}H\}$ NMR coupling constants ($^{1}J_{PAg}$) of [AgL^{P}(OTf)] at selected temperatures.

Complex[b]	T	J^{107}Ag–P (Hz)	J^{109}Ag–P (Hz)
[Ag((*S*)-H-MOP)OTf]	–60 °C	755	858
[Ag((*R*)-MeO-MOP)OTf]	–60 °C	743	857
(*S*)-**46a**	–40 °C	922	1065
(*R*)-**46b**	–40 °C	930	1072
(*S*)-**47a**	–60 °C	988	1140
(*R*)-**47b**	–80 °C	996	1149
(*S*)-**48a**	–20 °C	982	1133
(*R*)-**48b**	–20 °C	984	1135

$^{31}P\{^{1}H\}$ NMR measurements were taken at 202 MHz in CD_2Cl_2.

4.2.3 Copper coordination Chemistry

Complexes of the type [Cu(L^{P})(MeCN)$_2$]PF$_6$ were synthesised by reaction of one equivalent of the phosphonite ligand with [Cu(MeCN)$_4$]PF$_6$ in DCM. In this fashion, we were able to synthesise the following complexes: [Cu((*S*)-**28a**)(MeCN)$_2$]PF$_6$ (*S*)-**49a**, [Cu((*R*)-**28b**)(MeCN)$_2$]PF$_6$ (*R*)-**49b**, [Cu((*S*)-**29a**)(MeCN)$_2$]PF$_6$ (*S*)-**50a**, [Cu((*R*)-**29b**)(MeCN)$_2$]PF$_6$ (*R*)-**50b**, [Cu((*S*)-**30a**)(MeCN)$_2$]PF$_6$ (*S*)-**51a** and [Cu((*R*)-**30b**)(MeCN)$_2$]PF$_6$ (*R*)-**51b**. The cations were characterised by $^{31}P\{^{1}H\}$ NMR spectroscopy, which featured broad upfield resonances. We were also able to obtain single crystals of (*R*)-**51b**, suitable for analysis by X-ray diffraction, by slow diffusion of diethyl ether into a DCM solution. There are two crystallographically independent molecules in the asymmetric unit (Fig. 4.17), and the copper(I) is in a trigonal planar coordination environment in both independents.[224] The metal–arene distances are beyond the limiting value of 2.83 Å for a significant interaction, according to Echavarren *et al*.[208] The ligand bound to Cu1 shows a closest contact of 2.898(9) Å for the *ipso*-C (C1') of the lower naphthyl ring (Fig. 4.17), whereas the closest contact for the ligand bound to Cu2 is 2.959(10) Å, to one of the internal quaternary carbons of the lower naphthyl ring (Fig. 4.17, C31'). For both cations the closest metal contact to a centroid of a C$_6$ ring is for the ring containing the *ipso*-C, as reported for all of the gold complexes discussed: Cu1–centroid 3.070(5) Å and Cu2–centroid 3.048(6) Å (Fig. 4.17).

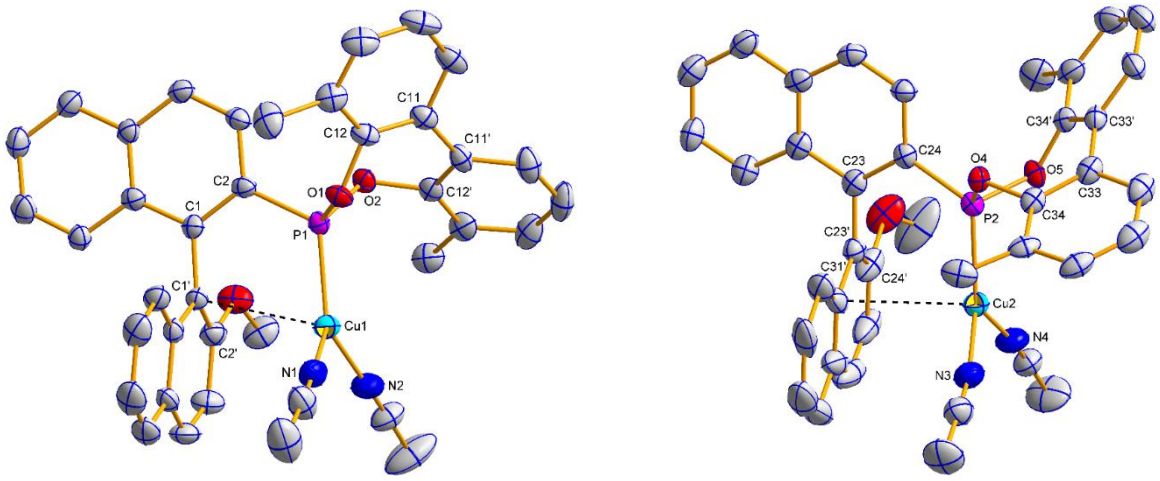

Fig. 4.17 Molecular structure of (*R*)-**51b** (the asymmetric unit comprises two cations in different conformations and two anions). Hydrogen atoms have been omitted for clarity. Selected average bond distances (Å) and angles (°): (left) P1–Cu1 2.1603(19), P1–C2 1.791(7), P1–O1 1.609(5), P1–O2 1.625(5), Cu1–N1 1.961(7), Cu1–N2 1.941(7); P1–Cu1–N1 122.3(2), P1–Cu1–N2 128.6(2), N1–Cu1–N2 107.3(3), Cu1–P1–C2 119.8(2), Cu1–P1–O1 105.90(19), Cu1–P1–O2 122.33(19), C2–C1–C1'–C2' –94.6(9), C12–C11–C11'–C12' 43.0(10); (right) P2–Cu2 2.1726(19), P1–C24 1.804(7), P2–O4 1.624(5), P2–O5 1.619(5), Cu2–N3 1.961(7), Cu2–N4 1.960(7); P2–Cu2–N3 127.8(2), P2–Cu2–N4 124.6(2), N3–Cu2–N4 105.3(3), Cu2–P2–C24 122.1(2), Cu2–P2–O4 120.54(19), Cu2–P2–O5 105.49(19), C24–C23–C23'–C24' –97.8(9), C34–C33–C33'–C34' –41.5(10).

We were unable to obtain crystals of (*S*)-**49a**; however, after repeated recrystallisation attempts, we did manage to crystallise the unusual dimer [Cu((*S*)-**28a**)(O_2PF_2)]$_2$ (*S*)-**52a** (Fig. 4.18). Complex (*S*)-**52a**, a possible decomposition product of (*S*)-**49a**, contains the bridging, tetrahedral difluorophosphate anion (Fig. 4.18), which most likely formed through partial hydrolysis of the octahedral hexafluorophosphate anion.[225] The metal-arene distances are longer than those seen in the mononuclear complex (*R*)-**51b**, and there appears to be no significant interaction. For the ligand bound to Cu1, the closest metal-arene contact is to the tertiary carbon *ortho* to the *ipso*-C (C2'), whereas for the ligand bound to Cu2, the closest contact is to C24': Cu1–C2' 3.050(5) Å and Cu2–C24' 2.995(6) Å (Fig. 4.18). Similar to the observations we made for the dimer [Ag((*R*)-**29b**)OTf]$_2$ (*R*)-**47b**, the ligand bound to Cu2 shows a shorter distance to a C_6 ring centroid for the ring containing C24' rather than C17', unlike that seen for the ligand bound to Cu1 which has a closest centroid contact for the C_6 ring containing C1': Cu1–centroid 3.858(2) Å and Cu2–centroid 3.813(3) Å (Fig. 4.18). We were unable to undertake NMR studies on (*S*)-**52a** due to its insolubility, as was also reported by Beck *et al.* for copper complexes with bridging difluorophosphate anions.[225b]

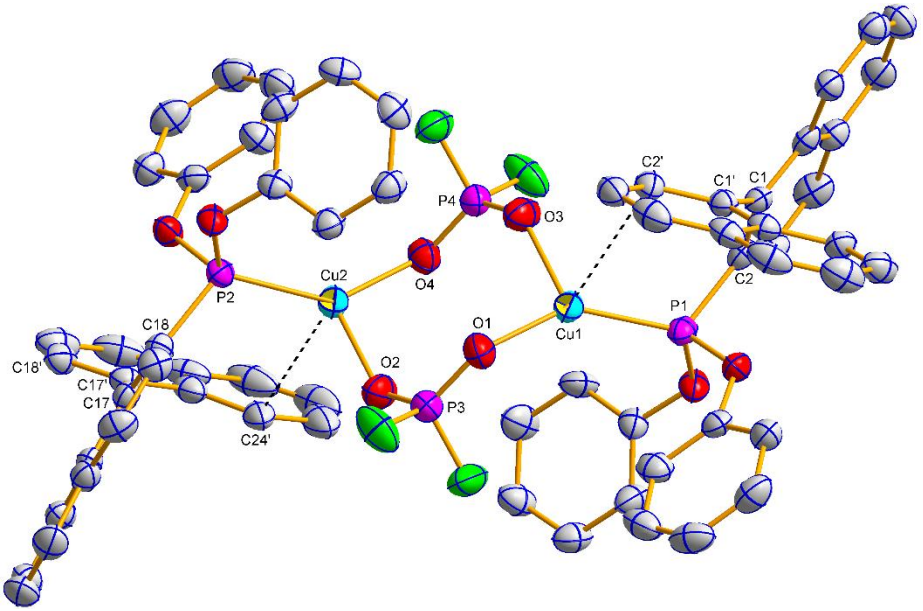

Fig. 4.18 Molecular structure of (*S*)-**52a**. Hydrogen atoms have been omitted for clarity. Selected average bond distances (Å) and angles (°): P1–Cu1 2.1344(13), P2–Cu2 2.1399(13), P1–C2 1.809(5), P2–C18 1.814(5), Cu1–O1 1.968(4), Cu1–O3 2.041(4), Cu2–O2 2.056(4), Cu2–O4 1.980(4), P3–O1 1.472(4), P3–O2 1.454(4), P4–O3 1.470(4), P4–O4 1.470(4); P1–Cu1–O1 141.17(12), P1–Cu1–O3 119.34(13), O1–Cu1–O3 99.09(17), P2–Cu2–O2 119.51(12), P2–Cu2–O4 139.15(11), O2–Cu2–O4 99.58(16), Cu1–P1–C2 117.88(15), Cu2–P2–C18 116.07(16), O1–P3–O2 122.4(2), O3–P4–O4 122.4(2), C2–C1–C1'–C2' –73.5(5), C18–C17–C17'–C18' –107.8(5).

4.3 Summary

Group 11 complexes of MOP ligands are uncommon, but have shown promise as asymmetric catalysts for a variety of organic transformations; the presence of M–π arene interactions have been deemed to play a role in some of these processes. We have prepared gold, silver and copper complexes of chiral MOP-phosphonites for the first time. Extensive NMR and X-ray crystallographic analyses were undertaken on these compounds, with the latter being especially useful in demonstrating that any M–π interactions appear weak, if present at all. Future work in the group will investigate the ramifications of these structural elements on the catalytic abilities of the complexes in asymmetric catalytic transformations.

4.4 Experimental Procedures

All air- and/or water-sensitive reactions were performed under a nitrogen atmosphere using standard Schlenk line techniques in oven dried glassware. Solvents were freshly distilled prior to use; toluene was dried over sodium, tetrahydrofuran and diethyl ether were dried over sodium/benzophenone, dichloromethane was dried over calcium hydride. Hexane was dried over sodium/benzophenone and *d*-chloroform was dried over phosphorus pentoxide, distilled and stored over molecular sieves. (*S*)-H-MOP,[126] (*R*)-MeO-MOP[127] and chloro(tetrahydrothiophene)gold(I)[226] were prepared according to literature procedures. All other chemicals were used as received without further purification. Melting

points were determined in open glass capillary tubes on a Stuart SMP3 melting point apparatus. Infrared spectra were measured on a Varian 800 FT-IR Scimitar Series spectrometer. ^{1}H, ^{13}C{^{1}H}, ^{19}F and ^{31}P{^{1}H} NMR spectra were recorded on a Brucker 500 (^{1}H 500.15 MHz), JEOL 400 (^{1}H 399.78 MHz) or Brucker 300 (^{1}H 300.13 MHz) spectrometer at room temperature (21-25°C) if not otherwise stated, using the indicated solvent as internal reference. 2D NMR experiments (^{1}H-^{1}H COSY, HSQC and HMBC) were used for the assignment of proton and carbon resonances, the numbering schemes are given in Fig. 3.25. High-resolution mass spectrometry was carried out by the EPSRC National Mass Spectrometry Facility, Swansea.

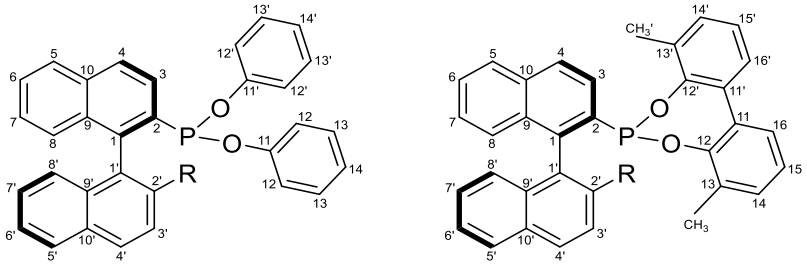

Fig. 4.19 Numbering schemes used to assign proton and carbon resonances in the NMR spectra: phenoxy-derived ligands (left), 2,2'-biphenoxy-derived ligands (right).

4.4.1 [Au((*S*)-**28a**)Cl] (*S*)-**42a**

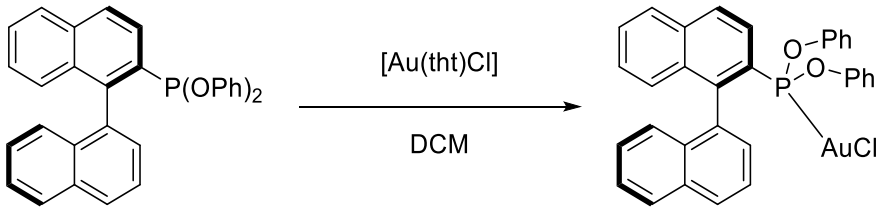

(*S*)-Diphenyl [1,1'-binaphthalen]-2-yl phosphonite ((*S*)-**28a**, 28.2 mg, 60.0 µmol, 1.0 eq.) and chloro(tetrahydrothiophene)gold(I) (19.2 mg, 60.0 µmol, 1.0 eq.) were dissolved in DCM (1.5 mL) and stirred for 30 min, after which the volatiles were removed *in vacuo*. The residue was washed with hexane and dried *in vacuo*, to yield the pure title compound quantitatively as a white solid. Single crystals were grown by pentane layering of a toluene solution.

MP: 140-142 °C (decomp.). **IR** (neat): ν = 3058.6 (w), 1588.3 (m), 1484.2 (s), 1369.2 (w), 1319.1 (w), 1200.6 (s), 1180.6 (s), 1158.0 (s), 1071.4 (w), 1023.0 (m), 914.8 (s), 802.5 (m), 767.8 (s), 688.0 (s), 642.2 (s), 615.3 (m) cm^{-1}. **^{1}H NMR** (300 MHz, $CDCl_3$): δ (ppm) = 8.24 (*apparent*-t (dd), $^{3}J_{HH/HP}$ = 9.0 Hz, 1H, *H*3), 8.13-8.04 (m, 2H, *H*4/*H*4'), 7.97-7.90 (m, 2H, *H*5/*H*5'), 7.60-7.53 (m, 3H, *H*2'/*H*3'/*H*6), 7.41 (ddd, $^{3}J_{HH}$ = 8.3 Hz, $^{3}J_{HH}$ = 6.8 Hz, $^{4}J_{HH}$ = 1.3 Hz, 1H, *H*6'), 7.32-7.15 (m, 5H, *H*7/*H*7'/*H*8/*H*13'), 7.11-6.97 (m, 5H, *H*8'/*H*13/*H*14/*H*14'), 6.96-6.90 (m, 2H, *H*12'), 6.56-6.50 (m, 2H, *H*12). **^{13}C{^{1}H} NMR** (75 MHz, $CDCl_3$): δ (ppm) = 152.3 (*overlapping*-d, *C*11/*C*11'), 145.1 (d, $^{2}J_{CP}$ = 22.3 Hz, *C*1), 135.3 (d, $^{4}J_{CP}$ = 1.8 Hz, *C*10),

133.8 (*C*10'), 133.5, 133.4, 133.3 (d, J_{CP} = 3.3 Hz), 130.1 (m), 130.0 (m), 129.1, 129.0, 128.8, 128.8, 128.2, 127.6 (d, J_{CP} = 2.6 Hz), 127.6 (d, J_{CP} = 1.1 Hz), 127.0, 126.5 (*C*6'), 126.1 (*C*8'), 125.9 (d, $^{5}J_{CP}$ = 1.9 Hz, *C*14'), 125.8 (d, $^{5}J_{CP}$ = 1.9 Hz, *C*14), 125.5, 125.0 (d, $^{2}J_{CP}$ = 8.2 Hz, *C*3), 121.0 (d, $^{3}J_{CP}$ = 6.2 Hz, *C*12'), 120.7 (d, $^{3}J_{CP}$ = 6.2 Hz, *C*12). **^{31}P{^{1}H} NMR** (121 MHz, $CDCl_3$): δ (ppm) = 132.9 (s). **HRMS** ($ASAP^+$, solid): Found: *m*/*z* = 667.1099. Calculated for $[M - Cl]^+$: *m*/*z* = 667.1096.

4.4.2 [Au((*R*)-**28b**)Cl] (*R*)-**42b**

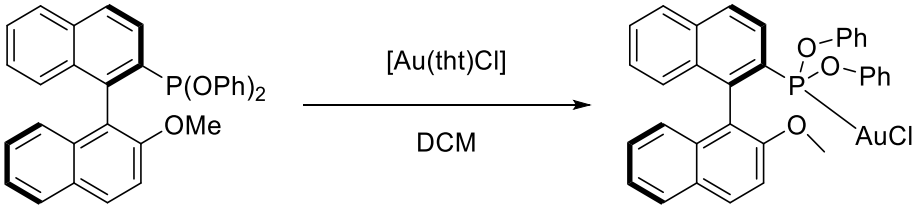

(*R*)-Diphenyl (2'-methoxy-[1,1'-binaphthalen]-2-yl)phosphonite ((*R*)-**28b**, 30.0 mg, 60.0 µmol, 1.0 eq.) and chloro(tetrahydrothiophene)gold(I) (19.2 mg, 60.0 µmol, 1.0 eq.) were dissolved in DCM (1.5 mL) and stirred for 30 min, after which the volatiles were removed *in vacuo*. The residue was washed with hexane and dried *in vacuo*, to yield the pure title compound quantitatively as a white solid. Single crystals were grown by slow diffusion of diethyl ether into a *d*-chloroform solution.

MP: 142-144 °C (decomp.). **IR** (neat): ν = 3057.2 (w), 1588.6 (m), 1483.7 (s), 1251.7 (m), 1198.6 (s), 1157.7 (s), 1079.3 (w), 1022.0 (w), 914.5 (s), 808.5 (m), 768.7 (s), 751.3 (m), 687.6 (s), 644.8 (s) cm^{-1}. **^{1}H NMR** (300 MHz, $CDCl_3$): δ (ppm) = 8.22 (*apparent*-t (dd), $^{3}J_{HH/HP}$ = 8.9 Hz, 1H, *H*3), 8.15-8.06 (m, 2H, *H*4/*H*4'), 7.94 (d, $^{3}J_{HH}$ = 8.2 Hz, 1H, *H*5), 7.85 (d, $^{3}J_{HH}$ = 8.2 Hz, 1H, *H*5'), 7.56 (ddd, $^{3}J_{HH}$ = 8.2 Hz, $^{3}J_{HH}$ = 6.3 Hz, $^{4}J_{HH}$ = 1.7 Hz, 1H, *H*6), 7.41 (d, $^{3}J_{HH}$ = 9.1 Hz, 1H, *H*3'), 7.33-6.89 (m, 12H, *H*6'/*H*7/*H*7'/*H*8/*H*12'/*H*13/*H*13'/*H*14/*H*14'), 6.85 (d, $^{3}J_{HH}$ = 8.6 Hz, 1H, *H*8'), 6.42-6.36 (m, 2H, *H*12), 3.75 (s, 3H, O*CH*$_3$). **^{13}C{^{1}H} NMR** (75 MHz, $CDCl_3$): δ (ppm) = 155.3 (*C*2'), 152.4 (*overlapping*-d, *C*11/*C*11'), 142.3 (d, $^{2}J_{CP}$ = 23.5 Hz, *C*1), 135.6 (d, $^{4}J_{CP}$ = 1.7 Hz, *C*10), 134.5 (*C*9'), 133.0 (d, $^{3}J_{CP}$ = 12.5 Hz, *C*9), 131.7 (*C*4'), 130.1 (*obscured*-d, *C*2), 130.0 (d, $^{4}J_{CP}$ = 0.8 Hz, *C*13 or *C*13'), 129.8 (d, $^{4}J_{CP}$ = 1.4 Hz, *C*13 or *C*13'), 129.0 (*C*6), 128.9 (*C*10'), 128.8 (d, $^{3}J_{CP}$ = 9.7 Hz, *C*4), 128.4 (*C*5'), 128.3 (*C*5), 127.5 (*C*7), 127.2 (*C*7'), 127.0 (d, $^{4}J_{CP}$ = 2.5 Hz, *C*8), 125.7 (*C*14 or *C*14'), 125.7 (*C*14 or *C*14'), 125.2 (d, $^{2}J_{CP}$ = 7.3 Hz, *C*3), 125.0 (*C*8'), 123.9 (*C*6'), 120.9 (*overlapping*-d, *C*12/*C*12'), 117.3 (d, $^{3}J_{CP}$ = 9.9 Hz, *C*1'), 113.5 (*C*3'), 56.0 (O*C*H$_3$). **^{31}P{^{1}H} NMR** (121 MHz, $CDCl_3$): δ (ppm) = 133.0 (s). **HRMS** (NSI^+, DCM/MeOH): Found: *m*/*z* = 750.1227. Calculated for $[M + NH_4]^+$: *m*/*z* = 750.1234.

4.4.3 [Au((*S*)-**29a**)Cl] (*S*)-**43a**

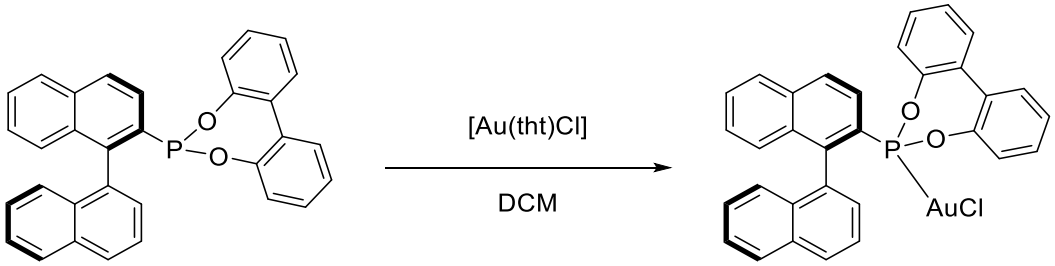

(*S*)-[1,1'-biphenyl]-2,2'-diyl [1,1'-binaphthalen]-2-yl phosphonite ((*S*)-**29a**, 28.1 mg, 60.0 µmol, 1.0 eq.) and chloro(tetrahydrothiophene)gold(I) (19.2 mg, 60.0 µmol, 1.0 eq.) were dissolved in DCM (1.5 mL) and stirred for 30 min, after which the volatiles were removed *in vacuo*. The residue was washed with hexane and dried *in vacuo*, to yield the pure title compound quantitatively as a white solid. Single crystals were grown by slow diffusion of diethyl ether into a DCM solution.

MP: 260-262 °C (decomp.). **IR** (neat): ν = 3057.7 (w), 1498.4 (m), 1475.1 (m), 1433.6 (s), 1367.7 (w), 1315.2 (w), 1246.5 (m), 1193.9 (s), 1094.9 (s), 1044.9 (w), 917.4 (s), 769.4 (s), 731.5 (m), 687.6 (m), 640.6 (s), 607.7 (s) cm^{-1}. **^{1}H NMR** (300 MHz, $CDCl_3$): δ (ppm) = 8.12 (d, $^3J_{HH}$ = 6.9 Hz, $^3J_{HH}$ = 2.4 Hz, 1H, *H*4'), 7.98 (d, $^3J_{HH}$ = 8.3 Hz, 1H, *H*5'), 7.86 (d, $^3J_{HH}$ = 8.3 Hz, 1H, *H*5), 7.79 (dd, $^3J_{HH}$ = 8.7 Hz, $^4J_{HP}$ = 2.3 Hz, 1H, *H*4), 7.66-7.41 (m, 7H, *H*2'/*H*3/*H*3'/*H*6/*H*6'/*H*16/*H*16'), 7.35-7.17 (m, 7H, *H*7/H7'/*H*8/*H*14/*H*14'/*H*15/*H*15'), 7.11 (d, $^3J_{HH}$ = 8.5 Hz, 1H, *H*8'), 7.05-6.98 (m, 1H, *H*13'), 6.90-6.85 (m, 1H, *H*13). **^{13}C{^{1}H} NMR** (75 MHz, $CDCl_3$): δ (ppm) = 147.8 (*overlapping*-d, *C*12/*C*12'), 145.1 (d, $^2J_{CP}$ = 24.4 Hz, *C*1), 134.4 (d, $^4J_{CP}$ = 1.7 Hz, *C*10), 132.9 (*C*9'), 132.6 (*C*10'), 132.2 (*C*9), 132.2 (d, $^1J_{CP}$ = 21.0 Hz, *C*2), 129.4 (d, $^4J_{CP}$ = 1.5 Hz, *C*16 or *C*16'), 129.4 (d, $^4J_{CP}$ = 1.6 Hz, *C*16 or *C*16'), 129.2 (m, *C*1'/*C*2'/*C*4'/*C*11'), 129.0 (d, $^3J_{CP}$ = 2.3 Hz, *C*11), 129.0 (d, $^4J_{CP}$ = 1.6 Hz, *C*8), 128.2 (*C*5'/*C*6), 127.1 (*C*5), 126.9 (d, $^3J_{CP}$ = 8.3 Hz, *C*4), 126.8 (*C*14 or *C*14'), 126.8 (*C*14 or *C*14'), 126.4 (*C*7), 126.1 (*C*7'), 125.9 (*C*6'), 125.7 (*C*15/*C*15'), 125.0 (*C*8'), 124.1 (*C*3'), 123.6 (d, $^2J_{CP}$ = 4.9 Hz, *C*3), 121.1 (d, $^3J_{CP}$ = 3.3 Hz, *C*13'), 120.7 (d, $^3J_{CP}$ = 3.0 Hz, *C*13). **^{31}P{^{1}H} NMR** (121 MHz, $CDCl_3$): δ (ppm) = 149.4 (s). **HRMS** ($ASAP^+$, solid): Found: *m*/*z* = 665.0932. Calculated for $[M - Cl]^+$: *m*/*z* = 665.0939.

4.4.4 [Au((*R*)-**29b**)Cl] (*R*)-**43b**

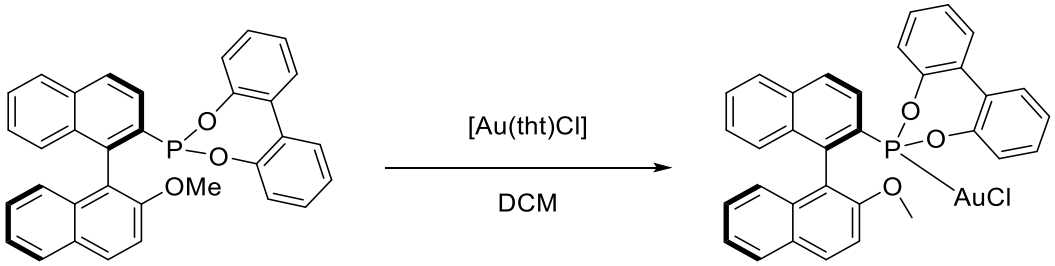

(*R*)-[1,1'-biphenyl]-2,2'-diyl (2'-methoxy-[1,1'-binaphthalen]-2-yl)phosphonite ((*R*)-**29b**, 29.9 mg, 60.0 µmol, 1.0 eq.) and chloro(tetrahydrothiophene)gold(I) (19.2 mg, 60.0 µmol, 1.0 eq.) were dissolved in DCM (1.5 mL) and stirred for 30 min, after which the volatiles were removed *in vacuo*. The residue was washed with hexane and dried *in vacuo*, to yield the pure title compound quantitatively as a white solid. Single crystals were grown by slow diffusion of diethyl ether into a DCM solution.

MP: 128-130 °C (decomp.). **IR** (neat): ν = 3057.3 (w), 1589.5 (m), 1499.0 (m), 1471.6 (m), 1434.5 (s), 1332.3 (w), 1314.6 (w), 1263.3 (m), 1249.3 (s), 1195.1 (s), 1175.5 (m), 1094.9 (m), 1051.5 (m), 1021.8 (m), 915.2 (s), 890.8 (s), 807.9 (m), 776.9 (s), 748.4 (s), 717.1 (m), 674.5 (m), 643.9 (s), 610.0 (s) cm^{-1}. **^{1}H NMR** (300 MHz, $CDCl_3$): δ (ppm) = 8.16 (d, $^{3}J_{HH}$ = 9.1 Hz, 1H, *H*4'), 7.90 (d, $^{3}J_{HH}$ = 8.2 Hz, 1H, *H*5'), 7.85 (d, $^{3}J_{HH}$ = 8.2 Hz, 1H, *H*5), 7.74 (dd, $^{3}J_{HH}$ = 8.7 Hz, $^{4}J_{HP}$ = 2.3 Hz, 1H, *H*4), 7.57-7.49 (m, 2H, *H*3/*H*6), 7.46-7.41 (m, 3H, *H*3'/*H*16/*H*16'), 7.36-7.15 (m, 8H, *H*6'/*H*7/*H*7'/*H*8/*H*14/*H*14'/*H*15/*H*15'), 6.99-6.90 (m, 2H, *H*13/*H*13'), 6.86 (d, $^{3}J_{HH}$ = 8.4 Hz, 1H, *H*8'), 3.86 (s, 3H, OCH_3). **^{13}C{^{1}H} NMR** (75 MHz, $CDCl_3$): δ (ppm) = 155.9 (*C*2'), 149.0 (*overlapping*-d, *C*12/*C*12'), 143.3 (d, $^{2}J_{CP}$ = 25.1 Hz, *C*1), 135.8 (d, $^{4}J_{CP}$ = 1.7 Hz, *C*10), 134.7 (*C*9'), 133.2 (d, $^{3}J_{CP}$ = 11.7 Hz, *C*9), 132.0 (*C*4'), 130.3 (m), 130.2 (d, J_{CP} = 2.4 Hz), 130.1 (d, J_{CP} = 1.5 Hz), 130.0 (d, J_{CP} = 1.5 Hz), 129.2 (*C*6), 128.9 (*C*5'), 128.3 (m, *C*5), 127.6 (d, $^{3}J_{CP}$ = 8.0 Hz, *C*4), 127.4, 127.2 (d, $^{4}J_{CP}$ = 2.5 Hz, *C*8), 126.8 (d, $^{5}J_{CP}$ = 1.8 Hz, *C*15'), 126.6 (d, $^{5}J_{CP}$ = 1.8 Hz, *C*15), 124.8 (m, *C*3/*C*8'), 124.1 (*C*6'), 122.2 (m, *C*13/*C*13'), 117.2 (d, $^{3}J_{CP}$ = 10.9 Hz, *C*1'), 113.1 (*C*3'), 56.2 (O*C*H_3). **^{31}P{^{1}H} NMR** (121 MHz, $CDCl_3$): δ (ppm) = 149.7 (s). **HRMS** (NSI^+, DCM/MeCN): Found: *m*/*z* = 753.0628. Calculated for $[M + Na]^+$: *m*/*z* = 753.0631.

4.4.5 [Au((*S*)-**30a**)Cl] (*S*)-**44a**

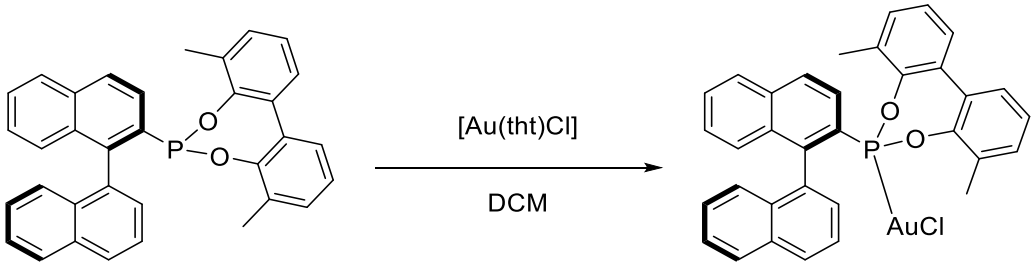

(*S*)-3,3'-dimethyl-[1,1'-biphenyl]-2,2'-diyl [1,1'-binaphthalen]-2-yl)phosphonite ((*S*)-**30a**, 29.8 mg, 60.0 µmol, 1.0 eq.) and chloro(tetrahydrothiophene)gold(I) (19.2 mg, 60.0 µmol, 1.0 eq.) were dissolved in DCM (1.5 mL) and stirred for 30 min, after which the volatiles were removed *in vacuo*. The residue was washed with hexane and dried *in vacuo*, to yield the pure title compound quantitatively as a white solid. Single crystals were grown by slow diffusion of diethyl ether into a DCM solution.

MP: 144-146 °C. **IR** (neat): ν = 3056.5 (w), 1452.5 (m), 1417.8 (m), 1369.4 (w), 1249.4 (m), 1181.6 (s), 1123.7 (m), 1085.2 (m), 1026.4 (w), 904.9 (s), 799.7 (m), 766.7 (s), 727.8 (s), 688.7 (m), 641.4 (m) cm^{-1}. **^{1}H NMR** (300 MHz, $CDCl_3$): *δ* (ppm) = 8.02 ($^{3}J_{HH}$ = 8.2 Hz, 1H, *H*4'), 7.97 (d, $^{3}J_{HH}$ = 8.2 Hz, 1H, *H*5'), 7.85 (d, $^{3}J_{HH}$ = 8.2 Hz, 1H, *H*5), 7.77 (dd, $^{3}J_{HH}$ = 8.7 Hz, $^{4}J_{HP}$ = 1.9 Hz, 1H, *H*4), 7.59-7.43 (m, 5H, *H*2'/*H*3/*H*3'/*H*6/*H*6'), 7.32-7.05 (m, 10H, *H*7/*H*7'/*H*8/*H*8'/*H*14/*H*14'/*H*15/*H*15'/*H*16/*H*16'), 2.12 (s, 3H, C*H*$_3$'), 1.84 (s, 3H, C*H*$_3$). **^{13}C{^{1}H} NMR** (75 MHz, $CDCl_3$): *δ* (ppm) = 147.2 (*overlapping*-d, *C*12/*C*12'), 145.8 (d, $^{2}J_{CP}$ = 24.9 Hz, *C*1), 135.5 (d, $^{4}J_{CP}$ = 1.8 Hz, *C*10), 134.0 (*C*10'), 133.9 (*C*9'), 133.7 (d, $^{3}J_{CP}$ = 10.6 Hz, *C*1'), 133.3 (d, $^{3}J_{CP}$ = 11.4 Hz, *C*9), 131.8 (d, $^{4}J_{CP}$ = 1.2 Hz, *C*14'), 131.4 (d, $^{4}J_{CP}$ = 1.5 Hz, *C*14), 130.8 (d, J_{CP} = 3.5 Hz), 130.7 (d, J_{CP} = 2.8 Hz), 130.6 (d, J_{CP} = 3.2 Hz), 130.3 (d, J_{CP} = 2.5 Hz), 130.1 (*C*4'), 129.6 (m, *C*2/*C*2'), 129.3, 129.3 (*C*5'), 128.6 (d, J_{CP} = 1.6 Hz), 128.2 (m, *C*4/*C*5/*C*7), 127.5 (d, J_{CP} = 1.1 Hz), 127.1 (*C*7'), 126.5 (*C*6'), 126.4 (d, J_{CP} = 1.8 Hz), 126.2 (d, J_{CP} = 1.7 Hz), 125.8, 125.0 (*C*3'), 124.4 (d, $^{2}J_{CP}$ = 5.8 Hz, *C*3), 17.2 (*C*H$_3$'), 16.9 (*C*H$_3$). **^{31}P{^{1}H} NMR** (121 MHz, $CDCl_3$): *δ* (ppm) = 145.5 (s). **HRMS** (NSI^+, DCM/MeOH + NH_4OAc): Found: *m*/*z* = 693.1246. Calculated for $[M - Cl]^+$: *m*/*z* = 693.1252.

4.4.6 [Au((*R*)-**30b**)Cl] (*R*)-**44b**

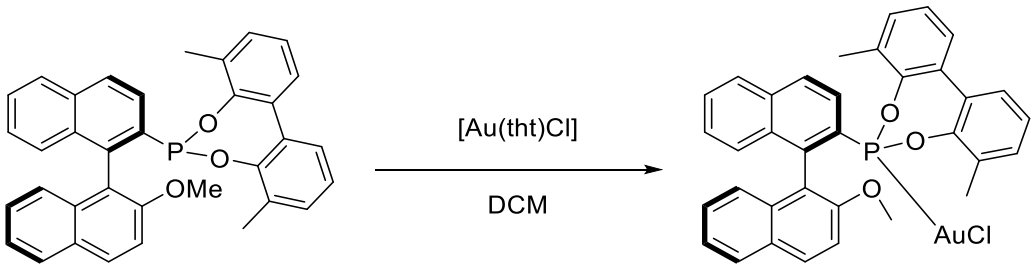

(*R*)-3,3'-dimethyl-[1,1'-biphenyl]-2,2'-diyl (2'-methoxy-[1,1'-binaphthalen]-2-yl) ((*R*)-**30b**, 31.6 mg, 60.0 µmol, 1.0 eq.) and chloro(tetrahydrothiophene)gold(I) (19.2 mg, 60.0 µmol, 1.0 eq.) were

dissolved in DCM (1.5 mL) and stirred for 30 min, after which the volatiles were removed *in vacuo*. The residue was washed with hexane and dried *in vacuo*, to yield the pure title compound quantitatively as a white solid. Single crystals could not be grown, despite repeated attempts.

MP: 146-148 °C. **IR** (neat): ν = 2935.0 (w), 1622.1 (w), 1591.8 (m), 1509.9 (m), 1455.4 (m), 1418.1 (m), 1311.9 (w), 1249.8 (s), 1182.2 (s), 1123.2 (m), 1080.6 (s), 1052.2 (w), 1021.6 (w), 903.7 (s), 810.3 (s), 766.2 (s), 727.9 (s), 685.2 (m), 644.1 (s) cm^{-1}. **^{1}H NMR** (300 MHz, $CDCl_3$): *δ* (ppm) = 8.19 (d, $^{3}J_{HH}$ = 9.1 Hz, 1H, *H*4'), 7.90 (d, $^{3}J_{HH}$ = 8.1 Hz, 1H, *H*5'), 7.83 (d, $^{3}J_{HH}$ = 8.2 Hz, 1H, *H*5), 7.71 (dd, $^{3}J_{HH}$ = 8.7 Hz, $^{4}J_{HP}$ = 1.8 Hz, 1H, *H*4), 7.52 (ddd, $^{3}J_{HH}$ = 8.2 Hz, $^{3}J_{HH}$ = 6.5 Hz, $^{4}J_{HH}$ = 1.5 Hz, 1H, *H*6), 7.41 (d, $^{3}J_{HH}$ = 9.1 Hz, 1H, *H*3'), 7.38 (dd, $^{3}J_{HH}$ = 8.7 Hz, $^{3}J_{HP}$ = 7.1 Hz, 1H, *H*3), 7.33-7.11 (m, 10H, *H*6'/*H*7/*H*7'/*H*8/*H*14/*H*14'/*H*15/*H*15'/*H*16/*H*16'), 6.84 (d, $^{3}J_{HH}$ = 8.4 Hz, 1H, *H*8'), 3.80 (s, 3H, OCH_3), 2.05 (s, 3H, CH_3'), 1.92 (s, 3H, CH_3). **^{13}C{^{1}H} NMR** (75 MHz, $CDCl_3$): *δ* (ppm) = 155.8 (*C*2'), 147.6 (d, $^{2}J_{CP}$ = 11.8 Hz, *C*12), 147.3 (d, $^{2}J_{CP}$ = 9.6 Hz, *C*12'), 142.9 (d, $^{2}J_{CP}$ = 26.7 Hz, *C*1), 135.8 (d, $^{4}J_{CP}$ = 1.7 Hz, *C*10), 134.9 (*C*9'), 133.0 (d, $^{3}J_{CP}$ = 12.0 Hz, *C*9), 131.9 (*C*4'), 131.7 (d, J_{CP} = 0.7 Hz), 131.4 (d, J_{CP} = 1.2 Hz), 131.0 (d, J_{CP} = 3.1 Hz), 130.7 (d, J_{CP} = 3.3 Hz), 130.6 (d, J_{CP} = 2.7 Hz), 130.3 (d, J_{CP} = 2.4 Hz), 129.3 (*C*10'), 129.2 (*C*6), 128.9 (m, *C*5'), 128.5 (d, J_{CP} = 1.3 Hz), 128.2 (m, *C*5), 127.9 (d, $^{3}J_{CP}$ = 7.8 Hz, *C*4), 127.5 (m, *C*7/*C*8), 127.3 (*C*7'), 126.3 (d, $^{5}J_{CP}$ = 1.7 Hz, *C*15 or *C*15'), 126.2 (d, $^{5}J_{CP}$ = 1.6 Hz, *C*15 or *C*15'), 124.4 (m, *C*3/*C*8'), 124.1 (*C*6'), 117.8 (d, $^{3}J_{CP}$ = 11.3 Hz, *C*1'), 113.0 (*C*3'), 56.2 (O*C*H_3), 17.0 (*C*H_3'), 16.3 (*C*H_3). **^{31}P{^{1}H} NMR** (121 MHz, $CDCl_3$): *δ* (ppm) = 146.7 (s). **HRMS** (NSI^+, DCM/MeOH): Found: *m*/*z* = 781.0937. Calculated for $[M + Na]^+$: *m*/*z* = 781.0944.

4.4.7 [Au((*S*)-**30a**)$_2$]SbF_6 (*S*)-**45a**

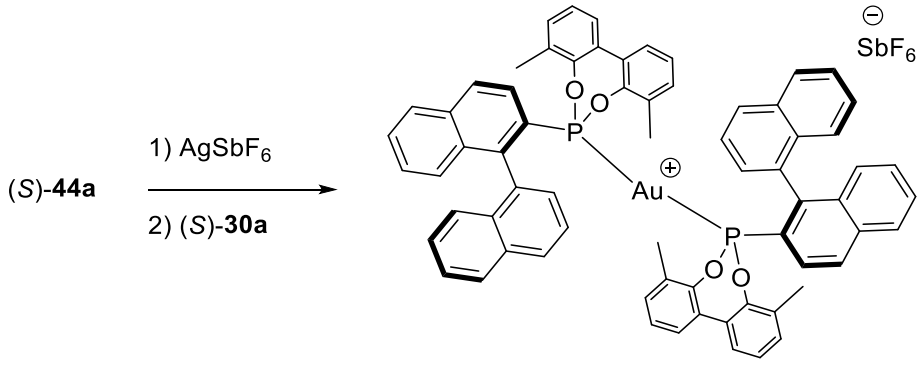

(*S*)-3,3'-dimethyl-[1,1'-biphenyl]-2,2'-diyl [1,1'-binaphthalen]-2-yl)phosphonite ((*S*)-**30a**, 19.9 mg, 40.0 µmol, 1.0 eq.) and chloro(tetrahydrothiophene)gold(I) (12.8 mg, 40.0 µmol, 1.0 eq.) were dissolved in DCM (2.0 mL) and stirred for 30 min, after which the volatiles were removed *in vacuo*. The residue was washed with hexane, redissolved in DCM (2.0 mL) and silver(I) hexafluoroantimonate (13.7 mg, 40.0 µmol, 1.0 eq.) was added. After stirring for 15 min, a second equivalent of (*S*)-**30a** (19.9 mg, 40.0 µmol, 1.0 eq.) was added and the reaction mixture stirred for 30 min. The precipitate

was filtered and the volatiles were removed *in vacuo* to yield the pure title compound quantitatively as an off-white solid. Single crystals were grown by hexane layering of a DCM solution.

MP: 262-264 °C (decomp.). **IR** (neat): ν = 3060.4 (w), 1453.7 (m), 1416.9 (m), 1370.3 (w), 1316.0 (w), 1249.0 (m), 1168.0 (s), 1122.4 (m), 1087.2 (m), 1026.9 (w), 907.8 (s), 875.2 (m), 803.0 (m), 776.4 (s), 654.9 (m), 636.7 (s) cm^{-1}. **^{1}H NMR** (300 MHz, CD_2Cl_2): δ (ppm) = 7.94 (d, $^{3}J_{HH}$ = 8.2 Hz, 1H, *H*5'), 7.89 (d, $^{3}J_{HH}$ = 8.8 Hz, 1H, *H*4), 7.69 (d, $^{3}J_{HH}$ = 8.2 Hz, 1H, *H*5), 7.62-7.55 (m, 2H, *H*4'/*H*6'), 7.38 (m, *H*6), 7.30-7.16 (m, 6H, *H*3'/*H*7/*H*15/*H*15'/*H*16/*H*16'), 7.15-7.02 (m, 3H, *H*3/*H*7'/*H*14'), 7.01-6.89 (m, 3H, *H*2'/*H*8/*H*14), 6.83 (d, $^{3}J_{HH}$ = 6.9 Hz, 1H, *H*8'), 1.85 (s, 3H, CH_3'), 1.32 (s, 3H, CH_3). **^{13}C{^{1}H} NMR** (75 MHz, CD_2Cl_2): δ (ppm) = 146.7 (*apparent*-t, J_{CP} = 4.8 Hz, *C*12'), 146.2 (*apparent*-t, J_{CP} = 5.0 Hz, *C*12), 145.2 (*apparent*-t, J_{CP} = 9.0 Hz, *C*1), 135.8 (*C*10), 133.5 (*apparent*-t, J_{CP} = 4.0 Hz, *C*1'), 133.2 (*C*9 or *C*9'), 133.2 (*C*9 or *C*9'), 133.0 (*apparent*-t, J_{CP} = 5.4 Hz, *C*2), 131.8 (*C*14'), 131.6 (*C*14), 130.4 (*C*10'), 130.0 (m, *C*4'/*C*6'/*C*13/*C*13'), 129.6, 129.4, 129.1 (m, *C*4), 128.7, 128.6 (*C*5/*C*8'), 128.4 (*C*5'), 128.1, 127.9 (*C*8), 127.1, 127.0, 126.9, 126.6 (*C*6), 125.5 (*C*2'), 125.0 (m, *C*3), 16.7 (*C*H_3'), 15.8 (*C*H_3). **^{31}P{^{1}H} NMR** (121 MHz, CD_2Cl_2): δ (ppm) = 167.8 (s). **HRMS** (NSI^+, DCM/MeOH): Found: *m*/*z* = 1189.2838. Calculated for $[M - SbF_6]^+$: *m*/*z* = 1189.2844.

4.4.8 General procedure for the synthesis of silver(I) complexes.

Phosphonite ligand (35.0 µmol, 1.0 eq.) and silver(I) trifluoromethanesulfonate (9.0 mg, 35 µmol, 1.0 eq.) were dissolved in CD_2Cl_2 (0.6 mL) and stirred at room temperature for 30 min. The solution was transferred to an NMR tube and VT $^{31}P\{^{1}H\}$ NMR (202 MHz) experiments were performed (Figs. 4.9-4.16 and Table 4.2).

4.4.9 [Ag((*R*)-**29b**)OTf] (*R*)-**47b**

Single crystals were grown by slow diffusion of diethyl ether into a DCM solution.

^{1}H NMR (400 MHz, CD_2Cl_2): δ (ppm) = 8.29-8.23 (m, 1H), 8.07-7.94 (m, 2H), 7.90-7.84 (m, 1H), 7.69-7.51 (m, 5H), 7.49-7.26 (m, 8H), 7.17-7.02 (m, 2H), 7.00-6.92 (m, 1H), 3.94 (br s, 3H, OCH_3). **^{13}C{^{1}H} NMR** (101 MHz, CD_2Cl_2): δ (ppm) = 156.5 (*C*2'), 149.3 (*overlapping*-d, *C*12/*C*12'), 142.6 (d, J_{CP} = 30.2 Hz, *C*1), 136.0, 133.6, 132.7 (m), 130.9, 130.5, 130.5, 130.4, 130.1, 129.3, 128.6, 128.5 (m), 128.1, 127.6, 127.0, 126.7, 126.4, 124.2, 124.1, 121.9, 121.7, 116.2 (d, $^{3}J_{CP}$ = 13.4 Hz, *C*1'), 113.2 (*C*3'), 56.4 (O*C*H_3). **^{31}P{^{1}H} NMR** (162 MHz, CD_2Cl_2): δ (ppm) = 157.1 (br s).

4.4.10 General procedure for the synthesis of copper(I) complexes.

Phosphonite ligand (60.0 µmol, 1.0 eq.) and tetrakis(acetonitrile)copper(I) hexafluorophosphate (22.4 mg, 60.0 µmol, 1.0 eq.) were dissolved in DCM (2.0 mL) and stirred at room temperature for 2 h,

after which the reaction mixture was filtered and a $^{31}P\{^{1}H\}$ NMR spectrum obtained. The NMR spectra showed a broad singlet for the ligand and a characteristic upfield septet for the hexafluorophosphate.

$^{31}P\{^{1}H\}$ NMR (121 MHz): δ (ppm) = [Cu((*S*)-H-MOP)(MeCN)$_2$], –9.3; [Cu((*R*)-MeO-MOP)(MeCN)$_2$], –7.7; (*S*)-**49a**, 130.8; (*R*)-**49b**, 131.8; (*S*)-**50a**, 145.9; (*R*)-**50b**, 147.3; (*S*)-**51a**, 142.2; (*R*)-**51b**, 144.5.

4.4.11 [Cu((*R*)-**30b**)(MeCN)$_2$]PF_6 (*R*)-**51b**

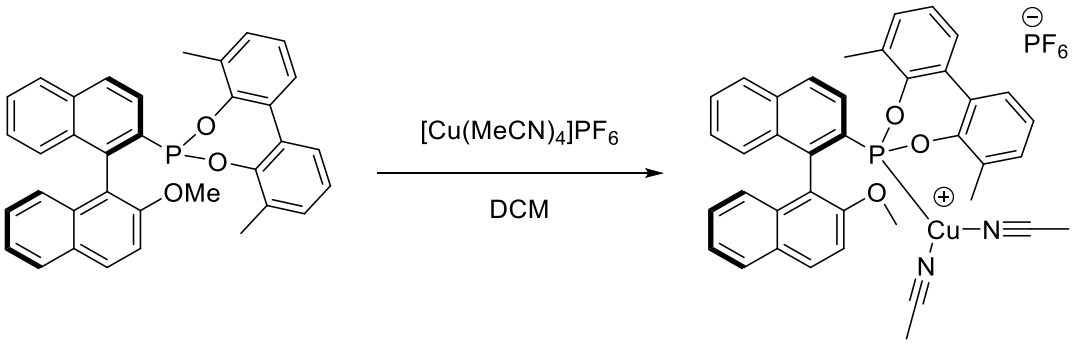

Single crystals were grown by slow diffusion of diethyl ether into a DCM solution.

MP: 192-194 °C. **IR** (neat): ν = 2963.4 (w), 1591.3 (w), 1508.1 (w), 1455.4 (m), 1418.91 (m), 1261.3 (m), 1188.9 (m), 1080.8 (s), 1020.4 (m), 900.0 (s), 836.3 (s), 807.8 (s), 773.9 (s), 682.6 (m), 637.8 (s) cm^{-1}. **^{1}H NMR** (500 MHz, CD_2Cl_2): δ (ppm) = 8.23 (br d, $^{3}J_{HH}$ = 8.5 Hz, 1H, *H*4'), 7.98 (br d, $^{3}J_{HH}$ = 7.5 Hz, 1H, *H*5'), 7.85 (d, $^{3}J_{HH}$ = 8.2 Hz, 1H, *H*5), 7.73 (d, $^{3}J_{HH}$ = 8.7 Hz, 1H, *H*4), 7.61 (br d, $^{3}J_{HH}$ = 8.5 Hz, 1H, *H*3'), 7.51 (m, 1H, *H*6), 7.36 (br *apparent*-t (dd), $^{3}J_{HH}$ = 7.5 Hz, 1H, *H*6'), 7.32-7.25 (m, 4H, *H*3/*H*7'/*H*16/*H*16'), 7.24-7.15 (m, 5H, *H*7/*H*14/*H*14'/*H*15/*H*15'), 6.98 (br d, $^{3}J_{HH}$ = 8.5 Hz, 1H, *H*8'), 6.84 (d, $^{3}J_{HH}$ = 8.6 Hz, 1H, *H*8), 3.80 (s, 3H, OCH_3), 1.99 (s, 3H, CH_3'), 1.98 (s, 6H, H_3CCN), 1.87 (s, 3H, CH_3). **$^{13}C\{^{1}H\}$ NMR** (126 MHz, CD_2Cl_2): δ (ppm) = 154.4 (*C*2'), 146.6 (*overlapping*-d, *C*12/*C*12'), 140.7 (d, $^{2}J_{CP}$ = 34.1 Hz, *C*1), 134.9 (*C*10), 132.8 (*C*9'), 131.4 (d, $^{3}J_{CP}$ = 9.7 Hz, *C*9), 131.1 (*C*4'), 130.3 (*obscured*-d, *C*2), 130.3 (*C*14'), 130.2 (*C*14), 129.9 (d, $^{3}J_{CP}$ = 2.1 Hz, *C*11 or *C*11'), 129.8 (*C*13), 129.5 (d, $^{3}J_{CP}$ = 2.3 Hz, *C*11 or *C*11'), 129.1 (d, $^{3}J_{CP}$ = 1.8 Hz, *C*13'), 128.4 (*C*10'), 127.9 (*C*6), 127.7 (*C*5'), 127.3 (*C*5), 127.2 (*C*4/*C*16/*C*16'), 126.7 (*C*7'), 126.3 (*C*7), 125.5 (*C*8), 124.9 (*C*15 or *C*15'), 124.9 (*C*15 or *C*15'), 123.6 (*C*8'), 123.3 (*C*6'), 122.5 (*C*3), 116.0 (H_3C*C*N), 115.8 (d, $^{3}J_{CP}$ = 11.5 Hz, *C*1'), 112.5 (*C*3'), 55.1 (O*C*H_3), 14.9 (*C*H_3'), 14.6 (*C*H_3), 0.90 (H_3*C*CN). **^{19}F NMR** (471 MHz, CD_2Cl_2): δ (ppm) = –73.1 (d, $^{1}J_{FP}$ = 710.4 Hz, P*F*$_6$). **$^{31}P\{^{1}H\}$ NMR** (202 MHz, CD_2Cl_2): δ (ppm) = 144.5 (br s, C*P*O_2), –144.4 (sep, $^{1}J_{PF}$ = 710.4 Hz, *P*F_6). **HRMS** (NSI$^+$, DCM/MeOH): Found: *m*/*z* = 589.0974. Calculated for [M – (2MeCN + PF_6)]$^+$: *m*/*z* = 589.0988.

4.5 X-ray Crystallography

Crystal structure data was collected on various diffractometers at temperatures ranging between 100-150 K using CuKα radiation (λ =1.54184 Å), MoKα radiation (λ = 0.71073 Å) or synchrotron (λ = 0.68890 Å) radiation. Cell parameters were refined from the observed positions of all strong reflections. Intensities were corrected for absorption, using a semi-empirical method based on symmetry-equivalent and repeated reflections for (*S*)-**42a**, (*R*)-**42b**, (*R*)-**43b**, (*S*)-**45a**, (*R*)-**47b**, (*R*)-**51b**, and (*S*)-**52a** and analytically using a multi-faceted crystal model for (*S*)-**43a** and (*S*)-**44a**.[133] All structures were solved by direct methods and refined on F2 values for all unique data. All non-hydrogen atoms were refined anisotropically, and H atoms were positioned with idealised geometry and the thermal parameters constrained using the riding model; U(H) was set at 1.2 times Ueq for the parent C atom. In the structure of (*S*)-**45a** there are solvent-accessible channels along the crystallographic [100] and [010] directions. The hexane molecules therein could not be modelled as discrete atoms and were hence treated with the SQUEEZE procedure using PLATON.[227] Oxford Diffraction CrysAlisPro was used for data collection and processing,[134] except for in the case of (*S*)-**45a** where CrystalClear was used.[228] Olex2[135] using SHELX[136] was used for structure solution and refinement and Crystal Impact Diamond was used to generate the molecular graphics with thermal ellipsoids drawn at the 50% probability level.[137]

	(*R*)-**42a**	(*S*)-**42b**	(*S*)-**43a**
Empirical formula	$C_{32}H_{23}O_2PClAu$	$C_{33}H_{25}O_3PClAu$	$C_{32}H_{21}O_2PClAu$
Formula weight	702.89	732.91	700.87
Temperature/K	150.0(2)	120.0	150.0(2)
Crystal system	triclinic	triclinic	monoclinic
Space group	P1	P1	$P2_1$
a/Å	8.68773(13)	8.9327(5)	11.1328(4)
b/Å	12.5934(2)	12.3201(7)	15.1475(4)
c/Å	13.1364(2)	13.2823(7)	15.0763(4)
α/°	107.4781(15)	73.9925(14)	90
β/°	103.5910(13)	77.1514(14)	90.611(3)
γ/°	90.4757(14)	88.9739(15)	90
Volume/Å^3	1327.66(4)	1368.41(13)	2542.22(13)
Z	2	2	4
ρ_{calc}g/cm^3	1.758	1.779	1.831
μ/mm^{-1}	12.130	5.566	5.984
F(000)	684.0	716.0	1360.0
Crystal size/mm^3	0.25 × 0.17 × 0.13	0.521 × 0.328 × 0.306	0.45 × 0.05 × 0.05
Radiation	CuKα (λ = 1.54184)	MoKα (λ = 0.71073)	MoKα (λ = 0.71073)
2Θ range for data collection/°	7.284 to 133.732	4.036 to 55.162	6.02 to 57.38
Index ranges	-10 ≤ h ≤ 10, -14 ≤ k ≤ 14, -15 ≤ l ≤ 15	-11 ≤ h ≤ 11, -16 ≤ k ≤ 16, -17 ≤ l ≤ 17	-15 ≤ h ≤ 13, -20 ≤ k ≤ 20, -20 ≤ l ≤ 20
Reflections collected	54307	19656	21800
Independent reflections	9130 [R_{int} = 0.0250, R_{sigma} = 0.0143]	12400 [R_{int} = 0.0337, R_{sigma} = 0.0464]	10648 [R_{int} = 0.0539, R_{sigma} = 0.0740]
Data/restraints/parameters	9130/3/667	12400/3/705	10648/637/667
Goodness-of-fit on F^2	1.063	1.032	1.090
Final R indexes [I>=2σ (I)]	R1 = 0.0165, wR_2 = 0.0420	R1 = 0.0234, wR_2 = 0.0606	R_1 = 0.0408, wR_2 = 0.0824
Final R indexes [all data]	R1 = 0.0166, wR_2 = 0.0421	R1 = 0.0239, wR_2 = 0.0609	R_1 = 0.0451, wR_2 = 0.0882
Largest diff. peak/hole / e Å^{-3}	0.33/-1.25	0.95/-0.97	1.67/-3.05
Flack parameter	-0.033(4)	-0.015(4)	-0.015(4)

	(*R*)-**43b**	(*S*)-**44a**	(*S*)-**45a**
Empirical formula	$C_{33}H_{23}O_3PClAu$	$C_{34}H_{25}O_2PClAu \cdot 0.88C_4H_{10}O$	$C_{68}H_{50}O_4P_2Au^+ \cdot SbF_6^- \cdot C_6H_{14}$
Formula weight	730.90	793.86	1511.90
Temperature/K	150.0(2)	150.0(2)	100(2)
Crystal system	monoclinic	monoclinic	monoclinic
Space group	$P2_1$	$P2_1$	$P2_1$
a/Å	11.3362(4)	11.64528(15)	12.1711(19)
b/Å	12.2678(3)	22.8679(3)	16.949(3)
c/Å	11.4833(4)	12.5763(2)	30.856(5)
α/°	90	90	90
β/°	119.535(5)	95.9000(14)	96.365(2)
γ/°	90	90	90
Volume/Å^3	1389.46(10)	3331.37(8)	6326.1(17)
Z	2	4	4
ρ_{calc}g/cm^3	1.747	1.583	1.587
μ/mm^{-1}	5.481	4.579	2.643
F(000)	712.0	1571.0	3016
Crystal size/mm^3	0.4 × 0.4 × 0.4	0.21 × 0.16 × 0.1	0.250 × 0.100 × 0.030
Radiation	MoKα (λ = 0.71073)	MoKα (λ = 0.71073)	synchrotron (λ = 0.6889)
2Θ range for data collection/°	6.642 to 56.7	5.772 to 58.932	1.3 to 27.3
Index ranges	-13 ≤ h ≤ 14, -12 ≤ k ≤ 15, -11 ≤ l ≤ 13	-15 ≤ h ≤ 15, -31 ≤ k ≤ 31, -17 ≤ l ≤ 16	-15 ≤ h ≤ 12, -22 ≤ k ≤ 19, -41 ≤ l ≤ 41
Reflections collected	12578	108491	55670
Independent reflections	5297 [R_{int} = 0.0243, R_{sigma} = 0.0371]	16205 [R_{int} = 0.0439, R_{sigma} = 0.0316]	25564 (R_{int} = 0.0363)
Data/restraints/parameters	5297/334/354	16205/715/801	25564/2305/1485
Goodness-of-fit on F^2	0.998	1.053	1.103
Final R indexes [I>=2σ (I)]	R_1 = 0.0181, wR_2 = 0.0322	R_1 = 0.0235, wR_2 = 0.0450	R1 = 0.0525, wR_2 = 0.1112
Final R indexes [all data]	R_1 = 0.0192, wR_2 = 0.0326	R_1 = 0.0286, wR_2 = 0.0470	R1 = 0.0595, wR_2 = 0.1133
Largest diff. peak/hole / e Å^{-3}	0.99/-0.86	0.81/-0.62	1.65/–3.62
Flack parameter	-0.002(3)	-0.0236(17)	0.087(3)

	(*R*)-**47b**	(*S*)-**51b**	(*S*)-**52a**
Empirical formula	$C_{68}H_{46}O_{12}P_2F_6S_2Ag_2 \cdot 2CH_2Cl_2$	$C_{39}H_{33}O_3PN_2Cu^{+} \cdot PF_6^{-} \cdot CH_2Cl_2$	$C_{64}H_{46}O_8P_4F_4Cu_2$
Formula weight	1680.70	902.08	1269.97
Temperature/K	150.0(2)	150.0(2)	150.0(2)
Crystal system	triclinic	triclinic	triclinic
Space group	P1	P1	P1
a/Å	11.1439(3)	12.4609(4)	9.2847(3)
b/Å	11.6528(3)	13.2453(4)	11.9004(3)
c/Å	14.4003(3)	14.9717(4)	12.7373(4)
α/°	92.665(2)	113.463(3)	84.837(2)
β/°	96.6293(18)	96.492(2)	89.150(2)
γ/°	115.865(3)	111.165(3)	80.158(2)
Volume/Å^3	1661.56(8)	2016.32(11)	1381.03(7)
Z	1	2	1
ρ_{calc}g/cm^3	1.680	1.486	1.527
μ/mm^{-1}	7.946	3.330	2.655
F(000)	844.0	920.0	648.0
Crystal size/mm^3	0.8 × 0.2 × 0.17	0.188 × 0.1371 × 0.0816	0.22 × 0.16 × 0.1
Radiation	CuKα (λ = 1.54184)	CuKα (λ = 1.54184)	CuKα (λ = 1.54184)
2Θ range for data collection/°	6.216 to 133.504	6.748 to 134.008	6.968 to 134.334
Index ranges	-13 ≤ h ≤ 13, -13 ≤ k ≤ 13, -17 ≤ l ≤ 17	-13 ≤ h ≤ 14, -15 ≤ k ≤ 15, -17 ≤ l ≤ 17	-11 ≤ h ≤ 11, -14 ≤ k ≤ 14, -15 ≤ l ≤ 15
Reflections collected	42848	45733	38044
Independent reflections	11444 [R_{int} = 0.0429, R_{sigma} = 0.0340]	13840 [R_{int} = 0.0387, R_{sigma} = 0.0380]	9465 [R_{int} = 0.0305, R_{sigma} = 0.0238]
Data/restraints/parameters	11444/18/917	13840/992/1033	9465/78/739
Goodness-of-fit on F^2	1.026	1.030	1.043
Final R indexes [I>=2σ (I)]	R_1 = 0.0312, wR_2 = 0.0771	R_1 = 0.0528, wR_2 = 0.1402	R_1 = 0.0274, wR_2 = 0.0678
Final R indexes [all data]	R_1 = 0.0353, wR_2 = 0.0805	R_1 = 0.0624, wR_2 = 0.1498	R_1 = 0.0319, wR_2 = 0.0709
Largest diff. peak/hole / e Å^{-3}	0.69/-0.36	1.19/-0.76	0.22/-0.34
Flack parameter	-0.030(4)	0.033(10)	-0.030(11)

5. References

1. K. J. Laidler, *Pure Appl. Chem.*, 1996, **68**, 149.
2. W. A. Herrmann and B. Cornils, *Angew. Chem., Int. Ed.*, 1997, **36**, 1048.
3. (a) J. F. Young, J. A. Osborn, F. H. Jardine and G. Wilkinson, *Chem. Commun.*, 1965, 131; (b) J. A. Osborn, F. H. Jardine, J. F. Young and G. Wilkinson, *J. Chem. Soc. A*, 1966, 1711; (c) F. H. Jardine, J. A. Osborn and G. Wilkinson, *J. Chem. Soc. A*, 1967, 1574.
4. L. Vaska and R. E. Rhodes, *J. Am. Chem. Soc.*, 1965, **87**, 4970.
5. D. Evans, J. A. Osborn and G. Wilkinson, *J. Chem. Soc. A*, 1968, 3133.
6. R. L. Pruett and J. A. Smith, *J. Org. Chem.*, 1969, **34**, 327.
7. D. G. Gilheany, *Chem. Rev.*, 1994, **94**, 1339.
8. (a) A. G. Orpen and N. G. Connelly, *J. Chem. Soc., Chem. Commun.*, 1985, 1310; (b) A. G. Orpen and N. G. Connelly, *Organometallics*, 1990, **9**, 1206; (c) B. J. Dunne, R. B. Morris and A. G. Orpen, *J. Chem. Soc., Dalton Trans.*, 1991, 653.
9. C. A. Tolman, *Chem. Rev.*, 1977, **77**, 313.
10. R. L. Harlow, R. J. McKinney and J. F. Whitney, *Organometallics*, 1983, **2**, 1839.
11. F. Allen, *Acta Cryst. B*, 2002, **58**, 380.
12. D. G. Gusev, *Organometallics*, 2009, **28**, 763.
13. T. L. Brown and K. J. Lee, *Coord. Chem. Rev.*, 1993, **128**, 89.
14. (a) N. Fey, S. E. Harris, J. N. Harvey and A. G. Orpen, *J. Chem. Inf. Model.*, 2006, **46**, 912; (b) N. Fey, A. C. Tsipis, S. E. Harris, J. N. Harvey, A. G. Orpen and R. A. Mansson, *Chem. Eur. J.*, 2006, **12**, 291; (c) R. A. Mansson, A. H. Welsh, N. Fey and A. G. Orpen, *J. Chem. Inf. Model.*, 2006, **46**, 2591.
15. (a) J. Jover, N. Fey, J. N. Harvey, G. C. Lloyd-Jones, A. G. Orpen, G. J. J. Owen-Smith, P. Murray, D. R. J. Hose, R. Osborne and M. Purdie, *Organometallics*, 2010, **29**, 6245; (b) N. Fey, S. Papadouli, P. G. Pringle, A. Ficks, J. T. Fleming, L. J. Higham, J. F. Wallis, D. Carmichael, N. Mézailles and C. Müller, *Phosphorus Sulfur Silicon Relat. Elem.*, 2014, **190**, 706.
16. N. Fey, M. F. Haddow, J. N. Harvey, C. L. McMullin and A. G. Orpen, *Dalton Trans.*, 2009, 8183.
17. (a) N. Fey, J. N. Harvey, G. C. Lloyd-Jones, P. Murray, A. G. Orpen, R. Osborne and M. Purdie, *Organometallics*, 2008, **27**, 1372; (b) J. Jover, N. Fey, J. N. Harvey, G. C. Lloyd-Jones, A. G. Orpen, G. J. J. Owen-Smith, P. Murray, D. R. J. Hose, R. Osborne and M. Purdie, *Organometallics*, 2012, **31**, 5302; (c) J. Jover and N. Fey, *Dalton Trans.*, 2013, **42**, 172.
18. N. Fey, A. G. Orpen and J. N. Harvey, *Coord. Chem. Rev.*, 2009, **253**, 704.
19. (a) *Phosphorus Ligands in Asymmetric Catalysis*, ed. A. Börner, Wiley-VCH, Weinheim, 2008; (b) *Phosphorus(III) Ligands in Homogeneous Catalysis: Design and Synthesis*, ed. P. C. J. Kamer and P. W. N. M. van Leeuwen, John Wiley & Sons, Chichester, 2012.
20. J. M. Hawkins and T. J. N. Watson, *Angew. Chem., Int. Ed.*, 2004, **43**, 3224.
21. (a) W. S. Knowles, *Angew. Chem., Int. Ed.*, 2002, **41**, 1998; (b) R. Noyori, *Angew. Chem., Int. Ed.*, 2002, **41**, 2008; (c) K. B. Sharpless, *Angew. Chem., Int. Ed.*, 2002, **41**, 2024.
22. A. Rauk, J. D. Andose, W. G. Frick, R. Tang and K. Mislow, *J. Am. Chem. Soc.*, 1971, **93**, 6507.
23. (a) L. Horner, H. Büthe and H. Siegel, *Tetrahedron Lett.*, 1968, **9**, 4023; (b) L. Horner, H. Siegel and H. Büthe, *Angew. Chem., Int. Ed.*, 1968, **7**, 942.
24. W. S. Knowles and M. J. Sabacky, *Chem. Commun.*, 1968, 1445.
25. W. S. Knowles, M. J. Sabacky and B. D. Vineyard, *J. Chem. Soc., Chem. Commun.*, 1972, 10.
26. K. M. Pietrusiewicz and M. Zablocka, *Chem. Rev.*, 1994, **94**, 1375.
27. (a) T. P. Dang and H. B. Kagan, *J. Chem. Soc. D*, 1971, 481; (b) H. B. Kagan and T. P. Dang, *J. Am. Chem. Soc.*, 1972, **94**, 6429.
28. (a) R. F. Service, *Science*, 2001, **294**, 503; (b) S. Goodman, *Nature*, 2001, **414**, 239.
29. W. S. Knowles, M. J. Sabacky, B. D. Vineyard and D. J. Weinkauff, *J. Am. Chem. Soc.*, 1975, **97**, 2567.
30. W. S. Knowles, *Acc. Chem. Res.*, 1983, **16**, 106.

31. G. Bringmann, A. J. Price Mortimer, P. A. Keller, M. J. Gresser, J. Garner and M. Breuning, *Angew. Chem., Int. Ed.*, 2005, **44**, 5384.
32. G. P. Moss, *Pure Appl. Chem.*, 1996, **68**, 2193.
33. R. S. Cahn, C. Ingold and V. Prelog, *Angew. Chem., Int. Ed.*, 1966, **5**, 385.
34. E. Masson, *Org. Biomol. Chem.*, 2013, **11**, 2859.
35. M. Kranz, T. Clark and P. v. R. Schleyer, *J. Org. Chem.*, 1993, **58**, 3317.
36. A. Miyashita, A. Yasuda, H. Takaya, K. Toriumi, T. Ito, T. Souchi and R. Noyori, *J. Am. Chem. Soc.*, 1980, **102**, 7932.
37. M. Berthod, G. Mignani, G. Woodward and M. Lemaire, *Chem. Rev.*, 2005, **105**, 1801.
38. R. Schmid, E. A. Broger, M. Cereghetti, Y. Crameri, J. Foricher, M. Lalonde, R. K. Müller, M. Scalone, G. Schoettel and U. Zutter, *Pure Appl. Chem.*, 1996, **68**, 131.
39. T. Saito, T. Yokozawa, T. Ishizaki, T. Moroi, N. Sayo, T. Miura and H. Kumobayashi, *Adv. Synth. Catal.*, 2001, **343**, 264.
40. M. McCarthy and P. J. Guiry, *Tetrahedron*, 2001, **57**, 3809.
41. R. Noyori and H. Takaya, *Acc. Chem. Res.*, 1990, **23**, 345.
42. (a) T. Ikariya, Y. Ishii, H. Kawano, T. Arai, M. Saburi, S. Yoshikawa and S. Akutagawa, *J. Chem. Soc., Chem. Commun.*, 1985, 922; (b) H. Kawano, T. Ikariya, Y. Ishii, M. Saburi, S. Yoshikawa, Y. Uchida and H. Kumobayashi, *J. Chem. Soc., Perkin Trans. 1*, 1989, 1571.
43. A. Miyashita, H. Takaya, T. Souchi and R. Noyori, *Tetrahedron*, 1984, **40**, 1245.
44. F. Lagasse and H. B. Kagan, *Chem. Pharm. Bull.*, 2000, **48**, 315.
45. T. Hayashi, M. Konishi, M. Fukushima, T. Mise, M. Kagotani, M. Tajika and M. Kumada, *J. Am. Chem. Soc.*, 1982, **104**, 180.
46. T. Hayashi and Y. Uozumi, *Pure Appl. Chem.*, 1992, **64**, 1911.
47. T. Hayashi, *Acc. Chem. Res.*, 2000, **33**, 354.
48. (a) M. Brynda, *Coord. Chem. Rev.*, 2005, **249**, 2013; (b) J. T. Fleming and L. J. Higham, *Coord. Chem. Rev.*, 2015, **297–298**, 127.
49. (a) H. Gali, K. R. Prabhu, S. R. Karra and K. V. Katti, *J. Org. Chem.*, 2000, **65**, 676; (b) K. V. Katti, N. Pillarsetty and K. Raghuraman, in *New Aspects in Phosphorus Chemistry III*, ed. J.-P. Majoral, Springer, Berlin Heidelberg, 2003, vol. 229, pp. 121-141; (c) R. M. Hiney, A. Ficks, H. Müller-Bunz, D. G. Gilheany and L. J. Higham, in *Organometallic Chemistry: Volume 37*, ed. I. J. S. Fairlamb and J. M. Lynam, The Royal Society of Chemistry, Cambridge, 2011, pp. 27-45.
50. T. Hanaya and H. Yamamoto, *Bull. Chem. Soc. Jpn.*, 1989, **62**, 2320.
51. E. P. Kyba and S. T. Liu, *Inorg. Chem.*, 1985, **24**, 1613.
52. K. V. Katti, H. Gali, C. J. Smith and D. E. Berning, *Acc. Chem. Res.*, 1998, **32**, 9.
53. H. Dorn, R. A. Singh, J. A. Massey, A. J. Lough and I. Manners, *Angew. Chem., Int. Ed.*, 1999, **38**, 3321.
54. B. Stewart, A. Harriman and L. J. Higham, *Organometallics*, 2011, **30**, 5338.
55. L. D. Quin, *A Guide to Organophosphorus Chemistry*, John Wiley & Sons, New York, 2000.
56. K. R. Prabhu, N. Pillarsetty, H. Gali and K. V. Katti, *J. Am. Chem. Soc.*, 2000, **122**, 1554.
57. B. Stewart, A. Harriman and L. J. Higham, in *Organometallic Chemistry : Volume 38*, ed. I. J. S. Fairlamb and J. M. Lynam, The Royal Society of Chemistry, Cambridge, 2012, vol. 38, pp. 36-47.
58. R. A. Bartlett, M. M. Olmstead, P. P. Power and G. A. Sigel, *Inorg. Chem.*, 1987, **26**, 1941.
59. M. Yoshifuji, K. Shibayama, N. Inamoto, T. Matsushita and K. Nishimoto, *J. Am. Chem. Soc.*, 1983, **105**, 2495.
60. B. Twamley, C.-S. Hwang, N. J. Hardman and P. P. Power, *J. Organomet. Chem.*, 2000, **609**, 152.
61. N. Pillarsetty, K. Raghuraman, C. L. Barnes and K. V. Katti, *J. Am. Chem. Soc.*, 2005, **127**, 331.
62. N. J. Goodwin, W. Henderson and B. K. Nicholson, *Chem. Commun.*, 1997, 31.
63. N. J. Goodwin, W. Henderson, B. K. Nicholson, J. Fawcett and D. R. Russell, *J. Chem. Soc., Dalton Trans.*, 1999, 1785.
64. W. Henderson and S. R. Alley, *J. Organomet. Chem.*, 2002, **656**, 120.

65. C. Spang, F. T. Edelmann, M. Noltemeyer and H. W. Roesky, *Chem. Ber.*, 1989, **122**, 1247.
66. R. M. Hiney, L. J. Higham, H. Müller-Bunz and D. G. Gilheany, *Angew. Chem., Int. Ed.*, 2006, **45**, 7248.
67. (a) H. W. Thompson and N. S. Kelland, *J. Chem. Soc.*, 1933, 1231; (b) P. D. Bartlett, E. F. Cox and R. E. Davis, *J. Am. Chem. Soc.*, 1961, **83**, 103; (c) M. M. Rauhut and H. A. Currier, *J. Org. Chem.*, 1961, **26**, 4626; (d) S. A. Buckler, *J. Am. Chem. Soc.*, 1962, **84**, 3093; (e) R. L. Powell and C. D. Hall, *J. Am. Chem. Soc.*, 1969, **91**, 5403; (f) H. D. Burkett, W. E. Hill and S. D. Worley, *Phosphorus Sulfur Silicon Relat. Elem.*, 1984, **20**, 169; (g) Z. B. Alfassi, P. Neta and B. Beaver, *J. Phys. Chem. A*, 1997, **101**, 2153; (h) B. Beaver, D. Rawlings, P. Neta, Z. B. Alfassi and T. N. Das, *Heteroat. Chem.*, 1998, **9**, 133; (i) S. Yasui, S. Tojo and T. Majima, *J. Org. Chem.*, 2005, **70**, 1276; (j) S. Yasui, S. Tojo and T. Majima, *Org. Biomol. Chem.*, 2006, **4**, 2969; (k) T. E. Barder and S. L. Buchwald, *J. Am. Chem. Soc.*, 2007, **129**, 5096; (l) S. Yasui, M. M. R. Badal, S. Kobayashi and M. Mishima, *Chem. Lett.*, 2013, **42**, 866; (m) S. Yasui, Y. Ogawa, K. Shioji and S. Yamazaki, *Chem. Lett.*, 2013, **42**, 1478; (n) S. Sasaki, K. Sutoh, Y. Shimizu, K. Kato and M. Yoshifuji, *Tetrahedron Lett.*, 2014, **55**, 322.
68. (a) X. Pan, X. Chen, T. Li, Y. Li and X. Wang, *J. Am. Chem. Soc.*, 2013, **135**, 3414; (b) G. Ménard, J. A. Hatnean, H. J. Cowley, A. J. Lough, J. M. Rawson and D. W. Stephan, *J. Am. Chem. Soc.*, 2013, **135**, 6446.
69. (a) F. L. Laughlin, A. L. Rheingold, N. Deligonul, B. J. Laughlin, R. C. Smith, L. J. Higham and J. D. Protasiewicz, *Dalton Trans.*, 2012, **41**, 12016; (b) S. Wu, N. Deligonal and J. D. Protasiewicz, *Dalton Trans.*, 2013, **42**, 14866; (c) F. L. Laughlin, N. Deligonul, A. L. Rheingold, J. A. Golen, B. J. Laughlin, R. C. Smith and J. D. Protasiewicz, *Organometallics*, 2013, **32**, 7116.
70. M. Yoshifuji, D.-L. An, K. Toyota and M. Yasunami, *Chem. Lett.*, 1993, **22**, 2069.
71. A. R. Jupp and J. M. Goicoechea, *J. Am. Chem. Soc.*, 2013, **135**, 19131.
72. T. Asamizu, W. Henderson, B. K. Nicholson and E. Hey-Hawkins, *Inorg. Chim. Acta*, 2014, **414**, 181.
73. S. Tschirschwitz, P. Lönnecke, J. Reinhold and E. Hey-Hawkins, *Angew. Chem., Int. Ed.*, 2005, **44**, 2965.
74. (a) S. Tschirschwitz, P. Lonnecke and E. Hey-Hawkins, *Dalton Trans.*, 2007, 1377; (b) C. Limburg, P. Lönnecke, S. Gómez-Ruiz and E. Hey-Hawkins, *Organometallics*, 2010, **29**, 5427.
75. F. Labrue, B. Pons, L. Ricard and A. Marinetti, *J. Organomet. Chem.*, 2005, **690**, 2285.
76. R. S. Drago, *Organometallics*, 1995, **14**, 3408.
77. I. V. Kourkine, S. V. Maslennikov, R. Ditchfield, D. S. Glueck, G. P. A. Yap, L. M. Liable-Sands and A. L. Rheingold, *Inorg. Chem.*, 1996, **35**, 6708.
78. H. Dorn, R. A. Singh, J. A. Massey, J. M. Nelson, C. A. Jaska, A. J. Lough and I. Manners, *J. Am. Chem. Soc.*, 2000, **122**, 6669.
79. R. Guterman, A. Rabiee Kenaree, J. B. Gilroy, E. R. Gillies and P. J. Ragogna, *Chem. Mater.*, 2015, **27**, 1412.
80. A. J. Bloomfield, J. M. Qian and S. B. Herzon, *Organometallics*, 2010, **29**, 4193.
81. J. S. Spiridonova, A. A. Karasik and O. G. Sinyashin, *Phosphorus Sulfur Silicon Relat. Elem.*, 2011, **186**, 764.
82. A. Benié, C. G. Kodjo, K. S. Traoré, J.-M. Denis and Y.-A. Békro, *Phys. Chem. News*, 2011, **59**, 73.
83. Y. S. Ganushevich, V. A. Miluykov, F. M. Polyancev, S. K. Latypov, P. Lönnecke, E. Hey-Hawkins, D. G. Yakhvarov and O. G. Sinyashin, *Organometallics*, 2013, **32**, 3914.
84. M. C. Fermin and D. W. Stephan, *J. Am. Chem. Soc.*, 1995, **117**, 12645.
85. R. Waterman, *Organometallics*, 2007, **26**, 2492.
86. M. B. Ghebreab, C. A. Bange and R. Waterman, *J. Am. Chem. Soc.*, 2014, **136**, 9240.
87. C. A. Bange, M. B. Ghebreab, A. Ficks, N. T. Mucha, L. J. Higham and R. Waterman, *Dalton Trans.*, 2016, **45**, 1863.
88. T. van Dijk, S. Burck, M. K. Rong, A. J. Rosenthal, M. Nieger, J. C. Slootweg and K. Lammertsma, *Angew. Chem., Int. Ed.*, 2014, **53**, 9068.

89. D. J. Brauer, K. W. Kottsieper, S. Roßenbach and O. Stelzer, *Eur. J. Inorg. Chem.*, 2003, 1748.
90. A. Ficks, C. Sibbald, S. Ojo, R. W. Harrington, W. Clegg and L. J. Higham, *Synthesis*, 2013, **45**, 265.
91. A. Ficks, I. Martinez-Botella, B. Stewart, R. W. Harrington, W. Clegg and L. J. Higham, *Chem. Commun.*, 2011, **47**, 8274.
92. A. Ficks, W. Clegg, R. W. Harrington and L. J. Higham, *Organometallics*, 2014, **33**, 6319.
93. (a) A. Ficks, R. M. Hiney, R. W. Harrington, D. G. Gilheany and L. J. Higham, *Dalton Trans.*, 2012, **41**, 3515; (b) A. Ficks, R. W. Harrington and L. J. Higham, *Dalton Trans.*, 2013, **42**, 6302.
94. J. Hopewell, P. Jankowski, C. L. McMullin, A. G. Orpen and P. G. Pringle, *Chem. Commun.*, 2010, **46**, 100.
95. B. J. Anderson, M. A. Guino-o, D. S. Glueck, J. A. Golen, A. G. DiPasquale, L. M. Liable-Sands and A. L. Rheingold, *Org. Lett.*, 2008, **10**, 4425.
96. L. Leseurre, F. Le Boucher d'Herouville, A. Millet, J.-P. Genêt, M. Scalone and V. Michelet, *Catal. Commun.*, 2015, **69**, 129.
97. M. M. Pereira, R. M. B. Carrilho and M. J. F. Calvete, in *Organophosphorus Chemistry: Volume 44*, ed. D. W. Allen, D. Loakes and J. C. Tebby, The Royal Society of Chemistry, Cambridge, 2015, vol. 44, pp. 56-103.
98. R. P. Feazell, C. E. Carson and K. K. Klausmeyer, *Inorg. Chem.*, 2005, **44**, 996.
99. Y. Xu, N. W. Alcock, G. J. Clarkson, G. Docherty, G. Woodward and M. Wills, *Org. Lett.*, 2004, **6**, 4105.
100. M. Mewald, A. Weickgenannt, R. Fröhlich and M. Oestreich, *Tetrahedron: Asymmetry*, 2010, **21**, 1232.
101. (a) A. Alexakis, J. Burton, J. Vastra, C. Benhaim, X. Fournioux, A. van den Heuvel, J.-M. Levêque, F. Mazé and S. Rosset, *Eur. J. Org. Chem.*, 2000, 4011; (b) A. Martorell, R. Naasz, B. L. Feringa and P. G. Pringle, *Tetrahedron: Asymmetry*, 2001, **12**, 2497; (c) M. T. Reetz, A. Gosberg and D. Moulin, *Tetrahedron Lett.*, 2002, **43**, 1189.
102. (a) W. Goertz, P. C. J. Kamer, P. W. N. M. van Leeuwen and D. Vogt, *Chem. Eur. J.*, 2001, **7**, 1614; (b) A. P. V. Göthlich, M. Tensfeldt, H. Rothfuss, M. E. Tauchert, D. Haap, F. Rominger and P. Hofmann, *Organometallics*, 2008, **27**, 2189; (c) L. Bini, C. Muller and D. Vogt, *Chem. Commun.*, 2010, **46**, 8325.
103. R. Bayersdörfer, B. Ganter, U. Englert, W. Keim and D. Vogt, *J. Organomet. Chem.*, 1998, **552**, 187.
104. T. Kamei, A. H. Sato and T. Iwasawa, *Tetrahedron Lett.*, 2011, **52**, 2638.
105. M. T. Reetz, D. Moulin and A. Gosberg, *Org. Lett.*, 2001, **3**, 4083.
106. (a) D. Selent, K.-D. Wiese, D. Röttger and A. Börner, *Angew. Chem., Int. Ed.*, 2000, **39**, 1639; (b) D. Selent, W. Baumann, R. Kempe, A. Spannenberg, D. Röttger, K.-D. Wiese and A. Börner, *Organometallics*, 2003, **22**, 4265; (c) J. I. van der Vlugt, J. M. J. Paulusse, E. J. Zijp, J. A. Tijmensen, A. M. Mills, A. L. Spek, C. Claver and D. Vogt, *Eur. J. Inorg. Chem.*, 2004, 4193.
107. (a) M. T. Reetz, A. Gosberg, R. Goddard and S.-H. Kyung, *Chem. Commun.*, 1998, 2077; (b) C. Claver, E. Fernandez, A. Gillon, K. Heslop, D. J. Hyett, A. Martorell, A. G. Orpen and P. G. Pringle, *Chem. Commun.*, 2000, 961; (c) M. T. Reetz and T. Sell, *Tetrahedron Lett.*, 2000, **41**, 6333; (d) A. Zanotti-Gerosa, C. Malan and D. Herzberg, *Org. Lett.*, 2001, **3**, 3687; (e) Y. Fu, G.-H. Hou, J.-H. Xie, L. Xing, L.-X. Wang and Q.-L. Zhou, *J. Org. Chem.*, 2004, **69**, 8157.
108. J.-i. Sakaki, W. B. Schweizer and D. Seebach, *Helv. Chim. Acta*, 1993, **76**, 2654.
109. W. C. Corbin, K. M. Mai, J. L. Freeman, S. D. Hastings and G. M. Gray, *Inorg. Chim. Acta*, 2013, **407**, 223.
110. J. M. Brunel, *Chem. Rev.*, 2005, **105**, 857.
111. D. Seebach, A. K. Beck and A. Heckel, *Angew. Chem., Int. Ed.*, 2001, **40**, 92.
112. T. Hayashi and K. Yamasaki, in *Comprehensive Organometallic Chemistry III*, ed. R. H. Crabtree and D. M. P. Mingos, Elsevier, Oxford, 2007, pp. 815-838.

113. Y. Uozumi, K. Kitayama, T. Hayashi, K. Yanagi and E. Fukuyo, *Bull. Chem. Soc. Jpn.*, 1995, **68**, 713.
114. (a) T. Hayashi, S. Hirate, K. Kitayama, H. Tsuji, A. Torii and Y. Uozumi, *J. Org. Chem.*, 2001, **66**, 1441; (b) J. W. Han and T. Hayashi, *Tetrahedron: Asymmetry*, 2014, **25**, 479.
115. A. J. Chalk and J. F. Harrod, *J. Am. Chem. Soc.*, 1965, **87**, 16.
116. S. B. Duckett and R. N. Perutz, *Organometallics*, 1992, **11**, 90.
117. Y. Uozumi, H. Tsuji and T. Hayashi, *J. Org. Chem.*, 1998, **63**, 6137.
118. H. L. Pedersen and M. Johannsen, *J. Org. Chem.*, 2002, **67**, 7982.
119. G. L. Larson, in *Organic Silicon Compounds Volume 1 and Volume 2*, ed. S. Patai and Z. Rappoport, John Wiley & Sons, Chichester, 1989, pp. 763-808.
120. K. Tamao, in *Advances in Silicon Chemistry*, ed. G. L. Larson, JAI Press, London, 1996, vol. 3, pp. 1-62.
121. P. G. A. Kumar, P. Dotta, R. Hermatschweiler, P. S. Pregosin, A. Albinati and S. Rizzato, *Organometallics*, 2005, **24**, 1306.
122. K. Kitayama, Y. Uozumi and T. Hayashi, *J. Chem. Soc., Chem. Commun.*, 1995, 1533.
123. A. M. Fournier, R. A. Brown, W. Farnaby, H. Miyatake-Ondozabal and J. Clayden, *Org. Lett.*, 2010, **12**, 2222.
124. J. H. Hutchinson, T. J. Seiders, B. Wang, J. M. Arruda, J. R. Roppe and T. Parr, *Br. Pat.*, GB2470833, 2010.
125. S. Hashiguchi, A. Fujii, K.-J. Haack, K. Matsumura, T. Ikariya and R. Noyori, *Angew. Chem., Int. Ed.*, 1997, **36**, 288.
126. Y. Uozumi, N. Suzuki, A. Ogiwara and T. Hayashi, *Tetrahedron*, 1994, **50**, 4293.
127. Y. Uozumi, A. Tanahashi, S. Y. Lee and T. Hayashi, *J. Org. Chem.*, 1993, **58**, 1945.
128. R. A. Fernandes and S. V. Mulay, *J. Org. Chem.*, 2010, **75**, 7029.
129. S. Green, A. Nelson, S. Warriner and B. Whittaker, *J. Chem. Soc., Perkin Trans. 1*, 2000, 4403.
130. T. Yamato, C. Hideshima, G. K. S. Prakash and G. A. Olah, *J. Org. Chem.*, 1991, **56**, 3192.
131. S. Kawabata, H. Tokura, H. Chiyojima, M. Okamoto and S. Sakaguchi, *Adv. Synth. Catal.*, 2012, **354**, 807.
132. D. J. Mathre, A. S. Thompson, A. W. Douglas, K. Hoogsteen, J. D. Carroll, E. G. Corley and E. J. J. Grabowski, *J. Org. Chem.*, 1993, **58**, 2880.
133. R. C. Clark and J. S. Reid, *Acta Cryst. A*, 1995, **51**, 887.
134. CrysAlisPro (Version 1.171.35), Oxford Diffraction, 2010.
135. O. V. Dolomanov, L. J. Bourhis, R. J. Gildea, J. A. K. Howard and H. Puschmann, *J. Appl. Crystallogr.*, 2009, **42**, 339.
136. G. M. Sheldrick, *Acta Cryst. A*, 2008, **64**, 112.
137. K. Brandenburg and H. Putz, Diamond (Version 3.2i), Crystal Impact, 2012.
138. J. T. Fleming, A. Ficks, P. G. Waddell, R. W. Harrington and L. J. Higham, *Dalton Trans.*, 2016, **45**, 1886.
139. (a) W. McFarlane and D. S. Rycroft, *J. Chem. Soc., Chem. Commun.*, 1972, 902; (b) W. McFarlane and D. S. Rycroft, *J. Chem. Soc., Dalton Trans.*, 1973, 2162.
140. (a) R. P. Pinnell, C. A. Megerle, S. L. Manatt and P. A. Kroon, *J. Am. Chem. Soc.*, 1973, **95**, 977; (b) D. W. Allen and B. F. Taylor, *J. Chem. Soc., Dalton Trans.*, 1982, 51.
141. (a) S. Vastag, B. Heil and L. Markó, *J. Mol. Catal.*, 1979, **5**, 189; (b) A. Roodt, S. Otto and G. Steyl, *Coord. Chem. Rev.*, 2003, **245**, 121.
142. R. A. Baber, M. F. Haddow, A. J. Middleton, A. G. Orpen, P. G. Pringle, A. Haynes, G. L. Williams and R. Papp, *Organometallics*, 2007, **26**, 713.
143. M. Carreira, M. Charernsuk, M. Eberhard, N. Fey, R. van Ginkel, A. Hamilton, W. P. Mul, A. G. Orpen, H. Phetmung and P. G. Pringle, *J. Am. Chem. Soc.*, 2009, **131**, 3078.
144. (a) A. Pidcock, R. E. Richards and L. M. Venanzi, *J. Chem. Soc. A*, 1966, 1707; (b) S. O. Grim, R. L. Keiter and W. McFarlane, *Inorg. Chem.*, 1967, **6**, 1133.
145. K. B. Dillon, A. E. Goeta, P. K. Monks and H. J. Shepherd, *Polyhedron*, 2010, **29**, 606.

146. K. M. Anderson and A. G. Orpen, *Chem. Commun.*, 2001, 2682.
147. M. J. Atherton, J. Fawcett, A. P. Hill, J. H. Holloway, E. G. Hope, D. R. Russell, G. C. Saunders and R. M. J. Stead, *J. Chem. Soc., Dalton Trans.*, 1997, 1137.
148. (a) A. D. Becke, *J. Chem. Phys.*, 1993, **98**, 5648; (b) P. J. Stephens, F. J. Devlin, C. F. Chabalowski and M. J. Frisch, *J. Phys. Chem.*, 1994, **98**, 11623.
149. (a) H. M. Senn, D. V. Deubel, P. E. Blöchl, A. Togni and G. Frenking, *J. Mol. Struct. Theochem*, 2000, **506**, 233; (b) C. H. Suresh and N. Koga, *Inorg. Chem.*, 2002, **41**, 1573.
150. K. D. Cooney, T. R. Cundari, N. W. Hoffman, K. A. Pittard, M. D. Temple and Y. Zhao, *J. Am. Chem. Soc.*, 2003, **125**, 4318.
151. J. Mathew, T. Thomas and C. H. Suresh, *Inorg. Chem.*, 2007, **46**, 10800.
152. K. G. Orrell, in *Annu. Rep. NMR Spectrosc.*, ed. G. A. Webb, Academic Press, London, 1999, vol. Volume 37, pp. 1-74.
153. (a) A. Almenningen, O. Bastiansen, L. Fernholt, B. N. Cyvin, S. J. Cyvin and S. Samdal, *J. Mol. Struct.*, 1985, **128**, 59; (b) S. Charbonnier, S. T. Beguemsi, Y. T. N'Guessan, D. Legoff, A. Proutiere and R. Viani, *J. Mol. Struct.*, 1987, **158**, 109; (c) F. Grein, *J. Phys. Chem. A*, 2002, **106**, 3823.
154. E. L. Eliel and S. H. Wilen, *Stereochemistry of Organic Compounds*, John Wiley & Sons, New York, 1994.
155. R. Shintani, C. Takagi, T. Ito, M. Naito and K. Nozaki, *Angew. Chem., Int. Ed.*, 2015, **54**, 1616.
156. R. Shintani, H. Kurata and K. Nozaki, *Chem. Commun.*, 2015, **51**, 11378.
157. (a) M. Sakai, M. Ueda and N. Miyaura, *Angew. Chem., Int. Ed.*, 1998, **37**, 3279; (b) E. F. Clarke, E. Rafter, H. Müller-Bunz, L. J. Higham and D. G. Gilheany, *J. Organomet. Chem.*, 2011, **696**, 3608.
158. X. Shen and S. L. Buchwald, *Angew. Chem., Int. Ed.*, 2010, **49**, 564.
159. J. Jeener, B. H. Meier, P. Bachmann and R. R. Ernst, *J. Chem. Phys.*, 1979, **71**, 4546.
160. (a) E. M. Viviente, P. S. Pregosin and D. Schott, in *Mechanisms in Homogeneous Catalysis*, ed. B. Heaton, Wiley-VCH, Weinheim, 2005, pp. 1-80; (b) H. Günther, *NMR Spectroscopy: Basic Principles, Concepts and Applications in Chemistry, 3rd Edition*, Wiley-VCH, Weinheim, 2013.
161. R. E. Blumer, F. Lianza, P. S. Pregosin, H. Ruegger and A. Togni, *Inorg. Chem.*, 1993, **32**, 2663.
162. (a) P. Barbaro, A. Currao, J. Herrmann, R. Nesper, P. S. Pregosin and R. Salzmann, *Organometallics*, 1996, **15**, 1879; (b) P. Leoni, M. Pasquali, M. Sommovigo, A. Albinati, P. S. Pregosin and H. Rüegger, *Organometallics*, 1996, **15**, 2047.
163. H. Bircher, B. R. Bender and W. von Philipsborn, *Magn. Reson. Chem.*, 1993, **31**, 293.
164. J. D. Heise, D. Raftery, B. K. Breedlove, J. Washington and C. P. Kubiak, *Organometallics*, 1998, **17**, 4461.
165. A. R. O'Connor, W. Kaminsky, D. M. Heinekey and K. I. Goldberg, *Organometallics*, 2011, **30**, 2105.
166. J. M. Brown, *Organometallics*, 2014, **33**, 5912.
167. *Chiral Amine Synthesis: Methods, Developments and Applications*, ed. T. C. Nugent, Wiley-VCH, Weinheim, 2010.
168. M. T. Reetz and G. Mehler, *Angew. Chem., Int. Ed.*, 2000, **39**, 3889.
169. (a) M. van den Berg, A. J. Minnaard, E. P. Schudde, J. van Esch, A. H. M. de Vries, J. G. de Vries and B. L. Feringa, *J. Am. Chem. Soc.*, 2000, **122**, 11539; (b) Y. Fu, X.-X. Guo, S.-F. Zhu, A.-G. Hu, J.-H. Xie and Q.-L. Zhou, *J. Org. Chem.*, 2004, **69**, 4648.
170. M. Soleilhavoup, L. Viau, G. Commenges, C. Lepetit and R. Chauvin, *Eur. J. Inorg. Chem.*, 2003, 207.
171. R. Franke, D. Selent and A. Börner, *Chem. Rev.*, 2012, **112**, 5675.
172. F. Agbossou, J.-F. Carpentier and A. Mortreux, *Chem. Rev.*, 1995, **95**, 2485.
173. J. Klosin and C. R. Landis, *Acc. Chem. Res.*, 2007, **40**, 1251.
174. G. Erre, S. Enthaler, K. Junge, S. Gladiali and M. Beller, *J. Mol. Catal. A: Chem.*, 2008, **280**, 148.
175. R. Shintani, M. Inoue and T. Hayashi, *Angew. Chem., Int. Ed.*, 2006, **45**, 3353.

176. P. G. Gildner and T. J. Colacot, *Organometallics*, 2015, **34**, 5497.
177. N. Miyaura and A. Suzuki, *Chem. Rev.*, 1995, **95**, 2457.
178. A. Suzuki, *Angew. Chem., Int. Ed.*, 2011, **50**, 6722.
179. (a) U. Christmann and R. Vilar, *Angew. Chem., Int. Ed.*, 2005, **44**, 366; (b) R. Martin and S. L. Buchwald, *Acc. Chem. Res.*, 2008, **41**, 1461.
180. J. Jover, N. Fey, M. Purdie, G. C. Lloyd-Jones and J. N. Harvey, *J. Mol. Catal. A: Chem.*, 2010, **324**, 39.
181. D. Zhang and Q. Wang, *Coord. Chem. Rev.*, 2015, **286**, 1.
182. (a) J. Yin and S. L. Buchwald, *J. Am. Chem. Soc.*, 2000, **122**, 12051; (b) X. Shen, G. O. Jones, D. A. Watson, B. Bhayana and S. L. Buchwald, *J. Am. Chem. Soc.*, 2010, **132**, 11278.
183. Y.-N. Ma and S.-D. Yang, *Chem. Eur. J.*, 2015, **21**, 6673.
184. (a) S. Wang, J. Li, T. Miao, W. Wu, Q. Li, Y. Zhuang, Z. Zhou and L. Qiu, *Org. Lett.*, 2012, **14**, 1966; (b) W. Wu, S. Wang, Y. Zhou, Y. He, Y. Zhuang, L. Li, P. Wan, L. Wang, Z. Zhou and L. Qiu, *Adv. Synth. Catal.*, 2012, **354**, 2395.
185. (a) Y. Zhou, S. Wang, W. Wu, Q. Li, Y. He, Y. Zhuang, L. Li, J. Pang, Z. Zhou and L. Qiu, *Org. Lett.*, 2013, **15**, 5508; (b) Y. Zhou, X. Zhang, H. Liang, Z. Cao, X. Zhao, Y. He, S. Wang, J. Pang, Z. Zhou, Z. Ke and L. Qiu, *ACS Catalysis*, 2014, **4**, 1390.
186. K. Sawai, R. Tatumi, T. Nakahodo and H. Fujihara, *Angew. Chem., Int. Ed.*, 2008, **47**, 6917.
187. P. Dotta, P. G. A. Kumar, P. S. Pregosin and A. Albinati, *Helv. Chim. Acta*, 2004, **87**, 272.
188. A. M. Z. Slawin, P. G. Waddell and J. D. Woollins, *Acta Cryst. E*, 2010, **66**, m321.
189. T. G. Schenck, J. M. Downes, C. R. C. Milne, P. B. Mackenzie, T. G. Boucher, J. Whelan and B. Bosnich, *Inorg. Chem.*, 1985, **24**, 2334.
190. M. Aydemir, N. Meric, C. Kayan, F. Ok and A. Baysal, *Inorg. Chim. Acta*, 2013, **398**, 1.
191. M. Kitamura, M. Tsukamoto, Y. Bessho, M. Yoshimura, U. Kobs, M. Widhalm and R. Noyori, *J. Am. Chem. Soc.*, 2002, **124**, 6649.
192. N. Weding, R. Jackstell, H. Jiao, A. Spannenberg and M. Hapke, *Adv. Synth. Catal.*, 2011, **353**, 3423.
193. C. J. Mathews, P. J. Smith and T. Welton, *J. Mol. Catal. A: Chem.*, 2003, **206**, 77.
194. C. W. Lim, O. Tissot, A. Mattison, M. W. Hooper, J. M. Brown, A. R. Cowley, D. I. Hulmes and A. J. Blacker, *Org. Process Res. Dev.*, 2003, **7**, 379.
195. M. C. Kroon, J. van Spronsen, C. J. Peters, R. A. Sheldon and G.-J. Witkamp, *Green Chem.*, 2006, **8**, 246.
196. M. J. Burk, J. E. Feaster, W. A. Nugent and R. L. Harlow, *J. Am. Chem. Soc.*, 1993, **115**, 10125.
197. T. T. Adint, G. W. Wong and C. R. Landis, *J. Org. Chem.*, 2013, **78**, 4231.
198. Á. Mosquera, M. A. Pena, J. Pérez Sestelo and L. A. Sarandeses, *Eur. J. Org. Chem.*, 2013, 2555.
199. A. Bermejo, A. Ros, R. Fernández and J. M. Lassaletta, *J. Am. Chem. Soc.*, 2008, **130**, 15798.
200. L. Benhamou, C. Besnard and E. P. Kündig, *Organometallics*, 2014, **33**, 260.
201. *Modern Gold Catalyzed Synthesis*, ed. A. S. K. Hashmi and F. D. Toste, Wiley-VCH, Weinheim, 2012.
202. M. P. Muñoz, J. Adrio, J. C. Carretero and A. M. Echavarren, *Organometallics*, 2005, **24**, 1293.
203. Y.-W. Sun, Q. Xu and M. Shi, *Beilstein J. Org. Chem.*, 2013, **9**, 2224.
204. N. Delpont, I. Escofet, P. Perez-Galan, D. Spiegl, M. Raducan, C. Bour, R. Sinisi and A. M. Echavarren, *Catal. Sci. Technol.*, 2013, **3**, 3007.
205. P. McGee, G. Bellavance, I. Korobkov, A. Tarasewicz and L. Barriault, *Chem. Eur. J.*, 2015, **21**, 9662.
206. A. S. K. Hashmi, B. Bechem, A. Loos, M. Hamzic, F. Rominger and H. Rabaa, *Aust. J. Chem.*, 2014, **67**, 481.
207. M. Touil, B. Bechem, A. S. K. Hashmi, B. Engels, M. A. Omary and H. Rabaâ, *J. Mol. Struct. Theochem*, 2010, **957**, 21.
208. P. Pérez-Galán, N. Delpont, E. Herrero-Gómez, F. Maseras and A. M. Echavarren, *Chem. Eur. J.*, 2010, **16**, 5324.

209. L.-S. Zheng, L. Li, K.-F. Yang, Z.-J. Zheng, X.-Q. Xiao and L.-W. Xu, *Tetrahedron*, 2013, **69**, 8777.
210. M. Naodovic, M. Wadamoto and H. Yamamoto, *Eur. J. Org. Chem.*, 2009, 5129.
211. J. Song, C. Guo, P.-H. Chen, J. Yu, S.-W. Luo and L.-Z. Gong, *Chem. Eur. J.*, 2011, **17**, 7786.
212. G. Hattori, K. Sakata, H. Matsuzawa, Y. Tanabe, Y. Miyake and Y. Nishibayashi, *J. Am. Chem. Soc.*, 2010, **132**, 10592.
213. J.-X. Chen, J. F. Daeuble and J. M. Stryker, *Tetrahedron*, 2000, **56**, 2789.
214. B. Tian, Q. Liu, X. Tong, P. Tian and G.-Q. Lin, *Org. Chem. Front.*, 2014, **1**, 1116.
215. T. Osako and Y. Uozumi, *Org. Lett.*, 2014, **16**, 5866.
216. A. Bondi, *The Journal of Physical Chemistry*, 1964, **68**, 441.
217. R. J. Staples, C. King, M. N. I. Khan, R. E. P. Winpenny and J. P. Fackler Jnr, *Acta Cryst. C*, 1993, **49**, 472.
218. J.-C. Wang, *Acta Cryst. C*, 1996, **52**, 611.
219. (a) D. Gudat, A. W. Holderberg, S. Kotila and M. Nieger, *Chem. Ber.*, 1996, **129**, 465; (b) J. Thomaier, S. Boulmaâz, H. Schönberg, H. Rüegger, A. Currao, H. Grützmacher, H. Hillebrecht and H. Pritzkow, *New J. Chem.*, 1998, **22**, 947; (c) K. M. A. Malik and P. D. Newman, *Dalton Trans.*, 2003, 3516.
220. (a) R. Terroba, M. B. Hursthouse, M. Laguna and A. Mendia, *Polyhedron*, 1999, **18**, 807; (b) M. Bardají, O. Crespo, A. Laguna and A. K. Fischer, *Inorg. Chim. Acta*, 2000, **304**, 7.
221. L. H. Davies, R. W. Harrington, W. Clegg and L. J. Higham, *Dalton Trans.*, 2014, **43**, 13485.
222. (a) E. L. Muetterties and C. W. Alegranti, *J. Am. Chem. Soc.*, 1972, **94**, 6386; (b) S. M. Socol and J. G. Verkade, *Inorg. Chem.*, 1984, **23**, 3487; (c) E. C. Alyea, J. Malito and J. H. Nelson, *Inorg. Chem.*, 1987, **26**, 4294.
223. (a) R. G. Goel and P. Pilon, *Inorg. Chem.*, 1978, **17**, 2876; (b) E. C. Alyea, S. A. Dias and S. Stevens, *Inorg. Chim. Acta*, 1980, **44**, L203; (c) L. J. Baker, G. A. Bowmaker, D. Camp, Effendy, P. C. Healy, H. Schmidbaur, O. Steigelmann and A. H. White, *Inorg. Chem.*, 1992, **31**, 3656.
224. G. A. Abakumov, A. V. Krashilina, V. K. Cherkasov and L. N. Zakharov, *Doklady Chemistry*, 2003, **391**, 185.
225. (a) S. Kitagawa, M. Kondo, S. Kawata, S. Wada, M. Maekawa and M. Munakata, *Inorg. Chem.*, 1995, **34**, 1455; (b) S. Mihan, K. Sünkel and W. Beck, *Chem. Eur. J.*, 1999, **5**, 745.
226. R. Uson, A. Laguna, M. Laguna, D. A. Briggs, H. H. Murray and J. P. Fackler, in *Inorg. Synth.*, John Wiley & Sons, Hoboken, 2007, pp. 85-91.
227. A. Spek, *Acta Cryst. D*, 2009, **65**, 148.
228. CrystalClear, Rigaku/MSC, 2008.